Arsonium and phosphonium-functionalized gold nanoparticles for mitochondria targeted therapeutics

LALWANI, Nikhil Narendra

Arsonium and Phosphonium-functionalized Gold Nanoparticles for Mitochondria Targeted Therapeutics

Nikhil Narendra Lalwani

A thesis submitted in partial fulfilment of the requirement of Sheffield Hallam University for the degree of Doctor of Philosophy.

August 2017

DECLARATION

The work presented in this thesis was carried out by Nikhil Lalwani at the Biomedical Research Centre, Faculty of Health and Wellbeing, between October 2012 and March 2017. The author declares that this work has not been submitted for any other degree. The work is original except where acknowledged by reference.

Nikhil Lalwani

Abstract

This thesis presents a body of original research describing the synthesis, characterisation and biological properties of novel arsonium- and phosphonium- alkylthiosulfate zwitterions and thioacetate salts and gold nanoparticles functionalized with triphenylarsoniumpropylthiolate ligands.

Chapter 1 presents a systematic literature review of the preparation of functionalized gold nanoparticles, their biomedical properties, the biological applications of phosphonium and arsonium ions and phosphonium-functionalized nanomaterials.

Details of the analytical methods employed to characterize all the compounds produced in this study are outlined in chapter 2.

Chapter 3 reports the synthesis of the triphenylarsoniopropylthiosulfate zwitterion and ω-thioacetylpropyl(triphenyl)arsonium bromide salt. Both compounds have been characterized spectroscopically and by single crystal X-ray diffraction. The thiosulfate group of the triphenylarsoniopropylthiosulfate zwitterion and the thioacetate group of the ω-thioacetylpropyl(triphenyl)arsonium salt undergo reductive cleavage, forming the corresponding triphenylarsoniumpropylthiolate ions that attach to the surface of gold in a modification of the established Brust-Schiffrin method for preparing gold nanoparticles. TEM studies show the triphenylarsonium-functionalized gold nanoparticles to be spherical with diameters of c.a. 3nm. The presence of the triphenylarsonium groups has been confirmed by Raman and XPS spectroscopy and mass spectrometry. It also describes the synthesis, characterisation and biological properties of a family of phosphoniopropylthiosulfate zwitterions and ω-thioacetylpropyl(triaryl)phosphonium salts derived from tri(4-methoxyphenyl)phosphine, tri(2,6-dimethoxyphenyl)phosphine and tri(2,4,6-trimethoxyphenyl)phosphine.

The IC_{50} values of the triphenylarsoniopropylthiosulfate zwitterion, ω-thioacetylpropyl-(triphenyl)arsonium bromide salt, triphenylarsonium-functionalized gold nanoparticles and family of phosphoniopropylthiosulfate zwitterions and ω-thioacetylpropyl(triaryl)phosphonium salts derived from tri(4-methoxyphenyl)phosphine, tri(2,6-dimethoxyphenyl)phosphine and tri(2,4,6-trimethoxyphenyl)phosphine have been determined against PC3 prostate cancer cells using MTT and CellTiter-Glo assays and are reported in Chapter 4. The uptake of the triphenylarsonium-functionalized gold nanoparticles by PC3 and Human Fibroblast cells has also been determined by ICP-OES spectroscopy.

Conclusion and suggestions for future work are presented in chapter 5.

Acknowledgement:

I would like to express my sincere gratitude to my supervisor **Prof Neil Bricklebank** for the continuous support of my Ph.D. study and related research, for his patience, motivation, and immense knowledge. His guidance helped me in all the time of research and writing of this thesis. I could not have imagined having a better advisor and mentor for my Ph.D. study.

Besides him, I would like to thank **Dr Neil Cross** for their insightful comments and encouragement, but also for the hard question which incented me to widen my research into cell culture. I would also take this opportunity to thank all the technical laboratory staff of Sheffield Hallam University for their tireless support, especially Kevin Osbourne for the NMR analysis and Daniel Kinsman for the training on the ESI-MS and MALDI instrument.

I would first like to thank my family without their continuous support and encouragement I never would have been able to achieve my goals. This one is for you mom!

Second, a special thank you to my wife **Pranjal Lalwani**. Words cannot describe how lucky I am to have her in my life. She has selflessly given more to me than I ever could have asked for. I love you, and look forward to our lifelong journey.

TABLE OF CONTENT

CHAPTER 1 ..... **1**

INTRODUCTION **1**

1.0 Introduction 2

1.1 Nanotechnology 2

1.1.1 Gold Nanoparticles 3

1.1.1.1 Synthesis of Gold Nanoparticles 3

1.1.1.2 Role of the Capping Ligand 5

1.1.1.3 Optical Properties of gold nanoparticles 7

1.1.1.4 Biomedical applications of AuNPs: 8

1.2 Cancer 9

1.2.1 Causes of Cancer 9

1.2.1.1 Chemical Carcinogens 10

1.2.1.2 Viruses 11

1.2.1.3 Radiation 11

1.2.2 Cancer Therapeutics 12

1.2.3 Cancer nanotechnology 15

1.2.3.1 Nanoparticles as Drug Delivery Carriers 16

1.2.3.2 Passive Targeting 16

1.2.3.3 Active Targeting 17

1.3 Mitochondria 18

1.3.1 Role of Mitochondria in Cell Death 19

1.3.2 Targeting Mitochondria for Cancer Therapy 20

1.3.3 Strategies for Mitochondrial Pharmacology 20

1.4 Lipophilic cations 21
1.4.1 Lipophilic Phosphonium Cations 23
1.4.2 Mitochondrial Accumulation of Lipophilic Phosphonium Cations 24
1.4.2.1 Phosphonium-conjugated Antioxidants 26
1.4.2.2 Mitochondria Targeted Photodynamic therapy 27
1.4.2.3 Mitochondria Targeted Radiotracers for Tumour imaging 28
1.5 Phosphonium-mediated Pharmaceutical Nanotechnology 28
1.5.1 Liposomes 29
1.5.2 Macromolecules 30
1.5.3 Metal nanoparticles 32
1.6 Arsonium Cations 36
1.7 Aims of this Thesis. 38
1.8 References 39
CHAPTER 2 62
EXPERIMENTAL METHODS 62
2.1 Melting point 63
2.2 Elemental analysis 63
2.3 Thin layer Chromatography 63
2.4 Nuclear Magnetic Resonance 63
2.5 Ultraviolet-visible absorption spectroscopy 64
2.6 Fourier Transform Infrared spectroscopy 64
2.7 Electrospray Ionization Mass Spectrometry 64
2.8 X-Ray Crystallography 64
2.9 Transmission Electron Microscopy 65
2.10 X-ray Photoelectron Spectroscopy 65
2.11 Cell Culture 66

2.12 Cytotoxicity assay 66

2.13 ICP-OES 67

2.14 References 68

CHAPTER 3 69

A) THE SYNTHESIS AND CHARACTERISATION OF TRIPHENYLARSONIUM- FUNCTIONALIZED GOLD NANOPARTICLES AND THEIR PRECURSOR LIGANDS 69

3.1 Introduction 70

3.2 Material and methods 71

3.2.1 Chemicals 71

3.2.2 Synthesis of Triphenylalkyl arsonium compounds 71

3.3 Characterization of Arsonium ligands. 73

3.3.1 Triphenylarsoniopropyl thiosulfate zwitterion (2): 73

3.3.2 ω-Thioacetylpropyl(triphenyl)arsonium bromide (3): 73

3.3.3 Single Crystal X-ray crystallography Studies of the Triphenylarsoniopropyl thiosulfate zwitterion (2). 73

3.3.4 Single Crystal X-ray crystallography Studies of the Thioacetylpropyl (triphenyl) arsonium bromide (3) 76

3.4 Synthesis and characterization of Triphenylarsonium functionalized gold nanoparticles. 79

3.4.1 The Synthesis of Triphenylarsonium- functionalized gold nanoparticles. 79

3.4.2 Characterization of Triphenylarsonium-Functionalized Gold Nanoparticles 83

3.4.2.1 Spectroscopic Characterization of Triphenylarsonium-capped AuNPs 83

3.4.2.2 X-Ray Photoelectron Spectroscopy (XPS) 88

3.4.2.3 Transmission Electron Microscopy (TEM) 98

3.5 Conclusion 103

3B) THE SYNTHESIS, CHARACTERISATION AND BIOLOGICAL PROPERTIES OF THE (METHOXY-PHENYL) PHOSPHONIOPROPYLTHIOSULFATE ZWITTERIONS AND ω-THIOACETYLPROPYL (METHOXYPHENYL) PHOSPHONIUM SALTS. 104

3.6 Methoxyphenyl phosphonium substituents 105

3.7 Material and methods 107

3.7.1 Chemicals 107

3.7.2 Methods 107

3.7.2.1 Cytotoxicity assay 107

3.8 Results and Discussion 108

3.9 Synthesis and Spectroscopic Characterisation of 5 -10 111

3.9.1 Single Crystal X-ray Analysis of tris(2,4,6-trimethoxyphenyl) phosphoniopropylthiosulfate 114

3.10 Conclusion 118

3.11 References 119

CHAPTER 4 126

4A) INVESTIGATION OF THE CYTOTOXICITY AND CELLULAR UPTAKE OF ARSONIUM LIGANDS AND GOLD NANOPARTICLES IN CELLS. 126

4.0 Introduction 127

4.1 Material and methods 129

4.1.1 Chemicals 129

4.1.2 Methods 129

4.1.2.1 Cytotoxicity and MTT assay 129

4.1.2.2 Quantification of the Uptake of Arsonium-functionalized gold nanoparticles in cells by ICP-OES 130

4.2 Results and Discussion 131

4.2.1 Cytotoxicity of Triphenylarsonium ligands 131

4.2.2 Cytotoxicity of Triphenylarsoniopropylthiolate-functionalized gold nanoparticles 133

4.3 Quantification of the Uptake by PC3 cells on Arsonium-functionalized gold nanoparticles in cells by ICP- OES spectrometry. 135

4.4 Conclusion 138

4B) Investigation of the cytotobxicity and cellular uptake of Methoxy substituents……140

4.5 Introduction 141

4.6 Material and methods 141

4.6.1 Chemicals 141

4.6.2 Methods 142

4.6.2.1 Cytotoxicity assay 142

4.7 Solubility studies of methoxy-phenyl phosphonium compounds 143

4.8 Cytotoxicity Screening of methoxy-phenyl phosphonium compounds 5 - 10. 143

4.9 Conclusion 148

4.10 References: 149

CHAPTER 5 154

CONCLUSIONS AND SUGGESTIONS FOR FUTURE WORK 154

5.1 Conclusion and Future Work 155

5.2 References 159

CHAPTER 6 160

ASSOCIATED WORK 160

6.1 Publications: 161

6.2 Conferences attended 161

6.3 Poster Presentations 161

6.4 Appendices 162

List of Figures

CHAPTER 1.

Figure 1.1 Synthesis of Gold Nanoparticles……5

Figure 1.2 Mercaptobenzoic acid……6

Figure 1.3 Naphthalene……8

Figure 1.4 Picloram……8

Figure 1.5 Phorbol……10

Figure 1.6 Nitrosamine 4-(methylnitrosamino)-1-(3-pyridyl)-1-butanone……11

Figure 1.7 Methotrexate……13

Figure 1.8 1-Ethyl-2-[[3-ethyl-5-(3-methyl-2(3H)-benzothiazolylidene)-4-oxo-2 thiazolidinylidene] methyl]-pyridinium chloride (MKT-077)… ……23

Figure 1.9 The proposed uptake of the triphenylarsonium cation by mitochondria through the mitochondrial membrane potential……...25

Figure 1.10 Molecular structure of the triphenyl phosphonium-vitamin E compound (MitoQ)……26

Figure 1.11 Liposomal drug delivery system surface modified with tripheylphosphonium moieties……29

Figure 1.12 Triphenylphsophonium-functionalized Dendrimers……30

Figure 1.13 poly(D,L-lactic-co-glycolic acid)-block (PLGA-b)-poly(ethyleneglycol) (PEG)-triphenylphosphonium (TPP) polymer (PLGA-b-PEG-TPP)……31

Figure 1.14 Triphenylphosphonium-conjugated Poly-L-Lysine nanoparticles……32

Figure 1.15 Scheme showing synthetic pathway for phosphonium zwitterions and salts……33

Figure 1.16 Structure of Triphneylphosphonium-functionalized mesoporous silica nanoparticles (MCM41)……35

Figure 1.17 Structure of Triphneylphosphonium-functionalized core-shed nanoparticles with a CdSe or ZnS core and a biocompatible γ-Fe_2O_3 shell.$_3$ shell……35

Figure 1.18 Structure of Water soluble triphenylphosphonium-functionalized Zro_2 nanoparticles……..35

CHAPTER 3.

Figure 3.1 Synthesis schemes of Arsonium ligands. ……72

Figure 3.2 An Ortep representation of the molecular structure of 2. Thermal ellipsoids are drawn at 50% probability level……74

Figure 3.3 S-[4-(trimethyammonio) phenyl] thiosulfate……75

Figure 3.4 An Ortep representation of the molecular structure of 3. Thermal ellipsoids are drawn at 50% probability level……77

Figure 3.5 Reaction scheme for synthesis of Triphenylarsonium-functionalized AuNPs…….81

Figure 3.6 UV-vis spectra of triphenylarsonium-functionalized AuNPs: (a) A-Au-Z0.1, (b) A-Au-Z1.5, (c) A-Au-Z0.5, (d) A-Au-Z2, (e) A-Au-Z1……84

Figure 3.7 Raman spectrum of **A-Au-Z0.5** in region 4000-500cm^{-1}. Insert, expansion of region 400 200cm^{-1}……86

Figure 3.8 Raman spectrum of **A-Au-Z1** in region 4000-500cm^{-1}. Insert, expansion of region 400-200cm^{-1}……86

Figure 3.9 Raman spectrum of **A-Au-Z1.5** in region 4000-500cm^{-1}. Insert, expansion of region 400-200cm^{1}……87

Figure 3.10 Raman spectrum of **A-Au-Z2** in region 4000-500cm^{-1}. Insert, expansion of region 400-200cm^{1}……87

Figure 3.11 Wide angle XPS spectrum of triphenylarsonium-AuNPs (a) A-Au-Z2 (b) (c) (d) A-AuT2……93

Figure 3. 12 High resolution Au XPS spectrum of triphenylarsonium-AuNPs (a) A-Au-Z2 (b) A-AuZ2w (c) A-Au-Z1w (d) A-AuT2……94

Figure 3.13 High resolution S ($2p_{3/2}$) XPS spectrum of triphenylarsonium-AuNPs (a) A-Au-Z2 (b) A-Au-Z2w (c) A-Au-Z1w (d) A-Au-T2……95

Figure 3.14 High resolution As (3d) XPS spectrum of triphenylarsonium-AuNPs (a) A-Au-Z2 (b) A-Au-Z2w (c) A-Au-Z1w (d) A-Au-T2……96

Figure 3.15 High resolution S XPS spectrum of ligands (a) 2 and (b) 3……97

Figure 3.16 High resolution As (3d) XPS spectrum of triphenylarsonium-AuNPs (a) 2 and (b)3……97

Figure 3.17 TEM micrographs and the core size histogram of arsonium-functionalized AuNPs (a) A-Au-Z0.5, (b) A-Au-Z1, (c) A-Au-Z1.5 and (d) A-Au-Z2……99

Figure 3.18 TEM micrograph and the core size histogram of the washed arsonium-functionalized AuNP sample A-Au-Z2w……102

Figure 3.19 TEM micrograph and the core size histogram of the arsonium-functionalized AuNP A-Au-T2, derived from ω-(triphenylarsonium)propylthioacetate bromide salt 3…….102

Figure 3.20 Molecular structure of 5……116

CHAPTER 4.

Figure 4.1 Schematic representation of AuNPs functionalized with sulfonated triphenylphosphine ligands……128

Figure 4.2 CellTiter-Glo (CTG) and MTT assay on arsonium zwitterions (1) and arsonium salt (2), Prostate cancer (PC3) cells were incubated with increasing concentration of compound (1 and 2). The IC_{50} was then determined for each drug (1 and 2) from a plot of log drug concentration versus percentage of cell normalised to control……132

Figure 4.3 Cytotoxicity assay on arsonium AuNPs (3)**.** Prostate cancer (PC3) cells were incubated with increasing concentration of compound (3). The IC_{50} values determined from a plot of log drug concentration versus percentage of cell normalised to control……134

Figure 4.4 Cytotoxicity assay on arsonium AuNPs (3)**.** Human Fibroblast cell were incubated with increasing concentration of compound (3). The IC_{50} values determined from a plot of log drug concentration versus percentage of cell normalised to control……134

Figure 4.5 ICP-OES data showing the percentage uptake of Triphenylarsonium-functionalized AuNP (A-AuNPs): Sigma AuNPs (S-AuNPs)……..136

Figure 4.6 PC3 cells treated with 5 - 10 for 24, 48, 72 hours. Cell proliferation was determined by the MTT assay. Data are expressed as a percentage of living cells normalized to control…….145

Figure 4.7 PC3 cells treated with 5-10 for 24, 48, 72 hours. Cell proliferation was determined by the CellTiter-Glo luminescent cell viability assay kit. Data are expressed as a percentage of living cells normalized to control……146

List of Tables

CHAPTER 3.

Table 3.1 Selected bond lengths [Å] and angles [°] in 2……..74

Table 3.2 Selected bond lengths [Å] and angles [°] in 3.3……78

Table 3.3 Varying ratio of Gold and Arsonium ligand……..82

Table 3.4 Position of Au-S band in Raman Spectra of triphenylarsoniumpropylthiolate-capped AuNPs……..85

Table 3.5 Summary of gold, sulphur and arsenic XPS binding energies for triphenylarsonium-functionalized AuNPs……88

Table 3.6 Average particle size of Triphenylarsonium-functionalized AuNPs. Mean particle size was calculated from 1000 nanoparticles……..98

Table 3.7 Selected bond lengths [Å] and angles [°] in compound 5……117

CHAPTER 4.

Table 4.1 IC_{50} values of **1** and **2** against PC3 Cell line (μM)……131

Table 4.2 IC_{50} values of Arsonium functionalized gold nanoparticles by PC3 and Human Fibroblast cell line (μM)……..134

Table 4.3 Percentage uptake of Triphenylarsonium-functionalized-AuNP (A-AuNPs): Sigma-AuNPs (S-AuNPs)……..137

Table 4.4 Comparison of Percentage uptake of Triphenylarsoniopropylthiolate-AuNPs (**A-Au-Z2**) and Triphenylphosphoniopropylthiolate-AuNPs (**P-Au-Z2**)……138

Table 4.5 IC_{50} values of methoxy-phenyl phosphoniopropylthiosulfate zwitterions (5 - 7) and ω-thioacetylpropyl(methoxyphenyl)phosphonium bromide salts (8 - 10). Units for data values are μM……144

Abbreviations

AuNPs	Gold Nanoparticles
CMP-tPP	Core Modified Porphyrin-mono-Triphenylphosphonium Cation
CPDs	Cyclobutane Diners
CTG	CellTiter-Glo
DECA	deconate
DIABLO	direct inhibitor of apoptosis-binding protein with low pl
DLC	Delocalised Lipophilic Cations
DMSO	Dimethyl sulfoxide
EPR	Enhanced Permeability and Retention
ESI-MS	Electrospray ionisation mass spectrometer
FDA	Food and Drug Administration
FITC	Fluorescein Isothiocyanate
FTIR	Fourier transform infrared
IMS	Intermembrane Space
kV	Kilovolt
MBA	Mercaptobenzoic Acid
MCM-41	Mesoporous silica nanoparticles
MitoQ	Molecular structure of the triphenyl phosphonium-vitamin E compound
MOMP	Mitochondrial Membrane Permeabilisation
mt DNA	mitochondrial DNA
MTT	3-(4,5-dimethyltiazol-2-yl)-2,5- diphenyltetrazolium bromide
PAH	Polycyclic Aromatic Hydrocarbons
PAMAM	Poly(amidoamine)
PC3	Prostate Cancer Cells
PDT	Photodynamic Therapy
PEG	Poly(ethyleneglycol)
PET	Positron Emission Tomography
PLGA	Poly(D,L-lactic-co-glycolic acid)-block

PLL	Poly-L-lysine
QDs	Quantum Dots
RNA	Ribonucleic Acid
Smac	Second mitochondria-derived activator of caspase
SPECT	Single-Photon Emission Computed Tomography
SPR	Surface Plasmon Resonance
TEM	Transmission Electron Microscopy
THF	Tertrahydrofuran
THPC	Tetrakis(hydroxymethyl) phosphonium chloride
TLC	Thin Layer Chromatography
TPMP	Triphenylmethylphosphonium
TPP	Tetraphenylphosphonium
UV-Vis	Ultraviolet visible
UVA	Ultraviolet A Radiation
UVB	Ultraviolet B Radiation
UVR	UV Radiation
XPS	X-ray photoelectron spectroscopy

Chapter 1

Introduction

1.0 Introduction

Arsenic and phosphorus both sit in group 15 of the periodic table. Both elements display an extensive and varied chemistry forming a wide range of compounds. Although the compounds of phosphorus and arsenic show some similarities, they also display important differences. For example, inorganic phosphates are essential for the existence of life whereas inorganic arsenic oxides are very toxic. Organo-phosphorus and -arsenic compounds have been very thoroughly investigated and find diverse application, especially in synthesis e.g. the Wittig reaction. Organophosphorus compounds find use in the field of nanotechnology, and as outlined below, are finding application in biomedical science. Similarly, the potential biomedical application of organoarsenic compounds is a topic that has received much attention since the advent of medicinal chemistry and has been revisited recently. This chapter provides a background to the work presented in this thesis, introducing the broad topics of nanotechnology and cancer before focusing on the biomedical applications of phosphonium- and arsonium- compounds and associated functionalized nanomaterials.

1.1 Nanotechnology

Nanotechnology is a multidisciplinary subject that encompasses physics, chemistry, biotechnology, engineering and medicine. Nanomaterials can be synthesized from a diverse range of substances including metals, metal oxides, semi-conductors, polymers, magnetic compounds, liposomes, carbon and silica-based materials. The field of nanotechnology is rapidly advancing and is constantly attracting immense interest from researchers from all over the world. These include industries such as electronic, textiles, cosmetics,

pharmaceuticals and environmental remediation (Daniel and Astruc, 2004). Gold nanoparticles are amongst the most widely studied nanomaterials due to their ease of preparation, stability, biocompatibility, and perceived biological inertness.

1.1.1 Gold Nanoparticles

The past twenty-five years have witnessed an explosion of interest in gold nanoparticles, due to their applications in drug delivery, solar cells, diagnostics, sensors and catalysis (Peer et al., 2007). Gold nanoparticles have been of significant interest in biomedical research owing to their surface functionalizing properties (Papasani et al., 2012). They have found application particularly in disease diagnosis and treatment, due to their larger surface area, reactivity in living cells and small size (Tiwari et al., 2011).

However, due to their smaller size, transport of nanoparticles into cells has been an issue. Consequently, strategies have been focused in binding these gold nanoparticles with various ligands and bio-molecules to achieve targeted delivery (Papasani et al., 2012).

1.1.1.1 Synthesis of Gold Nanoparticles

A wide variety of routes have been developed for the synthesis of gold nanoparticles (Fig 1.1). The most common method is the citrate reduction of gold(III) chloride salts in water, the citrate forming a loosely bound shell around the gold core. This method was first reported by Turkevitch in 1951 and leads to gold nanoparticles of approximately 20 nm in diameter (Turkevitch et al., 1951). The method was refined by Frens, who found that the size of the gold nanoparticles could be controlled by varying the ratio of gold salt and citrate

(Frens, 1973). A significant breakthrough came through the seminal work of Brust and Schiffrin who devised a method for producing gold nanoparticles with good polydispersity, which are very easily handled and can be isolated and re-dissolved in common organic solvents without aggregation or decomposition (Chen PhD Thesis, 2014). The initial method utilized an aqueous-toluene two-phase system with dodecanethiol as the capping ligand, sodium borohydride as the reducing agent, and tetraoctylammonium bromide as a phase transfer agent. The size of the particles can be varied by modifying the relative amounts of capping ligand and gold salt; the greater the amount of capping ligand the smaller the average particle size. Varying the temperature of the reaction also affects the particle size. Brust and co-workers refined the initial method by developing a single-phase method that obviated the need for the phase transfer agent, which can be difficult to remove from the metallic particles produced using the two-phase method (Brust et al., 1995). Subsequently, many workers have adopted the Brust–Schiffrin method and have prepared gold nanoparticles functionalized with a huge variety of thiolate ligands.

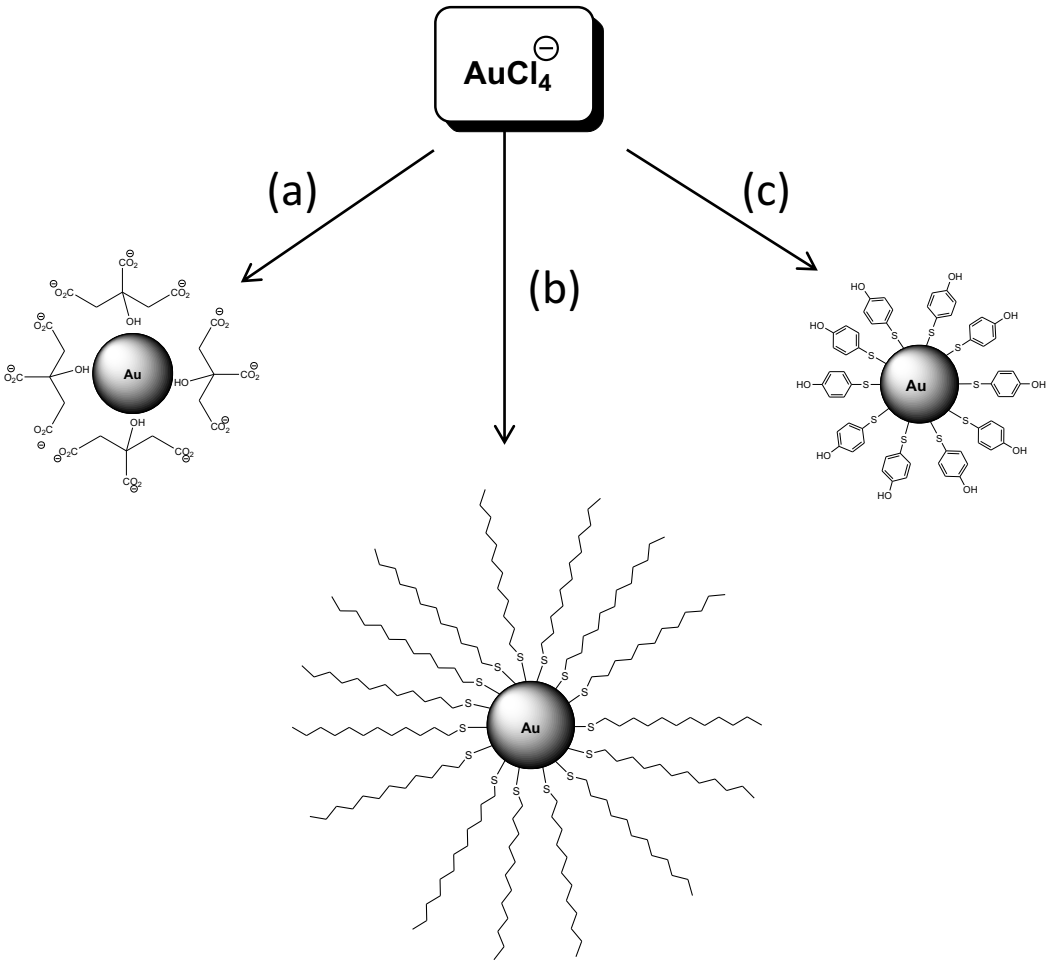

(a) Citrate reduction (Turkevitch et al., 1951).

(b) Brust-schiffrin two-phase system (Brust et al., 1994).

(c) Brust-schiffrin one-phase system (Brust et al., 1995).

Figure 1.1 Synthesis of Gold Nanoparticles

1.1.1.2 Role of the Capping Ligand

The capping ligand is a crucial component in both the synthesis and subsequent use of gold nanoparticles, stabilizing the particle, and preventing uncontrolled growth and

agglomeration. The choice of capping ligand influences the size and shape of the resulting particles. The most frequently used species are organic thiolates (RS^-, where R = alkyl or aryl), usually derived from the corresponding thiols or disulfides. Other common ligands include tertiary phosphines or alkyl amines. Organic thiolates have been widely studied because of the high affinity of sulphur for gold and the stability of the resulting S–Au bonds. The nature of the bond formed between the donor atom of capping ligand and the surface of the nanoparticle has been the subject of much investigation and speculation. However, a significant breakthrough came in 2007 with the reporting of the single crystal X-ray diffraction study of a sample of monodisperse gold particles functionalized with mercaptobenzoic acid (MBA) (Jadzinsky et al., 2007) (Fig 1.2). The structure revealed a core containing 102 gold atoms that is surrounded by 44 MBA ligands. The gold core comprises 89 Au atoms, 49 of which are arranged in a Marks decahedron with two 20-atom caps. The remaining 13 atoms form a band around the equator of the core. A significant finding was that the MBA ligands not only bind to the gold through Au–S bonds but also interact with each other through a series of face-to-face and face-to-edge interactions between adjacent phenyl rings and also phenyl–sulphur interactions. The inter-ligand interactions observed in this system may provide an indication of how capping ligands are ordered on the particle surface.

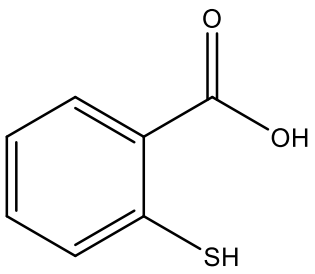

Fig 1.2 Mercaptobenzoic acid

In addition to their stabilizing role, the capping ligands can be used to functionalize the particles, enabling them to be used as sensors, for biomolecular recognition, or as transport vectors. Functionalization can be achieved by a number of ways. The organic groups that are attached to the particle during the initial synthesis can be modified by subjecting the particle to further chemical protocols. Alternatively, the particles can be used to form conjugates with biomolecules. The capping ligands that are utilized in the synthesis stage can be displaced by other species that exhibit the required functionality or biocompatibility through ligand exchange procedures.

1.1.1.3 Optical Properties of gold nanoparticles

Gold nanoparticles are widely studied because of their unique properties, including large optical field enhancements and their intense color which results in strong scattering and absorption of light. In the presence of the oscillating electromagnetic field of the light, the free electrons of the gold nanoparticle undergo a collective coherent oscillation with respect to the positive metallic lattice (Link and El-Sayed, 1999). This process is resonant at a particular frequency of the light and is also known as Surface Plasmon Resonance (SPR). The SPR depends on the particle size, temperature, shape and the surrounding of the gold nanoparticles. (Jain et al, 2008). The distinctive feature of this SPR band is its position around 520nm and as the size of the gold nanoparticles varies it shows a sharp decrease with decreasing core size. The SPR band is absent when the AuNPs are less than 2nm and for bulk gold. The SPR λ_{max} was observed at 517, 520, 533 and 575nm for AuNP size ranging from 9, 15, 48 and 99nm respectively (Daniel and Astruc, 2004).

1.1.1.4 Biomedical applications of AuNPs:

The field of nanotechnology has grown rapidly and was estimated to have a market value of around $53 billion in 2014. (Akhter et al, 2013). Functionalization of these gold nanoparticles facilitates targeted delivery to various cell types, bio-imaging, gene delivery, drug delivery, and other therapeutic and diagnosis applications. (Tiwari et al, 2011).

Functionalities that observe changes in response to enzymatic activity or other alterations can be used as sensors to provide information about a tumor or the efficiency of treatment. These sensors depend on the ability of the gold nanoparticles to undergo a change in their SPR when aggregated. Many methods have been developed to improve the biosensor activity by modifying nanomaterials for fabrication which permits applications of various signal transductions in biosensors. Colloidal gold nanocrystals were synthesized to develop biosensors that identify special DNA sequences and they were able to detect single base mutation in a homogenous format. Electro-catalytic sensors to detect tumor cells were also synthesized, AuNPs conjugated with DNA and using ethylene blue as an electroactive label and differential pulse voltammetry for DNA sensing (Maxwell et al, 2002). Many other examples including the detection of carcinogenic substances such as uocra-toxin A, Aflatoxin, naphthalene (Fig 1.3) and the herbicide picloram (Fig 1.4), were completed using electrochemical immunosensors. (Khan et al, 2013).

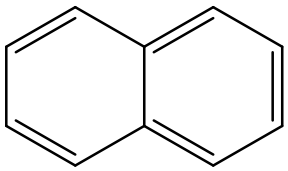

Fig 1.3 Naphthalene

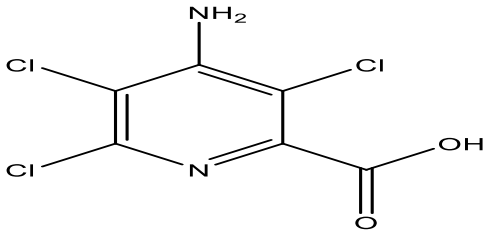

Fig 1.4 Picloram

1.2 Cancer

Cancer is a collective term for a group of diseases characterized by invasive abnormal cell growth, and is a common terminology for describing a malignant tumour (Hesketh, 2013). While the origin of the word cancer is credited to the Greek physician Hippocrates who described tumours as karkinos and karkinona, it was Galen who described the appearance of a tumour as similar to the legs of a crab, and this resemblance lead to the name of the disease- karkinos (cancer) which means crab in Greek (Papavramidou et al.,2010).

Cancer is a major cause of death in economically developed countries; this is predominantly driven by increasing average life-span, in addition to unhealthy lifestyle choices including smoking, lack of physical activity and poor diets. In 2014, approximately 14.7 million cancer cases were diagnosed with 7.6 million deaths globally. However, more than half the cases and deaths (56% and 64% respectively) occurred in economically developing countries, despite being the second leading cause of death in developing countries (Jemal et al., 2011). In the UK alone, 325,000 people were diagnosed with cancer in 2014 and someone is diagnosed with cancer every two minutes (Cancer Research UK).

1.2.1 Causes of Cancer

Cancer is perceived as a genetic disease involving a series of irreversible genetic changes, encompassing single point mutations, gene amplification and the loss of large regions of the genome (Tlsty and Coussens, 2006). The concept of cancer being a genetic disease of somatic cells was proposed in 1914 by Theodor Boveri (Knudson, 2001). Alterations in genetics may result in the gene no longer functioning normally and can acquire new cellular phenotypes that are beneficial to the cell such as resistance to cell death which are also

known as the hallmarks of cancer (Hanahan and Weinberg, 2011). The transition of normal cell into malignant phenotype is facilitated through the occurrence of genetic mutation, which can be induced by a variety of chemical, physical and biological agents.

1.2.1.1 Chemical Carcinogens

Chemical carcinogens are substances that are generally genotoxic and are able to induce DNA damage either through deletions, amplifications, single point mutations or re-arrangements. To-date a large number of chemical carcinogens have been identified (Wogan et al., 2004, Cohen and Arnold, 2011). However, not all cancer-causing agents result in DNA damage; phorbol (Fig 1.5) esters are a class of tumour promoters which induce cellular proliferation but are not mutagenic themselves (Goel et al., 2007).

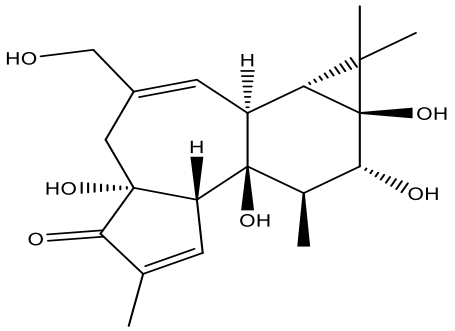

Fig 1.5 Phorbol

The role of cigarette smoking as a cause of cancer is unquestionable and more than 60 carcinogens from cigarette smoke have been verified to be carcinogenic in either animals or humans. (Pfeifer et al., 2002, Peto et al., 2000). Among all tobacco-specific carcinogens the nitrosamine 4-(methylnitrosamino)-1-(3-pyridyl)-1-butanone(NNK) (Fig 1.6) and polycyclic aromatic hydrocarbons (PAH) have shown to be predominately involved in the induction of lung cancer (Hecht, 1999).

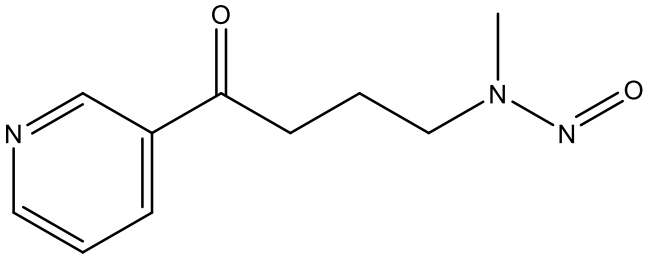

Fig 1.6 Nitrosamine 4-(methylnitrosamino)-1-(3-pyridyl)-1-butanone

1.2.1.2 Viruses

It has been estimated that 15% of all human cancers are caused by viruses, contributing to a substantial proportion of the cancer burden worldwide (Liao, 2006). Retroviruses cover a diverse class of ribonucleic acid (RNA) viruses which are small viruses containing only RNA in their genome and are associated with an array of immunodeficiency, neurological disorders and malignancies (D'Souza and Summers, 2005). Human T lymphotrophic virus type 1 and hepatitis C virus are two RNA viruses that have shown to contribute towards the development of cancers (Liao, 2006). Retroviruses can either be non-transforming or transforming, depending on the absence or presence of oncogene in their viral genome (Uren et al., 2005). Although no human retroviruses have this ability, many viruses in other species do and these viruses produce an enzyme called reverse transcriptase, enabling the host cell to make a replica of the viral genome and integrate into the host cell genome (Weinberg, 2013).

1.2.1.3 Radiation

Acute or prolonged exposure to high dose of ionizing radiation can lead to damaging consequences in humans including, but not limited to, cancer. In contrast, the effects of very low levels of radiation remain unclear (Brenner et al., 2003). The carcinogenic effect of

radiation has been well documented and is undisputed; radiation exposure in Hiroshima and Nagasaki in Japan has been associated with a number of different cancers, predominately leukemia. Underground miners exposed to radon sources were prone to develop lung cancer and luminous dial painters exposed from radium have been linked with bone cancer (Gilbert, 2009).

DNA damage from ionizing radiation can occur from either a direct interaction between DNA and radiation or via the creation of free radicals, which can result in cell death or non-lethal DNA modification including DNA cross-linking, mutations, chromosomal loss and single and double strand breaks (Wakeford, 2004, Cwikel et al., 2010). It is well known that UV radiation (UVR) present in sunlight is a potent carcinogen and chronic repeated exposure of UVR is the main cause of skin cancers. Both ultraviolet A radiation (UVA) (320-400 nm) and ultraviolet B radiation (UVB) (280-320 nm) have important biological significances for the skin; UVA has a crucial role in the carcinogenesis of stems cells of the skin while UVB produces DNA damage and subsequently gene mutations, oxidative stress, immunosuppression and tumorigenesis (Narayanan et al., 2010). UVB-induced DNA damage by forms dimeric photoproducts at "hot spots" of UV-induced mutations between adjacent pyrimidine bases on the same strand; pyrimidine-pyrimidone (6-4) photoproducts and cyclobutane diners (CPDs) are the two most prevalent adducts formed (Ichihashi et al., 2003).

1.2.2 Cancer Therapeutics

To date the most common types of cancer treatment include surgery, radiotherapy and chemotherapy. Surgery is most effective for the treatment of localized primary tumours and

associated metastases in regional lymphatics (Urruticoechea et al., 2010). Radiotherapy utilizes high energy radiation sources to cause damage to the DNA of cancer cells hence blocking their cell division cycle and is an effective treatment for early cancers including prostate, lung, cervix, head and neck, lymphomas, and skin cancers, all of which are curable with radiation therapy alone. Furthermore, radiotherapy is commonly used in conjunction with surgery and chemotherapy; around 50% of all patients will receive radiotherapy during the course of their illness contributing towards 40% of curative treatment of cancer (Baskar et al., 2012).

The use of chemotherapy to treat cancer dates back to the early 20th century with the use of nitrogen mustards and anti-folate drugs. Since this time cancer drugs have become one of the most extensively researched areas and have evolved into a multi-billion-dollar industry (Chabner and Roberts, 2005, Devita and Chu, 2008). Chemotherapy involves the use of cytotoxic drugs that disrupt the cell cycle; alkylating agents such as cisplatin and cyclophosphamide form adducts with DNA bases primarily at the guanine sites and interfere with DNA replication (Emadi et al., 2009, Zamble and Lippard, 1995). Antimetabolites including methotrexate (Fig 1.7) and 5-fluorouracil inhibit vital enzymes in the metabolic processes, thus halting cell growth (Kaye, 1998).

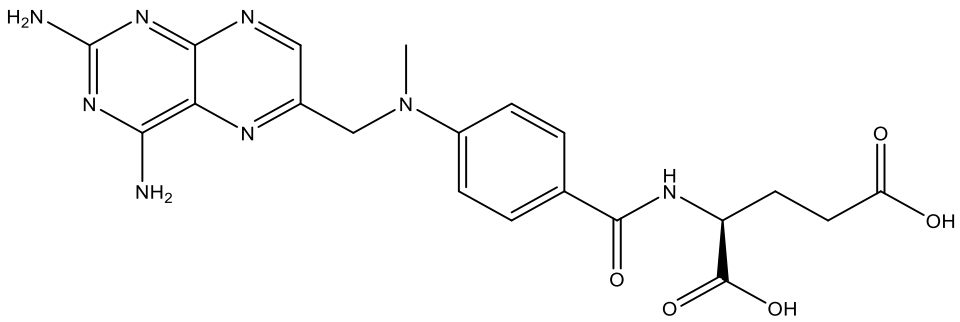

Fig 1.7 Methotrexate

Existing cancer treatments possess several drawbacks; surgery is limited to large accessible tumors, radiation therapy is non-specific and kills both normal and abnormal cells in the radiated pathway, chemotherapeutic drugs have a narrow therapeutic index and are carcinogenic, cause immuno-suppression, and are highly expensive. Consequently, research has focused on the development of new, novel therapies to decrease drug toxicity in healthy cells and increase efficacy and this has led to the development of targeted therapies (Arruebo et al.,2011).

One approach is to use monoclonal antibodies to target receptors overexpressed on the surface of cancer cells. Antibody-based therapy has become established over the past 15 years and is now often the preferred choice in the treatment of hematological malignancies and solid tumours (Scott et al., 2012). Over the years several fully human monoclonal antibodies (e.g. Herceptin) have been approved by regulatory agencies and others are under clinical trial (Arruebo et al., 2011). Alternative methods include targeting specific cellular signaling pathways with the use of tyrosine kinase inhibitors (e.g. Imatinib) (Arora and Scholar, 2005), triggering the extrinsic apoptotic pathway via the use of apoptosis-inducing ligands (e.g. TRAIL) (Mahmood and Shukla 2010, Wang, 2010) and targeting the p53 gene therapy pathway to reactivate the p53 apoptosis pathway (Bykov and Wiman, 2003. The use of nanomaterials for novel applications in the field of oncology has emerged a hot topic, with many publications in this area.

1.2.3 Cancer nanotechnology

At present, there is a strong focus on the applications of nanotechnology in cancer research; cancer nanotechnology is a comparatively new field of interdisciplinary research cutting across chemistry, engineering, biology and medicine, and is anticipated to revolutionize the detection, diagnosis and treatment of cancer (Llevot and Astruc, 2012, Portmey and Ozkan, 2006, Srinivas et al., 2002, Ferrari, 2005, Davis et al., 2008).

The utilization of nanomaterials for imaging applications has been widely investigated; Cellular labelling using quantum dots (QDs) has advanced the most and has provided a useful new class of fluorescent probes for in vivo biomolecular and cellular imaging, (Walling et al., 2009, Gao et al., 2004, Li et al., 2009, Bentolila et al., 2009). Furthermore, QDs have been used in cell tracking for the study of tumour metastasis (Voura et al., 2004) and the binding of EGF to EGFR (Lidke et al., 2004) magnetic nanoparticles has been exploited for magnetic resonance imaging and cell tracking (Arbab et al., 2006, Pankhurst et al., 2003, Singh, 2001, McCarthy and Weissleder, 2008).

The application of nano-size devices for drug delivery has blossomed (Wagner et al., 2006, Kumar et al., 2013). A range of nanometric delivery vehicles has been proposed, including polymeric micelles, dendrimers, and liposomes, QDs, carbon nanotubes and inorganic nanoparticles, especially gold (Rivera Gil et al., 2010, Bawarski et al., 2008, Elhissi et al., 2012, Riggio et al., 2011, Akhter et al., 2012, Ahmad et al., 2013, Han et al., 2007).

1.2.3.1 Nanoparticles as Drug Delivery Carriers

As mentioned above, the majority of current anti-cancer agents are not specific and lack the ability to differentiate between normal and cancerous cells, leading to systemic toxicity. Furthermore, because of the rapid elimination and widespread distribution of agents into non-targeted organs and tissues, a higher dosage is required which is not economical and often result in adverse side effects due to non-specific toxicity (Nie et al., 2007). The use of nanomaterials to delivery anti-cancer drugs to tumour sites is a promising platform, and can be achieved by either passive or active targeting.

1.2.3.2 Passive Targeting

Passive targeting refers to the accumulation of a drug or drug delivery system at a desired site due to physio-chemical or pharmacological factors; AuNPs take advantage of their inherent size in the nature of the tumour microenvironment. Tumour vasculature differs dramatically compared to normal tissue. Blood vessel walls in tumours are generally more porous and leaky owing to the formation of new blood vessel, a process also known angiogenesis (Carmeliet and Jain, 2000, Nishida et al., 2006). Angiogenic blood vessels in tumour tissues have gaps as large as 600-800 nm between adjacent endothelial cells. Furthermore, tumours have a dysfunctional lymphatic drainage resulting in AuNPs being retained longer at the tumour site. Together these effects induce a phenomenon called enhanced permeability and retention (EPR) effects, enabling nanoparticles to extravagate through these large gaps into extravascular spaces and accumulate inside tumour tissues (Misra et al., 2010, Ghosh et al., 2008, Nie et al., 2007).

A significant increase in tumour drug concentration can be achieved when the drug is delivered by a nanoparticle in comparison to the free drug form. However, passive targeting does suffer from several limitations. It is not always feasible to target all cells within a tumour as some drugs cannot diffuse efficiently. In addition, the random nature of passive targeting makes it difficult to control the process and can lead to multiple-drug resistance (Peer et al., 2007). Furthermore, the permeability of vessels may not be identical throughout the tumour and certain tumours do not exhibit the EPR effect. Nanocarriers may potentially suffer from non-specific uptake and degradation in macrophages and therefore targeting is critical for achieving maximum drug efficacy with minimal size effects (Ghosh et al., 2008).

1.2.3.3 Active Targeting

The development of nanocarriers with the capability of binding to specific cells/tumour sites of interest is an attractive proposition, and can be achieved by attaching targeting moieties onto the nanoparticle scaffold to enable their selective uptake by specific interactions such as ligand-receptor, antibody-antigen and lectin-carbohydrate (Allen, 2002). Lectin-carbohydrate binding is very specific and delivery based on this system has been developed to target organs as a whole (Yamazaki et al., 2000, Kannagi et al., 2004). The fact that receptors or antigens are usually over-expressed in human cancer cells has been exploited as receptor-ligand binding facilitates internalization via receptor-mediated endocytosis. The strength of NP interactions with antigens or membrane receptors can be controlled by the property of the ligand (e.g. affinity) and by changing the ligand density (e.g. avidity) attached to the surface of the particle (Chou et al., 2011).

Surface functionalization of nanoparticles plays a major role in active targeting enabling scientists to engineer specific AuNPs with active targeting capabilities via clever surface modifications. These targeting groups can be broadly classified as proteins (antibodies and their fragments), nucleic acids or other receptor ligands (small molecules, peptides, vitamins and carbohydrates) (Chou et al., 2011, Scheinberg et al., 2010).

Folate receptors are overexpressed on the surfaces of many tumour cells and have been explored as a target. Dixit and co-workers (Dixit et al., 2006) have shown that 10 nm AuNPs conjugated to folic acid were selectively taken-up by folate receptor positive KB cells, with minimal uptake in cells that do not overexpress the folate receptor. Chen and colleagues (Chen et al., 2007) have demonstrated that 13 AuNPs conjugated to methotrexate, a dihydrofolate reductase inhibitor that destroys folate metabolism, are rapidly taken-up and are more cytotoxic compared to methotrexate alone.

1.3 Mitochondria

Mitochondria are essential to cell function because they control critical cellular parameters including energy production, modulation of redox status, generation of reactive oxygen species and maintenance of calcium homeostasis. Furthermore, they are involved in a number of metabolic and biosynthetic pathways and the regulation of apoptosis or programmed cell death. Mitochondrial dysfunction is associated with a number of human disorders such as diabetes, neurodegenerative diseases (e.g. Parkinsons and Alzheimers), ischemia-reperfusion injury and cancer (Gupta et al., 2009, Wallace, 2005, Weissig et al., 2004). Mitochondrial research has become one of the fastest growing disciplines in

biomedicine and current research activities include targeting the mitochondrial apoptotic mechanism (D'Souza et al., 2011, Fulda, 2010, Wallace, 2012, Wang, 2001), protecting mitochondria from oxidative stress (Kelso et al., 2002, James et al., 2004, Coulter et al., 2000, Sheu et sl., 2006) and diseases caused by mutated mitochondrial DNA (mt DNA) (Pulkes and Hanna, 2001, Tuppen et al., 2010, D'Souza and Weissig, 2004).

1.3.1 Role of Mitochondria in Cell Death

At the center of the intrinsic apoptotic pathway is the mitochondrion. It is the cell's reservoir of pro-apoptotic factors which reside in the mitochondrial intermembrane space (IMS). Following an apoptotic stimulus, pores are formed in the outer mitochondrial membrane permeabilisation (MOMP) and this is a crucial event, referred to as the "point of no return" of cell death. Subsequently IMS proteins are released into the cytosol; while some of these proteins are considered to be "innocent bystanders" and do not cause any cellular response, cytochrome c and Smac/DIABLO (Second mitochondria-derived activator of caspase/ direct inhibitor of apoptosis-binding protein with low pl) promotes cell death via the activation of caspases (Parssons and Green, 2010, Gupta et al., 2009).

Caspases are very important in the apoptotic response and to date eleven human caspase proteins have been identified. Of these, seven are thought to have functions in apoptosis, including the initiator caspases (caspases-3, -6 and -7). In normal cells, caspases exist as zymogens (catalytically inactive) and must undergo proteolytic activity to become active (Riedl and Shi, 2004).

1.3.2 Targeting Mitochondria for Cancer Therapy

Mitochondria have emerged as an attractive novel pharmacological target for cancer therapeutics (Gupta et al., 2009, Frantz and Wipf, 2010, Modica-Napolitano and Singh, 2002, Costantini et al., 2000, Weissig, 2003). Interestingly cancer cell mitochondria are structurally and functionally different in comparison to their normal counterparts (Gogvadze et al., 2008, Modica-Napolitano and Singh, 2004). These notable differences have been exploited as potential targets for anti-cancer therapy by using agents that either interact directly at the site of mitochondria or target metabolic alterations caused by mitochondrial dysfunction.

1.3.3 Strategies for Mitochondrial Pharmacology

With mitochondria emerging as a novel pharmacological targets, there has been a growing interest in delivering biologically active molecules including proteins, enzymes and drugs to the site of mitochondria for therapeutic effects (Smith et al., 2012, Malhi and Murthy, 2012). The main strategy employed in mitochondrial pharmacology for site specific delivery involves the conjugation of small molecules to a lipophilic cation, and this has been reviewed extensively elsewhere (Murphy, 1997, Murphy and Smith, 2007, Murphy and Smith, 2000, Ross et al., 2005). Other strategies include mitochondria-targeted peptides (Yousif et al., 2009, Yousif et al., 2009, Jacotot et al., 2006, Cai et al., 2010) and making use of the high affinity mitochondria-specfic binding sites(Smith et al., 2004).

1.4 Lipophilic cations

Lipophilic cations are known to be lipid-soluble, despite carrying a positive charge. These cations pass through phospholipid bilayers of cells and are accumulated in the mitochondria. The activation energy for these cations is much lower compared to hydrophilic cations, mostly due to the fact that energy demand for the latter compounds is much higher when they pass through the biological membrane. The lipophilic cations adsorb on the membrane surface and travel via the hydrophobic core of the membrane to the other side before desorbing from the membrane. This passage helps the lipophilic cations to pass through the phospholipid bilayers, and hence these cations travel through the mitochondrial inner membrane (Le Gall et al., 2010).

The mitochondrial transmembrane proton-motive force which is powered by oxidative phosphorylation consists of a chemical component and an electrical component. The electrical component or mitochondrial membrane potential is higher in carcinoma cells than in normal epithelial cells. Lipophilic cations having a delocalized positive charge (delocalized lipophilic cations) penetrate the hydrophobic barriers of the plasma and mitochondrial membrane and accumulate in mitochondria in response to the negative charge inside transmembrane potentials.

$$E_k = \quad 2.303 \frac{RT}{zF} log10 \frac{[ion\ outside\ cell]}{[ion\ inside\ cell]}$$

Equation 1: Nernst potential equation. (E_k= Equilibrium constant)

The Nernst equation (Equation 1) is used to calculate the potential of an ion of charge *z* across a membrane. According to the Nernst equation, a difference of 60 mV membrane potential between carcinoma and control epithelial cells is enough to produce a 10-fold greater accumulation of the compound in carcinoma mitochondria. The higher plasma membrane potential observed in some carcinoma cells vs. control epithelial cells, thus further contributes to increased DLC accumulation in carcinoma mitochondria (Josephine S 2001).

Lipophilic cations are widely used as molecular probes for studying mitochondrial function and have demonstrated applications in antineoplastic, antioxidant, antimicrobial transport into mitochondria (Le Gall et al., 2010). The increased mitochondrial membrane potential in carcinoma cells which leads to selective accumulation of DLCs and consequent mitochondrial toxicity suggests a rationale for the selective chemotherapy of cancer cells. Rhodamine123 was the first DLC to demonstrate anticancer activity (Josephine et al, 2001). In a study, 1-Ethyl-2-[[3-ethyl-5-(3-methyl-2(3H)-benzothiazolylidene)-4-oxo-2 thiazolidinylidene]methyl]-pyridinium chloride, (MKT-077) (Fig 1.8) was shown to significantly inhibit the growth of a variety of keratin-positive human cancer cell lines, as measured by clonogenic assays and growth inhibition of cultured cells (Josephine et al, 2001). The same compound demonstrated significant in-vivo anti-tumor activity in nude mice implanted with human melanoma LOX, human renal carcinoma A498, and human prostate remaining viable nandrolone deconate (DECA) treated versus untreated control carcinoma DU-145, all of which are highly refractory to a variety of traditional therapies. MKT-077 was the first DLC to be approved by the US Food and Drug Administration (FDA) for clinical trials for the treatment of carcinoma (Le Gall et al., 2010). However, trials were

discontinued in phase II, since efficacy in tumour cell killing was not demonstrated at the particular approved dosage and drug regimen (Josephine et al, 2001).

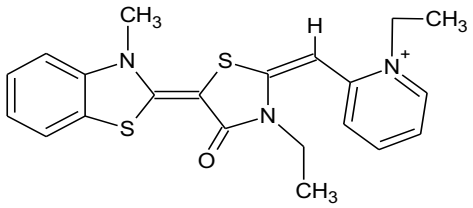

Figure 1.8: 1-Ethyl-2-[[3-ethyl-5-(3-methyl-2(3H)-benzothiazolylidene)-4-oxo-2-thiazolidinylidene] methyl]-pyridinium chloride **(MKT-077).**

1.4.1 Lipophilic Phosphonium Cations

Organophosphonium cations are species with the formula R_4P^+, i.e they contain four organic groups bound to a central phosphorus atom. Phosphonium compounds have been extensively studied because of their use in the Wittig reaction (Joseph et al., 2009). However, organophosphonium compounds are also of interest because of their applications in biomedical science; the compounds act as delocalised lipophilic cations (DLC) and are readily taken-up by cells. The ability of the tetraphenylphosphonium ion (Ph_4P^+) to act as a DLC was discovered by Liberman in 1969, who was investigating the membrane potential of cells.

In 1969, studies by Liberman had significant influence regarding understanding the passage of compounds through mitochondrial membranes aided by membrane potentials (Liberman et al., 1969). Delocalized lipophilic compounds (DLCs) such as tetraphenylphosphonium (TPP) chloride and triphenylmethylphosphonium (TPMP) iodide are known to accumulate selectively in cancer cells (Joseph et al., 2009). The salts display remarkable tumor selectivity

as they are able to easily traverse the lipophilic mitochondrial membrane of a tumor cell as its membrane potential is ca. 60 mV higher than that of a healthy cell (Ross et al., 2005)

As noted above, mitochondrial dysfunction is associated with a number of disorders and there is increasing awareness of the importance of targeting drugs to this organelle. (Malhi and Murthy 2012). Lipophilic cations, especially phosphonium species, have been found to be extremely valuable for mitochondria-targeted therapeutics and diagnostics. Recent work has demonstrated the potential of combining phosphonium moieties with nanotechnological approaches to traffic pharmaceutical and diagnostic moieties into cells (Malhi and Murthy 2012).

1.4.2 Mitochondrial Accumulation of Lipophilic Phosphonium Cations

Lipophilic phosphonium cations such as tetraphenylphosphonium and methyltriphenylphosphonium are attracted to the negative energy potentials of cellular and sub-cellular membranes. Despite their net positive charge, LPCs have the unusual properties of being relatively lipid-soluble, enabling their passage through the lipid bilayers and accumulate specifically inside the mitochondrial matrix, (Weissig, 2005, Yousif et al., 2009, Murphy, 1997, Porteous et al., 2010, Ross et al., 2008).

The uptake of LPCs into mitochondria is primarily governed by the large membrane potential across the mitochondrial inner membrane of up to 150-160 mV (negative inside) (Fig 1.9). The plasma membrane potential (usually 30-60 mV, negative inside) also drives the uptake of cations into the cell where they further accumulate inside the mitochondria, with

the majority of the intracellular cation (90 - 95%) localizing in the mitochondria (Burns and Murphy, 1997).

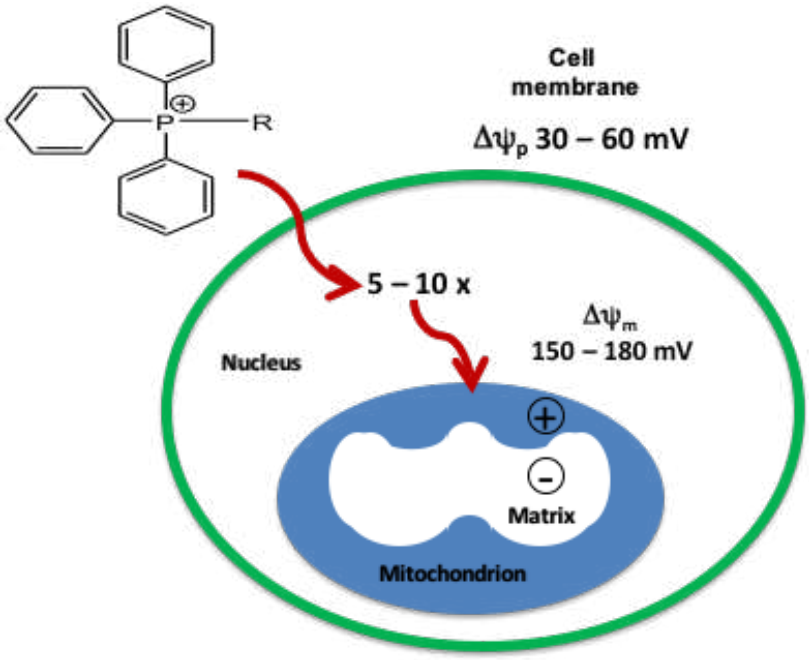

Figure 1.9: The proposed uptake of the phosphonium cation by mitochondria through the mitochondrial membrane potential.

Given the observation that lipophilic cations are taken-up by the mitochondria in cells it was natural to consider linking molecules of interest to a lipophilic cation for targeted delivery to mitochondria in *vivo* (Murphy, 1997, Smith et al., 2003, Weissig, 2005 Le Gall. et al 2010). The synthesis of alkyltriphenylyphosphonium cations from the reaction of triphenylphosphine with an appropriate precursor (Smith et al., 2004, Kelso et al., 2001, Smith et al., 1999) or by conjugation of a pre-formed alkyltriphenylphosphonium cation to a molecule is relatively simple (Murphy et al., 2003, James et al., 2003). This property has been exploited to direct a broad range of potential probes or therapeutic agents to the site of mitochondria and some of these are outlined below.

1.4.2.1 Phosphonium-conjugated Antioxidants

Conjugating lipophilic cations such as triphenylphosphonium to an antioxidant is an approach in designing drugs for selectively targeting mitochondria. A number of antioxidant compounds could be targeted to the mitochondria conjugating the triphenyl phosphonium moiety, such as ubiquinone, tocopherol, lipoic acid, spin traps and the peroxidise mimetic Ebselen. The most widely used and best known from this class is ubiquinol known as MitoQ (Fig 1.10). These compounds are taken up rapidly by mitochondria driven by the membrane potential, importantly all the accumulated vitamin E compound MitoQ is adsorbed in the matrix surface of the inner membrane. MitoQ satisfies the entire requirement within isolated mitochondria for antioxidant targeting mitochondria (Smith et al., 2004).

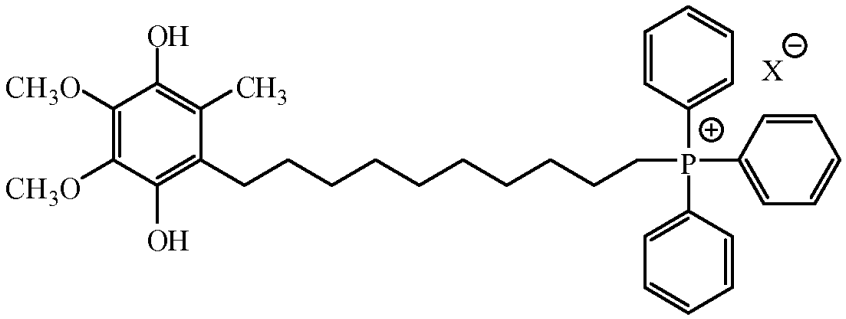

Figure 1.10: Molecular structure of the triphenyl phosphonium-vitamin E compound (MitoQ).

The most essential feature that mitochondria targeting antioxidants, such as MitoQ, is not to get extensively accumulated in the mitochondria and help in keeping the integrity of the membrane intact; thus it helps in preventing disruption of the respiration cycle and ATP synthesis. The antioxidants attached to TPP pass from cell to isolated mitochondria and get accumulated at 5-10 fold by the plasma membrane potential. Experiments show that binding this antioxidant with TPP cations results in total mitochondrial uptake within the

cells, which clearly indicates that almost all accumulated lipophilic cations are present in mitochondria (Murphy et al, 2003). More recent work has focused on targeting antioxidants to mitochondria *in vivo*, based on the observation that TPP cations easily pass through phospholipid bilayers from the gut to the bloodstream and from bloodstream to various tissues in body. Experiments clearly showed that once these compounds enter the bloodstream alkylTPP compounds distribute into organs. These alkyltriphenylphosphonium compounds can be administered orally with good bioavailability and they are rapidly cleared from the plasma accumulating in mitochondria within tissues. (Murphy, 2008).

1.4.2.2 Mitochondria Targeted Photodynamic therapy

Photodynamic therapy (PDT) is a novel treatment modality for several types of cancer; it involves photoreactions mediated by three key elements: photo sensitizers, light and oxygen to generate Reactive-Oxygen-Species (ROS) such as singlet oxygen, superoxide anion radical and hydroxyl radicals. PDT benefits from the cytotoxic effects generated from the ROS to induce apoptosis or necrosis in cytotoxic effects generated from the ROS to induce apoptosis or necrosis in cancerous cells (Lei et al., 2010). The photo sensitizer displayed a time-dependent cytotoxicity effect in ovarian carcinoma cells (SKOV-3), the conjugated (Mce6) exhibiting greater cytotoxicity (Cuchelkar et al., 2008).

Meso-tetraphenylporphyrin derivatives incorporating a TPP ion terminated alkoxy group at either para-or meta-position of one meso-phenyl group have been shown to be photoxic in human breast cancer (MCF-7) (Lei et al., 2010). More recently, a core-modified porphyrin-mono-triphenylphosphonium cation (CMP-tPP) has shown improvement in cellular uptake

and photodynamic activity compared to the mono-hydroxy core-modified porphyrin alone (Rajaputra et al., 2013).

1.4.2.3 Mitochondria Targeted Radiotracers for Tumour imaging

Conventional cationic radiotracers such as ^{99m}Tc-Tetrofosmin and ^{99m}Tc-Sestamibi have been used for the diagnosis of cancer by Single-photon emission computed tomography (SPECT) and the monitoring of the multidrug resistance transport functions in tumors of different origin. However, they suffer from low tumor selectivity and insufficient tumor localization which limits their diagnostic and prognostic values in a clinical setting (Zhou and Liu, 2011).

Nearly 30 years ago, radiolabeled quaternary phosphonium cations were first investigated as perfusion radiotracers for myocardial perfusion imaging (Srivastava et al., 1985), and since then several groups have proposed the use of radiolabeled triphenylphosphonium cations as PET radiotracers which include ^{18}F labelled probes and ^{64}Cu labelled phosphonium cations including ^{64}Cu-labelled 2-(diphenylphosphoryl)-ethyldiphenylphosphonium cations (Yang et al., 2008, Liu et al., 2009, Yang et al., 2007). Copper-64 labelled phosphonium cations have been developed as a new class of PET radiotracers with high tumour selectivity and uptake (Wang et al., 2007, Zhou and Liu, 2011).

1.5 Phosphonium-mediated Pharmaceutical Nanotechnology

Pharmaceutical nanotechnology is a term that has been coined to describe the biomedical and pharmaceutical applications of nanomaterials. As described above (section 1.4.2.1), organophosphonium compounds are readily taken-up by cells and accumulated in mitochondria and recent years have seen phosphonium moieties being combined with nanomaterials, including liposomes, macromolecules and nanoparticles.

1.5.1 Liposomes

Liposomes are hollow vesicle-like species made from lipids that can be used for drug delivery. Weislg and co-workers prepared liposomes from DOPC (1,2-dioleoyl-*sn*-glycero-3-phosphocholine) and cholesterol and stearyltriphenylphosphonium bromide (Boddapati et al., 2010); the triphenylphosphonium salt intercalates the lipid bilayer (Fig 1.11). They demonstrated that liposome surface-modified phosphonium cation can be used to transport drugs to subcellular organelles without the need for chemical modification of the drug molecules.

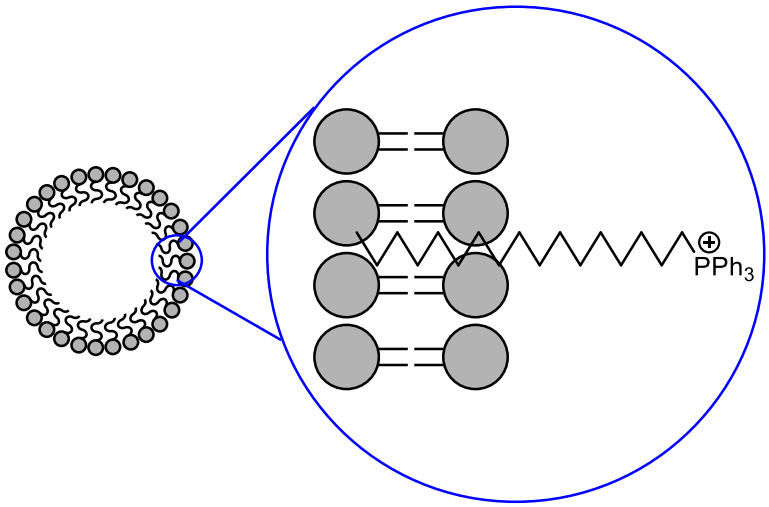

Figure 1.11 Liposomal drug delivery system surface modified with triphenylphosphonium moieties.

Liposomes modified with stearyltriphenylphosphoniumcations have been loaded with the anticancer drug Paclitaxel (Solomon et al., 2013). They showed improved mitochondrial colocalization and cytotoxicity in a paclitaxel-resistant cell line. The improvement in cytotoxicity was attributed to the increased accumulation of paclitaxel in mitochondria and to the specific toxicity of stearyltriphenylphosphonium compounds towards the resistant cell line. Mechanistic studies revealed that the cytotoxicity of the stearyl

triphenylphosphonium ion was associated with a decrease in mitochondrial membrane potential and other hallmarks related to caspase-independent cell death.

1.5.2 Macromolecules

Phosphonium compounds been incorporated into polymeric species, including polymers (Monge et al., 2011), hydrogels and dendrimers, in order to improve their biocompatibility. Tetrakis(hydroxymethyl)phosphonium chloride (THPC) has been used as a gelling gent for the production of protein hydrogels, which proved useful materials for cell encapsulation. Dendrimers are repetitively hyper-branched macromolecules that have found widespread interest for pharmaceutical drug delivery. Torchilin and coworkers conjugated triphenylphosphonium groups to the surface of generations 5 of poly(amidoamine) (PAMAM) dendrimers(G(5)-D) (Fig 1.12). These dendrimers were fluorescently labelled with fluorescein isothiocyanate (FITC) to quantify cell association by flow cytometry and for visualization under confocal laser scanning microscopy to assess the mitochondrial targeting *in vitro*. The triphenylphosphonium-conjugated dendrimer (G(5)-D-Ac-TPP) was efficiently taken up by the cells and demonstrated good mitochondrial targeting. *In vitro* cytotoxicity experiments carried out on normal mouse fibroblast cells (NIH-3T3) had greater cell viability in the presence of the G(5)-D-Ac-TPP compared to the parent unmodified G(5)-D dendrimers.

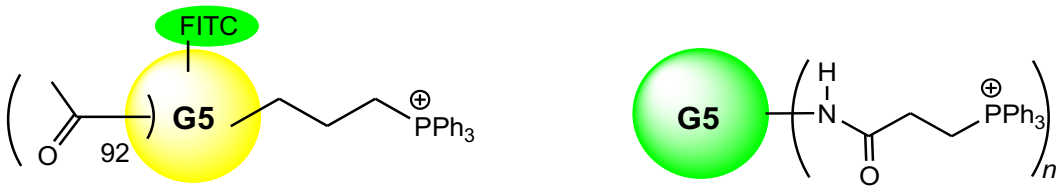

Figure. 1.12 Triphenylphosphonium-functionalized Dendrimers

Wang *et al*., have also prepared generation 5(G5) PAMAM dendrimers functionalized with triphenylphosphonium groups (Fig 1.12), albeit using a different methodology to Torchilin, which utilizes alkyl amide triphenylphosphonium derivatives, and investigated their ability to act as gene vectors. Their triphenylphosphonium-conjugated dendrimers effectively targeted mitochondria and showed efficient transfection efficacy on HeLa (a human cervical carcinoma cell line), and COS-7 (an African green monkey kidney fibroblast-like cell line), with low cytotoxicity on the transfected cells.

Biodegradable macromolecular nanoparticles composed of block co-polymers of poly(D,L-lactic-co-glycolic acid)-block (PLGA) and poly(ethyleneglycol) (PEG) have been prepared and conjugated with triphenylphosphonium groups (Figure 1.13) (Marrache et al., 2012). Different size particles were synthesised, with different levels of surface functionalization of phosphonium groups. It was found that the nanoparticles were able to cross the mitochondrial membrane and it was postulated that the materials could be used as nanocarriers for various mitochondrial dysfunction-related disorders, including Alzheimer's disease, obesity, and cancer.

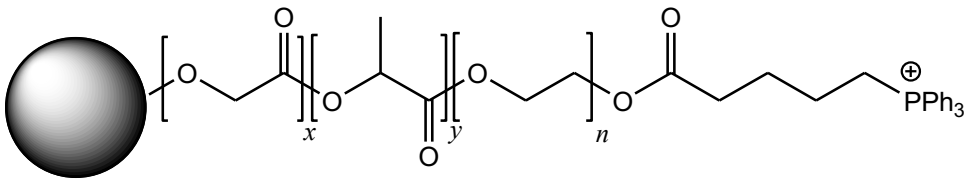

Figure. 1.13 poly(D,L-lactic-co-glycolic acid)-block (PLGA-b)-poly(ethyleneglycol) (PEG)-triphenylphosphonium (TPP) polymer (PLGA-b-PEG-TPP)

Teng and coworkers prepared Poly-L-lysine (PLL) nanoparticles by a one-step precipitation-encapsulation method assisted by positively charged poly-L-lysine (PLL). The effect of the

molecular weight of PLL on the formation of the particles was studied in terms of morphology, size and zeta potential, and medium-sized PLL proved to be the optimum one (Wang et al., 2013). Triphenylphosphonium groups were conjugated to the PLL-NPs (Fig 1.14), and exhibited a low cytotoxic effect and efficient cellular uptake. The authors suggest that the materials are promising mitochondria-targeted nanocarriers for imaging or anti-cancer therapies. The same group then developed their methodology to encapsulate the dioxygen probe Pt(II)-*meso*-tetra(pentafluorophenyl)porphine embedded in a hydrophobic polystyrene core, with triphenylphosphonium-conjugated PLL (Wang et al., 2014). They then used these core-shell nanoparticles to determine the oxygen consumption rates of HepG2 and LO2 cells under respiratory conditions.

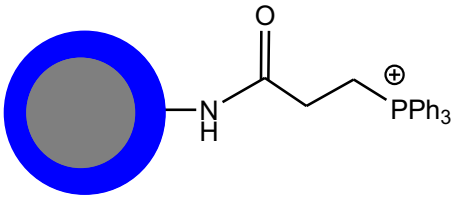

Figure. 1.14: Triphenylphosphonium-conjugated Poly-L-Lysine nanoparticles

1.5.3 Metal nanoparticles

As noted in section 1.1.1, gold nanoparticles (AuNPs) have attracted considerable interest for their potential biomedical applications. The first published report of the preparation of AuNPs functionalized with phosphonium compounds was by Bricklebank and coworkers in 2008. They devised a synthetic methodology, illustrated in figure 1.15, that was used to prepare a family of phosphonioalkylthiosulfate zwitterions and ϖ-thioacetylalkylphosphonium salts (Chen et al., 2017), that act as '*masked thiolate*' ligands

in which the thiolate is 'protected' as a thiosulfate or thioacetate group, respectively. These compounds have greater stability and are easier to handle than the corresponding thiol ligands. Cytotoxicity studies show that these compounds have low cytotoxicity towards cells (Chen PhD Thesis, 2014).

The phosphonioalkylthiosulfate zwitterions and ϖ-thioacetylalkylphosphonium salts can be used to prepare AuNPs protected by triorganophosphonioalkylthiosulfate groups using a modification of the well-known Brust-Schiffrin method (Brust et al., 1995). Under reductive conditions cleavage of the sulfur–sulfur or sulfur–carbon bonds in the thiosulfate and thioacetate species, respectively, generate thiolate anions *in situ* which bond with the surface of the growing nanoparticles leading to water-soluble, cationic, phosphonium-functionalized AuNPs. The nanoparticles prepared using this method are small, *ca.* 3.5 - 4.0 nm diameter.

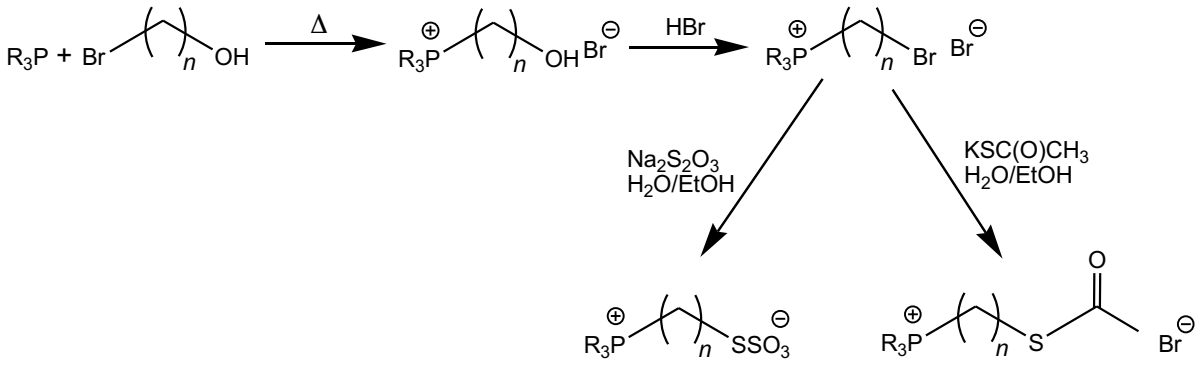

Figure 1.15: Scheme showing synthetic pathway for phosphonium zwitterions and salts

Subsequent research completed by Yu-Su Chen at Sheffield Hallam University showed that the triphenylphosphonium-functionalized gold nanoparticles are taken-up by PC3 prostate cancer cells and are located in the mitochondria (Chen PhD Thesis, 2014). Yang *et.al.*, have

taken the methodology devised by the Bricklebank group and used it to functionalize much larger gold nanoparticles (*ca.* 50 nm diameter) (Yang et al., 2015). The phosphonium-functionalized AuNPs were shown to accumulate in the mitochondria of MCF10A human breast cancer and MBD-MB-231 human mammary epithelial cell lines and enhance the formation of reactive oxygen species in 5-aminolevulinic-acid-assisted photodynamic therapy. This resulted in a higher rate of destruction of the breast cancer cells and demonstrated the value of phosphonium-functionalized AuNPs in cancer therapeutics.

Mesoporous materials, often containing silica or alumina, have pores in the size range 2 - 50 nm. They are of interest through their potential applications in drug delivery and as sensors. Mesoporous silica nanoparticles (MCM-41), loaded with the antineoplastic drug topotecan, have been conjugated with triphenylphosphonium groups and the antibiotic peptide $(KLAKLAK)_2$ (Fig 1.16) (Luo et al., 2014). It was found that the cationic charge promoted cellular take-up *via* endocytosis and that the pharmacological agents are released from the nanoparticle and induce damage to the tumour mitochondria. Triphenylphosphonium derivatives of magnetic mesoporous silica nanoparticles (Fe_3O_4@$mSiO_2$) conjugated with fluorescent carbon quantum dots have been reported (Zhang et al., 2015). The compounds were found to localize in the mitochondria and showed very low cytotoxicity in a range of cell lines.

Figure 1.16 Structure of Triphneylphosphonium-functionalized mesoporous silica nanoparticles (MCM-41) (Luo et al., 2014).

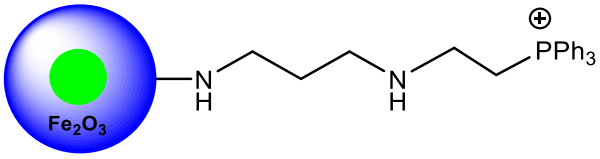

Figure 1.17 Structure of Triphneylphosphonium-functionalized core-shed nanoparticles with a CdSe or ZnS core and a biocompatible γ-Fe_2O_3 shell (Chakraborthy et al., 2015).

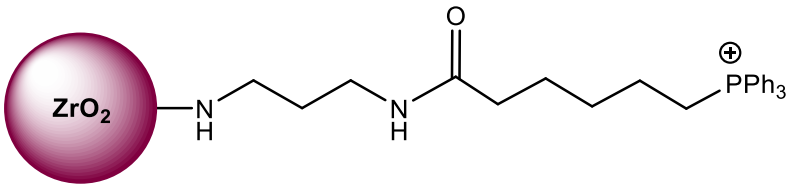

Figure 1.18 Structure of Water soluble triphenylphosphonium-functionalized Zro_2 nanoparticles (Tahir et al., 2015).

Core-shell nanoparticles comprising a CdSe or ZnS core and a γ-Fe_2O_3 (Fig 1.17) shell with diameters in the range 30 - 40 nm have been prepared and decorated with triphenylphosphonium groups (Chakraborthy et al., 2015). The materials are predicted to act as subcellular nanoprobes for imaging applications. Zirconium dioxide (Fig 1.18) 5 nm particles bearing phosphonium groups have been prepared (Tahir et al., 2015). The compounds are dispersible in water and are photostable making them potentially valuable photoluminescent materials. Molybdenum trioxide nanoparticles functionalized with triphenylphosphonium groups have been investigated as a potential therapy for sulfite

oxidase deficiency (Ragg et al., 2014). The functionalized MoO_3 nanoparticles were shown to cross the cellular membrane and accumulate at the mitochondria. They are highly soluble in water and have a low toxicity profile while increasing the SuOx activity in chemically induced SuOx knockdown cells.

1.6 Arsonium Cations

Arsenic has attracted the attention of scientists for centuries and its compounds have a variety of applications ranging from electronic and semiconductor materials (Mudhoo et al., 2011) to organic reagents, arsonium ylides finding utility in the Wittig reaction (He et al., 2005). Historically, arsenic compounds have been widely investigated for their medicinal properties although interest declined as greater understanding of their toxicity became apparent (Chen et al., 2011 and Swindell et al., 2013). Generally inorganic As(III) and As(V) species are highly toxic, whereas organic arsenic compounds are significantly less toxic (Mudhoo et al., 2011 and Jomova et al., 2011). More recently there has been a resurgence of interest in the medicinal properties of arsenic compounds, including the use of arsenic trioxide and organic arsenic derivatives as treatments for leukemia and other cancers (Mudhoo et al., 2011, Chen et al., 2011 and Swindell et al., 2013), the characterization of an arsenic trioxide analogue of cisplatin (Miodragovic et al., 2013), and the observation that ^{72}As and ^{74}As radiopharmaceuticals could be useful in positron emission tomography (PET) (Mudhoo et al., 2011).

The chemistry of arsenic is broadly similar to that of phosphorus, and organic phosphonium salts are known to act as lipophilic cations that are preferentially accumulated in the

mitochondria of cells (Hoyle et al., 2011). Similarly, arsonium cations are also lipophilic and tetraphenylarsonium cations have been used to investigate the membrane potential of cells.

In devising strategies to target mitochondria, Cle´ment and Floch et al. substituted ammonium cations of phosphonolipids with phosphonium or arsonium groups (**1**) (Picquet et al., 2005, Le Gall et al., 2010, Berchel et al., 2012). Similar work to this was done previously by Stekar et al., who replaced the ammonium group of edelfosine and miltefosine with phosphonium and arsonium groups. The phosphonium and arsonium derivatives were found to have significantly lower toxicity while maintaining the antitumor activity. The reduced toxicity of the edelfosine and miltefosine analogues was attributed to the increased atomic radii of As and P compared to N, which resulted in the formation of larger cationic complexes with reduced charge densities. Gene transfer studies conducted by Cle´ment and Floch et al. have shown that phosphonolipids with arsonium and phosphonium cations exhibit significantly lower cytotoxicity than the ammonium analogues. In addition, in vivo gene transfer studies using lipophosphoramidates showed up to a 3600-fold increase in gene transfer efficiency for the phosphonium and arsonium derivatives (Mintzer MA, Simanek EE, 2009). Other examples of the mitochondria-targeting potential of triphenylarsonium ions include ^{64}Cu-labelled complexes of 1,4,7,10-tetraazacyclododecane-4,7,10-triacetic acid-conjugated triphenylarsonium cations which have been found to act as tumour-selective PET imaging agents (Wang et al., 2007).

1.7 Aims of this Thesis.

1. To investigate the synthesis and characterization of the triphenylarsonio propylthiosulfate zwitterion and the triphenylarsoniopropyl thioacetate salt, from triphenylarsine and dibromopropane.

2. Investigate the attachment of the triphenylarsoniopropylthiolate anion derived from the zwitterion or thioacetate salt onto the surface of gold nanoparticles.

3. Investigate the mechanism of uptake of gold nanoparticles by cells and determine whether it is through endocytosis or passive penetration. Toxicity studies of gold nanoparticles are of importance, consequently the cell biology of the triphenylarsonio propylthiosulfate zwitterion, triphenylarsoniopropyl thioacetate salt and triphenylarsonium-capped gold nanoparticles will be studied on prostate cancer (PC3) cells by using MTT and CellTiter-Glo assays.

4. Previous research in the Bricklebank group on the biological chemistry of phosphonium compounds has focused on triphenylphosphonium derivatives. Studies have revealed that these compounds can have limited solubility in cell culture. Therefore it was decided to investigate the synthesis of phosphonium thiosulfate derivatives of tris(2,4,6-trimethoxyphenyl)phosphine and related compounds to see if the methoxy groups improved the solubility of the compounds in water.

1.8 References

AHMAD, M. Z., AKHTER, S., RAHMAN, Z., AKHTER, S., ANWAR, M., MALLIK, N. & AHMAD, F. J. 2013. Nanometric gold in cancer nanotechnology: current status and future prospect. *Journal of Pharmacy and Pharmacology*, 65, 634-651.

AKHTER, S., AHMAD, I., AHMAD, M. Z., RAMAZANI, F., SINGH, A., RAHMAN, Z., KOK, R. J. 2013. Nanomedicines as cancer therapeutics: Current status. *Current Cancer Drug Targets,* 13, 362-378.

AKHTER, S., AHMAD, M. Z., AHMAD, F. J., STROM, G. & KOK, R. J. 2012. Gold nanoparticles in theranostic oncology: current state-of-the-art. *Experts Opinion on Drug Delivery*, 9, 1225-1243.

ALLEN, T. M. 2002. Ligand-targeted therapeutics in anticancer therapy. *Nature Reviews Cancer*, 2, 750-763.

ARBAB, A. S., LIU, W. & FRANK, J. A. 2006. Cellular magnetic resonance imaging: Current status and future prospects. *Expert Review of Medical devices*, 3, 427-439.

ARORA, A. & SCHOLAR, E. M. 2005. Role of tyrosine kinase inhibitors in cancer therapy. *Journal of Pharmacology and Experimental Therapeutics*, 315, 971-979.

ARRUEBO, M., VILABOA, N., S EZ-GUTIERREZ, B., LAMBEA, J., TRES, A., VALLADARES, M. & GONZ LEZ-FERN NDEZ, A. 2011. Assessment of the evolution of cancer treatment therapies. *Cancers*, 3, 3279-3330.

BASKAR, R., LEE, K. A., YEO, R. & YEOH, K.-W. 2012. Cancer and Radiation Therapy: Current Advances and Future Directions. *International Journal of Medical Sciences*, 9, 193-199.

BAWARSKI, W. E., CHIDLOWSKY, E., BHARALI, D. J. & MOUSA, S. A. 2008. Emerging nanopharmaceuticals. *Nanomedicine: Nanotechnology, Biology, and Medicine*, 4, 273-282.

BENTOLILA, L. A., EBENSTEIN, Y. & WEISS, S. 2009. Quantum dots for in vivo small-animal imaging. *Journal of Nuclear Medicine*, 50, 493-496.

BERCHEL, M., LE GALL, T., COUTHON-GOURVÈS, H., HAELTERS, J., MONTIER, T., MIDOUX, P., JAFFRÈS, P. 2012. Lipophosphonate/lipophosphoramidates: A family of synthetic vectors efficient for gene delivery. *Biochimie,* 1, 33-41.

BODDAPATI, S. V., D'SOUZA, G. G. & WEISSIG, V. 2010. Liposomes for drug delivery to mitochondria. *Methods in Molecular Biology (Clifton, N. J.)*, 605, 295-303.

BRENNER, D. J., DOLL, R., GOODHEAD, D. T., HALL, E. J., LAND, C. E., LITTLE, J. B., LUBIN, J. H., PRESTON, D. L., PRESTON, R. J., PISKIN, J. S., RON, E., SACHS, R. K., SAMET, J. M., SETLOW, R. B. & ZAIDER, M. 2003. Cancer risks attributable to low doses of ionizing radiation: Assessing what we really know. *Proceedings of the National Academy of Sciences*, 100, 13761-13766.

BRUST, M., FINK, J., BETHELL, D., SCHIFFRIN, D. J., & KIELY, C. 1995. Synthesis and reactions of functionalized gold nanoparticles. *Journal of the Chemical Society, Chemical Communications,* 16, 1655-1656.

BRUST, M., WALKER, M., BETHELL, D., SCHIFFRIN, D. J. & WHYMAN, R. 1994. Synthesis of thiol-derivatised gold nanoparticles in a two-phase liquid-liquid system. *Journal of the Chemical Society, Chemical Communications*, 801-802.

BURNS, R. J. & MURPHY, M. P. 1997. Labeling of mitochondrial proteins in living cells by the thiol probe thiobutyltriphenylphosphonium bromide. *Archives of Biochemistry and Biophysics*, 339, 33-39.

BYKOV, V. J. N. & WINMAN, K. G. 2003. Novel cancer therapy by reactivation of the p53 apoptosis pathway. *Annals of Medicine*, 35, 458-465.

CAI, H., YANG, H., XIANG, B., LI, S., LIU, S., WAN, L., ZHANG, J., LI, Y., CHENG, J. & LU, X. 2010. Selective apoptotic killing of solid and hematologic tumor cells by bombesin-targeted delivery of mitochondria-disrupting peptides. *Molecular Pharmaceutics*, 7, 586-596.

CARMELIET, P. & JAIN, R. K. 2000. Angiogenesis in cancer and other diseases. *Nature*, 407, 249-257.

CHABNER, B. A. & ROBERTS, T. G. 2005. Timeline- Chemotherapy and the war on cancer. *Nature Reviews Cancer*, 5, 65-72.

CHAKRABORTY, A., & JANA, N. R. 2015. Design and synthesis of triphenylphosphonium functionalized nanoparticle probe for mitochondria targeting and imaging. *The Journal of Physical Chemistry C,* 5, 2888-2895.

CHEN, J. WANG, D., XI, J., AU, L., SIEKKINEN, A., WARSEN, A., LI, Z, Y., ZHANG, H., XIA, Y. & LI, X. 2007a. Immuno gold nanocages with tailored optical properties for targeted photothermal destruction of cancer cells. *Nano Letters*, 7, 1318-1322.

CHEN, Y, S. 2014. PhD Thesis, Sheffield Hallam University.

CHEN, Y. H., TSAI, C. Y., HUANG, P. Y., CHANG, M. Y., CHENG, P. C., CHOU, C. H., CHEN, D. H., WANG, C. R., SHIAU, A. L. & WU, C. L. 2007b. Methotrexate conjugated to gold nanoparticles inhibits tumor growth in a syngenic lung tumor model. *Molecular Pharmaceutics*, 4, 713-722.

CHEN, Y., ALLEN, D. W., TIZZARD, G. J., PITAK, M. B., COLES, S. J., CROSS, N. A., & BRICKLEBANK, N. 2017. Biological and structural studies of phosphonium 'masked thiolate' compounds. *European Journal of Medicinal Chemistry, 125*, 528-537.

CHOU, L. Y. T., MING, K. & CHAN, W. C. W. 2011. Strategies for the intracellular delivery of nanoparticles. *Chemical Society Reviews*, 40, 233-245.

COHEN, S. M. & ARNOLD, L. L. 2011. Chemical carcinogenesis. *Toxicological Sciences*, 120, S76-S92.

COSTANTINI, P., JACOTOT, E., DECAUDIN, D. & KROEMER, G. 2000. Mitochondria as a novel target of anticancer chemotherapy. *Journal of the National Cancer Institute*, 92, 1042-1053.

COULTER, C. V., KELSO, G. F., LIN, T. K., SMITH, R. A. J. & MURPHY, M. P. 2000. Mitochondrially targeted antioxidants and thiol reagents. *Free Radical Biology and Medicine*, 28, 1547-1554.

CUCHELKAR, V., KOPECKOV, P. & KOPECEK, J. 2008. Novel HPMA copolymer-bound constructs for combined tumor and mitochondrial targeting. *Molecular Pharaceutics*, 5, 776-786.

CWIKEL, J. G., GIDRON, Y. & QUASTEL, M. 2010. Low dose environmental radiation, DNA damage, and cancer: The possible contribution of psychological factors. *Psychology Health & Medicine*, 14, 1-16.

D'SOUZA, G. G. M. & WEISSIG, V. 2004. Approaches to mitochondrial gene therapy. *Current Gene Therapy*, 4, 317-328.

D'SOUZA, G. G. M., WAGLE, M. A., SAXENA, V. & SHAH, A. 2011. Approaches for targeting mitochondria in cancer therapy. *Biochimica Et Biophysica Acta-Bioenergetics*, 1807, 689-696.

D'SOUZA, V. & SUMMERS, M. F. 2005. How retroviruses select their genomes. *Nature Reviews Microbiology*, 3, 643-655.

DANIEL, M. C. & ASTRUC, D. 2004. Gold nanoparticles: Assembly, supramolecular chemistry, quantum-size-related properties, and applications toward biology, catalysis, and nanotechnology. *Chemical Reviews*, 104, 293-346.

DAVIS, M. E., CHEN, Z. & SHIN, D. M. 2008. Nanoparticle therapeutics: An emerging treatment modality for cancer. *Nature Reviews Drug Discovery*, 7, 771-782.

DEVITA, V. T., JR. & CHU, E. 2008. A History of Cancer Chemotherapy. *Cancer Research*, 68, 8643-8653.

DIXIT, V., VAN DEN BOSSCHE, J., SHERMAN, D. M., THOMPSON, D. H. & ANDRES, R. P. 2006. Synthesis and grafting of thioctic acid-PEG-folate conjugates onto Au nanoparticles for selective targeting of folate receptor-positive tumor cells. *Bioconjugate Chemistry*, 17, 603-609.

ELHISSI, A., AHMED, W., DHANAK, V. R. & SUBRAMANI, K. 2012. *Carbon nanotubes in cancer therapy and drug delivery*, 241, 20-22.

EMADI, A., JONES, R. J. & BRODSKY, R. A. 2009. Cyclophosphamide and cancer: golden anniversary. *Nature Reviews Clinical Oncology*, 6, 638-647.

FERRARI, M. 2005. Cancer nanotechnology: Opportunities and challenges. *Nature Reviews Cancer*, 5, 161-171.

FRANTZ, M. C. & WIPF, P. 2010. Mitochondria as a target in treatment. *Environmental and Molecular Mutagenesis*, 51, 462-475.

FRENS, G. 1973. Controlled Nucleation for the regulation of the particles size in monodisperse gold suspension. *NATURAL PHYSICS AND SCIENCE,* 241, 20-22.

FULDA, S. 2010. Exploiting mitochondrial apoptosis for the treatment of cancer. *Mitochondrion*, 10, 598-603.

GAO, X., CUI, Y., LEVENSON, R. M., CHUNG, L. W. K. & NIE, S. 2004. In vivo cancer targeting and imaging with semiconductor quantum dots. *Nature Biotechnology*, 22, 969-976.

GHOSH, P., HAN, G., DE, M., KIM, C. K. & ROTELLO, V. M. 2008. Gold nanoparticles in delivery applications. *Advanced Drug Delivery Reviews*, 60, 1307-1315.

GILBERT, E. S. 2009. Ionizing radiation and cancer risks: What have we learned from epidemiology? *International Journal of Radiation Biology*, 85, 467-482.

GOEL, G., MAKKAR, H. P. S., FRANCIS, G. & BECKER, K. 2007. Phorbol esters: Structure, biological activity, and toxicity in animals. *International Journal of Toxicology*, 26, 279-288.

GOGVADZE, V., ORRENIUS, S. & ZHIVOTOVSKY, B. 2008. Mitochondria in cancer cells: what is so special about them? *Trends in Cell Biology*, 18, 165-173.

GUPTA, S., KASS, G. E. N. SZEGEZDI, E. & JOSEPH, B. 2009. The mitochondrial death pathway: a promising therapeutic target in diseases. *Journal of Cellular and Molecular Medicine*, 13, 1004-1033.

HALESTRAP, A. 2005. Biochemistry: A pore way to die. *Nature*, 434, 578-579.

HAN, G., GHOSH, P. & ROTELLO, V. M. 2007. Functionalized gold nanoparticles for drug delivery. *Nanomedicine*, 2, 113-123.

HANAHAN, D. & WEINBERG, R.A. 2011. Hallmarks of Cancer: The Next Generation. *Cell*, 144, 646-674.

HE, H. S., CHUNG, C. W. Y., BUT, T. Y. S., & TOY, P. H. 2005. Arsonium ylides in organic synthesis. *Tetrahedron*, 6, 1385-1405.

HECHT, S. S. 1999. Tobacco smoke carcinogens and lung cancer. *Journal of the National Cancer Institute*, 91, 1194-1210.

HESKETH, R. 2013. *Introduction to Cancer Biology, United States of America Cambridge University Press*.

HOYE, A. T., DAVOREN, J. E., WIPF, P., FINK, M. P., & KAGAN, V. E. 2008. Targeting mitochondria. *Accounts of Chemical Research,* 1, 87-97.

ICHIHASHI, M., UEDA, M., BUDIYANTO, A., BITO, T., OKA, M., FUKUNAGA, M., TSURU, K. & HORIKAWA, T. 2003. UV-induced skin damage. *Toxicology*, 189, 21-39.

JACOTOT, E., DENIAUD, A., BORGNE-SANCHEZ, A., TOUAT, Z., BRAIND, J. P., LE BRAS, M. & BRENNER, C. 2006. Therapeutic peptides: Targeting the mitochondrion to modulate apoptosis. *Biochimica et Biophysica Acta- Bioenergettics*, 1757, 1312-1323.

JADZINSKY, P., CALERO, G., ACKERSON, C., BUSHNELL, D., KORNBERG, R., 2007. Structure of a Thiol Monolayer-Protected Gold Nanoparticle at 1.1 Å Resolution. *American Association for the Advancement of Science*, 318, 430-433.

JAIN, P. K., HUANG, X., EL-SAYED, I. H. & EL-SAYED, M. A. 2008. Noble metals on nanoscale: optional and photothermal properties and some applications in imaging, sensing, biology, and medicine. Accounts of Chemical Research, 41, 1578-1586.

JAMES, A. M., SMITH, R. A. J. & MURPHY, M. P. 2004. Antioxidant and prooxidant properties of mitochondrial Coenzyme Q. *Archives of Biochemistry and Biophysics*, 423-47-56.

JAMES, A.M., BLAIKIE, F.H., SMITH, R.A.J., LIGHTOWLERS, R.N., SMITH, P.M. & MURPHY, M.P. 2003. Specific targeting of a DNA-alkylating reagent to mitochondria. *European Journal of Biochemistry,* 270, 2827-2836.

JEMAL, A., BRAY, F., CENTER, M. M., FERLAY, J., WARD, E. & FORMAN, D. 2011. Global Cancer Statistics, *Ca-a Cancer Journal for Clinicians*, 61, 69-90.

JOMOVA, K., JENISOVA, Z., FESZTEROVA, M., BAROS, S., LISKA, J., HUDECOVA, D., VALKO, M. 2011. Arsenic: Toxicity, oxidative stress and human disease. *Journal of Applied Toxicology,* 2, 95-107.

JOSEPH A, IOPPOLO, KASSIOU, MICHAEL AND RENDINA, LOUIS M. 2009. Water-soluble phosphonium salts containing 1,12-dicarba-closo-dodecaborane(12). *Tetrahedron letters,* 47, 6457-6461.

JOSEPHINE S. AND APRILLE, JUNE R. (2001). Delocalized lipophilic cations selectively target the mitochondria of carcinoma cells. *Advanced drug delivery reviews,* 1–2, 63-70.

JU-NAM, Y., ALLEN, D. W., GARDINER, P. H. E., & BRICKLEBANK, N. 2008. ω-Thioacetylalkylphosphonium salts: Precursors for the preparation of phosphonium-functionalized gold nanoparticles. *Journal of Organometallic Chemistry, 693*, 3504-3508.

JU-NAM, Y., BRICKLEBANK, N., ALLEN, D.W., GARDINER, P.H., LIGHT, M.E. & HURSTHOUSE, M.B. 2006. Phosphonioalkylthiosulfate zwitterions--new masked thiol ligands for the formation of cationic functionalized gold nanoparticles. *Organic & biomolecular chemistry,* 4, 4345-4351.

JU-NAM, Y., CHEN, Y., OJEDA, J. J., ALLEN, D. W., CROSS, N. A., GARDINER, P. H. E., & BRICKLEBANK, N. 2012. Water-soluble gold nanoparticles stabilized with cationic phosphonium thiolate ligands. *RSC Advances*, 2, 10345-10351.

KANNAGI, R., IZAWA, M., KOIKE, T., MIYAZAKI, K. & KIMURA, N. 2004. Carbohydrate-mediated cell adhesion in cancer metastasis and angiogenesis. *Cancer Science*, 95, 377-384.

KAYE, S. B. 1998. New antimetabolites in cancer chemotherapy and their clinical impact. *British Journal of Cancer*, 78, 1-7.

KELSO, G. F., PORTEOUS, C. M., HUGHES, G., LEDGERWOOD, E. C., GANE, A. M., SMITH, R. A. J. & MURPHY, M. P. 2002. Prevention of mitochondrial oxidative damage using targeting

antioxidants. *In*: HARMAN, D. (ed.). *Increasing Healthy Life Span: Conventional Measures and Slowing the Innate Aging Process*.

KELSO, G.F., PORTEOUS, C.M., COULTER, C.V., HUGHES, G., PORTEOUS, W.K., LEDGERWOOD, E.C., SMITH, R.A. & MURPHY, M.P., 2001. Selective targeting of a redox-active ubiquinone to mitochondria within cells: antioxidant and antiapoptotic properties. *The Journal of Biological Chemistry,* 276, 4588-4596.

KHAN, MOHAMMED S., VISHAKANTE, GOWDA D. AND SIDDARAMAIAH H 2013. Gold nanoparticles: A paradigm shift in biomedical applications. *Advances in colloid and interface science,* 0, 44-58.

KNUDSON, A. G. 2001. Two genetic hits (more or less) to cancer, *Nature Reviews Cancer*, 1, 157-162.

KUMAR, D., SAINI, N., JAIN, N., SAREEN, R. & PANDIT, V. 2013b. Gold nanoparticles: an era in bionanotechnology. *Expert Opinion on Drug Delivery*, 10, 397-409.

LE GALL, T., LOIZEAU, D., PICQUET, E., CARMOY, N., YAOUANC, J., BUREL-DESCHAMPS, L., MONTIER, T. 2010. A novel cationic lipophosphoramide with diunsaturated lipid chains: Synthesis, physicochemical properties, and transfection activities. *Journal of Medicinal Chemistry, 53*(4), 1496-1508.

LEE, K., LEE, H., BAE, K. H., & PARK, T. G. 2010. Heparin immobilized gold nanoparticles for targeted detection and apoptotic death of metastatic cancer cells. *Biomaterials,* 31, 6530-6536.

LEI, W., XIE, J., J., HOU, Y., JIANG, G., ZHANG, H., WANG, P., WANG, X. & ZHANG, B. 2010. Mitochondria-targeting properties and photodynamic activities of porphyrin derivatives bearing cationic pendant. *Journal of Photochemistry and Photobiology B*: Biology, 98, 167-171.

LI, J. L., WANG, L., LIU, X. Y., ZHANG, Z. P., GUO, H. C., LIU, W. M. & TANG, S. H. 2009a. In vitro cancer cell imaging and therapy using transferrin-conjugated gold nanoparticles. *Cancer Letters*, 274, 319-326.

LI, Z., LOPEZ, M., HARDY, M., MCALLISTER, D. M., KALYANARAMAN, B. & ZHAO, M. 2009b. A 99mTc-Labeled Triphenylphosphonium Derivative for the Early Detection of Breast Tumors. *Cancer Biotherapy and Radiopharmaceuticals*, 24, 579-587.

LIAO, J. B. 2006. Viruses and human cancer. *The Yale journal of biology and medicine*, 79, 115-22.

LIBERMAN, E. A., TOPALY, V. P., TSOFINA, L. M., JASAITIS, A. A. & SKULACHEV, V, P. 1969. Mechanism of coupling of oxidative phosphorylation and the membrane potential of mitochondria. *Nature*, 222, 1076-1078.

LIDKE, D. S., NAGY, P., HEINTZMANN, R., ARNDT-JOVIN, D. J., POST, J. N., GRECCO, H. E., JARES-ERIJMAN, E. A. & JOVIN, T. M. 2004. Quantum dot ligands provide new insights into erbB/HER receptor-mediated signal transduction. *Nature Biotechnology*, 22, 198-203.

LINK, STEPHAN AND EL-SAYED, MOSTAFA 1999. Size and temperature dependence of the plasmon absorption of colloidal gold nanoparticles. *The Journal of Physical Chemistry B,* 21, 4212-4217.

LLEVOT, A. & ASTRUC, D. 2012. Applications of vectorized gold nanoparticles to the diagnosis and therapy of cancer. *Chemical Society Reviews*, 41, 242-257.

LUO, G., CHEN, W., LIU, Y., LEI, Q., ZHUO, R., & ZHANG, X. 2014. Multifunctional enveloped mesoporous silica nanoparticles for subcellular co-delivery of drug and therapeutic peptide. *Scientific Reports, 4*, 6064.

MAHMOOD, Z. & SHUKLA, Y. 2010. Death receptors: Targets for cancer therapy. *Experimental Cell Research*, 316, 887-889.

MALHI, S.S. & MURTHY, R.S., 2012. Delivery to mitochondria: a narrower approach for broader therapeutics. *Expert Opinion on Drug Delivery,* 9, 909-935.

MARRACHE, S., & DHAR, S. 2012. Engineering of blended nanoparticle platform for delivery of mitochondria-acting therapeutics. *Proceedings of the National Academy of Sciences of the United States of America,* 40, 16288-16293.

MAXWELL, D. J., TAYLOR, J. R. and NIE, S. 2002. Self-assembled nanoparticle probes for recognition and detection of biomolecules. *Journal of the American Chemical Society,* 32, 9606-9612.

MCCARTHY, J. R. & WEISSLEDER, R. 2008. Multifunctional magnetic nanoparticles for targeted imaging and therapy. *Advanced Drug Delivery Reviews*, 60, 1241-1251.

MINTZER, M. A. and SIMANEK, E. E. 2009. Non-viral vectors for gene delivery. *Chemical Reviews,* 2, 259-302.

MIODRAGOVIĆ, Đ. U., QUENTZEL, J. A., KURUTZ, J. W., STERN, C. L., AHN, R. W., KANDELA, I., O'HALLORAN, T. V. 2013. Robust structure and reactivity of aqueous arsenous Acid–Platinum(II) anticancer complexes. *Angewandte Chemie International Edition,* 41, 10749-10752.

MISRA, R., ACHARYA, S. & SAHOO, S. K. 2010. Cancer nanotechnology: Application of nanotechnology in cancer therapy. *Drug Discovery Today*, 15, 842-850.

MODICA-NAPOLITANO, J.S. & SINGH, K.K. 2002. Mitochondria as targets for detection and treatment of cancer. *Expert Reviews in Molecular Medicine,* 4, 1-19.

MODICA-NAPOLITANO, J.S. & SINGH, K.K. 2004. Mitochondrial dysfunction in cancer. *Mitochondrion,* 4, 755-762.

MONGE, S., CANNICCIONI, B., GRAILLOT, A., & ROBIN, J. 2011. Phosphorus-containing polymers: A great opportunity for the biomedical field. *Biomacromolecules,* 6, 1973-1982.

MUDHOO, A., SHARMA, S, K., GARG, V, K., TSENG, C, H. 2011. Arsenic: An overview of applications, health, and environmental concerns and removal processes. *Critical Review Environmental Science Technology*, 41, 435–519.

MURPHY, M. P. & SMITH, R. A. J. 2007. Targeting antioxidants to mitochondria by conjugation to lipophilic cations.

MURPHY, M.P. & SMITH, R.A.J., 2000. Drug delivery to mitochondria: the key to mitochondrial medicine. *Advanced Drug Delivery Reviews,* 41, 235-250.

MURPHY, M.P., 1997. Selective targeting of bioactive compounds to mitochondria. *Trends in Biotechnology,* 15, 326-330.

MURPHY, M.P., ECHTAY, K.S., BLAIKIE, F.H., ASIN-CAYUELA, J., COCHEME, H.M., GREEN, K., BUCKINGHAM, J.A., TAYLOR, E.R., HURRELL, F., HUGHES, G., MIWA, S., COOPER, C.E., SVISTUNENKO, D.A., SMITH, R.A. & BRAND, M.D., 2003. Superoxide activates uncoupling proteins by generating carbon-centered radicals and initiating lipid peroxidation: studies using a mitochondria-targeted spin trap derived from alpha-phenyl-N-tert-butylnitrone. *The Journal of Biological Chemistry,* 278, 48534-48545.

MURPHY, MICHAEL P. 2008. Targeting lipophilic cations to mitochondria. *Biochimica et biophysica acta (BBA) - Bioenergetics,* 7–8, 1028-1031.

NARAYANAN, D. L., SALADI, R. N. & FOX, J. L. 2010. Ultraviolet radiation and skin cancer. *International Journal of Dermatology*, 49, 978-989.

NIE, S. M., XING, Y., KIM, G. J. & SIMONS, J. W. 2007. Nanotechnology applications in cancer. *Annual Review of Biomedical Engineering*.

NISHIDA, N., YANO, H., NISHIDA, T., KAMURA, T. & KOJIRO, M. 2006. Angiogenesis in cancer. *Vascular Health and Risk Management*, 2, 213-9.

PANKHURST, Q. A., CONNOLLY, J., JONES, S. K. & DOBSON, J. 2003. Applications of magnetic nanoparticles in biomedicine. *Journal of Physics D: Applied Physics*, 36, R167-R181.

PAPASANI, MADHUSUDHAN R., WANG, GUANKUI AND HILL, RODNEY A. 2012. Gold nanoparticles: The importance of physiological principles to devise strategies for targeted drug delivery. *Nanomedicine: Nanotechnology, Biology and Medicine,* 6, 804-814.

PAPAVRAMIDOU, N., PAPAVRAMIDIS, T. & DEMETRIOU, T. 2010. Ancient Greek and Greco-Roman Methods in Modern Surgical Treatment of Cancer. *Annals of Surgical Oncology*, 17, 665-667.

PARSONS, M. J. & GREEN, D. R. 2010. Mitochondria in cell death. *Essays in Biochemistry*, 47, 99-114.

PEER, D., KARP, J. M., HONG, S., FAROKHZAD, O. C., MARGALIT, R. & LANGER, R. 2007. Nanocarriers as an emerging platform for cancer therapy. *Nature Nanotechnology*, 2, 751-760.

PETO, R., DARBY, S., DEO, H., SILCOCKS, P., WHITLEY, E. & DOLL, R. 2000. Smoking cessation, and lung cancer in the UK since 1950: combination of national statistics with two case-control studies. *British Medical Journal*, 321, 323-329.

PFEIFER, G. P., DENISSENKO, M. F., OLIVIER, M., TRETYAKOVA, N., HECHT, S. S. & HAINAUT, P. 2002. Tobacco smoke carcinogens, DNA damage and p53 mutations in smoking-associated cancers. *Oncogene*, 21, 7435-7451.

PICQUET, E., LE NY, K., DEL´EPINE, P., MONTIER, T., YAOUANC, J., CARTIER, D., CL´EMENT, J. 2005. Cationic lipophosphoramidates and lipophosphoguanidines are very efficient for in vivo DNA delivery. *Bioconjugate Chemistry,* 5, 1051-1053.

PICQUET, E., LE NY, K., DEL´EPINE, P., MONTIER, T., YAOUANC, J., CARTIER, D., CL´EMENT, J. 2005. Cationic lipophosphoramidates and lipophosphoguanidines are very efficient for in vivo DNA delivery. *Bioconjugate Chemistry,* 5, 1051-1053.

PORTEOUS, C.M., LOGAN, A., EVANS, C., LEDGERWOOD, E.C., MENON, D.K., AIGBIRHIO, F., SMITH, R.A.J. & MURPHY, M.P., 2010. Rapid uptake of lipophilic triphenylphosphonium cations by mitochondria in vivo following intravenous injection: Implications for mitochondria-specific therapies and probes. *Biochimica et Biophysica Acta (BBA) - General Subjects,* 1800, 1009-1017.

PORTNEY, N. G. & OZKAN, M. 2006. Nano-oncology: Drug delivery, imaging, and sensing. *Analytical and Bioanalytical Chemistry*, 384, 620-630.

PULKES, T. & HANNA, M. G. 2001. Human mitochondrial DNA diseases. *Advanced Drug Delivery Reviews*, 49, 27-43.

RAGG, R., NATALIO, F., TAHIR, M. N., JANSSEN, H., KASHYAP, A., STRAND, D., TREMEL, W. 2014. Molybdenum trioxide nanoparticles with intrinsic sulfite oxidase activity. *ACS Nano,* 5, 5182-5189.

RAJAPUTRA, P., NKEPANG, G., WATLEY, R. & YOU, Y. 2013. Synthesis and in vitro biological evaluation of lipophilic cation conjugated photosensitizers for targeting mitochondria. *Bioorganic and Medicinal Chemistry*, 21, 379-387.

RIEDL, S. J. & SHI, Y. G. 2004. Molecular mechanisms of caspase regulation during apoptosis. *Nature Reviews Molecular Cell Biology*, 8, 405-413.

RIGGIO, C., PAGNI, E., RAFFA, V. & CUSCHIERI, A. 2011. Nano-oncology: Clinical application for cancer therapy and future perspectives. *Journal of Nanomaterials*, 2011.

RIVERA GIL, P., H HN, D., DEL MERCATO, L. L., SASSE, D. & PARAK, W. J. 2010. Nanopharmacy: Inorganic nanoscale devices as vectors and active compounds. *Pharmacological Research*, 62, 115-125.

ROSS, M. F., KELSO, G. F., BLAIKIE, F. H., JAMES, A. M., COCHEME, H. M., FILIPOVSKA, A., . . . MURPHY, M. P. 2005. Lipophilic triphenylphosphonium cations as tools in mitochondrial bioenergetics and free radical biology. *Biochemistry.Biokhimiia,* 70, 222-230.

ROSS, M.F., KELSO, G.F., BLAIKIE, F.H., JAMES, A.M., COCHEME, H.M., FILIPOVSKA, A., DA ROS, T., HURD, T.R., SMITH, R.A. & MURPHY, M.P., 2005. Lipophilic triphenylphosphonium cations as tools in mitochondrial bioenergetics and free radical biology. *Biochemistry.Biokhimiia,* 70, 222-230.

ROSS, M.F., PRIME, T.A., ABAKUMOVA, I., JAMES, A.M., PORTEOUS, C.M., SMITH, R.A. & MURPHY, M.P., 2008. Rapid and extensive uptake and activation of hydrophobic triphenylphosphonium cations within cells. *The Biochemical journal,* 411, 633-645.

SCHEINBERG, D. A., VILLA, C. H., ESCORCIA, F. E. & MCDEVITT, M. R. 2010. Conscripts of the infinite armada: systemic cancer therapy using nanomaterials. *Nature Reviews Clinical Oncology*, 7, 266-276.

SCOTT, A. M., WOLCHOK, J. D. & OLD, L. J. 2012. Antibody therapy of cancer. *Nature Reviews Cancer*, 12, 278-287.

SHEU, S. S., NAUDURI, D. & ANDERS, M. W. 2006. Targeting antioxidants to mitochondria: A new therapeutic direction. *Biochimica et Biophysica Acta-Molecular Basis of Disease*, 1762, 256-265.

SINGH, K. K. 2001. Mitochondrial me and the Mitochondrion journal. *Mitochondrion*, 1, 1-2.

SMITH, R.A., HARTLEY, R.C., COCHEME, H.M. & MURPHY, M.P. 2012. Mitochondrial pharmacology. *Trends in Pharmacological Sciences,* 33, 341-352.

SMITH, R.A., KELSO, G.F., JAMES, A.M. & MURPHY, M.P. 2004. Targeting coenzyme Q derivatives to mitochondria. *Methods in enzymology,* 382, 45-67.

SMITH, R.A., PORTEOUS, C.M., COULTER, C.V. & MURPHY, M.P. 1999. Selective targeting of an antioxidant to mitochondria. *European journal of biochemistry / FEBS,* 263, 709-716.

SMITH, R.A., PORTEOUS, C.M., GANE, A.M. & MURPHY, M.P., 2003. Delivery of bioactive molecules to mitochondria in vivo. *Proceedings of the National Academy of Sciences of the United States of America,* 100, 5407-5412.

SOLOMON, M.A., SHAH, A. A., D'SOUZA, G. G., 2013. *In vitro* assessment of the utility of stearyl triphenyl phosphonium modified liposomes in overcoming the resistance of ovarian carcinoma Ovcar-3 cells to paclitaxel. *Mitochondrion*, 13, 464–472.

SRINIVAS, P. R., BARKER, P. & SRIVASTAVA, S. 2002. Nanotechnology in early detection of cancer. *Laboratory Investigation*, 82, 657-662.

SRIVASTAVA, P.C., HAY, H.G. & KNAPP, F.F., JR. 1985. Effects of alkyl and aryl substitution on the myocardial specificity of radioiodinated phosphonium, arsonium, and ammonium cations. *Journal of Medicinal Chemistry,* 28, 901-904.

SWINDELL, E. P., HANKINS, P. L., CHEN, H., MIODRAGOVIÄ‡, Ä. U., & OÂ€™HALLORAN, T. V. 2013. Anticancer activity of small-molecule and nanoparticulate arsenic(III) complexes. *Inorganic Chemistry,* 21, 12292-12304.

TAHIR, M. N., RAGG, R., NATALIO, F., SAHOO, J. K., DANIEL, P., KOYNOV, K., TREMEL, W. 2015. Amine functionalized ZrO_2 nanoparticles as biocompatible and luminescent probes for ligand specific cellular imaging. *Journal of Materials Chemistry B,* 11, 2371-2377.

TIWARI, M. P., VIG, K., DENNIS, A. V., & SINGH, R. S. 2011. Functionalized gold nanoparticles and their biomedical applications. *Nanomaterials*, 1, 31-63.

TLSTY, T. D. & COUSSENS, L. M. 2006. Tumor stroma and regulation of cancer development. *Annual Review of Pathology-Mechanisms of Disease*.

TUPPEN, H. A. L., BLAKELY, E. L., TURNBULL, D. M. & TAYLOR, R. W. 2010. Mitochondrial DNA mutations and human disease. *Biochimica Et Biophysica Acta-Bioenergetics*. 1797, 113-128.

TURKEVITCH, J., STEVENSON, P. C., AND HILLIER, J. 1951. Nucleation and growth process in the synthesis of colloidal gold. *Discussion Faraday Society*, 11, 55-75

UREN, A. G., KOOL, J., BERNS, A. & VAN LOHUIZEN, M. 2005. Retroviral insertional mutagenesis: past, present and future. *Oncogene*, 24, 7656-7672.

URRUTICOECHEA, A., ALEMANY, R., BALART, J., VILLANUEVA, A., VINALS, F. & CAPELLA, G. 2010. Recent Advances in Cancer Therapy: An Overview. *Current Pharmaceutical Design*, 16, 3-10.

VOURA, E. B., JAISWAL, J. K., MATTOUSSI, H. & SIMON, S. M. 2004. Tracking metastatic tumor cell extravasation with quantum dot nanocrystals and fluorescence emission-scanning microscopy. *Nature Medicine*, 10, 993-998.

WAGNER, V., DULLAART, A., BOCK, A. K. & ZWECK, A. 2006. The emerging nanomedicine landscape. *Nature Biotechnology*, 24, 1211-1217.

WAKEFORD, R. 2004. The Cancer epidemiology of radiation. *Oncogene*, 23, 6404-6428.

WALLACE, D. C. 2005. A mitochondrial paradigm of metabolic and degenerative diseases, aging, and cancer. A dawn for evolutionary medicine.

WALLACE, D. C. 2012. Mitochondria and cancer. *Nature Reviews Cancer*, 12, 685-698.

WALLING, M. A., NOVAK, J. A. & SHEPARD, J. R. E. 2009. Quantum dots for live cell and in vivo imaging. *International Journal of Molecular Sciences*, 10, 441-491.

WANG, F., OGASAWARA, M. A. & HUANG, P. 2010. Small mitochondria targeting molecule as anti-cancer agents. *Molecular Aspects of Medicine*, 31, 75-92.

WANG, J., YANG, C.T., KIM, Y.S., SREERAMA, S.G., CAO, Q., LI, Z.B., HE, Z., CHEN, X. & LIU, S., 2007. 64Cu-Labeled triphenylphosphonium and triphenylarsonium cations as highly tumor-selective imaging agents. *Journal of medicinal chemistry,* 50, 5057-5069.

WANG, X. 2001. The expanding role of mitochondria in apoptosis. *Genes and Development*, 15, 2922-2933.

WANG, X., PENG, H., YANG, L., YOU, F., TENG, F., HOU, L., & WOLFBEIS, O. S. 2014. Targetable phosphorescent oxygen nanosensors for the assessment of tumor mitochondrial

dysfunction by monitoring the respiratory activity. *Angewandte Chemie International Edition,* 46, 12471-12475.

WANG, X., PENG, H., YANG, L., YOU, F., TENG, F., TANG, A., LI, X. 2013. Poly-l-lysine assisted synthesis of core-shell nanoparticles and conjugation with triphenylphosphonium to target mitochondria. *Journal of Materials Chemistry B,* 38, 5143-5152.

WEINBERG, R. A. 2013. *The Biology of Cancer, New York, Garland Science*.

Weissig, V. 2011. From serendipity to mitochondria-targeted nanocarriers. *Pharmaceutical Research,* 11, 2657.

WEISSIG, V., 2003. Mitochondrial-targeted drug and DNA delivery. *Critical reviews in therapeutic drug carrier systems,* 20, 1-62.

WEISSIG, V., BODDAPATI, S.V., JABR, L. & D'SOUZA, G.G., 2007. Mitochondria-specific nanotechnology. *Nanomedicine,* 2, 275-285.

WEISSIG, V., CHENG, S. M. & D'SOUZA, G. G. M. 2004. Mitochondrial pharmaceutics. *Mitochondrion*, 3, 229-244.

WOGAN, G. N., HECHT, S. S., FELTON, J. S., CONNEY, A. H. & LOEB, L. A. 2004. Environmental and chemical carcinogenesis. *Seminars in Cancer Biology*, 14, 473-486.

WONG, W.W. & PUTHALAKATH, H., 2008. Bcl-2 family proteins: the sentinels of the mitochondrial apoptosis pathway. *IUBMB life,* 60, 390-397.

YAMAZAKI, N., KOJIMA, S., BOVIN, N. V., ANDRE, S., GABIUS, S. & GABIUS, H. J. 2000. Endogenous lectins as targets for drug delivery. *Advanced Drug Delivery Reviews*, 43, 225-244.

YANG Y, GAO N, HU Y, JIA C, CHOU T, DU H, WANG H. 2015. Gold nanoparticle enhanced photodynamic therapy: effects of surface charge and mitochondrial targeting. *Therapeutic delivery*, 6, 307-321.

YANG, C.T., KIM, Y.S., WANG, J., WANG, L., SHI, J., LI, Z.B., CHEN, X., FAN, M., LI, J.J. & LIU, S., 2008. 64Cu-labeled 2-(diphenylphosphoryl)ethyldiphenylphosphonium cations as highly selective tumor imaging agents: effects of linkers and chelates on radiotracer biodistribution characteristics. *Bioconjugate chemistry,* 19, 2008-2022.

YANG, C.T., LI, Y. & LIU, S., 2007. Synthesis and structural characterization of complexes of a DO3A-conjugated triphenylphosphonium cation with diagnostically important metal ions. *Inorganic chemistry,* 46, 8988-8997.

YOUSIF, L.F., STEWART, K.M. & KELLEY, S.O., 2009b. Targeting mitochondria with organelle-specific compounds: strategies and applications. *Chembiochem,* 10, 1939-1950.

YOUSIF, L.F., STEWART, K.M., HORTON, K.L. & KELLEY, S.O., 2009a. Mitochondria-penetrating peptides: sequence effects and model cargo transport. *Chembiochem,* 10, 2081-2088.

ZAMBLE, D. B. & LIPPARD, S. J. 1995. CISPLATIN AND DNA-REPAIR IN CANCER-CHEMOTHERAPY. *Trends in Biochemical Sciences*, 20, 435-439.

ZHANG, Y., SHEN, Y., TENG, X., YAN, M., BI, H., & MORAIS, P. C. 2015. Mitochondria-targeting nanoplatform with fluorescent carbon dots for long time imaging and magnetic field-enhanced cellular uptake. *ACS Applied Materials & Interfaces,* 19, 10201-10212.

ZHOU, Y. & LIU, S., 2011. 64Cu-labeled phosphonium cations as PET radiotracers for tumor imaging. *Bioconjugate Chemistry,* 22, 1459-1472.

Chapter 2

Experimental methods

This chapter introduces the analytical methods used to characterize the compounds synthesized during this project.

2.1 Melting point

Determination of the melting point of compounds was carried out using an electro thermal melting point apparatus, with a temperature gradient from room temperature (Temperature ramp: 0.5°C) using a Techne Stuart Digital Melting Point Apparatus (Fisher scientific, Sheffield Hallam University, UK)

2.2 Elemental analysis

Elemental analysis (Carbon, Sulphur and Hydrogen) were carried out by MEDAC Ltd (Chobham, Surrey, UK).

2.3 Thin layer Chromatography

Analytical thin layer chromatography (TLC) was performed on Merck silica gel 60F254 plates using 70:30 DCM:MeOH as the mobile phase. All samples were dissolved in DCM.

2.4 Nuclear Magnetic Resonance

Deuterated solvents were used to dissolve samples (10-15mg mL^{-1}) for ^{1}H, ^{31}P and ^{13}C nuclear magnetic resonance spectra. The spectra were obtained using a Bruker AVANCE III (400MHz) NMR spectrometer (Bruker, Coventry, West Midlands, UK). Spectra were interpreted by comparison with published data and reference material (Duss and Roger., 1998, Rensen and Keeler., 2006).

2.5 Ultraviolet-visible absorption spectroscopy

Ultraviolet visible (UV-Vis) absorption spectra of aqueous colloidal solutions were recorded at room temperature on a Jenway 6715 UV/Vis spectrophotometer (Bibby Scientific Limited, Stone, Staffordshire, UK) with UV-quartz cuvettes (1m optical path). Assignments were made based on published data (Daniel and Astruc., 2004).

2.6 Fourier Transform Infrared spectroscopy

Fourier transform infrared (FTIR) spectra were recorded on a PerkinElmer spectrum 100 FTIR spectrometer (PerkinElmer, Waltham, Massachusetts, USA). The data was interpreted using interpretation tables (Gunzler and Gremlich, 2002, Larkin, 2011).

2.7 Electrospray Ionization Mass Spectrometry

Samples were dissolved in EtOH: DIH_2O (50:50) to a concentration of approximately 1mg/mL for molecular ion determination. Electrospray mass spectra were recorded using a Thermo Finnigan MAT LCQ classic electrospray ionisation mass spectrometer (ESI-MS) (Thermo Scientific, Sanjose, California, USA) in a positive ion mode. Samples were introduced by direct infusion using the syringe pump on the instrument at a flow rate of 5 µL/min with an acquisition time of one minute.

2.8 X-Ray Crystallography

Single crystals of selected compounds were grown by slow diffusion of diethyl ether into a solution of the compounds dissolved in DCM. Crystalline Samples isolated were then submitted for analysis to the UK National Crystallography Service at the University of

Southampton (School of Chemistry, Highfield, Southampton, UK). The full crystallographic reports for all crystal studies are included in Appendix 1.

2.9 Transmission Electron Microscopy

Transmission electron micrographs of AuNPs were conducted on a Jeol 2000 FX transmission electron microscope (TEM) (ETC, Brunel University, Middlesex, UK), set at 100kV. Freeze dried AuNPs samples were re-suspended in ethanol, and placed on a Holey coated copper gold grid, and the grids were left dry in air at room temperature. Particle size distribution was obtained over 1000 AuNPs using Abel imaging software. TEM was also done at Sheffield Hallam University using Philips CM20 TEM (200kV, LaB6 filament) using the same protocol as above.

2.10 X-ray Photoelectron Spectroscopy

The sample was deposited onto the carbon tape on the sample bar as a slurry, and the sample was left under vacuum in the instrument's load lock for approximately 48 hours to dry out. The sample was analyzed by X-ray Photoelectron Spectroscopy using a Kratos Alpha DLD instrument (ETC, Brunel University, Middlesex, UK). Monochromated aluminium radiation was used to collect a survey scan between 1200 to 0 eV at 0.5 eV resolution, and then quantified using calibrated relative sensitivity factors to give the elemental compositions. In addition, high-resolution scans were collected over the C1s, O 1s, S 2p, Au 4f and As 3d peaks at 0.05 eV resolution and 20 eV pass energy. The scans obtained are after curve fitting. The binding energies have all been adjusted such that the C-C/C-H component of the C 1s peak in the wide survey spectrum falls at 285.0 eV (Sheffield Surface Analysis Centre, University of Sheffield, Sheffield, South Yorkshire, UK). This is to adjust for

charging effects not sufficiently compensated for by the charge neutralization used during data collection.

2.11 Cell Culture

Human prostate cancer cells (PC3) and Human Fibroblast cells were maintained in complete media (cDMEM) which contains Dulbecco's modified Eagle medium with GlutaMAX, 4.5 g/L D-glucose and sodium pyruvate (Invitrogen Life Technologies, Paisley, Renfrewshire, UK) containing 10% heat-inactivated fetal bovine serum (Biosera, East Sussex, Sussex, UK) and 1% penicillin-streptomycin (Invitrogen Life Technologies, Paisley, Renfrewshire, UK) at 37°C in 5% CO_2 and 95% air. Cells were sub-cultured every 4 days and periodically screened for mycoplasma.

2.12 Cytotoxicity assay

Cytotoxicity was assessed using CellTiter-Glo luminescent cell viability assay kit (Promega Corporation, Southampton, Hamshire, UK). Cell viability was measured according to the manufacturer's instructions. In brief plates were equilibrated at room temperature for 30 minutes, 100µL of assay reagent was added to each well, placed on an orbital shaker for 2 minutes and read on a Wallac Victor2 1420 multilabel counter (PerkinElmer, Cambridge, Cambridgeshire, UK).

Data obtained are expressed a percentage of live cells normalised to control. The average, standard deviation and IC_{50} values were plotted and calculated using GraphPad Prism (GraphPad software, La Jolia, California, USA).

2.13 ICP-OES

The Au analysis was carried out by digestion of the sample in 8ml of aqua regia and the solution made up to 100ml. This solution was then analyzed by ICP-OES. The instrument used for this was a Varian Vista MPX ICP-OES at MEDAC (Chobham, Surrey, UK).

2.14 References

DANIEL, M. C. & ASTRUC, D. 2004. Gold nanoparticles: Assembly, supramolecular chemistry, quantum-size-related properties, and application toward biology, catalysis, and nanotechnology. *Chemical Reviews*, 104, 293-346.

DUUS, J. 2002. A complete introduction to modern NMR spectroscopy. Wiley, Chichester, 1998, ISBN 0471 15736 8. *Magnetic Resonance in Chemistry*, 40, 430-430.

GUNZLER, H. & GREMLICH, H.-U. 2002. IR Spectroscopy: an introduction, Weinheim, Wiley-VCH.

HOFFMAN, D., E & STROOTBANT, V. 2007. Mass spectrometry: principle and applications England, John Wiley & Sons Ltd.

LARKIN, P. 2011. Infrared and Raman spectroscopy: principles and spectral interpretation, Boston; Amsterdam, Elsevier.

RENSEN, O. W. 2006. Understanding NMR Spectroscopy. Magnetic Resonance in Chemistry, 44, 820-820.

Chapter 3

A) The synthesis and characterisation of triphenylarsonium- functionalized gold nanoparticles and their precursor ligands

3.1 Introduction

As outlined in chapter 1, triphenylphosphonium salts act as lipophilic cations and are preferentially accumulated in the mitochondria of cells, making them an attractive proposition for integration with nanomaterials for applications in pharmaceutical-nanotechnology (Hoyle et al., 2008). Arsonium cations are also lipophilic and have been investigated as intra-cellular transport vectors. For example, copper-64 labelled complexes of 1,4,7,10-tetraazacyclododecane-4,7,10-triacetic acid-conjugated triphenylarsonium cations have been found to act as tumour-selective PET imaging agents (Wang et al., 2007) and lipophosphoramidate derivatives containing arsonium head-groups have been studied as gene delivery systems (Berchel et al., 2012).

Previous work in the Bricklebank group has focused on the preparation and biological properties of triphenylphosphonioalkylthiosulfate zwitterions and ω-thioacetylalkyl-(triphenyl)phosphonium salts, and the use of these compounds to prepare phosphonium-functionalized gold nanoparticles which are accumulated by cells and localized in the mitochondria (Ju-Nam et al., 2012, Ju-Nam et al., 2006, Ju-Nam et al., 2008, Chen PhD Thesis, 2014). Given the success of using arsonium cations as intra-cellular transport vectors it was decided to broaden the scope of our phosphonium-chemistry research to encompass triphenylarsonium and methoxyphenylphosphonium compounds.

In this chapter (3A) the synthesis and characterization of triphenylarsoniopropylthiosulfate zwitterion, ω-thioacetylpropyl(triphenyl)arsonium bromide salt, (3B) (methoxy-phenyl) phosphoniopropylthiosulfate zwitterions and ω-thioacetylpropyl (methoxyphenyl) phosphonium

salts are described, together with investigations into the preparation of gold nanoparticles functionalized with triphenylarsonium groups.

3.2 Material and methods

3.2.1 Chemicals

All chemicals were used as received; triphenylarsine, 1,3 dibromopropane, potassium thioacetate, sodium thiosulfate, Potassium bromide, gold(III) chloride trihydrate, hydrobromic acid, magnesium sulfate, deuterated dichloromethane and chloroform were purchased from Sigma-Aldrich (Gillingham, Dorset, UK).

3.2.2 Synthesis of Triphenylalkyl arsonium compounds

3-bromopropyl (triphenyl)arsonium bromide **(1)** was prepared from 1,3-dibromopropane (3ml) and triphenylarsine (1g) following the method of Moorhoff (Moorhoff, 1998) as shown in figure 3.1. The triphenylarsoniopropylthiosulfate zwitterion **(2)** and ω-thioacetylpropyl(triphenyl)arsonium bromide salt **(3)** were obtained by adapting the methods described by Ju-Nam and colleagues (Ju-Nam et al., 2012, Ju-Nam et al., 2006).

The triphenylarsoniopropylthiosulfate zwitterion **(2)** were synthesized by refluxing 3-bromopropyl(triphenyl)arsonium bromide (1.0g, 2.15 x 10^{-3} mol) with $Na_2S_2O_3$ in aqueous EtOH (0.8g, 3.23 X 10^{-3} mol) to obtain the product. The completion of the reaction was checked by TLC using 70:30 DCM:MeOH as the mobile phase. After the reaction was completed, 20ml KBr solution, 10%w/v was added prior to isolating the bromide salt. Solvent extraction with DCM (3 x 10 ml) was done to obtain the product which was finally purified by trituration with diethyl ether, followed by characterization by elemental analysis FT-IR, ESI-MS and NMR.

The ω-thioacetylpropyl(triphenyl)arsonium bromide salt **(3)** were synthesized by stirring 3-bromopropyl(triphenyl)arsonium bromide under nitrogen with potassium thioacetate in aqueous EtOH (0.37g, 3.23 x 10^{-3} mol). The completion of the reaction was checked by TLC using 70:30 DCM:MeOH as the mobile phase. After the reaction was completed, 20ml KBr solution, 10%w/v was added prior to isolating the bromide salt. Solvent extraction with DCM (3 x 10 ml) was done to obtain the product which was finally purified by trituration with diethyl ether, followed by characterization by elemental analysis FT-IR, ESI-MS and NMR.

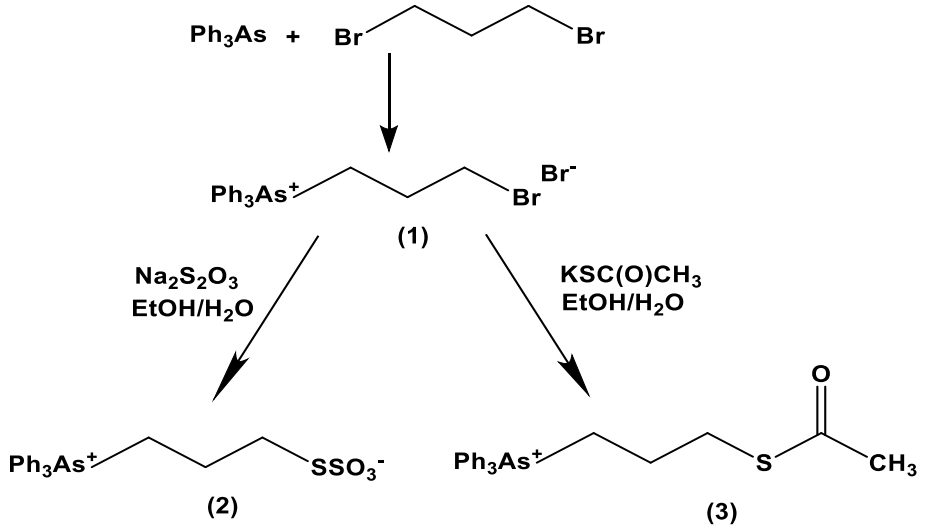

Figure 3.1 Synthesis schemes of Arsonium ligands.

3.3 Characterization of Arsonium ligands.

All arsonium compounds were characterized by elemental analysis and by ^{1}H and ^{13}C NMR, mass spectrometry and by FT-IR and FT-Raman spectroscopy and the data are reported below in section 3.3.1 and 3.3.2. Compounds **2** and **3** were also characterized by single crystal X-ray crystallography and X-ray photoelectron spectroscopy. The results of these analyses are discussed in detail in sections 3.3.4 and 3.4.2.2 respectively.

3.3.1 Triphenylarsoniopropyl thiosulfate zwitterion (2):

Colourless crystals, mp. 196°C. Elemental Analysis: found: C, 54.46%; H, 4.40%; S 13.94%. $C_{21}H_{21}AsO_3S_2$ requires: C, 54.78%; H, 4.56%; S 13.91%. ^{1}H NMR**:** δ 2.3 (2H, m), 3.2 (2H, t), 3.6 (2H, m), 7.6–7.9 (15H, m) ppm. IR υ_{max}/cm^{-1}=2912 (CH), 1483, 1438, 1209 (SO), 1082, 1010 (SO), 744, 688, 623, 523, 466. ESI-MS**:** 460.89 $[M]^+$, 461.97 $[M+H^+]$, 482.90 $[M+Na^+]$.

3.3.2 ω-Thioacetylpropyl(triphenyl)arsonium bromide (3):

Colourless crystals, mp. 234 - 238°C. Elemental Analysis: found: C, 54.97%; H, 4.81%; S 6.42%. $C_{22}H_{24}AsBrOS$ requires: C, 54.87%; H, 4.77%; S 6.36%. ^{1}H NMR**:** δ 1.6 (3H, s), 2.1 (2H, m), 3.2 (2H, t), 3.8 (2H, m), 7.6–7.9 (15H, m) ppm. IR υ_{max}/cm^{-1}=2911 (CH), 1483, 1436 (SO), 1082, 1022 (SO), 742, 687, 623, 466. ESI-MS**:** 423.13 $[M]^+$, 424.13 $[M+H^+]$.

3.3.3 Single Crystal X-ray crystallography Studies of the Triphenylarsoniopropyl thiosulfate zwitterion (2).

The structure of **2** was investigated by x-ray crystallography. Single crystals were grown by slow diffusion of diethyl ether into a DCM solution of **2,** which yielded colourless needles. The crystals were sent for full structure analysis at the EPSRC X-ray Crystallography service at the University of Southampton.

The molecular structure of **2** is shown in Figure 3.2, selected bond lengths and angles are listed in Table 3.1. Crystal data and structure refinement details are presented in appendix 1.

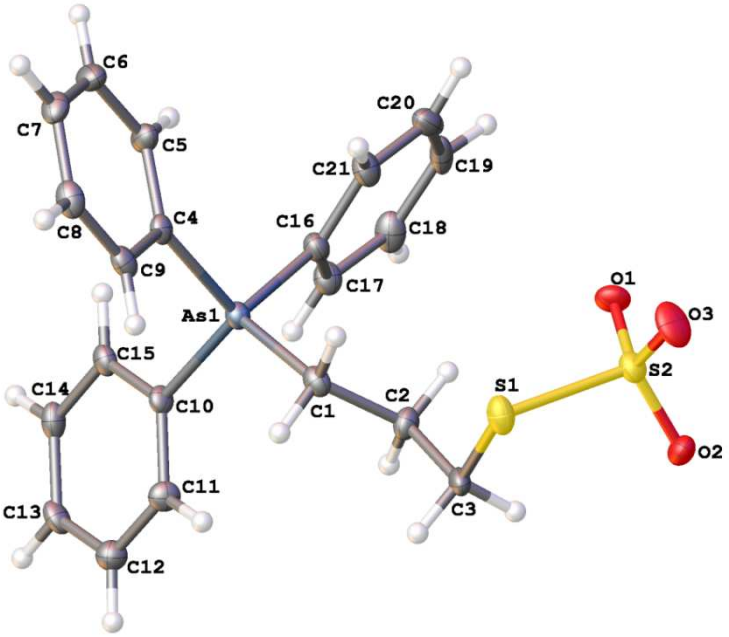

Figure 3.2 An Ortep representation of the molecular structure of **2**. Thermal ellipsoids are drawn at 50% probability level.

Table 3.1 Selected bond lengths [Å] and angles [°] in **2.**

C1–As1	1.923(5)	O1–S2	1.452(4)
C3–S1	1.817(5)	O2–S2	1.443(4)
C4–As1	1.910(5)	O3–S2	1.446(4)
C10–As1	1.916(4)	S1–S2	2.1081(18)
C16–As1	1.904(5)		
C3–S1–S2	99.84(17)	O2–S2–S1	105.78(16)
O2–S2–O3	114.6(2)	O3–S2–S1	101.28(17)
O2–S2–O1	113.7(2)	O1–S2–S1	107.13(16)
O3–S2–O1	113.0(2)		

The structures of several organic thiosulfate zwitterions have been described. The Bricklebank group has previously reported the structure of triphenylphosphoniopropylthiosulfate zwitterion (**4**), together with those of the tributylphosphoniopropylthiosulfate and (4-fluorophenyl)phosphoniopropylthiosulfate zwitterions (Ju-Nam et al., 2012, Ju-Nam et al., 2006). The only other crystallographically-characterized thiosulfate zwitterion is an ammonium derivative, *S*- [4- (trimethylammonio) phenyl] thiosulfate (**5**) (Chen et al., 2004).

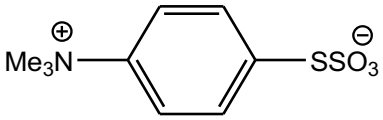

Figure 3.3 *S*- [4- (trimethylammonio) phenyl] thiosulfate **(5)**

Compound **2** displays the expected tetrahedral geometry around the arsenic atoms with a mean C–As–C bond angle of 109.5(2) °. The S–O bonds in the thiosulfate group are similar with a mean length of 1.447(4) Å, indicative of multiple bond character, and that the negative charge is delocalised over the entire sulfate group. The mean O–S–O angle [113.8(2)°] is consistent with those in other thiosulfate ions (Ju-Nam et al., 2012, Ju-Nam et al., 2006, Chen et al., 2004). The S–S bond length [2.1081(18) Å], is slightly shorter than that of the corresponding phosphonium compound **4** [2.1117(9) Å] (Ju-Nam et al., 2012), but longer than the S–S bond in ionic thiosulfate ions such as $Me_2HN(CH_2S_2O_3)_2^-Na^+$ (Ju-Nam et al., 2006). However, all are longer than the established length of a single S-S bond [2.05Å] (Huheey et al., 1972). The ammonium thiosulfate zwitterion **5** has an S-S bond length of 2.1137(7) Å, similar to those of **2** and **4**, but appreciably shorter than the S-S bond in the monoanion of thiosulfuric acid, $HSSO_3^-$ [2.155 Å] (K. Miaskiewicz and R. Steudel, 1992). The lengthening of the S-O and S-S bonds in the organic zwitterions is consistent with the

delocalization of the negative charge across the entire thiosulfate group. Furthermore, the longer and weaker S-S bond of the triphenyl-arsonium and -phosphonium zwitterions expedites the dissociation of the thiosulfate group with the concomitant formation of the corresponding thiolate ion which is a key step in the application of these compounds in the synthesis of metal nanoparticles.

Within the crystal lattice the triphenylarsonium thiosulfate zwitterions pack fairly loosely, held together by hydrogen-bonding interactions between the sulfate oxygen's and the phenyl hydrogens, but there is no close interaction between the arsonium centre and the thiosulfate moieties.

3.3.4 Single Crystal X-ray crystallography Studies of the Thioacetylpropyl (triphenyl) arsonium bromide (3)

The structure of arsonium salt **3** was investigated by x-ray crystallography. Single crystals were grown by slow diffusion of diethyl ether into a DCM solution of **3** which yielded the compound as colourless needles. The crystals were sent for full structure analysis at the EPSRC X-ray Crystallography service at the University of Southampton.

The molecular structure of **3** is shown in Figure 3.4, selected bond lengths and angles are listed in Table 3.2. Crystal data and structure refinement details are presented in appendix 1.

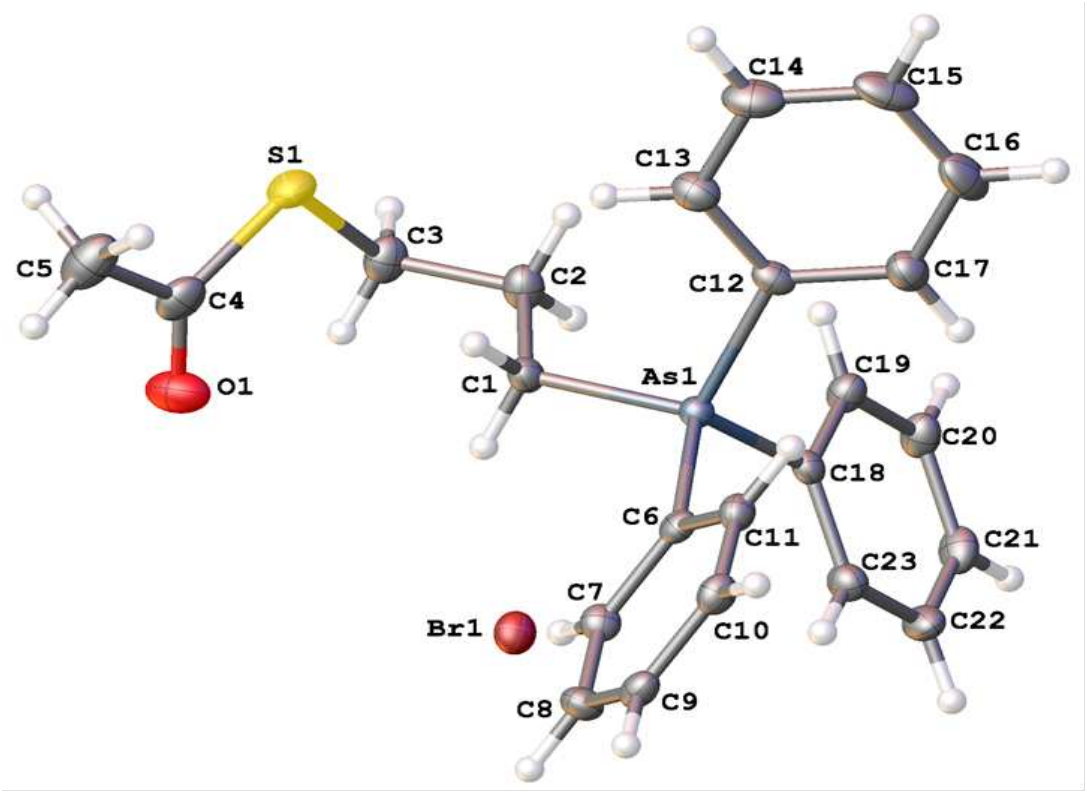

Figure 3.4 An Ortep representation of the molecular structure of **3**. Thermal ellipsoids are drawn at 50% probability level.

Table 3.2 Selected bond lengths [Å] and angles [°] in **3.**

C1–As1	1.927(2)	C6–As1	1.909(2)
C3–S1	1.806(3)	C12–As1	1.912(2)
C4–O1	1.204(3)	C18–As1	1.914(3)
C4–S1	1.777(3)		
C2–C1–As1	114.06(18)	C17–C12–As1	119.1(2)
As1–C1–H1A	108.7	C13–C12–As1	119.9(2)
As1–C1–H1B	108.7	C19–C18–As1	119.36(19)
C2–C3–S1	113.17(19)	C23–C18–As1	119.84(19)
S1–C3–H3A	108.9	C6–As1–C12	108.90(10)
S1–C3–H3B	108.9	C6–As1–C18	109.88(10)
O1–C4–C5	124.0(3)	C12–As1–C18	108.21(11)
O1–C4–S1	123.0(2)	C6–As1–C1	107.02(11)
C5–C4–S1	113.0(2)	C12–As1–C1	109.52(11)
C11–C6–As1	120.18(19)	C18–As1–C1	113.24(10)
C7–C6–As1	118.98(18)	C4–S1–C3	102.23(14)

Arsonium salt **3** displays the expected tetrahedral geometry around the arsenic atom with a mean C-As-C bond angle of 109.46(11)^{o} which is very similar to the mean C-As-C bond angle in **2** [109.5(2)^{o}]. The thioacetate moiety displays the expected angular geometry around the sulphur atom and the mean O–C–S angle [123.0(2)°] is consistent with those in other thioacetate ions (Ju-Nam et al., 2012). The C-S and C-O bond lengths of the thioacetate group in **3** are similar to the expected distances for C-S single and C=O bonds, *ca.*1.8 Å and 1.2 Å respectively, and are similar to the comparable bonds in ω-thioacetylpropyl(tri-4-fluorophenyl)phosphonium bromide (Ju-Nam et al., 2012), and dimethylmonothiocarbonate, $CH_3OC(S)CH_3$, which has C-S bond lengths of 1.791(2)Å, 1.759(1) Å and a C=O bond length of 1.195(2) Å (Erben et al., 2006).

3.4 Synthesis and characterization of Triphenylarsonium functionalized gold nanoparticles.

Phosphonioalkylthiosulfate zwitterions (Ju-Nam et al., 2012, Ju-Nam et al., 2006), and phosphonioalkylthioacetate salts (Ju-Nam et al., 2008) are known to act as 'masked thiolates' and, under reductive conditions, cleavage of the thiosulfate S-S or thioacetate S-C bonds takes place generating phosphonioalkylthiolate zwitterions that can coordinate to the surface of gold particles. The Bricklebank group have exploited this chemistry to generate water soluble cationic gold nanoparticles functionalized with alkylthiolate ligands bearing phosphonium head-groups, and hence it was of interest to investigate if the analogous arsonium thiosulfate zwitterion (**2**) and thioacetate salt (**3**) would undergo the same reaction. Recent work has reported rare examples of the coordination chemistry of tertiary arsine ligands bearing pendant thiolate groups towards Ni(II), Pt(II) and Pd(II) (Hildebrand et al., 2013). However, to the best of our knowledge, there are no reports of the coordination chemistry of triorganoarsonium thiolate species or of the use of tertiary arsines or arsonium compounds as capping ligands in the formation of functionalized nanoparticles, although nanoscale liposomes or nanobins, composed of lipids and metal salts, have been used to encapsulate and stabilize arsenic trioxide in order to extend the clinical utility of this compound (Swindell et al., 2013).

3.4.1 The Synthesis of Triphenylarsonium- functionalized gold nanoparticles.

The synthesis is based on methods developed previously by the Bricklebank group (Ju-Nam et al., 2012, Ju-Nam et al., 2006, Ju-Nam et al., 2008) as shown in Figure 3.5. A solution of the arsonium ligand (**2** or **3**) (0.25mmol) was prepared in dichloromethane. Solid

tetrachloroauric acid was added to form a homogenous solution. The mixture was stirred for 5-6 hours until the gold salt had completely dissolved. After the complete dissolution of the gold salt, the reduction was carried out by the addition an aqueous solution of sodium borohydride, drop-wise with vigorous stirring.

The first confirmation that the AuNPs had been successfully prepared was the visual observation of the color change of the solution during the synthesis; when $HAuCl_4$ (0.25mg) was added to the solution of the corresponding protecting ligands **2** and **3** in DCM (10mL), the stirring organic solution turned yellow. The drop by drop addition of $NaBH_4$ (10mL) induced a color change from yellow to a characteristic purple color which indicated that reduction had taken place (Daniel and Astruc review, 2004). When the reaction was stopped after 24 hours, the DCM layer was colorless and the aqueous phase was purple in color with no evidence of aggregation, indicating that functionalized AuNPs were present in the aqueous phase. The aqueous phase was subjected to three DCM extractions in order to remove the excess organic matter present. A series of experiments have been completed, as outlined in Table 3.3, varying the ratio of $HAuCl_4$ and arsonium ligand with the aim of investigating the effect on the size and polydispersity of the resulting AuNPs.

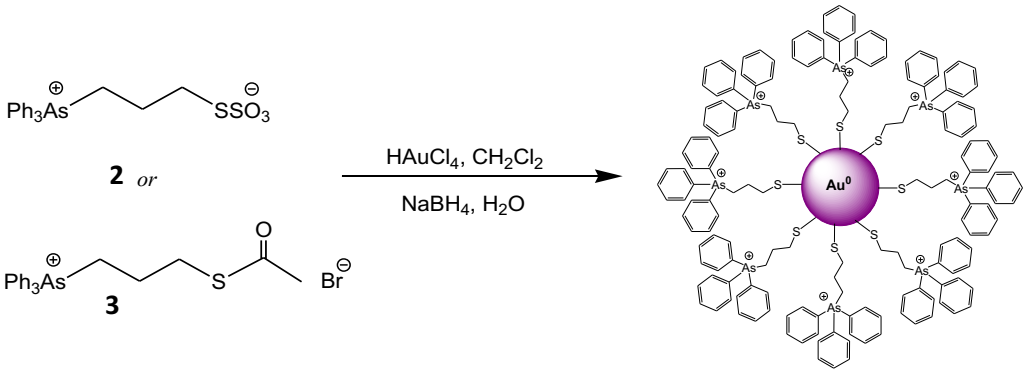

Figure 3.5 Reaction scheme for synthesis of **Triphenylarsonium-functionalized AuNP**

Table 3.3 Varying ratio of Gold and Arsonium ligand.

Sample*	Capping Ligand	Ratio of gold salt and capping ligand		Notes and observations
		$[AuCl_4]^-$	Ligand	
A-Au-Z0.1	**2**	1	0.1	No nanoparticles formed
A-Au-Z0.5	**2**	1	0.5	
A-Au-Z1	**2**	1	1	
A-Au-Z1.5	**2**	1	1.5	
A-Au-Z2	**2**	1	2	
A-Au-T2	**3**	1	2	

***NOTE**

In order to differentiate the samples an experimental notation has been developed as follows:

- The initial A or P represents Triphenyl**A**rsonium or triphenyl**P**hosphonium head group
- The Au represents a gold nanoparticle
- Z or T indicates whether the precursor ligand was a thiosulfate **Z**witterion or **T**hioacetate salt
- The numbers indicate the gold: ligand ratio in the reaction mixture, *e.g.* 2 indicates a $[AuCl_4]^-$:ligand ration of 1:2

Therefore, **A-Au-Z0.5** would be a gold nanoparticle, capped with triphenylarsonium ligand, prepared using the triphenylpropylthiosulfate zwitterion with gold: ligand ratio of 1:0.5.

The mechanism by which the triphenylarsonium-functionalized AuNPs are formed is not certain. Studies into the formation of monolayers on gold surfaces from alkylthiosulfates show hydrolysis by trace amounts of water present in the solvent to be crucial (Fealy et al., 2011, Pillai and Freund, 2011). The nanoparticles reported here were prepared in a two-phase water/dichloromethane mixture, i.e. more than a trace of water! However the possibility that the growing gold nanoparticles and/or the reducing agent are involved in the cleavage of the thiosulfate S–S or thioacetate S–C bonds cannot be excluded. Previous studies on the analogous phosphonium zwitterions and salts indicate that the cleavage step

is slower for the thioacetate ligands than for the thiosulfate zwitterions and so this results in slower monolayer formation and consequently a broader particle size distribution.

3.4.2 Characterization of Triphenylarsonium-Functionalized Gold Nanoparticles

The triphenylarsonium-functionalized AuNPs have been characterized using a range of techniques including UV-visible, IR and Raman spectroscopy, X-ray photoelectron spectroscopy (XPS) and Transmission Electron Microscopy (TEM), as discussed below.

3.4.2.1 Spectroscopic Characterization of Triphenylarsonium-capped AuNPs

To study the optical properties of nanoparticles UV-Vis absorption spectroscopy has been widely used, the UV-visible absorption band of gold nanoparticles being governed by a number of factors such as the shape and size of the metal nanoparticles. The evidence that the AuNPs were successfully synthesized was supported by the broad adsorption band in the visible region centered at ~520nm (Figure 3.6). This indicated that the AuNPs were between 2-10nm in diameter, according to the data for other thiolate-capped gold nanoparticles reported previously (Daniel and Astruc review, 2004).

The position of the λ_{max} of the absorption band is not significantly affected by the ratio of gold and capping ligand, except for experiment **A-Au-Z0.1**, indicating that the particle size of the AuNPs were very similar; this was later confirmed by TEM. The reaction with a gold: ligand molar ratio of 1:0.1 (**A-Au-Z0.1**) had insufficient ligand to be able to stabilize the growing nanoparticles and hence no absorption band was observed in the UV-visible spectrum.

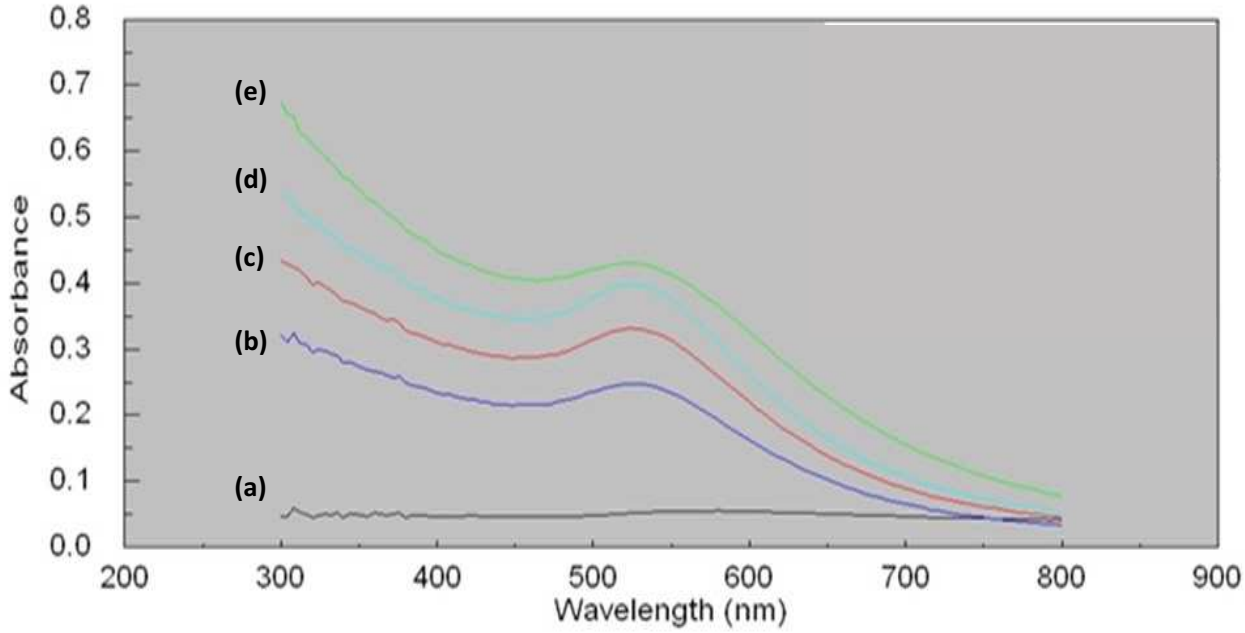

Figure 3.6 UV-vis spectra of triphenylarsonium-functionalized AuNPs: (a) **A-Au-Z0.1**, (b) **A-Au-Z1.5**, (c) **A-Au-Z0.5**, (d) **A-Au-Z2**, (e) **A-Au-Z1**.

ESI-MS data also provided useful information regarding the chemical composition of the surface ligands on the AuNPs. The ESI-MS spectra of **A-Au-Z1**, **A-Au-Z1.5**, and **A-Au-Z2**, **A-Au-T2** all contained a peak due to the triphenylarsoniopropylthiolate ion $(Ph_3AsCH_2CH_2CH_2S)^+$, with no evidence of the parent thiosulfate zwitterion or thioacetate cation. This indicated that the S-S bond of the thiosulfate group in **2** and the thioacetate group in **3** has been successfully cleaved. The spectra also included a fragment peak at m/z 306 due to the Ph_3As moiety.

Raman spectroscopy has previously been used to characterize thiolate-protected gold clusters and nanoparticles (Varnholt et al., 2014 and Holze and Wu., 2014). The spectra are dependent on the size of the particles and the nature and steric bulk of the ligand with Au-S

modes typically occurring in the region 250 - 325cm^{-1}. The Raman spectra of triphenylarsoniumpropylthiolate-capped AuNPs were recorded in the region 4000 - 150cm^{-1}. The spectra are illustrated in Figures 3.7 – 3.10. All of the nanoparticle samples showed significant fluorescence which diminished the quality of the data. Nonetheless, some deductions can be made. The spectra of all samples, contained peaks at 1600, 1021 and 999cm^{-1} that can be attributed to C-H ring bending modes (Varnholt et al., 2014). Furthermore, the compounds all show a band in the region 259 - 271 cm^{-1} (Table 3.4) that can be attributed to an Au-S vibrational mode (B Varnholt). These results confirm the presence of the triphenylarsoniumpropylthiolate groups on the surface of the AuNPs.

Table 3.4 Position of Au-S band in Raman Spectra of triphenylarsoniumpropylthiolate-capped AuNPs

Sample	Au-S / cm^{-1}	C-H / cm^{-1}
A-Au-Z0.5	266	999.9
A-Au-Z1	271	1000.1
A-Au-Z1.5	259	1000.3
A-Au-Z2	259	998.9

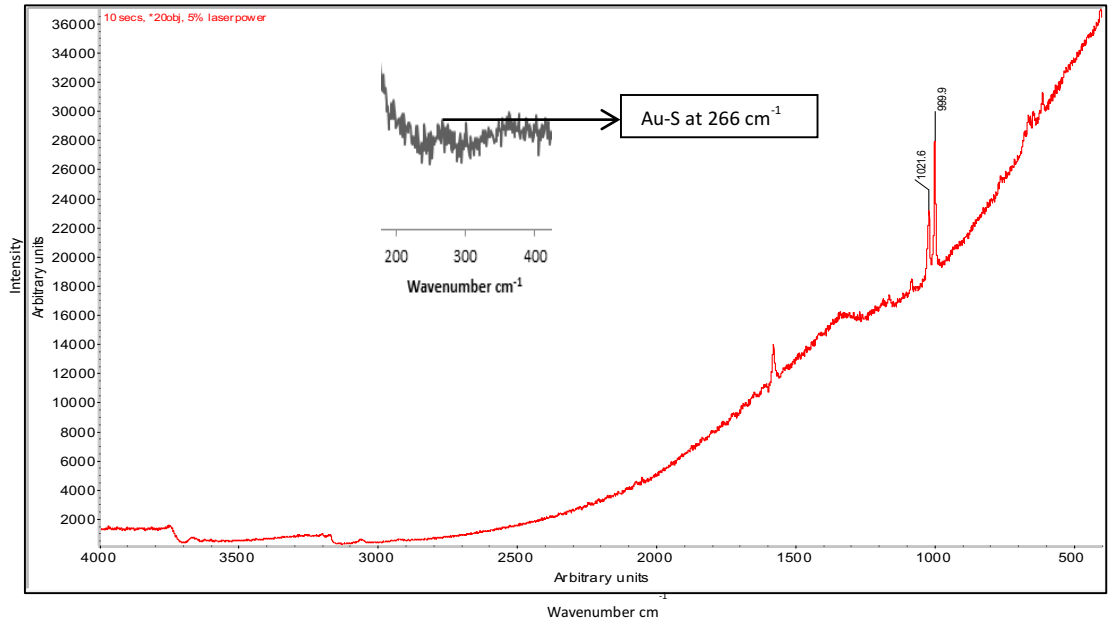

Figure 3.7 Raman spectrum of **A-Au-Z0.5** in region 4000-500cm^{-1}, (Inset) expansion of region 400-200cm^{-1}.

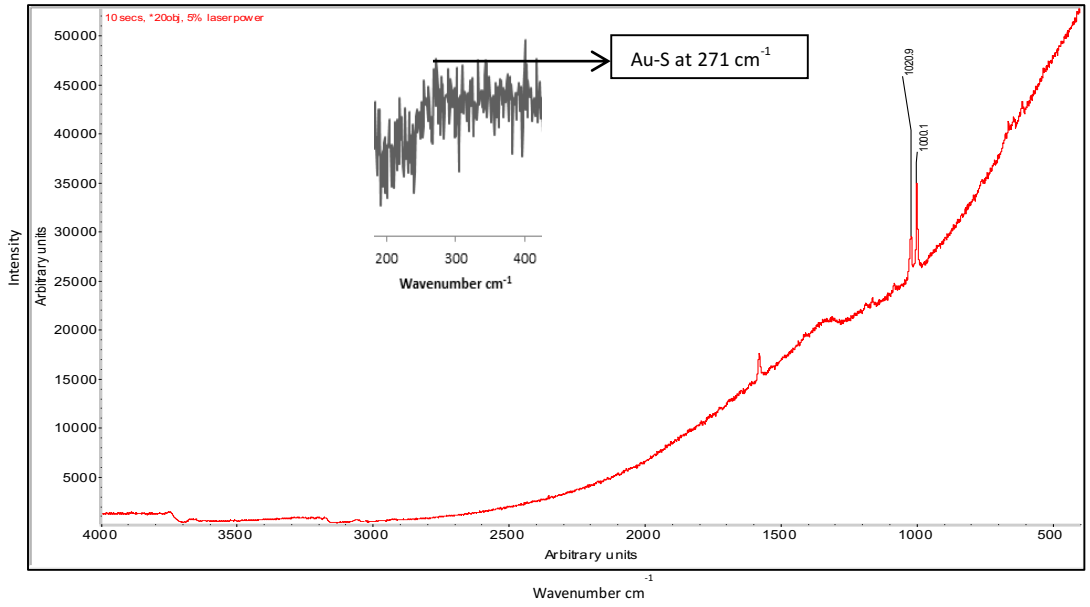

Figure 3.8 Raman spectrum of **A-Au-Z1** in region 4000-500cm^{-1}, (Inset) expansion of region 400-200cm^{-1}.

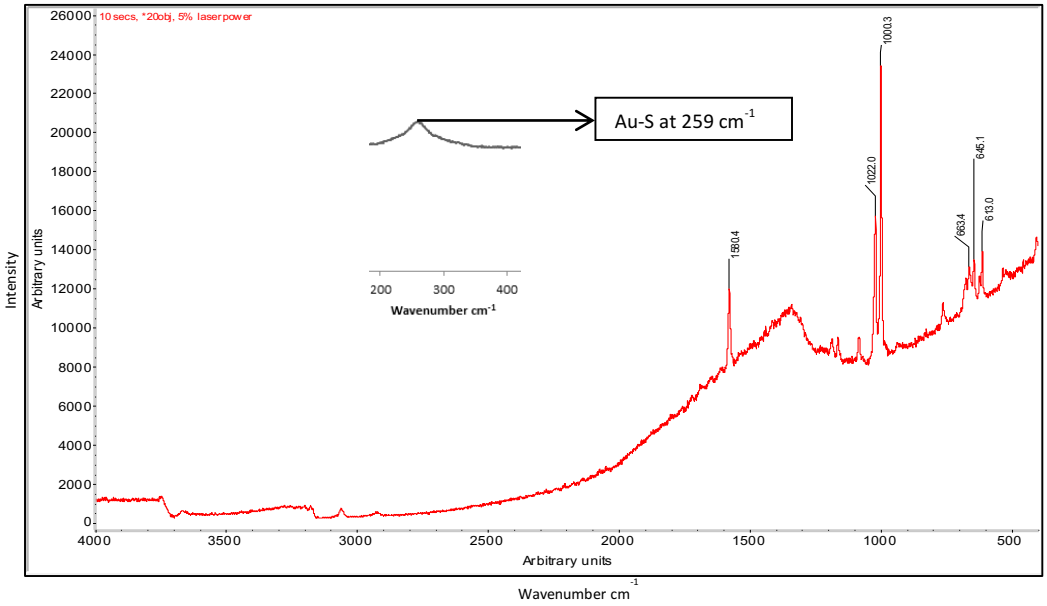

Figure 3.9 Raman spectrum of **A-Au-Z1.5** in region 4000-500cm^{-1}, (Inset) expansion of region 400-200cm^{-1}.

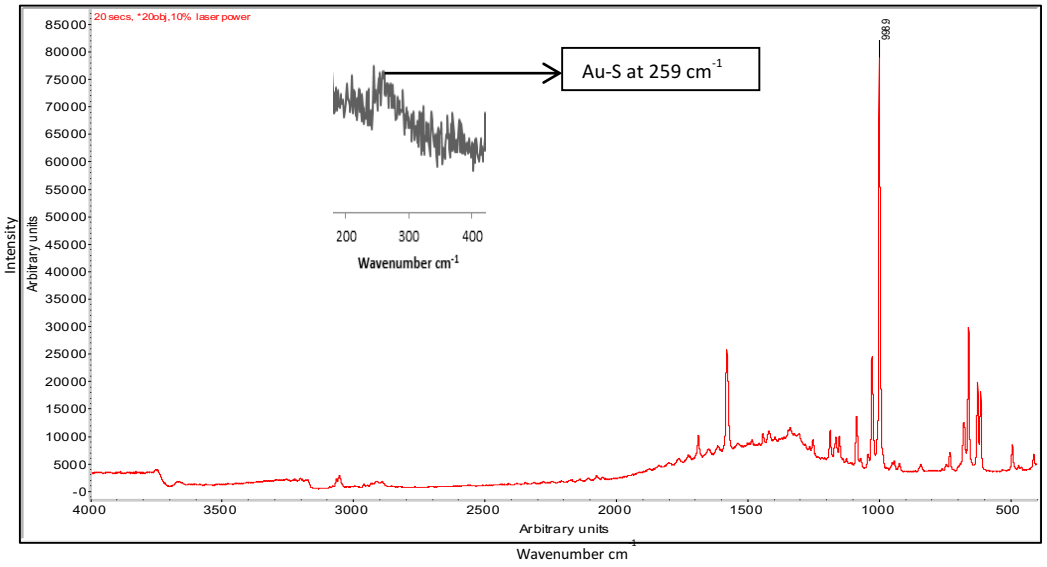

Figure 3.10 Raman spectrum of **A-Au-Z2** in region 4000-500cm^{-1}, (Inset) expansion of region 400-200cm^{-1}.

3.4.2.2 X-Ray Photoelectron Spectroscopy (XPS)

XPS is a powerful tool for understanding the surface analysis of numerous self-assembled monolayer systems and monolayer-protected metal clusters. For these experiments, XPS have been used to understand the nature of the Au-S linkages. XPS can also be used to determine the atomic composition and surface studies for the nanoparticles having surface layers (2-10nm depth) such as for the arsonium functionalized AuNPs (Baer and Engelhead, 2010).

Table 3.5 Summary of gold, sulphur and arsenic XPS binding energies for **triphenylarsonium-functionalized AuNPs**.

Sample	Au:As Ligand ratio	Conditions	XPS Binding Energies (eV)				
			Au		S		As
			$4f_{7/2}$	$4f_{5/2}$	$2p_{3/2}$		$3d_{5/2}$
A-Au-Z2	1:2	As prepared AuNPs	84.14	87.80	162.25	169.52	44.74
A-Au-Z2w	1:2	Sample washed with aqueous KBr before analysis	84.43	88.08	162.15		44.97
A-Au-Z1w	1:1	Sample washed with aqueous KBr before analysis	84.34	87.99	162.33		44.90
A-Au-T2	1:2	As prepared AuNPs	84.00	87.66	163.83		45.01
2	-		-	-	163.34	169.05	44.84
3	-		-	-	164.00		45.05

The data are summarised in Table 3.5. Wide scan spectra of the AuNPs (Figure 3.11) were very similar, showing signals due to gold, sulphur, arsenic, carbon, sodium, oxygen and chlorine. The high resolution Au(4f) spectra of all four samples contain a doublet for Au ($4f_{7/2}$) and Au ($4f_{5/2}$) with binding energies of c.a. 84.0 and 87.5 eV, respectively (Figure

3.12). These values are very similar to those reported for the analogous AuNPs capped with triphenylphosphoniumpropylthiolate ions. For example, phosphonium-AuNPs prepared from the triphenylphosphoniopropylthiosulfate zwitterion (**P-Au-Z2**) displayed Au $4f_{7/2}$ binding energies of 84.0 eV and 87.5 eV, and the phosphonium-AuNPs derived from ω-thioacetylpropyl(triphenyl)phosphonium bromide (**P-Au-Z2)** displayed Au $4f_{7/2}$ binding energies of 84.1 eV and 87.8 eV (Ju-Nam et al., 2012). Furthermore, the data reported here are similar to that reported by Brust (83.8 eV and 87.5 eV) (Brust et al., 1994) Yee (84.2 eV and 87.85 eV) (Yee et al., 2003) for AuNPs capped with dodecanethiol.

The binding energy of Au $4f_{7/2}$ from Au(0) in a metallic gold film is 84 eV, whereas the Au(I) in a gold thiolate has a binding energy of 86 eV and AuNPs that are reported to contain a fraction of their surface atoms in the Au(I) oxidation state show Au $4f_{7/2}$ peak with a binding energy of 84.9 eV (McNeillie et al., 1980). Therefore the Au ($4f_{7/2}$) observed at 84.0 eV in the triphenylarsonium-AuNPs strongly suggests that the bulk of the gold atoms are in the Au(0) oxidation state.

Figure 3.13 shows the high resolution S(2p) XPS spectrum of a freshly prepared sample of AuNP (**A-Au-Z2)** generated using the triphenylarsoniopropylthiosulfate zwitterion **2**. This material displayed two peaks with binding energies of 163.80 eV and 169.52 eV. The peak at 163.80 eV is typical of a thiolate-sulphur bound to gold, which occurs in the range (162.0 to 162.9 eV) (Bourg et al., 2000, Bain et al., 1989). The XPS spectrum of the analogous phosphonium-functionalized AuNPs (**P-Au-Z2**) show a thiolate-sulphur peak with a binding energy of 162.9 eV (Ju-Nam et al., 2012). The peak at 169.52 eV is characteristic of an oxidised sulphur species, such as a sulphonate or sulphite (Ju-Nam et al., 2012). Previous

studies of phosphonium-functionalized AuNPs showed that freshly prepared AuNPs contained only a single sulphur peak in the XPS spectrum, whereas samples that were over six months old showed two peaks, like that of **A-Au-Z2** reported here, with the second peak being due to the presence of oxidised sulphur. Given that the samples of arsonium-functionalized AuNPs analyzed here were freshly prepared, it seemed quite remarkable that the sample had oxidised so quickly. However, the synthetic procedure used to prepare the nanoparticles involves cleavage of the S-S bond in the thiosulfate zwitterion, generating a thiolate anion (which coordinates to the growing gold nanoparticle), and a sulphite anion. Therefore, another possibility was that the peak at 169.52 eV is due to residual sulphite species or the presence of unreacted zwitterion. To test this hypothesis a sample of the AuNPs were prepared and washed three times with a dilute aqueous KBr 10% w/v solution before analysis by XPS. The spectrum of this sample (**A-Au-Z2w**), showed only a single sulphur peak with a binding energy of 163.8 eV, indicating that the peak at 169.52 eV was due to residual SO_3^- ions. Furthermore, the wide angle scan of **(A-Au-Z2W)** also showed the presence of bromine from the bromide ions, with a lower amount of sulphur and oxygen, compared to the original unwashed sample **(A-Au-Z2)**. A sample of AuNPs prepared using a 1:1 ratio of gold salt and zwitterion **2** was prepared and washed with KBr solution (**A-Au-Z1w**), before analysis by XPS. The XPS spectrum of this material contained only a single $S(2p_{3/2})$ signal with a binding energy of 163.40 eV.

The XPS spectrum of a sample of AuNPs prepared from ω-thioacetylpropyl(triphenyl)arsonium bromide salt **3** (**A-Au-T2**) showed only a single $S(2p_{3/2})$ peak with a binding energy of 163.50 eV and no evidence for a peak at *ca.* 169 eV due to oxidised sulphur, providing further evidence that the peak at 169.52 eV in the XPS

spectrum of **A-Au-Z2** is due to residual sulphite. The XPS spectrum of a sample of phosphonium-AuNPs prepared from ω-thioacetylpropyl(triphenyl)phosphonium bromide (**P-Au-T2**) also showed just a single S($2p_{3/2}$) peak with a binding energy of 162.10 eV.[10](Ju-Nam et al., 2012) Gold nanoparticles capped with *n*-tetradecanethioacetate also have a S($2p_{3/2}$) peak of 162.19 eV (Zhang et al., 2009).

The XPS spectrum of the parent arsonium zwitterion **2** displays two S(2p) signals at 163.34 and 167.76 eV (Fig. 3.15), arising from the non-equivalent sulphurs bound to carbon and to oxygen, respectively. This result confirms the cleavage of the sulfur-sulfur bond in the zwitterions during the synthesis with the concomitant expulsion of SO_3^- (or some other sulfur species derived from it), at the ligand/Au interface. The spectrum of the precursor arsonium thioacetate ligand **3** contains a single S($2p_{3/2}$) peak with a binding energy of 161.1 eV, corresponding to a thiolate sulfur.

The high-resolution XPS spectrum of the arsenic component of the functionalized nanoparticles is shown in Figure 3.16. All of the nanoparticle samples, together with precursor ligands **2** and **3**, show a peak with a binding energy *ca* 45 eV that can be attributed to the As ($3d_{5/2}$) electron in an arsenic(V) compound. Although XPS data has been reported for many inorganic arsenic compounds, especially oxides and sulphides and semiconductor materials such as GaAs, there is a paucity of data on organic arsenic derivatives. The data for inorganic species shows that As(V) generally has a peak with a binding energy in the region of 44 - 45 eV and that under X-rays this can degrade forming As(III) species with a binding energy of 43 - 44 eV. For organic derivatives the four-coordinate, As(V) species tetraphenylarsonium cation $[Ph_4As]^+$ has a As (3d) binding energy

of 44.8 eV (Stec et al., 1972), whereas the three-coordinate As(III) species triphenylarsine (Ph_3As) has a As (3d) binding energy of 42.7 eV (Bain et al., 1989).

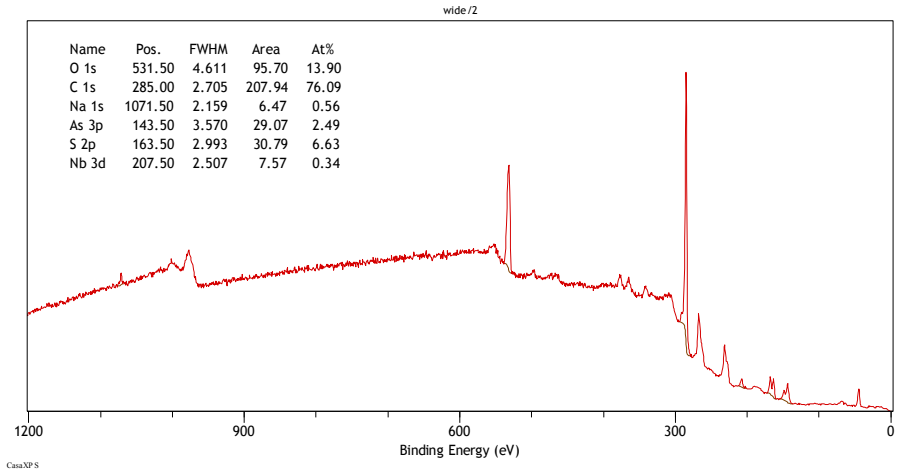

(a)

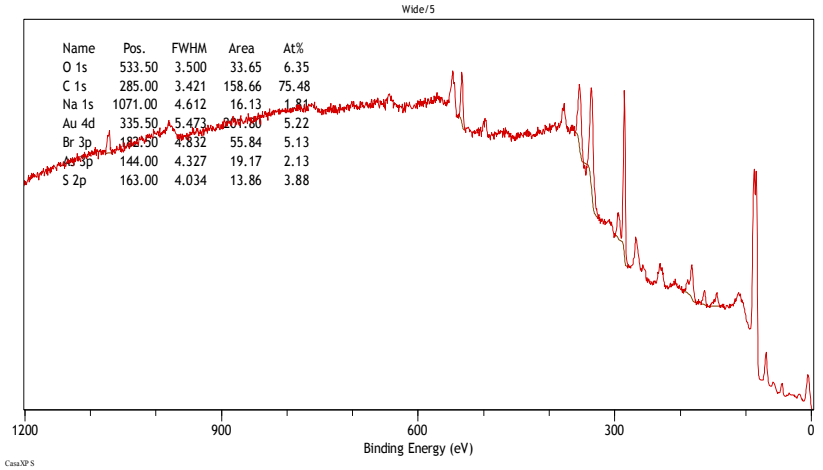

(b)

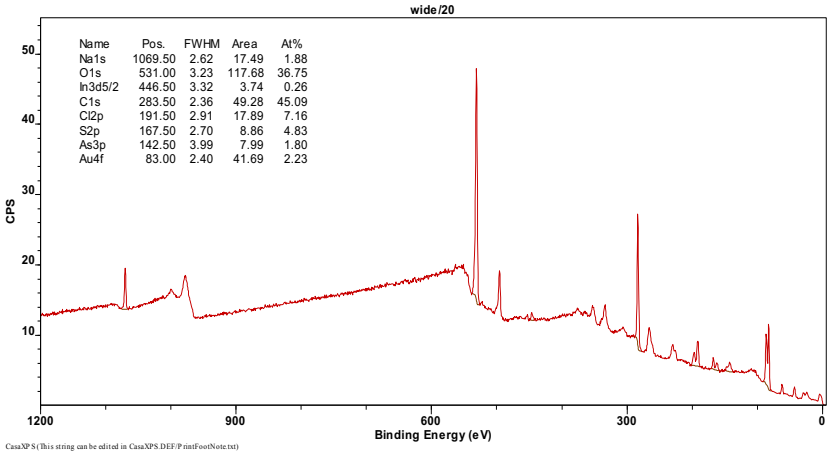

(c)

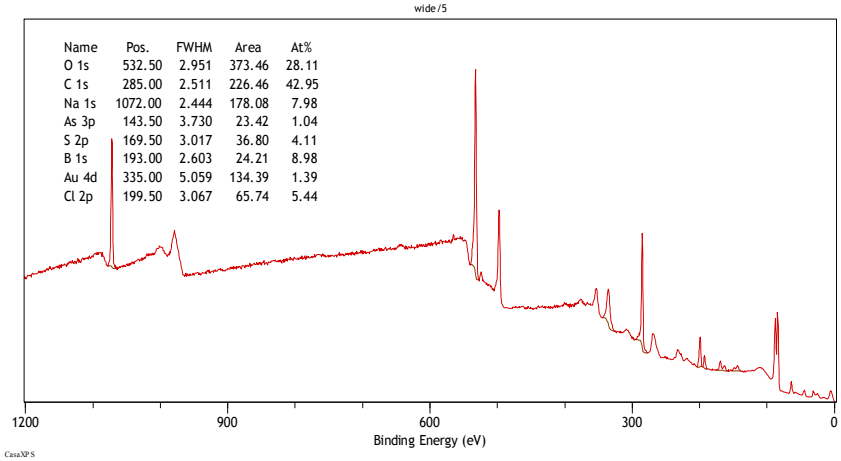

(d)

Figure 3.11 Wide angle XPS spectra of triphenylarsonium-AuNPs (a) **A-Au-Z2** (b) **A-Au-Z2w** (c) **A-Au-Z1w** (d) **A-Au-T2**

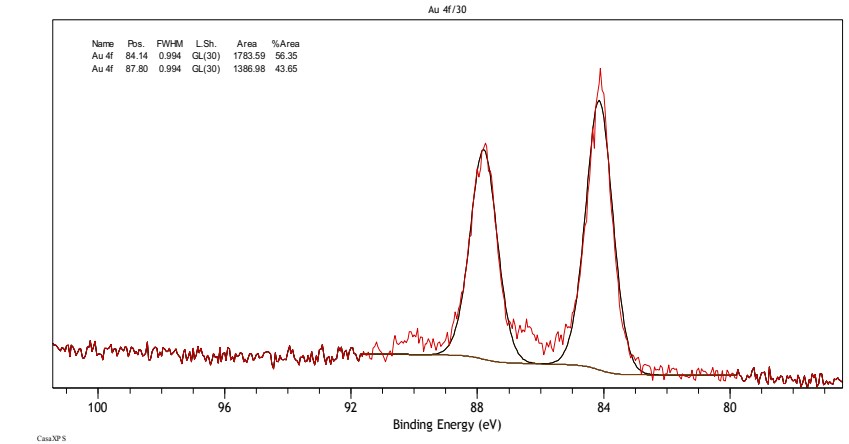

(a)

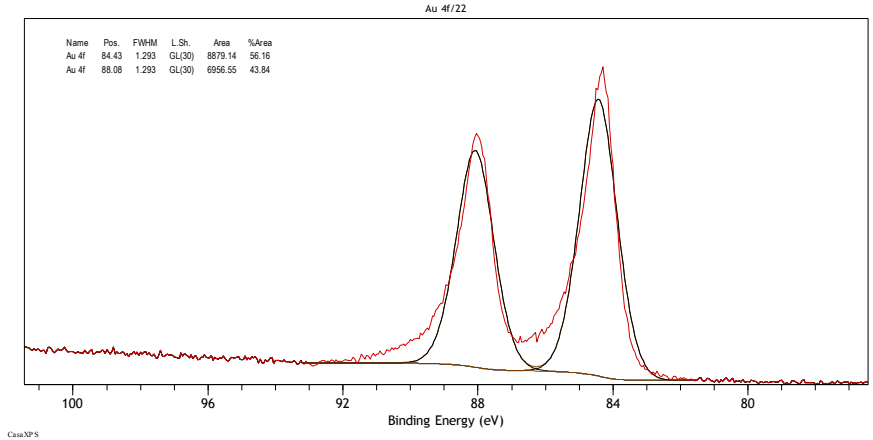

(b)

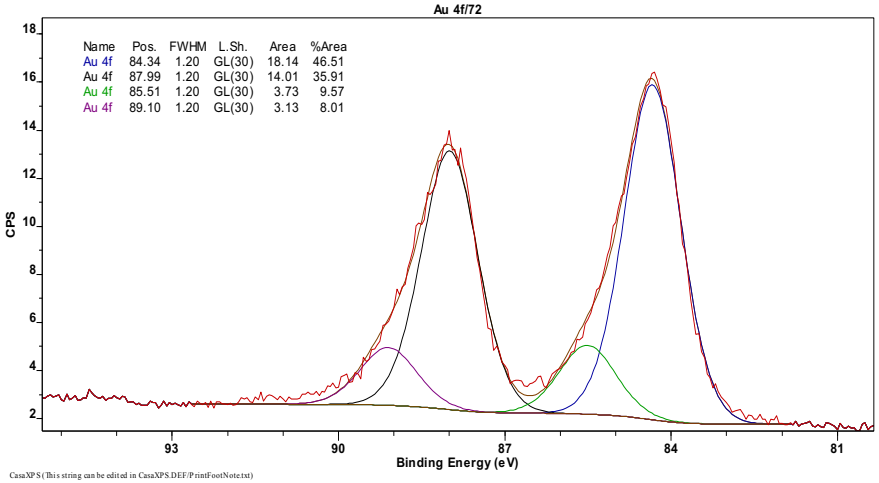

(c)

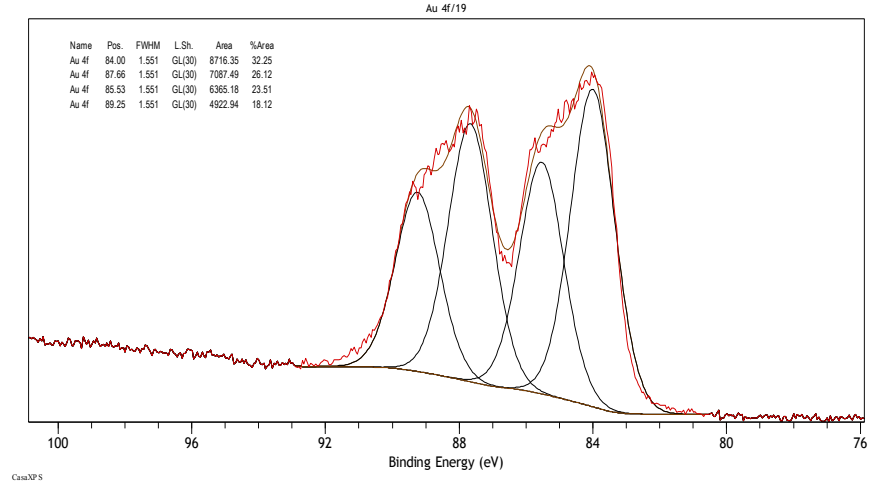

(d)

Figure 3.12 High resolution Au XPS spectra of triphenylarsonium-AuNPs (a) **A-Au-Z2** (b) **A-Au-Z2w** (c) **A-Au-Z1w** (d) **A-Au-T2**

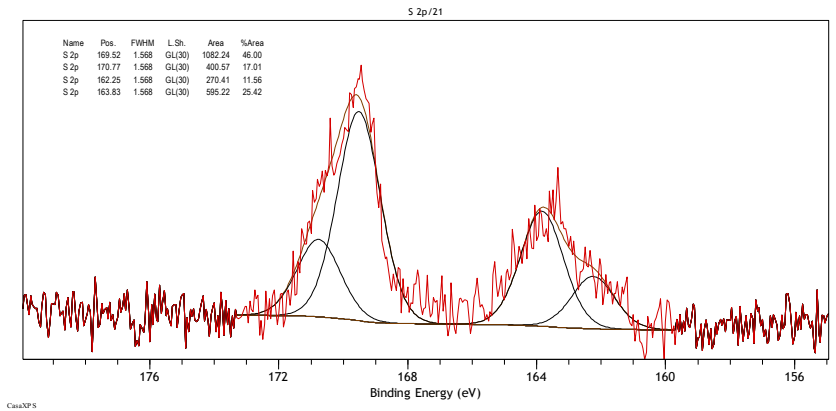

(a)

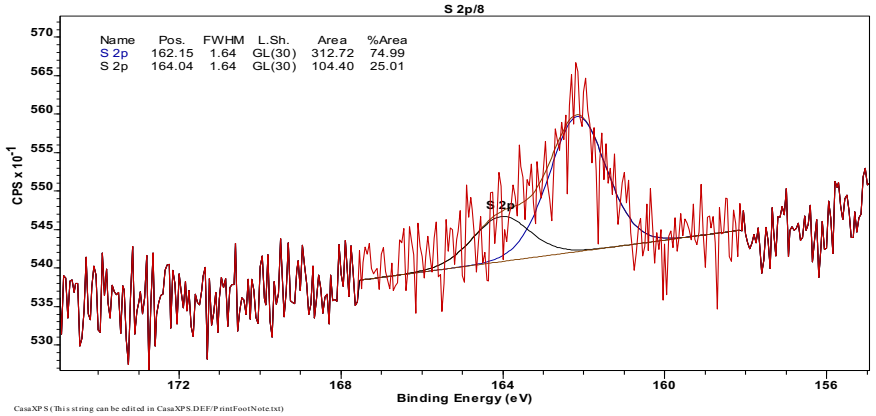

(b)

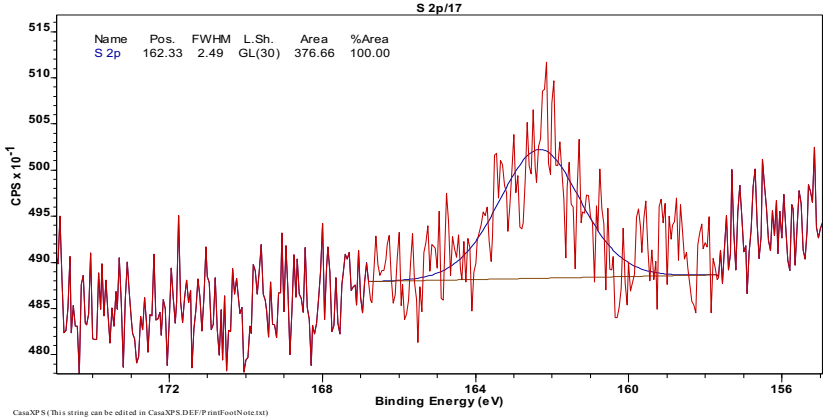

(c)

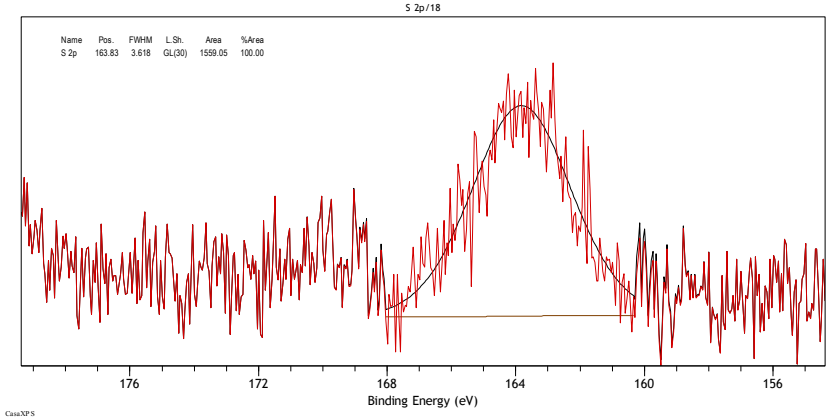

(d)

Figure 3.13 High resolution S ($2p_{3/2}$) XPS spectra of triphenylarsonium-AuNPs (a) **A-Au-Z2** (b) **A-Au-Z2w** (c) **A-Au-Z1w** (d) **A-Au-T2**

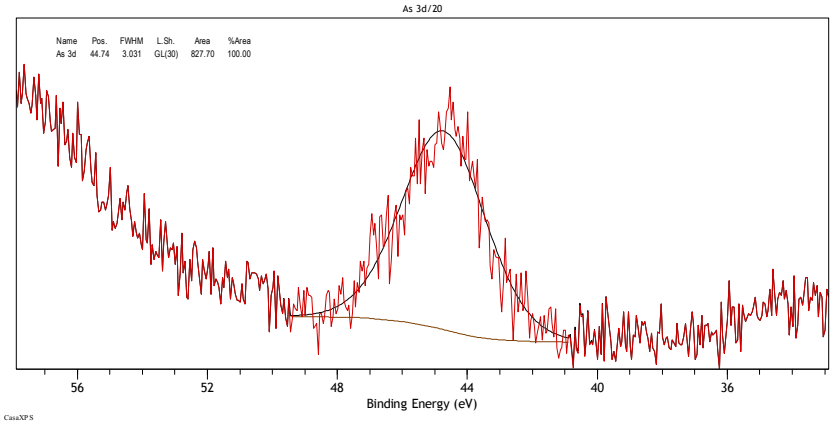

(a)

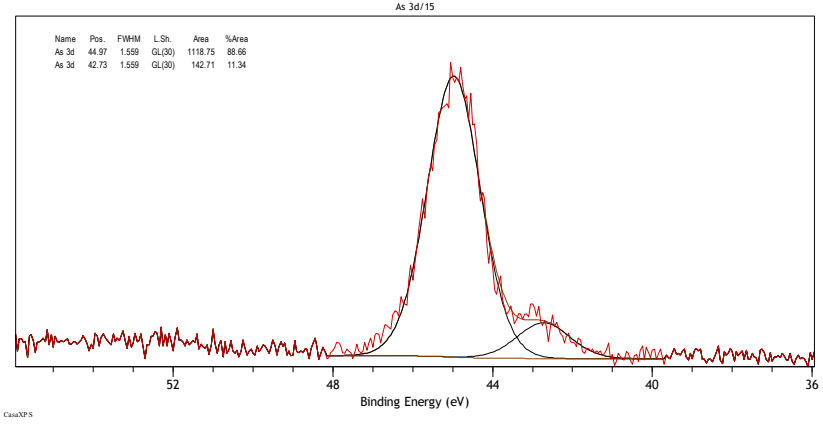

(b)

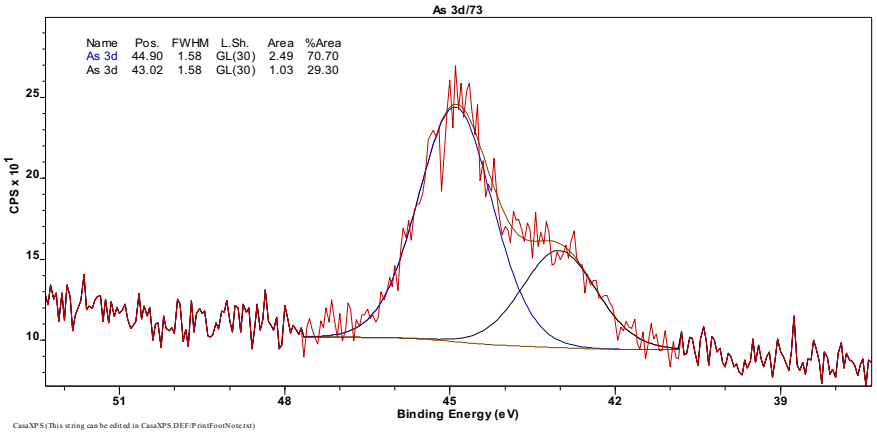

(c)

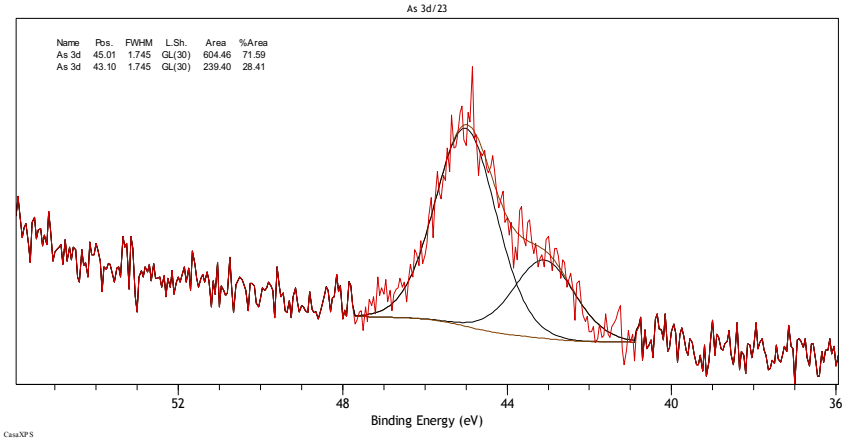

(d)

Figure 3.14 High resolution As (3d) XPS spectra of triphenylarsonium-AuNPs (a) **A-Au-Z2** (b) **A-Au-Z2w** (c) **A-Au-Z1w** (d) **A-Au-T2**

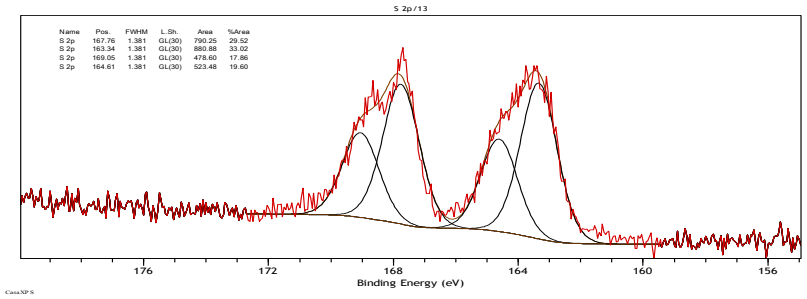

(a)

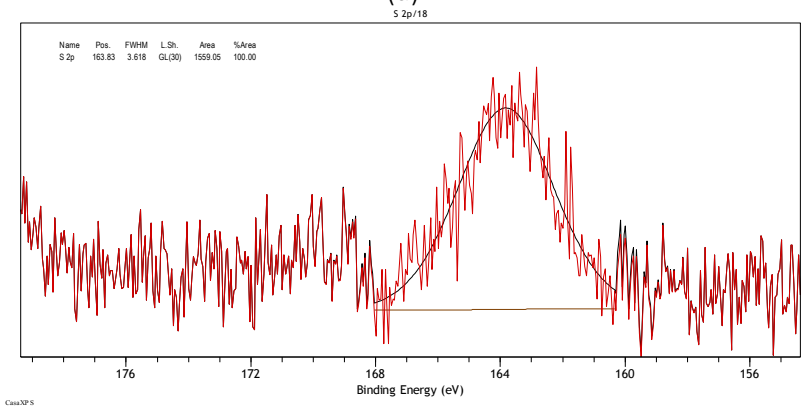

(b)

Figure 3.15 High resolution S XPS spectra of ligands (a) **2** and (b) **3**

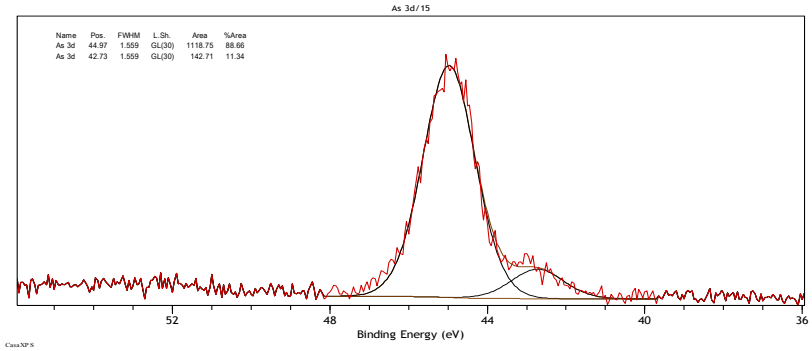

(a)

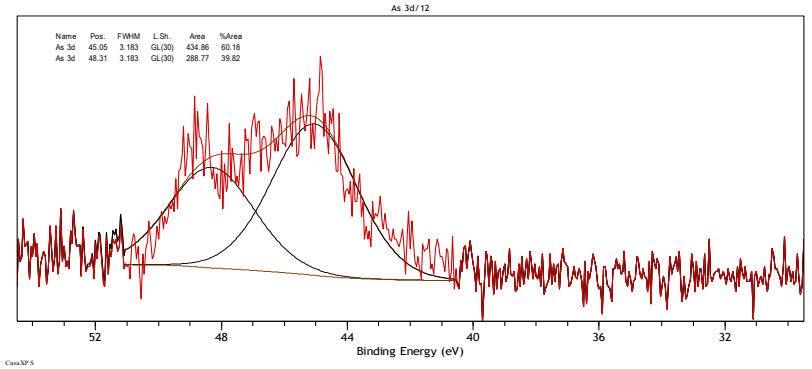

(b)

Figure 3.16 High resolution As (3d) XPS spectra of triphenylarsonium-AuNPs (a) **2** and (b) **3**

3.4.2.3 Transmission Electron Microscopy (TEM)

TEM is routinely used for the characterization of nanoparticles, which provides an image of the gold core and size information (Daniel and Astruc review, 2004). The size and morphology of AuNPs functionalized with different molar ratios of ligand **2** have been determined by TEM. The micrographs were recorded by Prof Alan Reynolds and Dr Jesus Ojeda at the Experimental Techniques Centre, Brunel University or by Paul Allender at the Materials and Engineering Research Institute at Sheffield Hallam University. The images were generated by putting a solution of the AuNPs dispersed in water drop-by-drop onto a carbon-copper grid. To remove the excess water on the grid, a piece of tissue was used and the samples were left overnight so any remaining solvent could evaporate. 1000 mesh copper grid was used for the experiment and the TEM data were obtained using a low voltage (kV) so as to prevent the decomposition of the organic matter, around 1000 nanoparticles were measured to calculate the mean of the particle size. The TEM images are shown in Figure 3.17 and the results summarised in Table 3.6.

Table 3.6 Average particle size of Triphenylarsonium-functionalized AuNPs. Mean particle size was calculated from 1000 nanoparticles.

Sample	Au:As Ligand ratio	Mean Particle size (nm)	Standard deviation
A-Au-Z0.5	1 : 0.5	3.63	1.03
A-Au-Z1	1 : 1	2.86	1.35
A-Au-Z1.5	1 : 1.5	3.84	0.89
A-Au-Z2	1 : 2	2.7	1.02
A-Au-Z2w	1 : 2	1.15	1.46
A-Au-T2	1 : 2	1.28	1.20

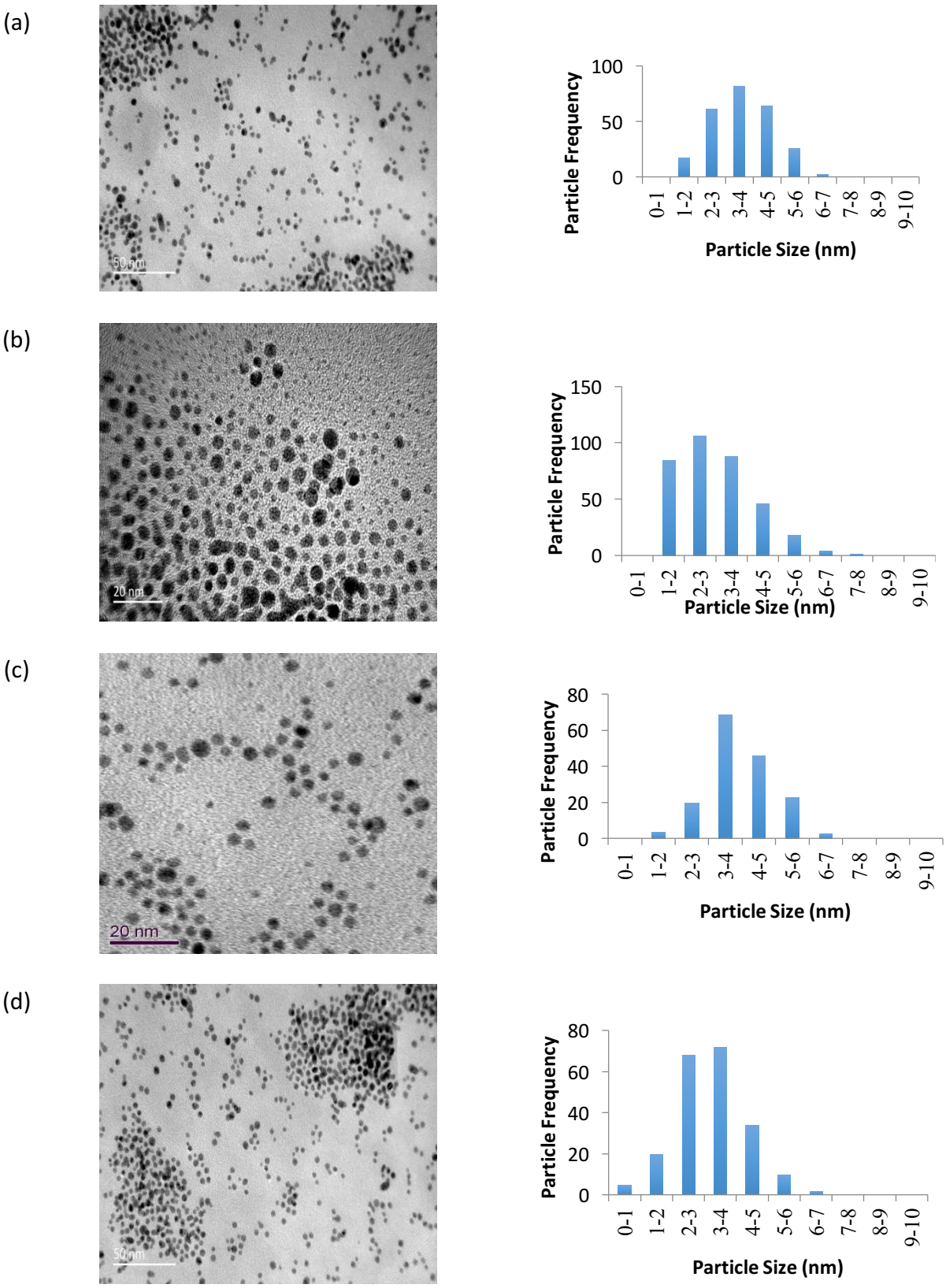

Figure 3.17 TEM micrographs and the core size histogram of arsonium-functionalized AuNPs (a) **A-Au-Z0.5,** (b) **A-Au-Z1,** (c) **A-Au-Z1.5 and** (d) **A-Au-Z2**.

The TEM images revealed the particles to have spherical shape. The particle size and polydispersity were similar, irrespective of the amount of starting ligand present. Furthermore, the particle size is very similar to that of the analogous triphenylphosphonium-functionalized AuNPs (**P-Au-Z2**), which have a mean diameter of 3nm ± 1.2nm (Ju-Nam et al., 2012). The TEM micrograph of the washed sample **A-Au-T2w** (Figure 3.18) shows that the washing process has minimal effect on the size or shape of the gold nanoparticles.

The morphology of the AuNPs derived from ω-thioacetylpropyl(triphenyl)arsonium bromide salt **3**, **A-Au-T2** (Figure 3.19) has also been studied showing that the particles derived from this ligand are slightly larger, and have a broader particle size distribution, compared to the nanoparticles synthesised from zwitterion **2**. This observation is in agreement with previous work on triphenylphosphonium-functionalized gold nanoparticles which showed that those prepared from ω-thioacetylpropyl(triphenyl)arsonium bromide salt are larger, and have a broader particle size distribution, than those obtained from the triphenylphosphoniumpropylthiosulfate zwitterion. These differences in size and particle size distribution can be explained on the basis of the differing passivation kinetics of the two types of ligand. (Lohse et al., 2010, Fealy et al., 2011, Pillai and Freund., 2011, Singh et al., 2010, Zhang et al., 2009). The first stage of the synthesis should be adsorption of the ligand on the surface of the growing particles and the thioacetate might be expected to be a more weakly binding ligand than the thiosulfate. Secondly, transformation of the thiosulfate or thioacetate to the thiolate occurs. The mechanism of this step in our system is unclear. Studies into the formation of monolayers on gold surfaces from alkylthiosulfates

show hydrolysis by trace amounts of water present in the solvent to be crucial. (Fealy et al., 2011, Pillai and Freund., 2011). The triphenylarsonium-AuNPs reported here were prepared in a two-phase water/dichloromethane mixture, *i.e.* with an excess of water. However, the possibility that the growing gold nanoparticles and/or the reducing agent are involved in the cleavage of the thiosulfate S–S or thioacetate S–C bonds cannot be excluded. It would appear that the cleavage step is slower for the thioacetate than for the thiosulfate and so results in slower monolayer formation and hence a larger size particle and a broader particle size distribution.

It was noteworthy that the ESI-MS spectrum of **A-AuT2** showed no evidence of the parent thioacetate salt **3**, whereas that of the related **P-AuT2** did indicate the presence of unreacted ω-thioacetylalkyl(triphenyl) phosphoniopropyl ions (Chen PhD thesis, 2014 and Ju-Nam et al., 2012).

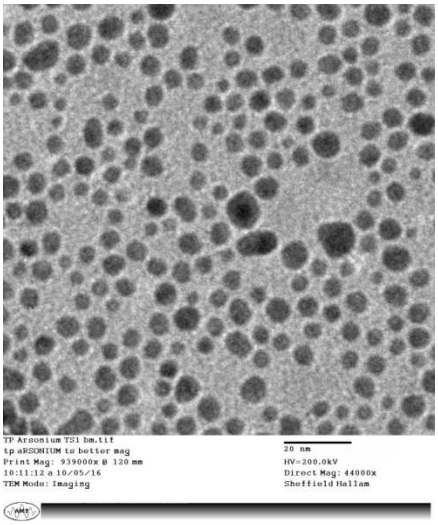

Figure 3.18 TEM micrograph and the core size histogram of the washed arsonium-functionalized AuNP sample **A-Au-Z2w**.

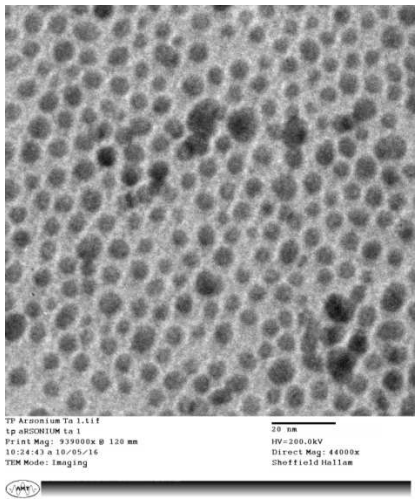

Figure 3.19 TEM micrograph and the core size histogram of the arsonium-functionalized AuNP **A-Au-T2**, derived from ω-thioacetylpropyl(triphenyl) arsonium bromide salt **3**

3.5 Conclusion

The results presented in this chapter confirmed the hypothesis that triphenylarsoniopropylthiosulfate (**2**) and ω-thioacetylpropyl(triphenyl)arsonium bromide salt (**3**) can be used to prepare cationic, triphenylarsonium-functionalized gold nanoparticles. The precursor arsonium compounds **2** and **3** have been characterized thoroughly using a range of spectroscopic techniques and by single-crystal X-ray crystallography.

The triphenylarsonium-functionalized gold nanoparticles have been characterized by TEM and XPS, and have been found to possess an average core size of 2.7-3.84 nm.

3B) The synthesis, characterisation and biological properties of the (methoxy-phenyl) phosphoniopropylthiosulfate zwitterions and ω-thioacetylpropyl (methoxyphenyl) phosphonium salts.

3.6 Methoxyphenyl phosphonium substituents

Previous work has shown that alkylthiosulfate zwitterion and alkylthioacetate salt derivatives of triphenylphosphine, and other trialkyl- and triaryl-phosphines, can be used as precursors for the formation of triphenylphosphonium-functionalized gold nanoparticles (Ju-nam et al., 2006; Ju-nam et al., 2012; Yang et al., 2015; Ju-nam et al., 2007; Ju-nam et al., 2015). Although the triphenylphosphonium-functionalized nanoparticles are soluble in water and biological media, and are taken-up by cells (Ju-nam et al., 2012), the parent triphenylphosphoniumalkylthiosulfate zwitterions are insoluble in aqueous media (Chen PhD thesis, 2014) This observation has prompted us to investigate alternative triarylphosphonium groups in an attempt to improve the aqueous solubility of the zwitterions.

Previous work by Liu and coworkers (Kim et al., 2008) showed that tri-(4-methoxyphenyl) - and tris (2, 4, 6-trimethoxyphenyl) phosphonium compounds can be used to functionalize macrocyclic derivatives **1** and **2**, that are soluble in biological media and which are readily taken up by cells. Their results showed that both the 4-methoxy- and the 2,4,6-trimethoxy-compounds are more effective at mitochondria-targeting than the analogous triphenylphosphine compound. Furthermore, compound **1** is more effective at mitochondria-targeting than the 2,4,6-trimethoxy species **2**.

Another biological application of tris(2,4,6-trimethoxyphenyl)phosphonium compounds such as the *S*-pentafluorophenylacetate (**3**) (Huang et al., 1997, Barry et al., 2003, Huang et al., 1999, Sadagopan et al., 2000, Shen et al., 2000) and alkylcarboxylates (**4**) (Leavens et al., 2002) is to derivatise a range of compounds including small molecules, such as amines

and carboxylic acids, alcohols, aldehydes and ketones, and large biomolecules such as proteins and peptides, to enhance their detection by mass spectrometry.

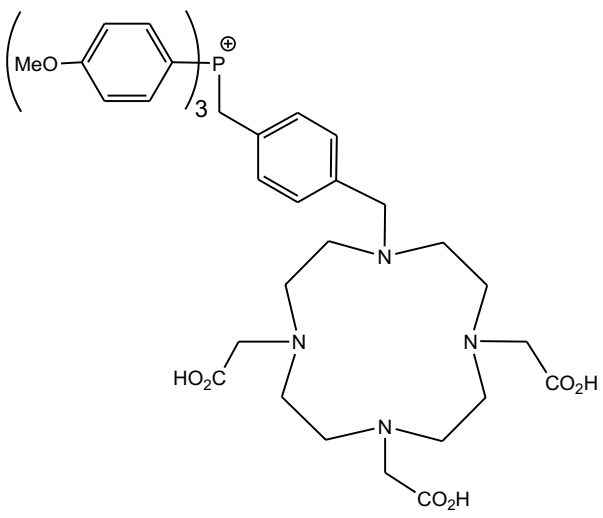

1

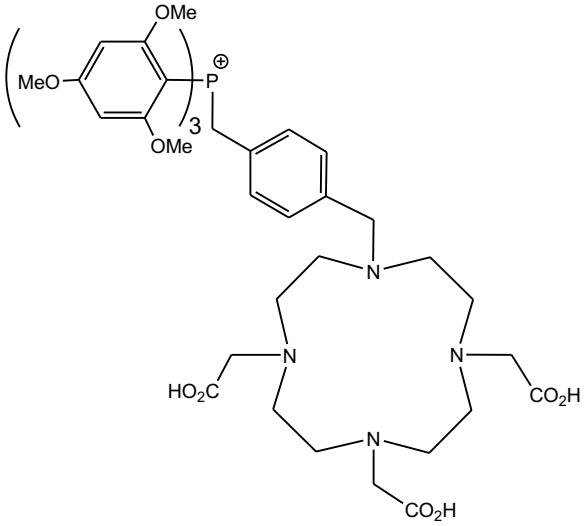

2

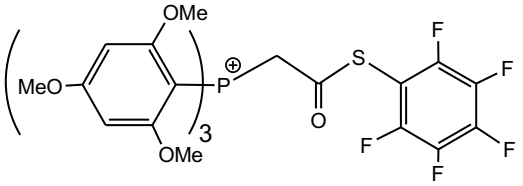

3

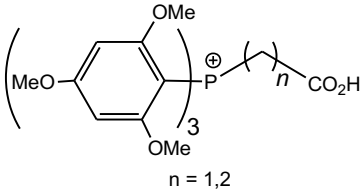

4

Tris (2, 4, 6-trimethoxyphenyl) phosphine is a very unusual tertiary aryl phosphine (Wada et al., 1984). The presence of the methoxy groups increases the basicity of the phosphine and also increases the steric bulk of the compound (Dunbar et al., 1994). Tris(2,6-dimethoxyphenyl)phosphine has a lower basicity, but similar steric properties to tris(2,4,6-trimethoxyphenyl)-phosphine, whereas tris(4-methoxyphenyl)phosphine has a lower basicity and lower steric bulk than tris(2,4,6-trimethoxyphenyl)phosphine. The aim of this chapter is to investigate the synthesis and biological properties of a series of alkylthiosulfate zwitterion and alkylthioacetate salt derivatives of methoxy-phenyl phosphines.

3.7 Material and methods

3.7.1 Chemicals

All chemicals were used as received; tris(2,4,6-trimethoxyphenyl)phosphine and tris(2,4 dimethoxyphenyl)phosphine and tris(4-methoxyphosphine) were purchased from Sigma Aldrich, UK and used without any further treatment. 1, 3- Dibromopropane was purchased from Acros Organics, UK. Potassium thioacetate ($KSCOCH_3$), sodium thiosulfate ($Na_2S_2O_3$), Potassium bromide (KBr), gold(III) chloride trihydrate, hydrobromic acid (HBr), magnesium sulfate ($MgSO_4$), deuterated dichloromethane, chloroform and ICP Au standard were purchased from Sigma-Aldrich (Gillingham, Dorset, UK).

3.7.2 Methods

3.7.2.1 Cytotoxicity assay

Cytotoxicity was assessed using a CellTiter-Glo luminescent cell viability assay kit (Promega Corporation, Southampton, Hamshire, UK).

PC3 cells were seeded in opaque-walled 96 well plates at a density of 10,000 cells/well and allowed to adhere overnight. Cells were subsequently treated with the corresponding phosphonium ligand (0-1000μm) for 24, 48, 72 hours. After each incubation period, cell viability was measured according to the manufacturer's instructions. In brief, plates were equilibrated at room temperature for 30 mins, 100μL of assay reagent was added to each well, placed on an orbital shaker for 2mins, left to stand at room temperature for 10 minutes and read on a Wallac Victor2 1420 multilabel counter (PerkinElmer, Cambridge, Cambridgeshire, UK).

Cytotoxicity studies were also done to assess IC_{50} using 3-(4,5-dimethyltiazol-2-yl)-2,5-diphenyltetrazolium bromide (MTT) assay. Cells were seeded in a 96 well plate with the corresponding ligand (0-1000μm) for 24, 48, 72 hours. An MTT mixture was added to each well to give a final concentration of 0.3mg/mL MTT. Cells were incubated with MTT for 3-4 hours at 37 ^{o}C. The supernatant liquid was then removed and DMSO was added to read the absorbance at 570nm.

All plates contain control wells and all measurements were performed in quadruplicates, three independent experiments were conducted (n=12). Data are expressed as a percentage of live cells normalized to control, the average, standard deviation and IC_{50} values were plotted and calculated using GraphPad Prism (GraphPad software, La Jolla, California, USA).

3.8 Results and Discussion

The established method for preparing triarylphosphonioalkyl thiosulfate zwitterions, and the associated phosphonioalkyl thioacetate salts is to reflux the parent tertiary phosphine with a bromoalcohol, such as bromopropanol, as shown in scheme 1. The resulting (3-hydroxypropyl) triarylphosphonium bromide salt is then refluxed with hydrobromic acid to generate a (3-bromopropyl) triarylphosphonium bromide that can be converted into the alkylthiosulfate zwitterion or the thioacetate salt. Unfortunately, this synthetic route is not possible for methoxyphenyl-phosphines because the hydrobromic acid used in the second step preferentially attacks the ether substituents. Consequently, an alternative route has been developed, shown in scheme 1. This involves treating the methoxyphenyl phosphine with an excess of α,ω-dibromoalkane, such as 1,3-dibromopropane. This leads directly to

the (3-bromopropyl) methoxyphenylphosphonium bromide that can be converted into the alkylthiosulfate zwitterion or the thioacetate salt by refluxing with sodium thiosulfate or potassium thioacetate respectively. The reaction leads to good yields of the phosphonium compounds although care has to be exercised in the initial step to avoid the methoxyphenyl phosphine reacting with both ends of the α,ω-dibromoalkane. This is done by using a significant excess of the dibromoalkane and adding the methoxyphenylphosphine in small amounts over an extended period of time.

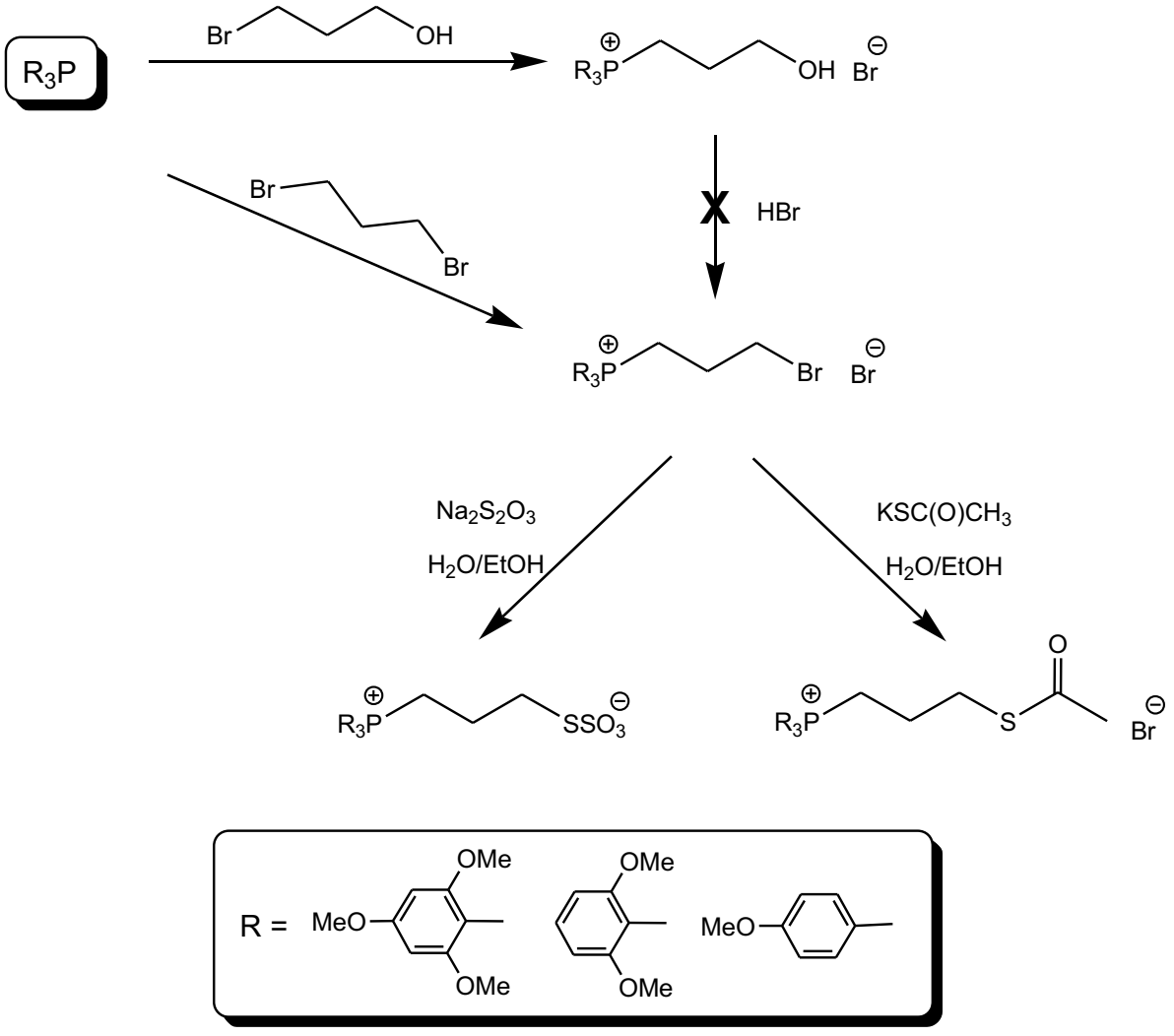

Scheme 1. Synthetic procedures employed in this study.

The structures of the compounds prepared in this study, their names and numbering, are shown below. Regarding the length of the alkyl chain in the phosphonioalkylthiosulfate zwitterions, and ω-thioacetylalkylphosphonium salts, previous studies have shown that a propyl chain is the ideal length. Longer alkyl chains tend to produce compounds that form as waxy solids or oils that are difficult to handle. Shorter alkyl chains would be less useful for forming functionalized nanoparticles. Therefore, in this study we have focused on the propyl derivatives.

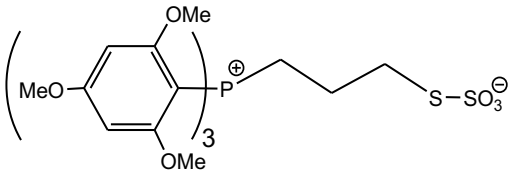

5
tris(2,4,6-trimethoxyphenyl)-phosphoniopropylthiosulfate

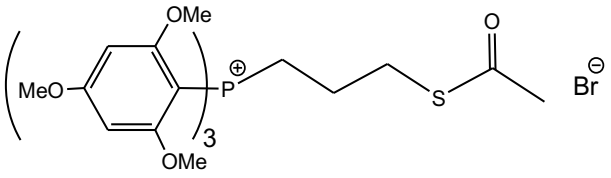

8
ω-thioacetylpropyltris(2,4,6-trimethoxyphenyl)phosphonium bromide

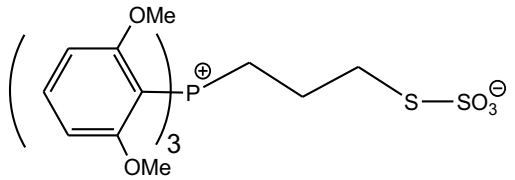

6
tris(2,6-dimethoxyphenyl)-phosphoniopropylthiosulfate

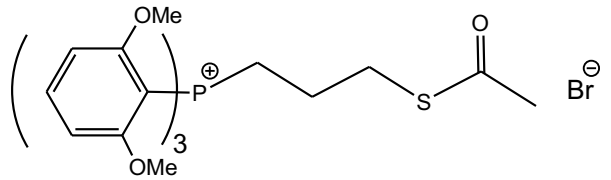

9
ω-thioacetylpropyltri(2,6-dimethoxyphenyl)phosphonium bromide

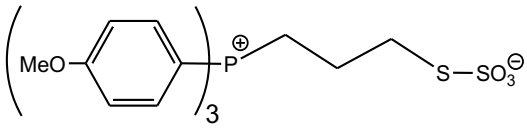

7
tri(4-methoxyphenyl)-phosphoniopropylthiosulfate

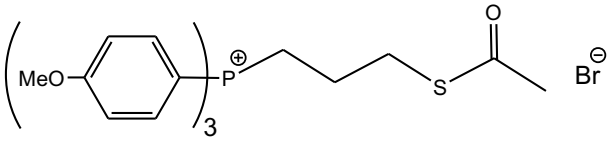

10
ω-thioacetylpropyltri(4-methoxyphenyl)phosphonium bromide

3.9 Synthesis and Spectroscopic Characterisation of 5 -10

All six compounds were prepared in a similar manner, as exemplified by the preparation of compounds **5** and **8**.

Tris(2,4,6-trimethoxyphenyl)phosphine (1.0g, 1.878 x 10^{-4} mol), dissolved in acetonitrile (20 mL), was added dropwise to a 1,3-dibromopropane (5 mL, 1.245 x 10^{-2} mol) under a nitrogen atmosphere. The mixture was refluxed overnight. The product, 3-bromopropyl[tris(2,4,6-trimethoxyphenyl)]phosphonium bromide was isolated by diluting the reaction mixture with deionised water (20mL) followed by liquid-liquid extraction using dichloromethane (3 x 10 ml). The dichloromethane extracts were combined, dried over $MgSO_4$, and the solvent removed by rotary evaporation yielding the product as a white solid. To produce zwitterion **5**, 3-bromopropyl tris(2,4,6-trimethoxyphenyl)phosphonium bromide (0.250 g, 3.82 x 10^{-4} mol) and $Na_2S_2O_3$ (0.212 g, 8.56 x 10^{-4} mol) were heated under reflux in aqueous ethanol under a nitrogen atmosphere. The thioacetate salt **8** was produced by refluxing 3-bromopropyl tris(2,4,6-trimethoxyphenyl)phosphonium bromide (0.250 g, 3.82 x 10^{-4} mol) and $KSC(O)CH_3$ (0.098 g, 8.56 x 10^{-4} mol) in aqueous ethanol. Both compounds were isolated from the reaction mixtures by extraction with dichloromethane (3 x 20 mL). Purification of the products, which form as white microcrystalline powders, was achieved by triturating with diethyl ether and recrystallising from dichloromethane/diethyl ether. The progress of all of the reactions was monitored by TLC using a mobile phase of 80% dichloromethane : 20% methanol.

Tris(2,4,6-trimethoxyphenyl)- phosphoniopropylthiosulfate **(5)**

White solid, M.P. - 218° Elemental Analysis: found: C, 52.76%; H, 5.86%; S, 9.29% requires: C, 52.47%; H, 5.67%; S 9.30%. ^{1}H NMR**:** δ 2.3 (2H, m), 3.1 (2H, t), 3.8 (2H,m), 7.3–7.6 (15H, m) ppm. ^{31}P NMR ($CDCl_3$) = 5.24 ppm ^{31}P NMR ($CDCl_3$) = 2.3(2H, m). IR υ_{max}/cm^{-1} = 2912 (CH), 1483, 1438, 1209 (SO), 1082, 1010 (SO), 744, 688, 623, 523, 466. ESI-MS**:** 686.4 $[M]^+$, 708.86 $[M+Na^+]$

Tris(2,6-dimethoxyphenyl)- phosphoniopropylthiosulfate **(6)**

White solid, M.P. = 237° Elemental Analysis: found: C, 52.42%; H, 5.51%; S 10.19%, requires: C, 52.34%; H, 5.53%; S 10.33%. ^{1}H NMR ($CDCl_3$)**:** δ 2.2 (2H, m), 3.1 (2H, t), 3.5 (2H,m), 7.2–7.5 (15H, m) ppm. ^{31}P NMR ($CDCl_3$) = 7.54 ppm. IR υ_{max}/cm^{-1} = 2912 (CH), 1483, 1438, 1209 (SO), 1082, 1010 (SO), 744, 688, 623, 523, 466. ESI-MS**:** 577.4 $[M]^+$, 619.33 $[M+Na^+]$

Tri(4-methoxyphenyl)- phosphoniopropylthiosulfate **(7)**

White solid, M.P. = 195° Elemental Analysis: found: C, 58.11%; H, 5.64% ; S 10.29%, requires: C, 57.01%; H, 5.33%; S 10.62%. ^{1}H NMR**:** δ 2.3 (2H, m), 3.2 (2H, t), 3.6 (2H,m), 7.6–7.9 (15H, m) ppm. ^{31}P NMR ($CDCl_3$) = 21.28 ppm. IR υ_{max}/cm^{-1} = 2912 (CH), 1483, 1438, 1209 (SO), 1082, 1010 (SO), 744, 688, 623, 523, 466. ESI-MS**:** 507.2 $[M]^+$, 529.2 $[M+Na^+]$

ω-thioacetylpropyltris(2,4,6-trimethoxyphenyl)phosphonium bromide **(8)**

White solid, M.P. = 243°, Elemental Analysis: found: C, 53.83%; H, 5.62%; S 5.03%, requires: C, 53.62%; H, 5.54%; S 5.03%. ^{1}H NMR ($CDCl_3$)**:** δ 2.4 (2H, m), 3.1 (2H, t), 3.3 (2H,m), 7.1–7.4 (15H, m) ppm. ^{31}P NMR ($CDCl_3$) = 5.27 ppm ^{31}P NMR ($CDCl_3$) = 2.4(2H, m). IR υ_{max}/cm^{-1} = 2912 (CH), 1483, 1438, 1209 (SO), 1082, 1010 (SO), 744, 688, 623, 523, 466. ESI-MS**:** 649.33 $[M]^+$, 650.38 $[M+H^+]$

ω-thioacetylpropyltri(2,6-dimethoxyphenyl)phosphonium bromide **(9)**

White solid, M.P. = 226° Elemental Analysis: found: C, 54.31%; H, 5.90%; S 4.98%, requires: C, 54.46%; H, 5.63%; S 5.00%. ^{1}H NMR**:** δ 2.2 (2H, m), 3.3 (2H, t), 3.5 (2H,m), 7.5–7.8 (15H, m) ppm. ^{31}P NMR ($CDCl_3$) = 7.31 ppm. IR υ_{max}/cm^{-1} = 2912 (CH), 1483, 1438, 1209 (SO), 1082, 1010 (SO), 744, 688, 623, 523, 466. ESI-MS**:** 559.37 $[M]^+$, 560.38 $[M+H^+]$

ω-thioacetylpropyltri(4-methoxyphenyl)phosphonium bromide **(10)**

White solid, M.P. = 207°**,** Elemental Analysis: found: C, 57.60%; H, 5.53%; S 5.88%, requires: C, 56.83%; H, 5.28%; S 5.82%. ^{1}H NMR ($CDCl_3$)**:** δ 2.3 (2H, m), 3.2 (2H, t), 3.6 (2H,m), 7.6–7.9 (15H, m) ppm. ^{31}P NMR ($CDCl_3$) = 21.33 ppm. IR υ_{max}/cm^{-1} = 2912 (CH), 1483, 1438, 1209 (SO), 1082, 1010 (SO), 744, 688, 623, 523, 466. ESI-MS**:** 469.34 $[M]^+$, 471.35 $[M+H^+]$.

3.9.1 Single Crystal X-ray Analysis of tris(2,4,6-trimethoxyphenyl) phosphoniopropylthiosulfate

Single crystals of **5** were grown by slow diffusion of diethyl ether into dichloromethane solution of the compound, resulting in the formation of colorless crystals. The crystals were sent for full structure analysis at the EPSRC X-ray Crystallography Service at the University of Southampton. The molecular structure of **5** is shown in Figure 3.20 and selected bond lengths and angles in Table 3.7. The detailed crystallographic report on compound **5** is presented in Appendix 1.

The Bricklebank group has previously reported the structure of the triphenylphosphoniopropylthiosulfate zwitterion (**11**) (Ju-Nam et al., 2006), together with those of the tri(4-fluorophenyl)phosphoniopropylthiosulfate, (Y-S Chen et al., 2017) and tributylphosphoniothiosulfate (**12**) zwitterions (Ju-Nam et al., 2006). The only other crystallographically-characterized thiosulfate zwitterions are the ammonium derivative *S*-[4-(trimethylammonio)phenyl]thiosulfate (**13**), (J-X Chen et al., 2004) and the triphenylarsoniopropylthiosulfate zwitterion described in chapter 3A.

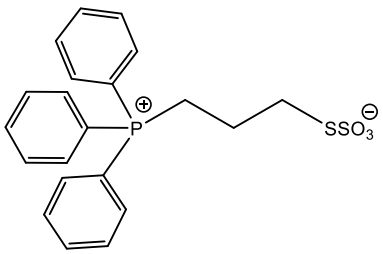

11

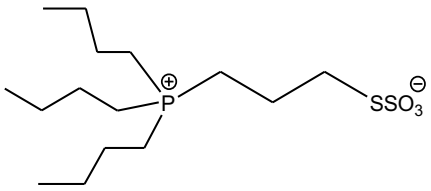

12

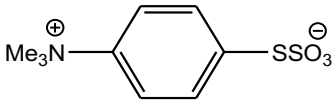

13

The asymmetric unit of **5** contains two independent molecules. The molecule containing atoms P1, S1 and S2 is referred to as **5A**, and that containing atoms P41, S41 and S42 is **5B**. The structure of **5** is highly disordered. This is not unusual for derivatives of tris(2,4,6-

trimethoxyphenyl)phosphine.

Both **5A** and **5B** display the expected tetrahedral geometry around the phosphorus atoms with a mean C-P-C bond angle of 109.2^{o} in 5A and 108.9^{o}. The corresponding values for the triphenyl and tributyl analogues **11** and **12** are 109.47(11)^{o} and 109.47(17)^{o} respectively. The bond lengths and angles in the aryl rings are unremarkable and are similar to those in the parent phosphine, [2,4, 6-$(MeO)_3C_6H_2]_3P$.

The S-O bonds in the thiosulfate group of **5** are all similar, with a mean lengths of 1.429(5)Å and 1.412(10)Å in **5A** and **5B** respectively, [*c.f.* 1.4478(19) Å in **11** and 1.440(3) Å in **12**],indicative of multiple bond character. The S-S bond lengths [2.059(3)Å in **5A** and 2.102(6)Å in **5B**], are slightly shorter than that of **11** [2.1117(9) Å], and similar to that in **12** [2.1030(14) Å], but all are longer than the established length of a single S-S bond [2.05Å] (Huheey, 1972). The ammonium thiosulfate zwitterion **13** has an S-S bond length of 2.1137(7) Å, similar to those of **5**, **11** and **12**, but all are appreciably shorter than S-S bond in the monoanion of thiosulfuric acid, $HSSO_3^-$ [2.155] (Miaskiewicz and Steudel, 1992).

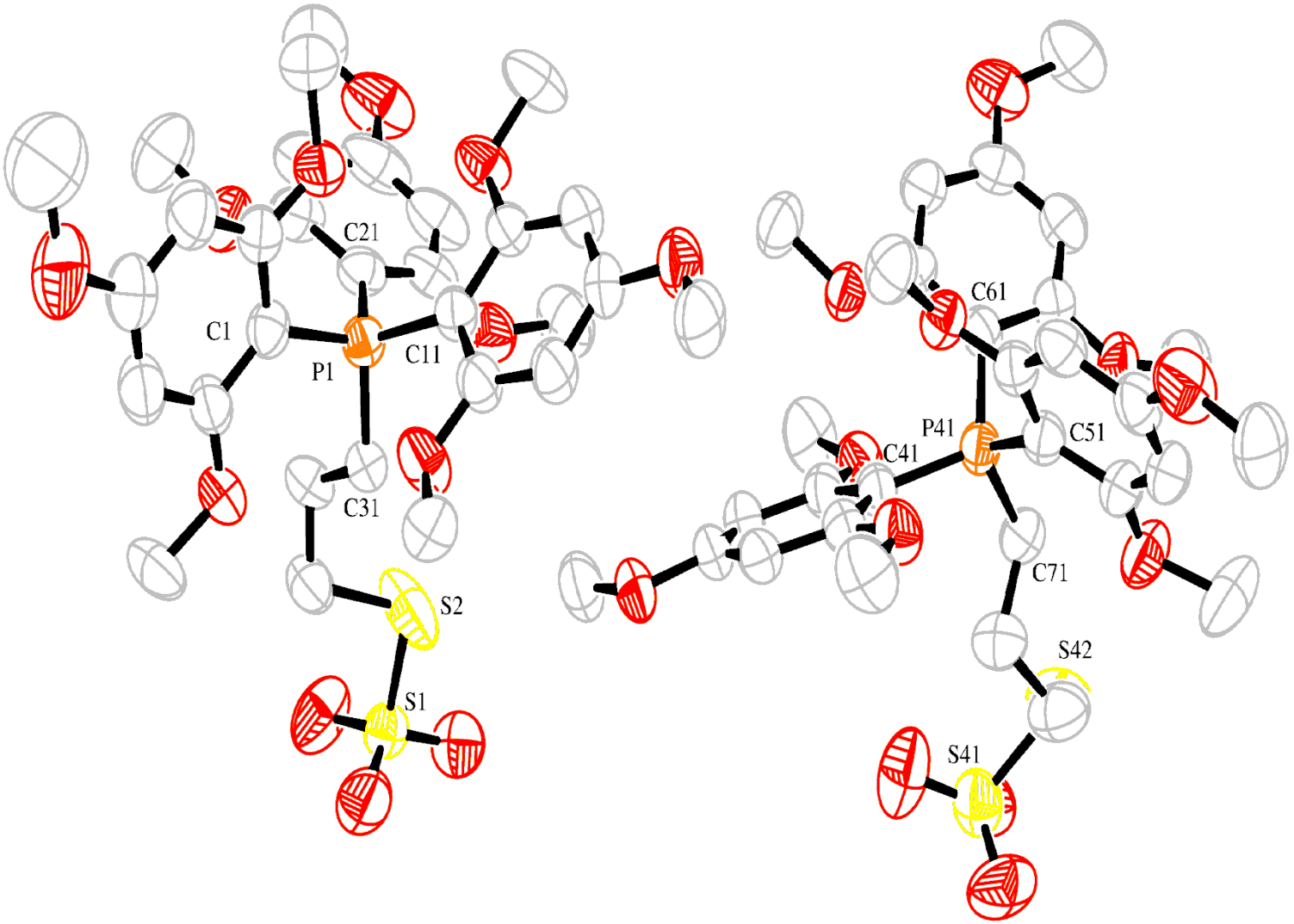

Figure 3.20 Molecular structure of **5**

Table 3.7 Selected bond lengths [Å] and angles [°] in compound 5.

5A			
C1–P1	1.844(6)	O31–S1	1.441(5)
C11–P1	1.798(4)	O32–S1	1.430(5)
C21–P1	1.798(5)	O33–S1	1.416(4)
C31–P1	1.801(15)	S1–S2	2.059(3)
P1–C131	1.811(5)	S101–S102	2.059(9)
P1–C101	1.812(6)		
C11–P1–C21	110.4(2)	O33–S1–O32	118.3(3)
C11–P1–C131	96.9(10)	O33–S1–O31	115.1(4)
C21–P1–C131	107.0(16)	O32–S1–O31	107.4(4)
C11–P1–C31	110.6(2)	O33–S1–S2	100.5(2)
C11–P1–C101	103.7(3)	O32–S1–S2	107.8(3)
C21–P1–C31	105.8(6)	O31–S1–S2	107.0(3)
C21–P1–C101	112.0(6)	C33–S2–S1	100.81(19)
C131–P1–C101	123(2)		
C11–P1–C1	110.1(6)		
C21–P1–C1	114.8(6)		
C31–P1–C1	107.0(4)		
5B			
C41–P41	1.807(4)	O71–S41	1.424(9)
C51–P41	1.785(5)	O72–S41	1.397(11)
C61–P41	1.802(4)	O73–S41	1.425(9)
C71–P41	1.830(10)	S41–S42	2.116(6)
P41–C171	1.814(11)	O171–S141	1.429(9)
S141–S142	2.087(6)	O172–S141	1.377(12)
		O173–S141	1.421(9)
C51–P41–C61	107.0(2)	O72–S41–S42	106.2(7)
C51–P41–C41	113.5(2)	O71–S41–S42	102.2(5)
C61–P41–C41	112.7(2)	O73–S41–S42	107.3(6)
C51–P41–C171	107.7(8)	C73–S42–S41	101.2(5)
C61–P41–C171	113.0(14)	O172–S141–O173	118.5(9)
C41–P41–C171	102.9(12)	O172–S141–O171	114.6(9)
C51–P41–C71	110.6(14)	O173–S141–O171	111.2(9)
C61–P41–C71	107.8(8)	O172–S141–S142	100.7(7)
C41–P41–C71	105.1(12)	O173–S141–S142	104.0(6)
O72–S41–O71	112.4(8)	O171–S141–S142	105.9(5)
O72–S41–O73	112.7(8)	C173–S142–S141	99.5(5)
O71–S41–O73	114.9(9)		

3.10 Conclusion

The aim of the work reported in this chapter (3B) was to synthesize methoxy-phenyl phosphoniopropylthiosulfate zwitterions (**5 - 7**) and ω-thioacetylpropyl(methoxyphenyl) phosphonium bromide salts (**8 - 10**) and determines their cytotoxicity in PC3 cells. All compounds are easily prepared and have been characterized thoroughly. Unlike other triarylphosphoniopropylthiosulfate zwitterions, the methoxy-phenyl compounds reported here are soluble in water and aqueous media.

3.11 References

BAER, D. R. & ENGELHARD, M. H. 2010. XPS analysis of nanostructured materials and biological surfaces. *Journal of Electron Spectrocopy and Related Phenomena*, 178-179, 415-432.

BAIN, C. D., BIEBUYCK, H. A. & WHITESIDES, G. M. 1989. Comparison of self-assembled monolayers on gold: Coadsorption of thiols and disulfides. Langmuir, 5, 723-727.

BARRY, S. J., CARR, R. M., LANE, S. J., LEAVENS, W. J., MANNING, C. O., MONTÉ, S., & WATERHOUSE, I. 2003. Use of S-pentafluorophenyl tris(2,4,6-trimethoxyphenyl)phosphonium acetate bromide and (4-hydrazino-4-oxobutyl) [tris(2,4,6-trimethoxyphenyl)phosphonium bromide for the derivatization of alcohols, aldehydes and ketones for detection by liquid chromatography/electrospray mass spectrometry. *Rapid Communications in Mass Spectrometry,* 5, 484-497.

BERCHEL, M., LE GALL, T., COUTHON-GOURVÈS, H., HAELTERS, J., MONTIER, T., MIDOUX, P., JAFFRÈS, P. 2012. Lipophosphonate/lipophosphoramidates: A family of synthetic vectors efficient for gene delivery. *Biochimie,* 1, 33-41.

BERGERON, K. L., MURPHY, E. L., MAJOFODUN, O., MUÑOZ, L. D., WILLIAMS, J. C., & ALMEIDA, K. H. 2009. Arylphosphonium salts interact with DNA to modulate cytotoxicity. *Mutation Research*, 2, 141–148.

BOURG, M. C., BADIA, A. & BRUCE LENNOX, R. 2000. Gold-sulfur bonding in 2D and 3D self-assembled monolayers: XPS characterization. *Journal of Physical Chemistry B*, 104, 6562-6567.

BRUST, M., WALKER, M., BETHELL, D., SCHIFFRIN, D. J. & WHYMAN, R. 1994. Synthesis of thiol-derivatised gold nanoparticles in a two-phase liquid-liquid system. *Journal of the Chemical Society, Chemical Communications*, 801-802.

CHEN, J.-X., XU, Q.-F., ZHANG, Y., ZAIN, S. M., NG, S. W. & LANG, J.-P. 2004. *Acta Crystallographica*, C60, 0572-0574.

CHEN, S., ZHOU, G., ZHANG, X., MAO, J., DE THE, H., & CHEN, Z. 2011. From an old remedy to a magic bullet: dunbarMolecular mechanisms underlying the therapeutic effects of arsenic in fighting leukemia. *Blood,* 24, 6425.

CHEN, Y, S. 2014. PhD Thesis, Sheffield Hallam University.

CHEN, Y., ALLEN, D. W., TIZZARD, G. J., PITAK, M. B., COLES, S. J., CROSS, N. A., & BRICKLEBANK, N. 2017. Biological and structural studies of phosphonium 'masked thiolate' compounds. *European Journal of Medicinal Chemistry, 125*, 528-537.

DANIEL, M. C. & ASTRUC, D. 2004. Gold nanoparticles: Assembly, supramolecular chemistry, quantum-size-related properties, and applications toward biology, catalysis, and nanotechnology. *Chemical Reviews*, 104, 293-346.

DUNBAR, K. R., AND HAEFNER, S. C. 1994. Synthesis and properties of tris(2,4,6-trimethoxyphenyl)phosphine and tris(2,4,6-trimethoxyphenyl)phosphine oxide. *Polyhedron*, 13, 527 - 536.

ERBEN, M. F., BOESE, R., DELLA VEDOVA, C. O., OBERHAMMER, H., & WILLNER, H. 2006. Toward an intimate understanding of the structural properties and conformational preference of oxoesters and thioesters: gas and crystal structure and conformational analysis of dimethyl monothiocarbonate, $CH_3OC(O)SCH_3$. *The Journal of Organic Chemistry,* 2, 616-622.

FEALY, R. J., ACKERMAN, S. R. & FERGUSON, G. S. 2011. Mechanism of spontaneous formation of monolayers on gold from alkyl thiosulfates. *Langmuir*, 27, 5371-5376.

HE, H. S., CHUNG, C. W. Y., BUT, T. Y. S., & TOY, P. H. 2005. Arsonium ylides in organic synthesis. *Tetrahedron,* 6, 1385-1405.

HILDEBRAND, A., SÃROSI, I., LÖNNECKE, P., SILAGHI-DUMITRESCU, L., SÃROSI, M. B., SILAGHI-DUMITRESCU, I., & HEY-HAWKINS, E. 2012. Heteropolytopic arsanylarylthiolato ligands: Cis-Trans isomerism of nickel(II), palladium(II), and platinum(II) complexes of 1-$AsPh_2$-2-SHC_6H_4. *Inorganic Chemistry,* 13, 7125-7133. (b) VĂLEAN, A., GÓMEZ-RUIZ, S., SILAGHI-DUMITRESCU, L., & HEY-HAWKINS, E. 2013. Variable coordination modes of potentially tetradentate phosphino- and arsinoarylthiolato ligands derived from E(2-SHC6H4)3 (E = P, as) in gallium(III) complexes. *Zeitschrift Für Anorganische Und Allgemeine Chemie,* 7, 1220-1226.

HOLZE, R., & WU, Y. P. 2014. Intrinsically conducting polymers in electrochemical energy technology: Trends and progress. *Electrochimica Acta, 122*, 93-107.

HOYE, A. T., DAVOREN, J. E., WIPF, P., FINK, M. P., & KAGAN, V. E. 2008. Targeting mitochondria. *Accounts of Chemical Research,* 1, 87-97.

HUANG, Z., SHEN, T., WU, J., GAGE, D. A., & WATSON, J. T. 1999. Protein sequencing by matrix-assisted laser desorption Ionization–Post source Decay–Mass spectrometry analysis of the N-tris(2,4,6-trimethoxyphenyl)phosphine-acetylated tryptic digests. *Analytical Biochemistry,* 2, 305-317.

HUANG, Z., WU, J., ROTH, K. D. W., YANG, Y., GAGE, D. A., & WATSON, J. T. 1997. A picomole-scale method for charge derivatization of peptides for sequence analysis by mass spectrometry. *Analytical Chemistry,* 2, 137-144.

HUHEEY, J. E. 1972. Inorganic chemistry: principles of structure and reactivity, Harper Row, New York.

JOMOVA, K., JENISOVA, Z., FESZTEROVA, M., BAROS, S., LISKA, J., HUDECOVA, D., VALKO, M. 2011. Arsenic: Toxicity, oxidative stress and human disease. *Journal of Applied Toxicology,* 2, 95-107.

JU-NAM, Y., ALLEN, D. W., GARDINER, P. H. E., & BRICKLEBANK, N. 2008. ω-Thioacetylalkylphosphonium salts: Precursors for the preparation of phosphonium-functionalized gold nanoparticles. *Journal of Organometallic Chemistry, 693*, 3504-3508.

JU-NAM, Y., BRICKLEBANK, N., ALLEN, D.W., GARDINER, P.H., LIGHT, M.E. & HURSTHOUSE, M.B. 2006. Phosphonioalkylthiosulfate zwitterions--new masked thiol ligands for the formation of cationic functionalized gold nanoparticles. *Organic & Biomolecular chemistry,* 4, 4345-4351.

JU-NAM, Y., CHEN, Y., OJEDA, J. J., ALLEN, D. W., CROSS, N. A., GARDINER, P. H. E., & BRICKLEBANK, N. 2012. Water-soluble gold nanoparticles stabilized with cationic phosphonium thiolate ligands. *RSC Advances*, 2, 10345-10351.

KIM, Y., YANG, C., WANG, J., WANG, L., LI, Z., CHEN, X., & LIU, S. 2008. Effects of targeting moiety, linker, bifunctional chelator, and molecular charge on biological properties of 64Cu-labeled triphenylphosphonium cations. *Journal of Medicinal Chemistry,* 10, 2971-2984.

LEAVENS, W. J., LANE, S. J., CARR, R. M., LOCKIE, A. M., & WATERHOUSE, I. 2002. Derivatization for liquid chromatography/electrospray mass spectrometry: Synthesis of tris(trimethoxyphenyl)phosphonium compounds and their derivatives of amine and carboxylic acids. *Rapid Communications in Mass Spectrometry,* 15, 433-441.

LOHSE, S. E., DAHL, J. A. & HUTCHISON, J. E. 2010. Direct synthesis of large water-soluble functionalized gold nanoparticles using Bunte salts as ligand precursor. *Langmuir*, 26, 7504-7511.

MANETTA, A., GAMBOA, G., NASSERI, A., PODNOS, Y. D., EMMA, D., DORION, G., RIDEOUT, D. 1996. *Novel phosphonium salts displayin vitroandin VivoCytotoxic activity against human ovarian cancer cell lines,* 60, 203-212.

MCNEILLIE, A., BROWN, D. H., SMITH, W. E., GIBSON, M., & WATSON, L. 1980. X-ray photoelectron spectra of some gold compounds. *Journal of the Chemical Society, Dalton Transactions,* 5, 767-770.

MIASKIEWICZ, K., & STEUDEL, R. 1992. The structures of thiosulfuric acid $H_2S_2O_3$ and its monoanion $HS_2O_3^-$. *Angewandte Chemie International Edition in English,* 1, 58-59.

MILLARD, M., PATHANIA, D., SHABAIK, Y., TAHERI, L., DENG, J., & NEAMATI, N. 2010. Preclinical evaluation of novel triphenylphosphonium salts with broad-spectrum activity. *Plos One,* 10, e13131.

MIODRAGOVIĆ, Đ. U., QUENTZEL, J. A., KURUTZ, J. W., STERN, C. L., AHN, R. W., KANDELA, I., O'HALLORAN, T. V. 2013. Robust structure and reactivity of aqueous arsenous Acid–Platinum(II) anticancer complexes. *Angewandte Chemie International Edition,* 41, 10749-10752.

MOORHOFF, C, M. 1998. A general method for the rapid high yield preparation of pure arsonium salts. Preparation of (3-alkoxy-carbonyl-2-oxopropyl)triphenylarsonium bromides. *Synthetic Communications*, 28, 2925 – 2935.

MUDHOO, A., SHARMA, S, K., GARG, V, K., TSENG, C, H. 2011. Arsenic: An overview of applications, health, and environmental concerns and removal processes. *Critical Review Environmental Science Technology*, 41, 435–519.

PILLAI, R. G. & FREUND, M. S. 2011. Self-assembly of alkylthiosulfate on gold: Role of electrolyte and trace water in the solvent. *Langmuir*, 27, 9028-9033.

RIDEOUT B.A., MONTALI R.J., WALLACE S., BUSH M., PHILLIPS L.G., ANTONOVYCH T.T., SABNIS S.G. 1989. Renal medullary amyloidosis in Dorcas gazelles. *Veterinary Pathology*, 26, 129–135.

SADAGOPAN, N., & WATSON, J. T. 2000. Investigation of the tris(trimethoxyphenyl)phosphonium acetyl charged derivatives of peptides by electrospray ionization mass spectrometry and tandem mass spectrometry. *Journal of the American Society for Mass Spectrometry,* 2, 107-119.

SEHY, D. W., SHAO, L., RIDEOUT, D., & YU, J. 1993. Sensitivity of committed hematopoietic progenitor cells in vitro (BFU-E, CFU-E, CFU-GM) and two human carcinoma cell lines toward rhodamine-123 and phosphonium salt II-41. *Leukemia Research,* 3, 247-253.

SHEN, T. L., & ALLISON, J. 2000. Interpretation of matrix-assisted laser desorption/ionization post source decay spectra of charge-derivatized peptides: Some examples of tris(2,4,6-trimethoxyphenyl) phosphonium]-tagged proteolytic digestion products of phosphoenolpyruvate carboxykinase. *Journal of the American Society for Mass Spectrometry,* 2, 145-152.

SINGH, A., DAHANAYAKA, D. H., BISWAS, A., BUMM, L. A. & HALTERMAN, R. L. 2010. Molecularly ordered decanethiolate self-assembled monolayers on Au(111) from in situ cleaved decanethioacetate: An NMR and STM study of the efficacy of reagents for thioacetate cleavage. *Langmuir*, 26, 13221-13226.

STEC, W. J., MORGAN, W. E., ALBRIDGE, R. G., & VAN WAZER, J. R. 1972. Measured binding energy shifts of "3p" and "3d" electrons in arsenic compounds. *Inorganic Chemistry,* 2, 219-225.

SWINDELL, E. P., HANKINS, P. L., CHEN, H., MIODRAGOVIÄ, Ä. U., & OTTHALLORAN, T. V. 2013. Anticancer activity of small-molecule and nanoparticulate arsenic(III) complexes. *Inorganic Chemistry,* 21, 12292-12304.

VARNHOLT, B., OULEVEY, P., LUBER, S., KUMARA, C., DASS§, A., & BÜRGI, T. 2014. Structural information on the Au-S interface of thiolate-protected gold clusters: A raman spectroscopy study. *The Journal of Physical Chemistry C,* 18, 9604-9611.

WADA, M., & HIGASHIZAKI, S. 1984. A highly basic triphenylphosphine, 2,4,6-$(MeO)_3C_6H_2]_3P$. *Journal of the Chemical Society, Chemical Communications,* 7, 482-483.

WANG, J., YANG, C.T., KIM, Y.S., SREERAMA, S.G., CAO, Q., LI, Z.B., HE, Z., CHEN, X. & LIU, S., 2007. 64Cu-Labeled triphenylphosphonium and triphenylarsonium cations as highly tumor-selective imaging agents. *Journal of Medicinal Chemistry,* 50, 5057-5069.

YANG Y, GAO N, HU Y, JIA C, CHOU T, DU H, WANG H. 2015. Gold nanoparticle-enhanced photodynamic therapy: effects of surface charge and mitochondrial targeting. *Therapeutic delivery*, 6, 307-321.

YEE, C. K., ULMAN, A., RUIZ, J. D., PARIKH, A., WHITE, H. & RAFAILOVICH, M. 2003. Alkyl Selenide-And Alkyl Thiolate-Functionalized Gold Nanoparticles: Chain Packing and Bond Nature. *Langmuir*, 19, 9450-9458.

ZHANG, S., LEEM, G. & RANDALL LEE, T. 2009. Monolayer-protected gold nanoparticles prepared using long-chain alkanethioacetates. *Langmuir*, 25, 13855-13860.

Chapter 4

4A) Investigation of the cytotoxicity and cellular uptake of Arsonium ligands and Gold nanoparticles in cells.

4.0 Introduction

The cytotoxicity of arsenic compounds is crucially dependent on the nature and oxidation state of the species. Inorganic compounds, such as arsenite and arsenate, show acute toxicity; for example, the IC_{50} of sodium arsenate was reported as 6 μM. In contrast, the organic derivative arsenobetaine, $Me_3As^+CH_2CO_2^-$, an important metabolite of arsenic which is widely distributed in marine ecosystems and found in comparatively high levels in seafood, is reported to have no toxic effects and was found to significantly enhance the cell viability of bone marrow cells *in vitro* in a concentration-dependent manner (Sakurai et al., 2001).

Nanotechnology is revolutionising the way in which materials are engineered today, mainly due to their surface to volume ratio and other favourable characteristics. Gold nanoparticles are known to passively target tumour cells because of the nature of the blood vessels and their inherent small size. It has been reported that AuNPs on their own do not target all cell types and hence it becomes essential to functionalize them with ligands which can interact with the surface and/or receptors on the cell. (Patra et al., 2007, Kirui et al., 2010).

The most commonly deployed ligands for protecting AuNPs are organic thiolates derived from thiols or disulfides. Other common ligands include citrate and tertiary phosphines. Pan and co-workers (Pan et al., 2009) have investigated the size-dependent cytotoxicity of AuNPs functionalized with water-soluble sulfonated triphenylphosphines (Fig. 4.1). Their results show that ultra-small AuNPs (1.5 nm) cause rapid cell death whereas larger, 15 nm AuNPs, are significantly less cytotoxic.

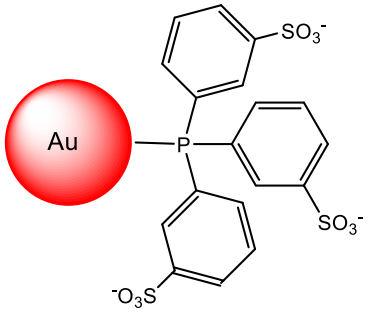

Figure 4.1 Schematic representation of AuNPs functionalized with sulfonated triphenylphosphine ligands.

The use of ionic species to functionalize the surface of AuNPs is an attractive proposition for improving the aqueous solubility of AuNPs and facilitating cellular uptake. Research by Goodman and co-workers (Goodman et al., 2004) has demonstrated that AuNPs bearing cationic ligands are significantly less cytotoxic than anionic ligands. The most widely studied ligands for the production of cationic charged AuNPs are thiolates bearing ammonium groups. As outlined in Chapter 1, there is increasing interest in the use of phosphonium cations to functionalize nanomaterials and the Bricklebank group has developed the synthesis of phosphonium-functionalized AuNPs and investigated their cellular uptake and cytotoxicity. However, there have been no published reports into the use of organoarsonium cations to functionalize AuNPs.

The synthesis and characterisation of AuNPs functionalized with triphenylarsoniumalkylthiolate ligands is described in Chapter 3. In this chapter the results of studies of the cytotoxicity of the triphenylarsoniopropylthiolate-AuNPs, and the parent triphenylarsoniopropylthiosulfate zwitterion, ω-thioacetylpropyl(triphenyl)arsonium bromide salts and methoxyphenyl compounds are reported.

4.1 Material and methods

4.1.1 Chemicals

Triphenylarsoniopropyllthiosulfate zwitterion (**1**), ω-thioacetylpropyl(triphenyl)arsonium bromide salts (**2**) salts and triphenylarsoniopropylthiolate-functionalized AuNPs were prepared as described in Chapter 3. CellTiter-Glo luminescent cell viability assay kit was purchased from Promega Corporation, Southampton, Hamshire UK, and 3-(4,5-dimethylthiazol-2-yl)-2,5- diphenyltetrazolium bromide (MTT) was purchased from Sigma Aldrich UK, and were used as received.

4.1.2 Methods

4.1.2.1 Cytotoxicity and MTT assay

Cytotoxicity was assessed using CellTiter-Glo luminescent cell viability assay kit. PC3 and Human Fibroblast cells were seeded in an opaque-walled 96 well plate at a density of 10,000 cells/well and allowed to adhere overnight. Cells were subsequently treated with the corresponding arsonium compound (0-1000μM) for 24, 48, 72 hours. After each incubation period cell viability was measured according to the manufacturer's instructions. In brief, plates were equilibrated at room temperature for 30 minutes, 100μL of assay reagent was added to each well, placed on an orbital shaker for 2mins, left to stand at room temperature for 10 minutes and read on a Wallac Victor2 1420 multilabel counter (PerkinElmer, Cambridge, Cambridgeshire, UK).

Cytotoxicity studies were also done to assess IC_{50} using the 3-(4,5-dimethylthiazol-2-yl)-2,5-diphenyltetrazolium bromide (MTT) assay. Both cell lines (PC3 and Human Fibroblast) were seeded in a 96 well plate with the corresponding ligand (0-1000μM) for 24, 48, 72 hours.

The MTT mixture was added to each well to give a final concentration of 0.3mg/mL MTT. Cells were incubated with MTT for 3-4 hours at 37^{o}C. The supernatant was then removed and DMSO was added to read the absorbance at 570nm.

All plates contain control well and all measurements were performed in quadruplicates; three independent experiments were conducted (n=12). Data are expressed as a percentage of live cells normalized to control and the average, standard deviation and IC_{50} values were plotted and calculated using GraphPad Prism (GraphPad software, La Jolla, California, USA).

4.1.2.2 Quantification of the Uptake of Arsonium-functionalized gold nanoparticles in cells by ICP-OES

PC3 cells were treated in a 6 well plate at a density of 500,000 cells/well and allowed to adhere overnight. Cells were treated with different concentration of triphenylarsoniopropylthiolate-AuNPs **A-Au-Z2**[#] or citrate-stabilised 5nm AuNPs purchased from Sigma-Aldrich. The concentrations of the nanoparticle solutions were 12.5, 25.0, 50.0 mg/mL. The cells were incubated with each of these solutions overnight. The following day the cells were trypsinised, washed with PBS, fixed in 100% EtOH and sent to MEDAC (Chobham, Surrey, UK) for ICP-OES analysis. The Au analysis was carried out by digestion of the sample in 8ml of *aqua regia* and the solution made up to 100ml. This solution was then analyzed by ICP-OES. The instrument used for this was a Varian Vista MPX ICP-OES.

Refer to Chapter 3, Table 3.3 for an explanation of compound labelling.

4.2 Results and Discussion

4.2.1 Cytotoxicity studies of Triphenylarsonium ligands.

In order to evaluate the efficacy of the triphenylarsoniumpropylthiolate-functionalized AuNPs as cellular transport systems were first screened against the PC3 prostate cancer cell lines in order to determine the IC_{50} of the parent triphenylarsoniopropylthiosulfate zwitterion (**1**), and ω-thioacetylpropyl(triphenyl)arsonium bromide salts (**2**). The results are summarised in Table 4.1

Table 4.1: Summary of IC_{50} values for triphenylarsoniopropylthiosulfate zwitterion (**1**), and ω-thioacetylpropyl(triphenyl)arsonium bromide (**2**) against PC3 Cell line (μM)

	CellTiter-Glo			MTT		
Compound	24hr	48hr	72hr	24hr	48hr	72hr
1	600.4	548.7	722.2	89.9	51.9	71.8
2	969.4	568.8	384.5	74.6	43.6	74.9

The MTT assay measures mitochondrial activity to determine the in vitro cytotoxic effects of chemical entities. The results (Fig. 4.2) showed **1** and **2** to have IC_{50} values of 75 mM and 72 mM, respectively, after 72 hours. There is limited published data on the IC_{50} values of arsonium compounds and the publication is based on the results reported in this thesis (Lalwani et al., 2015). As noted in the introduction to this chapter, arsenobetaine is believed to be essentially nontoxic, whereas inorganic arsenic compounds are very toxic.

These data reported here compare favourably with that for the analogous phosphonium compounds ω-thioacetylpropyl(triphenyl)phosphonium bromide and ω-thioacetylpropyl(tri-4-fluorophenyl)phosphonium bromide which showed IC_{50} values of

67.1μM and 252.6μM respectively (Chen et al., 2017). Millard and co-workers have screened a large number of triphenylphosphonium salts using MTT against PC3 cells. These displayed IC_{50} values in the range 0.4–5 μM (Millard et al., 2010). The results described here are also in accordance with cellular toxicity data for lipophosphoramidate derivatives, where phosphonium compounds show greater cytotoxicity than the corresponding arsonium compounds (Millard et al., 2010). The cytotoxicity results determined using the CellTiter-Glo assay (Fig 4.2), showed that the IC_{50} values were found to be 722 μM and 384 μM after 72 hours for **1** and **2** respectively. The difference between toxicity might be attributed to the zwitterionic (**1**) and cationic (**2**) nature of the respected compounds.

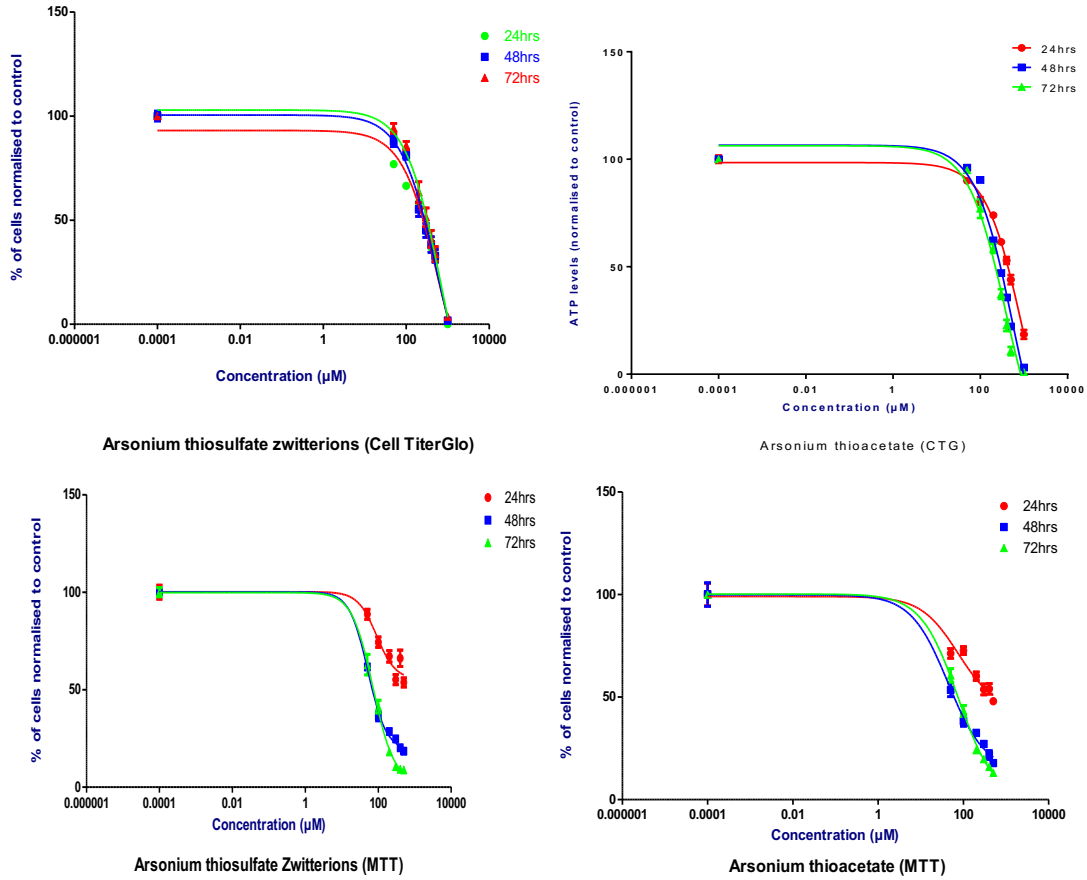

Figure 4.2: CellTiter-Glo (CTG) and MTT assay on triphenylarsoniopropylthiosulfate zwitterion (**1**) and ω-thioacetylpropyl(triphenyl)arsonium bromide (**2**)**.** Prostate cancer (PC3) cells were incubated with increasing concentration of compound **1** and **2**. The IC_{50} was then determined for each compound from a plot of log [drug concentration] versus percentage of cell normalised to control.

4.2.2 Cytotoxicity of Triphenylarsoniopropylthiolate-functionalized gold nanoparticles

Although there is a significant body of evidence, generated over a long period of time, pertaining to the toxic effects of arsenic compounds, there is no published work on the cytotoxicity of gold nanoparticles functionalized with organoarsonium compounds. Organic arsenic compounds have long been investigated as therapeutic drugs but their greatest drawback is their toxicity (Swindell EP et al, 2013). Most arsenic compounds display dose-limiting acute toxicity as well as chronic toxicities. Organic arsenic compounds are considered to be less toxic than inorganic arsenic. In all cases, exposure to trivalent arsenic As(III) is more toxic than exposure to pentavalent As(V). It is believed that the greater toxicity of As(III) compared to As(V) is due to the increased affinity of As(III) for sulfur ligands; arsenic exerts its effect in cells by interacting with the sulfhydryl groups of cysteine residues of proteins and peptides (Swindell EP et al, 2013).

The cytotoxicity of triphenylarsoniopropylthiolate-functionalized gold nanoparticles **A-Au-Z2** was assessed against the PC3 prostate cancer cell line and Human Fibroblast (Hfb) 'normal' cells, in order to establish if there is a difference between normal and cancerous cells. The IC_{50} values were determined using both MTT and CellTitre-Glo assays. The results are summarised in Table 4.2, Fig 4.3 and 4.4. It can be seen that the IC_{50} values are very similar for both the PC3 and the Hfb cells. Furthermore, the **A-Au-Z2** nanoparticles are significantly more toxic than the parent zwitterion **1** or ω-thioacetyl(triphenyl)arsonium bromide salt **2** (Table 4.1).

Table 4.2: IC_{50} values of **A-Au-Z2** nanoparticles in PC3 and Human Fibroblast cell lines (µM)

	Cell Titer-Glo (µM)			MTT (µM)		
Cell line	24hr	48hr	72hr	24hr	48hr	72hr
PC3	64.94	49.77	31.53	31.06	24.76	14.73
HFB	82.37	63.56	39.82	50.27	38.28	24.47

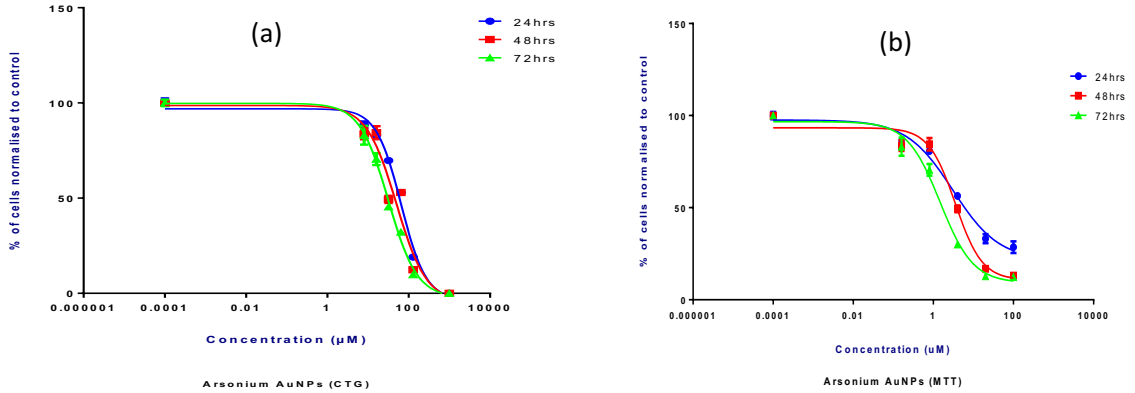

Fig 4.3: Cytotoxicity assay of **A-Au-Z2** nanoparticles against PC3 prostate cancer cells. The cells were incubated with increasing concentration of nanoparticles. The IC_{50} values determined from a plot of log [drug concentration] versus percentage of cell normalised to control using (a) CellTitre-Glo, and (b) MTT assay.

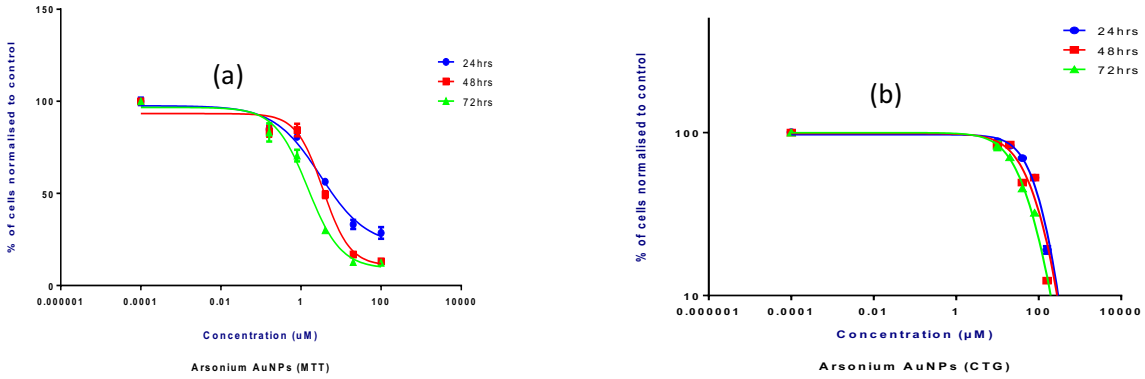

Figure 4.4: Cytotoxicity assay of **A-Au-Z2** nanoparticles against Human Fibroblast cells. The cells were incubated with increasing concentration of nanoparticles. The IC_{50} values determined from a plot of log [drug concentration] versus percentage of cell normalised to control using (a) CellTitre-Glo, and (b) MTT assay.

4.3 Quantification of the Uptake by PC3 cells on Arsonium-functionalized gold nanoparticles in cells by ICP- OES spectrometry.

Previous research on the cellular uptake and viability of PC3 cells exposed to AuNPs functionalized with triphenylhosphoniumpropylthiolate ligands (**P-Au-Z2**) showed that triphenyphosphoniopropylthiolate-AuNPs with a concentration of up to 5.0 mg/mL are relatively non-toxic to PC3 cells, with cell viability above 90% (Chen PhD thesis, 2014). At **P-Au-Z2** concentrations above 5.0 mg/mL, after 24 hours exposure the majority of cells were necrotic. Results for the analogous arsonium AuNPs **A-Au-Z2** (Fig 4.5) showed that at a concentration of 12.5 mg/ml 11.16% of cells were viable after 24 hours and that viability decreases markedly above this concentration.

In similar studies, Pan and co-workers (Pan et al., 2007) determined the cytotoxicity of tris-sulfonated triphenylphosphine and triphenylphosphine monosulfate AuNPs in logarithmic-phase HeLa cells. The toxicity was reported to be size dependent and AuNPs greater than 5nm were less toxic (30 and 46μM), whereas AuNPs having size in the range of 2-3nm showed much greater toxicity (140-250μm). It is not very clear at this stage, but the higher cytotoxicity of the triphenylarsonium-functionalized AuNPs reported in this thesis could be due to the toxicity of the small AuNPs rather than the triphenylarsonium ligands.

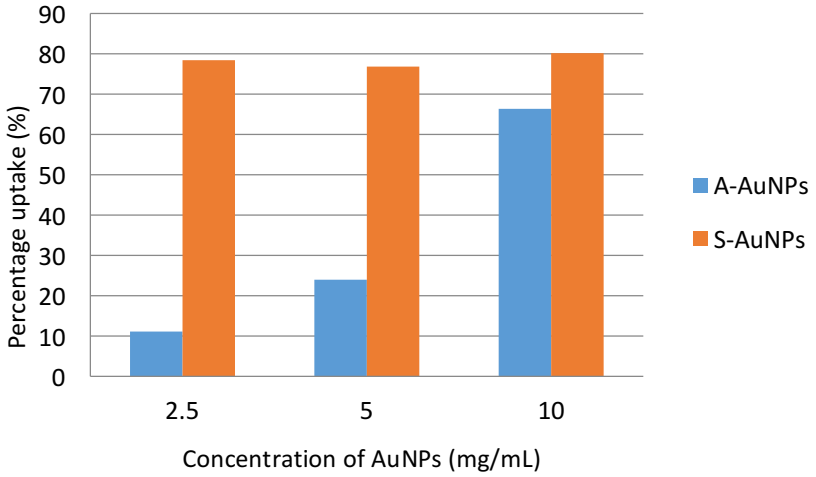

Figure 4.5 ICP-OES data showing the percentage uptake of Triphenylarsonium-functionalized AuNP (A-AuNPs): Sigma AuNPs (S-AuNPs).

A solution of **A-Au-Z2** with a concentration of 10mg/ml was analyzed by ICP-OES and found to contain 2 mg/ml of gold. Based on this result, a series of solutions containing 12.5, 25 and 50mg/ml of **A-Au-Z2** nanoparticles were produced. These solutions contained 2.5, 5 and 10 mg/ml of gold respectively. PC3 cells were incubated with each of these solutions for 24 hours. After incubation the cells were washed with PBS, fixed in 100% EtOH and sent to MEDAC for analysis. The amount of gold present in the cells was determined by ICP-OES spectrometry. The results are summarised in Table 4.3 (experiments 1-3). In a second series of experiments, PC3 cells were incubated with similar concentrations of gold nanoparticles purchased from Sigma Aldrich. The Sigma AuNPs have a mean particle size of 5nm and are spherical in shape and stabilised with citrate ligands. The Sigma AuNPs were diluted to create solutions containing 2.5, 5, and 10 mg/ml of gold. The PC3 cells were incubated with each of these Sigma solutions for 24 hours. After incubation the cells were washed with PBS, fixed in 100% EtOH. The amount of gold present in the cells was

determined by ICP-OES spectrometry. The results are summarised in Table 4.3 (experiments 4-6).

Table 4.3. Percentage uptake of Triphenylarsonium-functionalized-AuNP (A-AuNPs): Sigma-AuNPs (S-AuNPs).

Experiment	Source of gold	Initial concentration of gold (mg/ml)	Concentration of gold in PC3 cells after 72 hours incubation (mg/ml)	Percentage uptake of gold (%)
1	**A-Au-Z2**	2.5	0.279	11.16
2	**A-Au-Z2**	5.0	1.204	24.08
3	**A-Au-Z2**	10.0	6.646	66.46
4	Sigma-AuNPs	2.5	7.841	78.41
5	Sigma-AuNPs	5.0	7.688	76.88
6	Sigma-AuNPs	10.0	8.021	80.21

The quantification of AuNPs was done by ICP-OES (Allabashi et al., 2009). The result showed that 5nm AuNPs (stabilised suspension in citrate buffer) had a much higher percentage of uptake than the triphenylarsonioalkylthiolate-capped AuNPs. The highest percentage uptake for arsonium AuNPs was found to be 66.46% while uptake for 5nm AuNPs from Sigma Aldrich was found to be over 76% across all concentrations. This data is comparable to results obtained by Arnida and co-workers (Arnida et al., 2010) who reported that uptake of spherical AuNPs with a mean diameter of 30nm is steady across all concentrations tested (0-40nm) and this uptake may be due to the limited cationic sites available on cell surfaces (Wilhelm et al., 2003).

The percentage uptake of the triphenylarsonium AuNPs was also low compared to the analogous triphenylphosphonium AuNPs (Chen PhD thesis, 2014), as reported in Table 4.4. The reason for this is unclear; especially since studies comparing the cell biology of triphenylarsonium-functionalized macrocyclic copper complexes with their triphenylphosphonium-analogues did not note a significant difference in behaviour.

Table 4.4 Comparison of Percentage uptake of Triphenylarsoniopropylthiolate-AuNPs (**A-Au-Z2**) and Triphenylphosphoniopropylthiolate-AuNPs (**P-Au-Z2**)

Sample	Initial Concentration of gold mg/ml	Percentage uptake of **A-AuZ2**	Percentage uptake of **P-AuZ2**
1	2.5	11	88
2	5	24	76
3	10	66	102

4.4 Conclusion

Arsenic compounds have been widely investigated for their medicinal properties although interest declined as greater understanding of their toxicity became apparent (Chen et al., 2011 and Swindell et al., 2013). More recently there has been a resurgence of interest in the medicinal properties of arsenic compounds, including the use of arsenic trioxide and organic arsenic derivatives as treatments for leukaemia and other cancers (Mudhoo et al., 2011, Chen et al., 2011 and Swindell et al., 2013).

The data presented here show that triphenylarsonium-functionalized AuNPs are significantly more toxic then the parent triphenylarsoniopropylthiosulfate zwitterion and ω-thioacetylpropyl (triphenyl) arsonium bromide salts. In contrast, results for the

analogous triphenylphosphonium-AuNPs showed they were less toxic as compared to the parent ligands. As described in chapter 3, the triphenylarsonium-functionalized AuNPs are slightly smaller than analogous triphenylphosphonium-AuNPs and it is possible that the greater toxicity of the arsenic-containing materials is due to the size of the AuNPs. Further research is necessary to establish whether the cytotoxicity of the triphenylarsonium-AuNPs is due to the triphenylarsonium ligands, the AuNPs or a combination of both species.

The use of ICP-MS for quantifying the uptake of AuNPs in cells has also been reported. In this chapter, the related technique ICP-OES has been used to determine the amount of AuNPs in cells. The results indicate that the triphenylarsonium-AuNPs are taken-up at much lower levels than the triphenylphosphonium-AuNPs or citrate-stabilised AuNPs purchased from Sigma. It is difficult to compare data obtained with published studies, due to variations in reporting the data, as reviewed by Lévy and colleagues (Lévy *et al.*, 2010). For example the units of size vary between groups thereby making comparison a complicated task; Zhu *et al.* (2012) reported the uptake of AuNPs by ICP-MS in terms of pmol, while Arnida *et al.* (2010) reported the uptake of AuNPs by number per cell and Chithrani *et al.* (2006) reported the uptake by number of AuNPs per cell (10^3). Further work is also needed to establish if the triphenylarsonium-AuNPs are actually taken up by the cells.

4B) Investigation of the cytotoxicity and cellular uptake of Methoxyphenyl substituents

4.5 Introduction

Previous work has shown that alkylthiosulfate zwitterion and alkylthioacetate salt derivatives of triphenylphosphine, and other trialkyl- and triaryl-phosphines, can be used as precursors for the formation of triphenylphosphonium-functionalized gold nanoparticles (Ju-nam et al., 2006; Ju-nam et al., 2012; Yang et al., 2015; Ju-nam et al., 2007; Ju-nam et al., 2015). Although the triphenylphosphonium-functionalized nanoparticles are soluble in water and biological media, and are taken-up by cells (Ju-nam et al., 2012), the parent triphenylphosphoniumalkylthiosulfate zwitterions are insoluble in aqueous media (Chen PhD thesis, 2014) This observation has prompted us to investigate alternative triarylphosphonium groups in an attempt to improve the aqueous solubility of the zwitterions. The characterisation and synthesis has been reported in Chapter 3B.

4.6 Material and methods

4.6.1 Chemicals

All chemicals were used as received; tris(2,4,6-trimethoxyphenyl)phosphine and tris(2,4 dimethoxyphenyl)phosphine and tris(4-methoxyphosphine) were purchased from Sigma Aldrich, UK and used without any further treatment. 1, 3- Dibromopropane was purchased from Acros Organics, UK. Potassium thioacetate ($KSCOCH_3$), sodium thiosulfate ($Na_2S_2O_3$), Potassium bromide (KBr), gold(III) chloride trihydrate, hydrobromic acid (HBr), magnesium sulfate ($MgSO_4$), deuterated dichloromethane, chloroform and ICP Au standard were purchased from Sigma-Aldrich (Gillingham, Dorset, UK).

4.6.2 Methods

4.6.2.1 Cytotoxicity assay

Cytotoxicity was assessed using a CellTiter-Glo luminescent cell viability assay kit (Promega Corporation, Southampton, Hamshire, UK).

PC3 cells were seeded in opaque-walled 96 well plates at a density of 10,000 cells/well and allowed to adhere overnight. Cells were subsequently treated with the corresponding phosphonium ligand (0-1000μm) for 24, 48, 72 hours. After each incubation period, cell viability was measured according to the manufacturer's instructions. In brief, plates were equilibrated at room temperature for 30 mins, 100μL of assay reagent was added to each well, placed on an orbital shaker for 2mins, left to stand at room temperature for 10 minutes and read on a Wallac Victor2 1420 multilabel counter (PerkinElmer, Cambridge, Cambridgeshire, UK).

Cytotoxicity studies were also done to assess IC_{50} using 3-(4,5-dimethyltiazol-2-yl)-2,5-diphenyltetrazolium bromide (MTT) assay. Cells were seeded in a 96 well plate with the corresponding ligand (0-1000μm) for 24, 48, 72 hours. An MTT mixture was added to each well to give a final concentration of 0.3mg/mL MTT. Cells were incubated with MTT for 3-4 hours at 37 ^{o}C. The supernatant liquid was then removed and DMSO was added to read the absorbance at 570nm.

All plates contain control wells and all measurements were performed in quadruplicates, three independent experiments were conducted (n=12). Data are expressed as a percentage of live cells normalized to control, the average, standard deviation and IC_{50}

values were plotted and calculated using GraphPad Prism (GraphPad software, La Jolla, California, USA).

4.7 Solubility studies of methoxy-phenyl phosphonium compounds

Compounds **5** - **10** readily dissolve in a range of solvents including DCM, water and aqueous media. This makes them suitable for cell biology studies. The solubility of zwitterions **5** - **7** in aqueous media is notable. Previous research from our own group (Jenni Chen Thesis, 2014; Chen et al., 2017) and by others (Ju-nam 2015), has shown that triarylphosphoniopropylthiosulfate zwitterions prepared from triphenyl-, tri(p-fluorophenyl)- and tri(p-tolyl)-phosphine are not so soluble in aqueous media. In contrast, the corresponding ω-thioacetylpropyl(triaryl)phosphonium bromide salts are soluble in aqueous media. This difference in solubility between the phosphonium zwitterions and phosphonium salts was attributed to strong electrostatic interactions that exist between the zwitterions in the solid state. These interactions are not present in the phosphonium salts. The solubility of zwitterions **5** - **7** can be attributed to the electronic and steric effects of the methoxy-substituents.

4.8 Cytotoxicity Screening of methoxy-phenyl phosphonium compounds 5 - 10.

Phosphonium compounds are known to selectively accumulate in the mitochondria of cancer cells and their anti-cancer activity has been of interest and have been investigated by several groups (Millard et al., 2010, Rideout et al., 1989, Sehy et al., 1993, Manetta et al., 1996, Bergeron et al., 2009). Cell viability studies on compounds **5** - **10** were performed against the PC3 prostate cancer cell line using MTT and CellTitre-Glo assays. The results are presented below (Table 4.5 and Figures 4.6 and 4.7).

Table 4.5 IC_{50} values of methoxy-phenyl phosphoniopropylthiosulfate zwitterions (5 - 7) and ω-thioacetylpropyl(methoxyphenyl)phosphonium bromide salts (8 - 10). Units for data values are μM.

	CellTiter-Glo			MTT		
Compound	24hr	48hr	72hr	24hr	48hr	72hr
5	325.50	288.73	218.33	69.55	55.65	45.65
6	469.33	344.74	289.68	105.83	78.62	66.09
7	308.54	261.27	198.15	82.21	64.59	47.80
8	527.16	420.69	328.77	111.80	86.69	74.00
9	413.22	341.33	249.94	96.84	72.66	58.70
10	582.27	390.06	319.36	123.90	83.13	68.22
14*	137.95	127.07	67.14			
15*	654.73	367.75	252.63			
16¥						0.40
17¥						8.00

NOTES

*Data reported by Y-S Chen, PhD Thesis, Sheffield Hallam University, 2014

¥ Data reported by M. Millard, D. Pathania, Y. Shabaik, L. Taheri, J. Deng and N. Neamati, *PLoS One*, 2010, **5**, e13131.

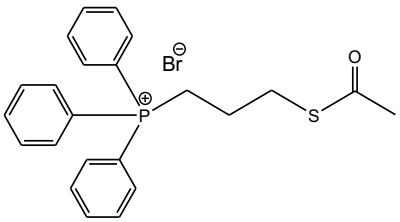

14

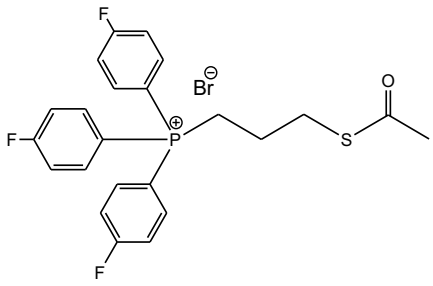

15

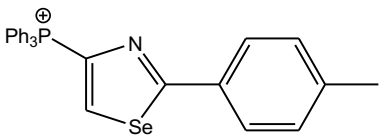

16

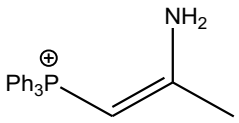

17

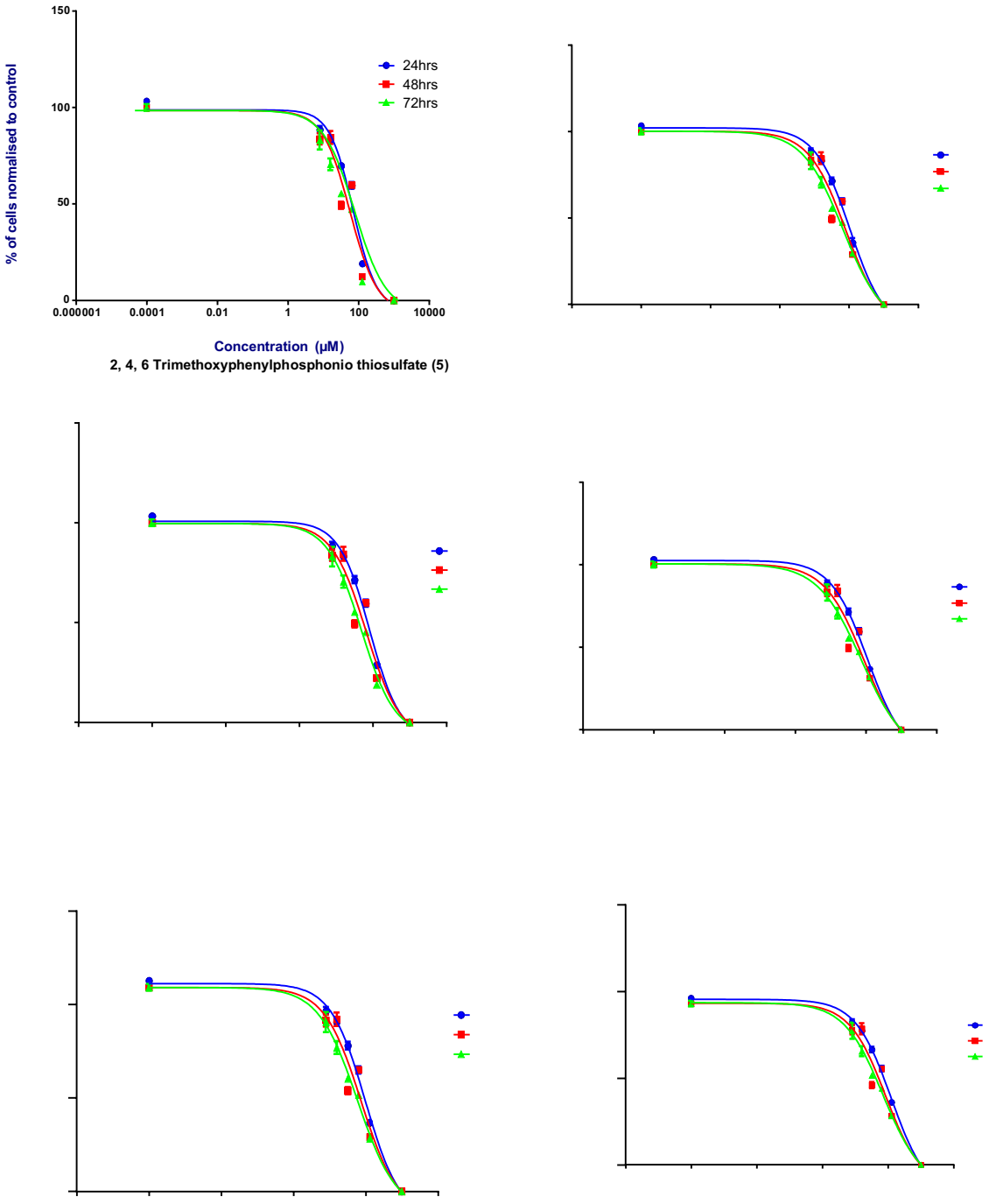

Figure 4.6 PC3 cells treated with 5 - 10 for 24, 48, 72 hours. Cell proliferation was determined by the MTT assay. Data are expressed as a percentage of living cells normalized to control.

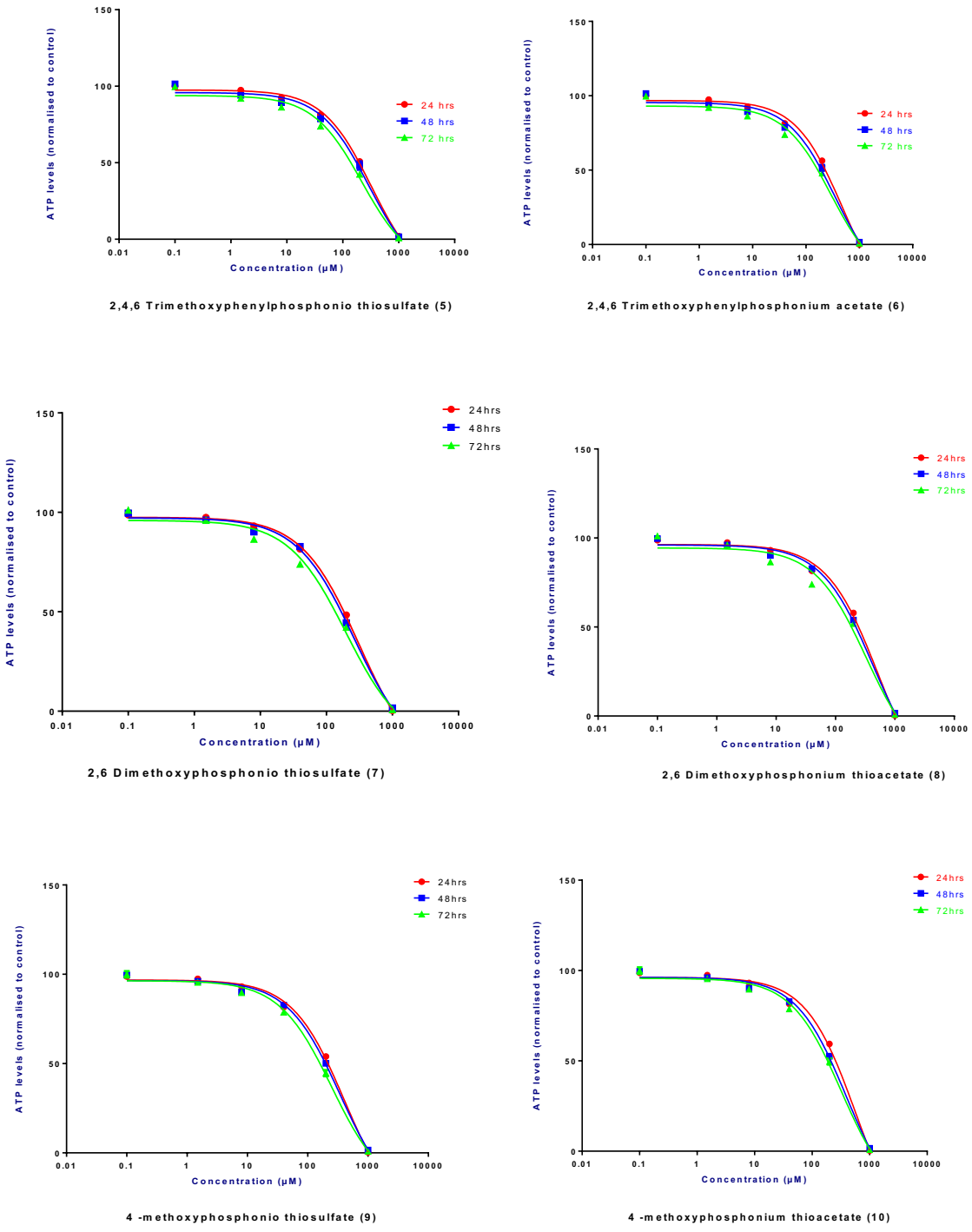

Figure 4.7 PC3 cells treated with 5-10 for 24, 48, 72 hours. Cell proliferation was determined by the CellTiter-Glo luminescent cell viability assay kit. Data are expressed as a percentage of living cells normalized to control.

MTT measures mitochondrial activity to determine the *in vitro* cytotoxic effects of chemical entities. The results showed that zwitterions **5 - 7** are more toxic to cells after 72 hours than the corresponding thioacetate salts **8** - **10**. These values compare very favorably with those of the triphenylphosphonium- and tri(p-fluorophenyl)phosphonium- thioacetate salts **14** and **15**. Millard and coworkers have reported IC_{50} values for 33 different phosphonium compounds (all contain the triphenylphosphonium moiety with different side chains) in five different cell lines, including PC3 cells, using the MTT assay (Millard et al., 2010). The compounds investigated had IC_{50} values between 0.4 – 4.1μM at 72 hours in PC3 cell lines. The most toxic compound reported by Millard et al., 2010 was TP 731 (**16**) having IC_{50} value of 0.40 μM while the least toxic was TP 764 (**17**) with IC_{50} value of 8 μM. The IC_{50} values which Millard reported showed that triphenyl-substituted phosphonium salts are significantly more toxic towards PC3 cells than **5** - **10**.

The viability of PC3 cells in the presence of compound **5** -**10** has also been determined using the CellTitre-Glo assay to confirm the MTT cytotoxicity data. This uses luminescence to determine the number of viable cells based on a quantification of ATP levels. Although, the IC_{50} for CTG is much higher then MTT; which is comparable to work done by Millard and co-worker (Millard et al., 2010), The data showed a similar trend to that determined using MTT, with zwitterions **5** - **7** showing slightly greater toxicity than thioacetate salts **8** - **10**.

4.9 Conclusion

Cell viability results show that all compounds are cytotoxic towards cells at very high concentrations and at prolonged period incubation times. The main purpose was also to synthesize compounds which were less toxic compared to the other phosphonium compounds studied previously (Millard et al., 2010, Rideout et al., 1989, Manetta et al., 1996) and this has been achieved. The IC_{50} values of **5** - **10** at 72 hours are significantly higher than other phosphonium derivatives which indicate that methoxy-phenyl phosphonium compounds could be ideal compounds for the surface-functionalization of AuNPs for biological applications.

4.10 References:

ALLABASHI, R., STACH, W., DE LA ESCOSURA-MU IZ, A., LISTE-CALLEJA, L. & MERKO I, A. 2009. ICP-MS: A powerful technique for quantitative determination of gold nanoparticles without dissolving. *Journal of Nanoparticles Research*, 11, 2003-2011.

ARNIDA, MALUGIN, A. & GHANDEHARI, H. 2010. Cellular uptake and toxicity of gold nanoparticles in prostate cancer cells: A comparative study of rods and spheres. *Journal of Applied Toxicology*, 30, 212-217.

BERCHEL, M., LE GALL, T., COUTHON-GOURVÈS, H., HAELTERS, J., MONTIER, T., MIDOUX, P., JAFFRÈS, P. 2012. Lipophosphonate/lipophosphoramidates: A family of synthetic vectors efficient for gene delivery. *Biochimie,* 1, 33-41.

BERGERON, K. L., MURPHY, E. L., MAJOFODUN, O., MUÑOZ, L. D., WILLIAMS, J. C., & ALMEIDA, K. H. 2009. Arylphosphonium salts interact with DNA to modulate cytotoxicity. *Mutation Research*, 2, 141–148.

CHEN, S., ZHOU, G., ZHANG, X., MAO, J., DE THE, H., & CHEN, Z. 2011. From an old remedy to a magic bullet: Molecular mechanisms underlying the therapeutic effects of arsenic in fighting leukemia. *Blood,* 24, 6425-6437.

CHEN, Y, S. 2014. PhD Thesis, Sheffield Hallam University.

CHEN, Y., ALLEN, D. W., TIZZARD, G. J., PITAK, M. B., COLES, S. J., CROSS, N. A., & BRICKLEBANK, N. 2017. Biological and structural studies of phosphonium 'masked thiolate' compounds. *European Journal of Medicinal Chemistry, 125*, 528-537.

CHITHRANI, B. D., GHAZINI, A. A., CHAN, W. C. W. 2006. Determining the size and shape dependence gold nanoparticle uptake into mammalian cells. *Nano Letters*, 6, 662-668

GOODMAN CM, MCCUSKER CD, YILMAZ T, ROTELLO VM. 2004. Toxicity of gold nanoparticles functionalized with cationic and anionic side chains. *Bioconjugate Chemistry*, 15, 897-900.

JOMOVA, K., JENISOVA, Z., FESZTEROVA, M., BAROS, S., LISKA, J., HUDECOVA, D., VALKO, M. 2011. Arsenic: Toxicity, oxidative stress and human disease. *Journal of Applied Toxicology,* 2, 95-107.

KIRUI, D. K., REY, D. A. & BATT, C. A. 2010. Gold hybrid nanoparticles for targeted phototherapy and cancer imaging. *Nanotechnology*, 21.

LALWANI, N., CHEN, Y., BROOKE, G., CROSS, N. A., ALLEN, D. W., REYNOLDS, A., OJEDA, J., TIZZARD, G, J., BRICKLEBANK, N. 2015. Triphenylarsonium-functionalized gold nanoparticles: Potential nanocarriers for intracellular therapeutics. *Chemical Communications,* 19, 4109-4111.

LE GALL, T., LOIZEAU, D., PICQUET, E., CARMOY, N., YAOUANC, J., BUREL-DESCHAMPS, L., MONTIER, T. 2010. A novel cationic lipophosphoramide with diunsaturated lipid chains: Synthesis, physicochemical properties, and transfection activities. *Journal of Medicinal Chemistry, 53*(4), 1496-1508.

LEVY, R., SHAHEEN, U., CESBRON, Y., S E, V. 2010. Gold nanoparticles delivery in mammalian cells: a critical revirew. *Nano Reviews*

MANETTA, A., GAMBOA, G., NASSERI, A., PODNOS, Y. D., EMMA, D., DORION, G., RIDEOUT, D. 1996. *Novel phosphonium salts displayin vitroandin VivoCytotoxic activity against human ovarian cancer cell lines,* 60, 203-212.

MILLARD, M., PATHANIA, D., SHABAIK, Y., TAHERI, L., DENG, J., & NEAMATI, N. 2010. Preclinical evaluation of novel triphenylphosphonium salts with broad-spectrum activity. *Plos One,* 10, e13131.

MUDHOO, A., SHARMA, S, K., GARG, V, K., TSENG, C, H. 2011. Arsenic: An overview of applications, health, and environmental concerns and removal processes. *Critical Review Environmental Science Technology*, 41, 435–519.

PAN, Y., NEUSS, S., LEIFERT, A., FISCHLER, M., WEN, F., SIMON, U., JAHNEN-DECHENT, W. 2007. Size-dependent cytotoxicity of gold nanoparticles. *Small,* 11, 1941-1949.

PATRA, H. K., BANERJEE, S., CHAUDHARI, U., LAHIRI, P. & DASGUPTA, A. K. 2007. Cell selective response to gold nanoparticles. *Nanomedicine: Nanotechnology, Biology, and Medicine*, 3, 111-119.

PICQUET, E., LE NY, K., DEL´EPINE, P., MONTIER, T., YAOUANC, J., CARTIER, D., CL´EMENT, J. 2005. Cationic lipophosphoramidates and lipophosphoguanidines are very efficient for in vivo DNA delivery. *Bioconjugate Chemistry, 16*(5), 1051-1053.

RIDEOUT B.A., MONTALI R.J., WALLACE S., BUSH M., PHILLIPS L.G., ANTONOVYCH T.T., SABNIS S.G. 1989. Renal medullary amyloidosis in Dorcas gazelles. *Veterinary Pathology*, 26, 129–135.

SAKURAI, T., & FUJIWARA, K. 2001. Modulation of cell adhesion and viability of cultured murine bone marrow cells by arsenobetaine, a major organic arsenic compound in marine animals. *British Journal of Pharmacology*, 1, 143–150.

SEHY, D. W., SHAO, L., RIDEOUT, D., & YU, J. 1993. Sensitivity of committed hematopoietic progenitor cells in vitro (BFU-E, CFU-E, CFU-GM) and two human carcinoma cell lines toward rhodamine-123 and phosphonium salt II-41. *Leukemia Research,* 3, 247-253.

SWINDELL, E. P., HANKINS, P. L., CHEN, H., MIODRAGOVIĆ, Đ. U., & O'HALLORAN, T. V. 2013. Anticancer activity of small-molecule and nanoparticulate arsenic(III) complexes. *Inorganic Chemistry,* 21, 12292-12304.

WILHELM, C., BILLOTEY, C., ROGER, J., PONS, J. N., BACRI, J. C. & GAZEAU, F. 2003. Intracellular uptake of anionic superparamagnetic nanoparticles as a function of their surface coating. *Biomaterials*, 24, 1001-1011.

ZHU, Z. J., TANG, R., YEH, Y. C., MIRANDA, O. R., ROTELLO, V. M., VACHET, R. W. 2012. Determination of the intracellular stability of gold nanoparticles monolayers using mass spectrometry. *Analytical Chemistry*, 84, 4321-4326.

JU-NAM, Y., ALLEN, D. W., GARDINER, P. H. E., & BRICKLEBANK, N. 2008. ω-Thioacetylalkylphosphonium salts: Precursors for the preparation of phosphonium-functionalized gold nanoparticles. *Journal of Organometallic Chemistry, 693*, 3504-3508.

JU-NAM, Y., BRICKLEBANK, N., ALLEN, D.W., GARDINER, P.H., LIGHT, M.E. & HURSTHOUSE, M.B. 2006. Phosphonioalkylthiosulfate zwitterions--new masked thiol ligands for the formation of cationic functionalized gold nanoparticles. *Organic & Biomolecular chemistry,* 4, 4345-4351.

JU-NAM, Y., CHEN, Y., OJEDA, J. J., ALLEN, D. W., CROSS, N. A., GARDINER, P. H. E., & BRICKLEBANK, N. 2012. Water-soluble gold nanoparticles stabilized with cationic phosphonium thiolate ligands. *RSC Advances*, 2, 10345-10351.

YANG Y, GAO N, HU Y, JIA C, CHOU T, DU H, WANG H. 2015. Gold nanoparticle-enhanced photodynamic therapy: effects of surface charge and mitochondrial targeting. *Therapeutic delivery*, 6, 307-321.

Chapter 5

Conclusions and Suggestions for Future Work

5.1 Conclusion and Future Work

This thesis presents a body of original research relating to the synthesis and chemical and biological characterization of triphenylarsonium-alkylthiosulfate zwitterions and alkylthioacetate salts, and the associated triphenylarsoniumalkylthiolate-protected gold nanoparticles, and a series of triarylphosphonium-alkylthiosulfate zwitterions and alkylthioacetate salts based on triarylphosphines bearing methoxyphenyl substituents.

Chapter 3A reports the synthesis of the triphenylarsoniopropylthiosulfate zwitterion and ω-thioacetylpropyl(triphenyl)arsonium salt. Both compounds have been characterized by single-crystal X-ray crystallography, elemental analysis, NMR and IR spectroscopy and mass spectrometry. Investigations into the cytotoxicity of the triphenylarsoniopropylthiosulfate zwitterions and ω-thioacetylpropyl(triphenyl)arsonium towards PC3 prostate cancer cells are described in chapter 4 and show that both compounds are toxic to the cells at high concentrations and at prolonged incubation times (Lalwani et al., 2015). However, the triphenylarsonium compounds reported here are less cytotoxic than the analogous phosphonium compounds. Similarly, Millard et al (2010) investigated the cytotoxicity of numerous triphenylphosphonium compounds in several cancer cell lines including the PC3 cells utilized in this study. Their most toxic compound has an IC_{50} value of 0.4 μM at 72 hours in PC3 which is significantly more toxic than the triphenylarsonium compounds described here. Further work should be carried out to determine the cytotoxicity of the triphenylarsoniopropylthiosulfate zwitterion and ω-thioacetylpropyl (triphenyl) arsonium salt towards other cell lines, including cancer cells and normal cell lines. Research should

also be done to determine how much of the compounds are taken-up by cells and to establish if the compounds are localized within the mitochondria of the cells.

The triphenylarsoniopropylthiosulfate zwitterion and ω-thioacetylpropyl(triphenyl)arsonium salt can be used to prepare AuNPs functionalized with triphenylarsoniumpropylthiolate ligands using a modification of the well-known Brust-Schiffrin synthesis (Brust et al., 1995). The resulting triphenylarsoniumpropylthiolate-capped AuNPs are cationic and water-soluble, making them potential candidates for biological applications. A number of analytical techniques have been used to characterize the triphenylarsoniumpropylthiolate-capped AuNPs, including XPS, TEM, mass spectrometry, UV-visible, IR and Raman spectroscopy. TEM results showed all triphenylarsoniumpropylthiolate-capped AuNPs synthesized have a uniform spherical shape with mean core sizes of *c.a.* 3 nm. The presence of triphenylarsonium-propylthiolate groups on the surface of the AuNPs was confirmed by TEM and mass spectrometry which show that the S-S bond of the thiosulfate group of the zwitterion and the S-C bond of the thioacetate group of the triphenylarsonium salt are cleaved under the reductive conditions employed in the Brust-Schiffrin method.

Chapter 3B reports the synthesis of a family of methoxy-phenyl substituted phosphoniopropylthiosulfate zwitterions and ω-thioacetylpropyl(triaryl)phosphonium salts. All compounds have been characterized by elemental analysis, NMR and IR spectroscopy and mass spectrometry. A single crystal X-ray diffraction study of tri(2,4,6-trimethoxyphenyl)phosphoniopropyl-thiosulfate zwitterions showed the compound to be very disordered. This is not unusual for derivatives of tri(2,4,6-

trimethoxyphenyl)phosphine. The next step is to investigate the use of the methoxy-phenyl substituted phosphoniopropylthiosulfate zwitterions and ω-thioacetylpropyl (methoxy-phenyl)phosphonium salts as capping ligands for the functionalized gold nanoparticles and to determine the biological properties of the resulting methoxyphenylphosphoniumalkylthiolate-capped AuNPs.

Chapter 4A reports the preliminary investigation into the cytotoxicity of the triphenylarsoniumpropylthiolate-capped AuNPs towards PC3 prostate cancer and human fibroblast normal cell lines. The results show that the AuNPs have a similar toxicity toward both cell lines. This result contrasts with previous studies on triphenylphosphoniumpropylthiolate-capped AuNPs which were not toxic towards cells (Chen PhD thesis, 2014). Previous studies by Pan and coworkers (Pan et al., 2007) have demonstrated that the cytotoxicity of AuNPs is size-dependent. Larger AuNPs, with diameters >15nm, are relatively non-toxic to cells whereas small AuNPs, with diameters <5nm, are toxic towards cells. It is not clear whether the toxicity of the triphenylarsoniumpropylthiolate-capped AuNPs is due to the small size of the AuNPs or some intra-cellular metabolite of the triphenylarsoniumpropylthiolate moiety, or possibly a combination of both. Further research could be undertaken to prepare larger AuNPs functionalized with triphenylarsoniumpropylthiolate ligands and determine their cytotoxicity towards different cell lines.

The amount of gold taken-up by the cells was determined by ICP-OES spectroscopy and showed that a much lower amount of the triphenylarsoniumpropylthiolate-capped AuNPs

were taken-up by the cells compared to triphenylphosphoniumalkylthiolate-capped AuNPs (Chen PhD thesis, 2014) and citrate-stabilized AuNPs purchased from Sigma-Aldrich. Further research is necessary to confirm this result and to investigate the why the triphenylarsoniumpropylthiolate-capped AuNPs do not appear to be taken-up as readily as the analogous triphenylphosphoniumalkylthiolate-capped AuNPs.

Chapter 4B reports preliminary investigation into the cytotoxicity of methoxy-phenyl substituted phosphoniopropylthiosulfate zwitterions and ω-thioacetylpropyl(triaryl)phosphonium salts towards PC3 prostate cancer lines. Previous work has shown that analogous triphenylphosphoniopropylthiosulfate zwitterions are essentially insoluble in water and biological media, which has prevented its cytotoxicity from being determined (Chen et al., 2017) In contrast, the tri(methoxyphenyl)phosphoniopropylthiosulfate zwitterions are soluble in water. The IC_{50} values of all of the methoxy-phenyl substituted phosphonio-propylthiosulfate zwitterions and ω-thioacetylpropyl(methoxy-phenyl) phosphonium salts towards PC3 prostate cancer have been determined. All of the compounds are less cytotoxic than the analogous ω-thioacetylpropyl(triphenyl)phosphonium salt and other triphenylphosphonium derivatives.

5.2 References

BRUST, M., FINK, J., BETHELL, D., SCHIFFRIN, D. J., & KIELY, C. 1995. Synthesis and reactions of functionalized gold nanoparticles. *Journal of the Chemical Society, Chemical Communications,* 16, 1655-1656.

BRUST, M., WALKER, M., BETHELL, D., SCHIFFRIN, D. J. & WHYMAN, R. 1994. Synthesis of thiol-derivatised gold nanoparticles in a two-phase liquid-liquid system. *Journal of the Chemical Society, Chemical Communications*, 801-802.

CHEN, Y, S. 2014. PhD Thesis, Sheffield Hallam University.

CHEN, Y., ALLEN, D. W., TIZZARD, G. J., PITAK, M. B., COLES, S. J., CROSS, N. A., & BRICKLEBANK, N. 2017. Biological and structural studies of phosphonium 'masked thiolate' compounds. *European Journal of Medicinal Chemistry, 125*, 528-537.

LALWANI, N., CHEN, Y., BROOKE, G., CROSS, N. A., ALLEN, D. W., REYNOLDS, A., OJEDA, J., TIZZARD, G, J., BRICKLEBANK, N. 2015. Triphenylarsonium-functionalized gold nanoparticles: Potential nanocarriers for intracellular therapeutics. *Chemical Communications,* 19, 4109-4111.

MILLARD, M., PATHANIA, D., SHABAIK, Y., TAHERI, L., DENG, J., & NEAMATI, N. 2010. Preclinical evaluation of novel triphenylphosphonium salts with broad-spectrum activity. *Plos One,* 10, e13131.

PAN, Y., NEUSS, S., LEIFERT, A., FISCHLER, M., WEN, F., SIMON, U., JAHNEN-DECHENT, W. 2007. Size-dependent cytotoxicity of gold nanoparticles. *Small,* 11, 1941-1949.

Chapter 6

Associated work

6.1 Publications:

Lalwani, N., Chen, Y., Brooke, G., Cross, N. A., Allen, D. W., Reynolds, A., Ojeda, J., Tizzard, G, J., Bricklebank, N. 2015. Triphenylarsonium-functionalized gold nanoparticles: Potential nanocarriers for intracellular therapeutics. *Chemical Communications,* 19, 4109-4111.

6.2 Conferences attended

1. Mass Spectrometry Showcase day (Jul 2014), Sheffield Hallam University, UK.

2. Northern Universities Postgraduate Symposium (Sep 2014), University of Sheffield, UK

3. Biomedical Research Centre Winter Poster Event (Dec 2013, Dec 2014, Dec 2015). Sheffield Hallam University, UK.

6.3 Poster Presentations

- **Lalwani, N.,** Cross, N. A., Bricklebank, N. 2014. Synthesis & Characterization of Arsonium functionalized nanoparticles. Physical Chemistry of Functional Biomedical Nanoparticles Faraday Discussion 175. Bristol, United Kingdom.

- **Lalwani, N.,** Cross, N. A., Bricklebank, N. 2015. Triphenylarsonium-conjugated gold nanoparticles: potential nanocarriers for mitochondria-targeted therapeutics. 12th International Conference on Materials Chemistry (MC12). York, United Kingdom.

6.4 Appendices

Appendix 1.

Crystal data and structure refinement details for triphenylarsoniopropylthiosulfate zwitterion. Compound 2, described in chapter 3A.

Table A1.1. Crystal data and structure refinement details.

Identification code	**2011ncs0152aa**	
Empirical formula	$C_{21}H_{21}AsO_3S_2$	
Formula weight	460.42	
Temperature	100(2) K	
Wavelength	0.71073 Å	
Crystal system	Monoclinic	
Space group	*P*21/*n*	
Unit cell dimensions	*a* = **11.687(5) Å**	α = **90°**
	b = **14.366(6) Å**	β = **106.254(5)°**
	c = **12.127(5) Å**	γ = **90°**
Volume	1954.7(14) $Å^3$	
Z	4	
Density (calculated)	1.565 Mg / m^3	
Absorption coefficient	1.972 mm^{-1}	
F(000)	944	
Crystal	Needle; Colourless	
Crystal size	0.30 × 0.15 × 0.02 mm^3	
θ range for data collection	3.19 – 27.48°	
Index ranges	$-15 \le h \le 15$, $-18 \le k \le 11$, $-15 \le l \le 11$	
Reflections collected	10357	
Independent reflections	4425 [R_{int} = 0.0510]	
Completeness to θ = 27.48°	98.7 %	
Absorption correction	Semi–empirical from equivalents	
Max. and min. transmission	0.9616 and 0.5892	
Refinement method	Full-matrix least-squares on F^2	
Data / restraints / parameters	4425 / 0 / 244	
Goodness-of-fit on F^2	1.143	
Final *R* indices [$F^2 > 2\sigma(F^2)$]	*R1* = 0.0730, *wR2* = 0.1111	
R indices (all data)	*R1* = 0.0858, *wR2* = 0.1173	
Largest diff. peak and hole	0.644 and –1.100 e $Å^{-3}$	

Diffractometer: *Rigaku Saturn724+* area detector (ϕ scans and ω scans to fill *asymmetric unit* sphere). **Cell determination:** *CrystalClear-SM Expert 2.0 r7* (Rigaku, 2011). **Data collection:** *CrystalClear-SM Expert 2.0 r7* (Rigaku, 2011). **Data reduction and cell refinement**: *CrystalClear-SM Expert 2.0 r7* (Rigaku, 2011). **Absorption correction**: *CrystalClear-SM Expert 2.0 r7* (Rigaku, 2011). S**tructure solution**: *SUPERFLIP* (Palatinus, L. & Chapuis, G. (2007). J. Appl. Cryst. 40, 786-790.) S**tructure refinement**:

SHELXL97 (G Sheldrick, G.M. (2008). Acta Cryst. A64, 112-122.). **Graphics:** *OLEX2* (Dolomanov, O. V., Bourhis, L. J., Gildea, R. J., Howard, J. A. K. & Puschmann, H. (2009). J. Appl. Cryst. 42, 339-341.)

Table A1.2 . Atomic coordinates [× 10^4], equivalent isotropic displacement parameters [Å^2 × 10^3] and site occupancy factors. U_{eq} is defined as one third of the trace of the orthogonalized U^{ij} tensor.

Atom	*x*	*y*	*z*	U_{eq}	*S.o.f.*
C1	10852(4)	2610(3)	223(4)	18(1)	1
C2	11673(4)	3452(3)	379(5)	19(1)	1
C3	12695(4)	3257(3)	−142(4)	20(1)	1
C4	8898(4)	1613(3)	1032(4)	15(1)	1
C5	8489(4)	1465(3)	1987(4)	20(1)	1
C6	8134(5)	573(4)	2186(5)	24(1)	1
C7	8179(4)	−141(3)	1444(5)	21(1)	1
C8	8559(4)	15(3)	478(5)	22(1)	1
C9	8926(4)	901(3)	258(4)	18(1)	1
C10	8238(4)	3486(3)	−372(4)	15(1)	1
C11	8406(5)	3749(3)	−1413(4)	19(1)	1
C12	7532(5)	4280(3)	−2164(5)	22(1)	1
C13	6513(4)	4541(3)	−1860(4)	20(1)	1
C14	6351(4)	4262(3)	−829(5)	21(1)	1
C15	7210(4)	3722(3)	−67(4)	18(1)	1
C16	9876(4)	3530(3)	2102(4)	19(1)	1
C17	9548(4)	4453(3)	2085(5)	20(1)	1
C18	9934(5)	4987(4)	3071(5)	26(1)	1
C19	10651(4)	4584(4)	4064(5)	24(1)	1
C20	10948(5)	3649(4)	4089(5)	25(1)	1
C21	10579(4)	3116(4)	3106(4)	23(1)	1
O1	14228(3)	3273(2)	2672(3)	22(1)	1
O2	15307(3)	3774(2)	1338(3)	24(1)	1
O3	15745(3)	2278(3)	2301(3)	32(1)	1
S1	13657(1)	2293(1)	505(1)	23(1)	1
S2	14873(1)	2999(1)	1861(1)	19(1)	1
As1	9451(1)	2811(1)	728(1)	15(1)	1

Table A1.3 Bond lengths [Å] and angles [°].

C1–C2	1.523(6)	C19–H19	0.9500
C1–As1	1.923(5)	C20–C21	1.380(7)
C1–H1A	0.9900	C20–H20	0.9500
C1–H1B	0.9900	C21–H21	0.9500
C2–C3	1.527(7)	O1–S2	1.452(4)
C2–H2A	0.9900	O2–S2	1.443(4)
C2–H2B	0.9900	O3–S2	1.446(4)
C3–S1	1.817(5)	S1–S2	2.1081(18)
C3–H3A	0.9900		
C3–H3B	0.9900	C2–C1–As1	113.8(3)
C4–C5	1.388(7)	C2–C1–H1A	108.8
C4–C9	1.395(7)	As1–C1–H1A	108.8
C4–As1	1.910(5)	C2–C1–H1B	108.8
C5–C6	1.388(7)	As1–C1–H1B	108.8
C5–H5	0.9500	H1A–C1–H1B	107.7
C6–C7	1.376(7)	C1–C2–C3	109.9(4)
C6–H6	0.9500	C1–C2–H2A	109.7
C7–C8	1.382(7)	C3–C2–H2A	109.7
C7–H7	0.9500	C1–C2–H2B	109.7
C8–C9	1.393(7)	C3–C2–H2B	109.7
C8–H8	0.9500	H2A–C2–H2B	108.2
C9–H9	0.9500	C2–C3–S1	115.0(4)
C10–C11	1.383(7)	C2–C3–H3A	108.5
C10–C15	1.395(7)	S1–C3–H3A	108.5
C10–As1	1.916(4)	C2–C3–H3B	108.5
C11–C12	1.391(7)	S1–C3–H3B	108.5
C11–H11	0.9500	H3A–C3–H3B	107.5
C12–C13	1.393(7)	C5–C4–C9	121.9(5)
C12–H12	0.9500	C5–C4–As1	120.9(4)
C13–C14	1.375(7)	C9–C4–As1	117.3(4)
C13–H13	0.9500	C6–C5–C4	118.4(5)
C14–C15	1.394(7)	C6–C5–H5	120.8
C14–H14	0.9500	C4–C5–H5	120.8
C15–H15	0.9500	C7–C6–C5	120.4(5)
C16–C17	1.379(7)	C7–C6–H6	119.8
C16–C21	1.396(7)	C5–C6–H6	119.8
C16–As1	1.904(5)	C6–C7–C8	121.0(5)
C17–C18	1.385(7)	C6–C7–H7	119.5
C17–H17	0.9500	C8–C7–H7	119.5
C18–C19	1.387(7)	C7–C8–C9	120.0(5)
C18–H18	0.9500	C7–C8–H8	120.0
C19–C20	1.386(8)	C9–C8–H8	120.0

C8–C9–C4	118.3(5)	O3–S2–S1	101.28(17)
C8–C9–H9	120.8	O1–S2–S1	107.13(16)
C4–C9–H9	120.8	C16–As1–C4	109.8(2)
C11–C10–C15	122.0(4)	C16–As1–C10	107.2(2)
C11–C10–As1	120.5(4)	C4–As1–C10	111.5(2)
C15–C10–As1	117.5(4)	C16–As1–C1	108.8(2)
C10–C11–C12	118.8(5)	C4–As1–C1	106.9(2)
C10–C11–H11	120.6	C10–As1–C1	112.6(2)
C12–C11–H11	120.6		
C11–C12–C13	120.0(5)		
C11–C12–H12	120.0		
C13–C12–H12	120.0		
C14–C13–C12	120.5(5)		
C14–C13–H13	119.8		
C12–C13–H13	119.8		
C13–C14–C15	120.6(5)		
C13–C14–H14	119.7		
C15–C14–H14	119.7		
C14–C15–C10	118.2(5)		
C14–C15–H15	120.9		
C10–C15–H15	120.9		
C17–C16–C21	121.0(5)		
C17–C16–As1	120.3(4)		
C21–C16–As1	118.6(4)		
C16–C17–C18	119.9(5)		
C16–C17–H17	120.1		
C18–C17–H17	120.1		
C17–C18–C19	119.3(5)		
C17–C18–H18	120.4		
C19–C18–H18	120.4		
C20–C19–C18	120.7(5)		
C20–C19–H19	119.6		
C18–C19–H19	119.6		
C21–C20–C19	120.2(5)		
C21–C20–H20	119.9		
C19–C20–H20	119.9		
C20–C21–C16	118.9(5)		
C20–C21–H21	120.6		
C16–C21–H21	120.6		
C3–S1–S2	99.84(17)		
O2–S2–O3	114.6(2)		
O2–S2–O1	113.7(2)		
O3–S2–O1	113.0(2)		
O2–S2–S1	105.78(16)		

Table A1.4. Anisotropic displacement parameters [Å^2× 10^3]. The anisotropic displacement factor exponent takes the form: $-2\pi^2[h^2a^{*2}U^{11} + \cdots + 2\,h\,k\,a^*\,b^*\,U^{12}]$.

Atom	U^{11}	U^{22}	U^{33}	U^{23}	U^{13}	U^{12}
C1	18(3)	16(2)	17(2)	−2(2)	1(2)	2(2)
C2	13(2)	18(2)	25(3)	0(2)	5(2)	0(2)
C3	16(3)	24(3)	17(3)	3(2)	−2(2)	−7(2)
C4	10(2)	16(2)	18(2)	−1(2)	1(2)	2(2)
C5	21(3)	21(2)	17(3)	−4(2)	6(2)	−6(2)
C6	26(3)	25(3)	19(3)	3(2)	5(2)	−8(2)
C7	19(3)	14(2)	27(3)	4(2)	3(2)	−2(2)
C8	20(3)	17(2)	26(3)	−5(2)	1(2)	2(2)
C9	14(2)	22(2)	17(3)	−2(2)	0(2)	4(2)
C10	11(2)	15(2)	18(2)	2(2)	1(2)	3(2)
C11	19(3)	19(2)	21(3)	0(2)	8(2)	4(2)
C12	22(3)	22(3)	21(3)	1(2)	6(2)	0(2)
C13	17(3)	19(2)	19(3)	0(2)	−3(2)	4(2)
C14	13(3)	20(2)	26(3)	−6(2)	2(2)	0(2)
C15	15(2)	16(2)	18(3)	−3(2)	0(2)	−1(2)
C16	16(3)	23(2)	16(2)	−1(2)	2(2)	−1(2)
C17	16(3)	19(2)	23(3)	−1(2)	3(2)	3(2)
C18	21(3)	25(3)	31(3)	−11(2)	8(2)	0(2)
C19	13(3)	39(3)	21(3)	−14(2)	6(2)	−6(2)
C20	18(3)	41(3)	16(3)	4(2)	4(2)	1(2)
C21	16(3)	25(3)	24(3)	−1(2)	1(2)	3(2)
O1	26(2)	27(2)	16(2)	−1(2)	10(2)	2(2)
O2	21(2)	29(2)	22(2)	1(2)	6(2)	−9(2)
O3	22(2)	29(2)	36(2)	1(2)	−5(2)	13(2)
S1	18(1)	24(1)	26(1)	−8(1)	2(1)	0(1)
S2	17(1)	19(1)	19(1)	0(1)	1(1)	1(1)
As1	14(1)	14(1)	16(1)	−1(1)	2(1)	1(1)

Table A1.5. Hydrogen coordinates [× 10^4] and isotropic displacement parameters [Å^2 × 10^3].

Atom	*x*	*y*	*z*	U_{eq}	*S.o.f.*
H1A	11303	2079	655	21	1
H1B	10602	2438	–600	21	1
H2A	11996	3593	1208	23	1
H2B	11217	4001	0	23	1
H3A	13188	3825	–74	24	1
H3B	12356	3126	–971	24	1
H5	8452	1962	2493	23	1
H6	7857	456	2839	29	1
H7	7946	–749	1597	25	1
H8	8570	–482	–35	26	1
H9	9189	1017	–403	22	1
H11	9106	3570	–1611	23	1
H12	7630	4464	–2885	26	1
H13	5926	4915	–2368	24	1
H14	5648	4438	–636	25	1
H15	7098	3521	642	21	1
H17	9058	4721	1399	24	1
H18	9711	5623	3066	31	1
H19	10941	4952	4734	29	1
H20	11406	3373	4785	30	1
H21	10800	2480	3112	27	1

Table A1.6. Torsion angles [°].

As1–C1–C2–C3	–174.9(3)
C1–C2–C3–S1	–61.7(5)
C9–C4–C5–C6	1.9(7)
As1–C4–C5–C6	–177.9(4)
C4–C5–C6–C7	–0.6(8)
C5–C6–C7–C8	–1.0(8)
C6–C7–C8–C9	1.3(8)
C7–C8–C9–C4	0.0(7)
C5–C4–C9–C8	–1.7(7)
As1–C4–C9–C8	178.2(4)
C15–C10–C11–C12	1.3(7)
As1–C10–C11–C12	–176.7(4)
C10–C11–C12–C13	0.3(7)
C11–C12–C13–C14	–1.4(8)
C12–C13–C14–C15	0.8(7)
C13–C14–C15–C10	0.8(7)
C11–C10–C15–C14	–1.8(7)
As1–C10–C15–C14	176.2(3)
C21–C16–C17–C18	1.1(8)
As1–C16–C17–C18	–175.4(4)
C16–C17–C18–C19	0.1(8)
C17–C18–C19–C20	–2.2(8)
C18–C19–C20–C21	3.1(8)
C19–C20–C21–C16	–1.9(8)
C17–C16–C21–C20	–0.2(8)
As1–C16–C21–C20	176.3(4)
C2–C3–S1–S2	–86.9(3)
C3–S1–S2–O2	–52.7(2)
C3–S1–S2–O3	–172.6(3)
C3–S1–S2–O1	68.8(2)
C17–C16–As1–C4	–136.6(4)
C21–C16–As1–C4	46.8(5)
C17–C16–As1–C10	–15.3(5)
C21–C16–As1–C10	168.1(4)
C17–C16–As1–C1	106.7(4)
C21–C16–As1–C1	–69.9(5)
C5–C4–As1–C16	20.8(5)
C9–C4–As1–C16	–159.1(3)
C5–C4–As1–C10	–97.9(4)
C9–C4–As1–C10	82.2(4)
C5–C4–As1–C1	138.7(4)
C9–C4–As1–C1	–41.2(4)

C11–C10–As1–C16	121.6(4)
C15–C10–As1–C16	–56.5(4)
C11–C10–As1–C4	–118.1(4)
C15–C10–As1–C4	63.8(4)
C11–C10–As1–C1	2.0(5)
C15–C10–As1–C1	–176.1(3)
C2–C1–As1–C16	–39.1(4)
C2–C1–As1–C4	–157.7(3)
C2–C1–As1–C10	79.6(4)

Appendix 2.

Crystal data and structure refinement details for ω-thioacetylpropyl(triphenyl)aronium bromide. Compound 3, described in chapter 3A.

Table A2.1. Crystal data and structure refinement details.

NCS Identification code	2012ncs0291a	
Empirical formula	$C_{23}H_{24}AsBrOS$	
Formula weight	503.31	
Temperature	120(2) K	
Wavelength	0.71075 Å	
Crystal system	Monoclinic	
Space group	*P*21/*n*	
Unit cell dimensions	*a* = 11.1700(3) Å	α = 90°
	b = 13.6075(4) Å	β = 91.738(7)°
	c = 14.4757(10) Å	γ = 90°
Volume	2199.23(18) Å^3	
Z	4	
Density (calculated)	1.520 Mg / m^3	
Absorption coefficient	3.467 mm^{-1}	
F(000)	1016	
Crystal	Block; Colourless	
Crystal size	0.52 × 0.32 × 0.14 mm^3	
θ range for data collection	2.99 – 27.44°	
Index ranges	$-14 \le h \le 13$, $-16 \le k \le 17$, $-18 \le l \le 18$	
Reflections collected	13491	
Independent reflections	4973 [R_{int} = 0.0274]	
Completeness to θ = 27.44°	99.0 %	
Absorption correction	Semi–empirical from equivalents	
Max. and min. transmission	0.6424 and 0.2658	
Refinement method	Full-matrix least-squares on F^2	
Data / restraints / parameters	4973 / 0 / 245	
Goodness-of-fit on F^2	0.960	
Final *R* indices [$F^2 > 2\sigma(F^2)$]	*R1* = 0.0267, *wR2* = 0.0530	
R indices (all data)	*R1* = 0.0398, *wR2* = 0.0641	
Largest diff. peak and hole	0.546 and –0.505 e Å^{-3}	

Diffractometer: *Rigaku R-Axis Spider* including curved Fujifilm image plate and a graphite monochromated sealed tube Mo generator. **Cell determination and data collection**: *CrystalClear-SM Expert 2.0 r11* (Rigaku, 2011). **Data reduction, cell refinement and absorption correction**: *CrystalClear-SM Expert 2.0 r13* (Rigaku, 2011). **Structure solution**: *SUPERFLIP* (Palatinus, L. & Chapuis, G. (2007). J. Appl. Cryst. 40, 786-790). **Structure refinement**: *SHELXL97* (Sheldrick, G.M. (2008). Acta Cryst. A64, 112-122). **Graphics:** *OLEX2* (Dolomanov, O. V., Bourhis, L. J., Gildea, R. J., Howard, J. A. K. & Puschmann, H. (2009). J. Appl. Cryst. 42, 339-341).

Table A2.2. Atomic coordinates [× 10^4], equivalent isotropic displacement parameters [Å^2 × 10^3] and site occupancy factors. U_{eq} is defined as one third of the trace of the orthogonalized U^{ij} tensor.

Atom	*x*	*y*	*z*	U_{eq}	*S.o.f.*
C1	6685(2)	1183(2)	1381(2)	18(1)	1
C2	6645(3)	501(2)	549(2)	24(1)	1
C3	6381(3)	1059(2)	−354(2)	26(1)	1
C4	6847(3)	3069(2)	−447(2)	26(1)	1
C5	7651(3)	3928(2)	−628(2)	39(1)	1
C6	6981(2)	1506(2)	3484(2)	16(1)	1
C7	5994(2)	2133(2)	3503(2)	19(1)	1
C8	5974(2)	2870(2)	4165(2)	21(1)	1
C9	6916(2)	2978(2)	4801(2)	20(1)	1
C10	7891(2)	2348(2)	4784(2)	20(1)	1
C11	7929(2)	1603(2)	4130(2)	19(1)	1
C12	8626(2)	−2(2)	2526(2)	18(1)	1
C13	9481(2)	422(2)	1968(2)	25(1)	1
C14	10641(3)	61(2)	2014(2)	32(1)	1
C15	10944(3)	−705(2)	2597(2)	33(1)	1
C16	10093(3)	−1132(2)	3146(2)	32(1)	1
C17	8924(3)	−779(2)	3115(2)	24(1)	1
C18	5955(2)	−514(2)	2795(2)	16(1)	1
C19	5949(2)	−1352(2)	2246(2)	21(1)	1
C20	5105(3)	−2080(2)	2395(2)	24(1)	1
C21	4298(2)	−1983(2)	3100(2)	26(1)	1
C22	4332(2)	−1158(2)	3664(2)	26(1)	1
C23	5155(2)	−416(2)	3512(2)	22(1)	1
As1	7043(1)	531(1)	2538(1)	15(1)	1
O1	5828(2)	3146(2)	−207(2)	37(1)	1
S1	7546(1)	1917(1)	−639(1)	30(1)	1
Br1	3579(1)	1232(1)	1856(1)	22(1)	1

Table A2.3. Bond lengths [Å] and angles [°].

C1–C2	1.521(3)	C18–C19	1.390(4)
C1–As1	1.927(2)	C18–C23	1.396(4)
C1–H1A	0.9900	C18–As1	1.914(3)
C1–H1B	0.9900	C19–C20	1.389(4)
C2–C3	1.533(4)	C19–H19	0.9500
C2–H2A	0.9900	C20–C21	1.388(4)
C2–H2B	0.9900	C20–H20	0.9500
C3–S1	1.806(3)	C21–C22	1.388(4)
C3–H3A	0.9900	C21–H21	0.9500
C3–H3B	0.9900	C22–C23	1.388(4)
C4–O1	1.204(3)	C22–H22	0.9500
C4–C5	1.501(4)	C23–H23	0.9500
C4–S1	1.777(3)		
C5–H5A	0.9800	C2–C1–As1	114.06(18)
C5–H5B	0.9800	C2–C1–H1A	108.7
C5–H5C	0.9800	As1–C1–H1A	108.7
C6–C11	1.396(3)	C2–C1–H1B	108.7
C6–C7	1.396(4)	As1–C1–H1B	108.7
C6–As1	1.909(2)	H1A–C1–H1B	107.6
C7–C8	1.387(4)	C1–C2–C3	111.9(2)
C7–H7	0.9500	C1–C2–H2A	109.2
C8–C9	1.385(4)	C3–C2–H2A	109.2
C8–H8	0.9500	C1–C2–H2B	109.2
C9–C10	1.387(4)	C3–C2–H2B	109.2
C9–H9	0.9500	H2A–C2–H2B	107.9
C10–C11	1.388(4)	C2–C3–S1	113.17(19)
C10–H10	0.9500	C2–C3–H3A	108.9
C11–H11	0.9500	S1–C3–H3A	108.9
C12–C17	1.392(4)	C2–C3–H3B	108.9
C12–C13	1.394(4)	S1–C3–H3B	108.9
		H3A–C3–H3B	107.8
C12–As1	1.912(2)	O1–C4–C5	124.0(3)
C13–C14	1.385(4)	O1–C4–S1	123.0(2)
C13–H13	0.9500	C5–C4–S1	113.0(2)
C14–C15	1.378(4)	C4–C5–H5A	109.5
C14–H14	0.9500	C4–C5–H5B	109.5
C15–C16	1.385(5)	H5A–C5–H5B	109.5
C15–H15	0.9500	C4–C5–H5C	109.5
C16–C17	1.390(4)	H5A–C5–H5C	109.5
C16–H16	0.9500	H5B–C5–H5C	109.5
C17–H17	0.9500	C11–C6–C7	120.8(2)
		C11–C6–As1	120.18(19)

C7–C6–As1	118.98(18)	C22–C21–H21	119.9
C8–C7–C6	119.0(2)	C20–C21–H21	119.9
C8–C7–H7	120.5	C23–C22–C21	120.1(3)
C6–C7–H7	120.5	C23–C22–H22	119.9
C9–C8–C7	120.5(2)	C21–C22–H22	119.9
C9–C8–H8	119.7	C22–C23–C18	119.4(2)
C7–C8–H8	119.7	C22–C23–H23	120.3
C8–C9–C10	120.2(2)	C18–C23–H23	120.3
C8–C9–H9	119.9	C6–As1–C12	108.90(10)
C10–C9–H9	119.9	C6–As1–C18	109.88(10)
C11–C10–C9	120.3(2)	C12–As1–C18	108.21(11)
C11–C10–H10	119.9	C6–As1–C1	107.02(11)
C9–C10–H10	119.9	C12–As1–C1	109.52(11)
C10–C11–C6	119.2(2)	C18–As1–C1	113.24(10)
C10–C11–H11	120.4	C4–S1–C3	102.23(14)
C6–C11–H11	120.4		
C17–C12–C13	120.9(2)		
C17–C12–As1	119.1(2)		
C13–C12–As1	119.9(2)		
C14–C13–C12	118.8(3)		
C14–C13–H13	120.6		
C12–C13–H13	120.6		
C15–C14–C13	120.6(3)		
C15–C14–H14	119.7		
C13–C14–H14	119.7		
C14–C15–C16	120.6(3)		
C14–C15–H15	119.7		
C16–C15–H15	119.7		
C17–C16–C15	119.8(3)		
C17–C16–H16	120.1		
C15–C16–H16	120.1		
C16–C17–C12	119.3(3)		
C16–C17–H17	120.4		
C12–C17–H17	120.4		
C19–C18–C23	120.8(2)		
C19–C18–As1	119.36(19)		
C23–C18–As1	119.84(19)		
C20–C19–C18	119.2(2)		
C20–C19–H19	120.4		
C18–C19–H19	120.4		
C19–C20–C21	120.4(3)		
C19–C20–H20	119.8		
C21–C20–H20	119.8		
C22–C21–C20	120.1(3)		

Table A2.4. Anisotropic displacement parameters [$Å^2 \times 10^3$]. The anisotropic displacement factor exponent takes the form: $-2\pi^2[h^2a^{*2}U^{11} + \cdots + 2\,h\,k\,a^*\,b^*\,U^{12}]$.

Atom	U^{11}	U^{22}	U^{33}	U^{23}	U^{13}	U^{12}
C1	19(1)	18(1)	18(1)	1(1)	−1(1)	2(1)
C2	30(1)	19(1)	21(1)	−1(1)	−4(1)	−2(1)
C3	32(2)	25(1)	20(1)	0(1)	−4(1)	−4(1)
C4	32(2)	31(2)	16(1)	−3(1)	1(1)	−7(1)
C5	52(2)	37(2)	29(2)	−1(1)	6(1)	−16(2)
C6	17(1)	16(1)	15(1)	1(1)	2(1)	−5(1)
C7	16(1)	21(1)	21(1)	1(1)	−2(1)	−1(1)
C8	19(1)	19(1)	25(1)	−2(1)	3(1)	3(1)
C9	27(1)	18(1)	16(1)	0(1)	4(1)	−4(1)
C10	21(1)	23(1)	16(1)	2(1)	−2(1)	−4(1)
C11	18(1)	20(1)	19(1)	4(1)	−1(1)	0(1)
C12	14(1)	19(1)	21(1)	−4(1)	−3(1)	2(1)
C13	21(1)	23(1)	31(1)	−3(1)	1(1)	−1(1)
C14	19(1)	38(2)	40(2)	−9(1)	6(1)	−3(1)
C15	18(1)	43(2)	37(2)	−13(1)	−6(1)	10(1)
C16	33(2)	35(2)	28(1)	−2(1)	−10(1)	14(1)
C17	25(1)	24(1)	24(1)	1(1)	−1(1)	4(1)
C18	16(1)	15(1)	18(1)	2(1)	−1(1)	2(1)
C19	25(1)	20(1)	19(1)	1(1)	1(1)	−2(1)
C20	32(2)	18(1)	22(1)	0(1)	−1(1)	−4(1)
C21	22(1)	21(1)	33(2)	8(1)	−1(1)	−6(1)
C22	24(1)	23(1)	32(1)	5(1)	11(1)	1(1)
C23	23(1)	18(1)	25(1)	0(1)	2(1)	1(1)
As1	14(1)	14(1)	16(1)	0(1)	1(1)	0(1)
O1	32(1)	33(1)	48(1)	−9(1)	11(1)	−2(1)
S1	27(1)	34(1)	29(1)	5(1)	10(1)	1(1)
Br1	19(1)	25(1)	23(1)	3(1)	−4(1)	−2(1)

Table A2. 5. Hydrogen coordinates [× 10^4] and isotropic displacement parameters [Å^2 × 10^3].

Atom	*x*	*y*	*z*	U_{eq}	*S.o.f.*
H1A	5900	1516	1420	22	1
H1B	7297	1696	1284	22	1
H2A	6019	–4	633	28	1
H2B	7425	159	508	28	1
H3A	5617	1421	–301	31	1
H3B	6277	579	–864	31	1
H5A	7236	4540	–480	59	1
H5B	7859	3932	–1281	59	1
H5C	8384	3872	–241	59	1
H7	5345	2057	3069	23	1
H8	5308	3303	4183	25	1
H9	6895	3486	5250	24	1
H10	8535	2426	5221	24	1
H11	8591	1166	4121	22	1
H13	9272	948	1564	30	1
H14	11233	345	1639	38	1
H15	11744	–943	2623	40	1
H16	10307	–1665	3542	38	1
H17	8336	–1065	3492	29	1
H19	6516	–1426	1774	26	1
H20	5079	–2647	2013	28	1
H21	3721	–2483	3197	31	1
H22	3792	–1101	4155	31	1
H23	5174	154	3891	26	1

Table A2.6. Torsion angles [°].

As1–C1–C2–C3	–178.94(19)
C1–C2–C3–S1	64.7(3)
C11–C6–C7–C8	1.1(4)
As1–C6–C7–C8	–177.16(19)
C6–C7–C8–C9	–0.3(4)
C7–C8–C9–C10	–0.2(4)
C8–C9–C10–C11	–0.1(4)
C9–C10–C11–C6	0.8(4)
C7–C6–C11–C10	–1.3(4)
As1–C6–C11–C10	176.91(19)
C17–C12–C13–C14	–0.4(4)
As1–C12–C13–C14	176.0(2)
C12–C13–C14–C15	0.3(4)
C13–C14–C15–C16	0.3(5)
C14–C15–C16–C17	–0.6(5)
C15–C16–C17–C12	0.4(4)
C13–C12–C17–C16	0.1(4)
As1–C12–C17–C16	–176.4(2)
C23–C18–C19–C20	2.4(4)
As1–C18–C19–C20	–175.73(19)
C18–C19–C20–C21	–1.7(4)
C19–C20–C21–C22	–0.2(4)
C20–C21–C22–C23	1.5(4)
C21–C22–C23–C18	–0.8(4)
C19–C18–C23–C22	–1.2(4)
As1–C18–C23–C22	177.0(2)
C11–C6–As1–C12	–11.0(2)
C7–C6–As1–C12	167.21(19)
C11–C6–As1–C18	107.3(2)
C7–C6–As1–C18	–74.4(2)
C11–C6–As1–C1	–129.3(2)
C7–C6–As1–C1	48.9(2)
C17–C12–As1–C6	86.1(2)
C13–C12–As1–C6	–90.5(2)
C17–C12–As1–C18	–33.3(2)
C13–C12–As1–C18	150.1(2)
C17–C12–As1–C1	–157.2(2)
C13–C12–As1–C1	26.3(2)
C19–C18–As1–C6	–173.19(19)
C23–C18–As1–C6	8.6(2)
C19–C18–As1–C12	–54.4(2)
C23–C18–As1–C12	127.4(2)

C19–C18–As1–C1	67.2(2)
C23–C18–As1–C1	–111.0(2)
C2–C1–As1–C6	–177.66(18)
C2–C1–As1–C12	64.4(2)
C2–C1–As1–C18	–56.4(2)
O1–C4–S1–C3	–1.6(3)
C5–C4–S1–C3	179.3(2)
C2–C3–S1–C4	–109.1(2)

Appendix 3.

Crystal data and structure refinement details for tri(2,4,6-trimethoxyphenyl) phosphoniopropylthiosulfate zwitterion. Compound 5, described in chapter 3B.

Table A3.1. Crystal data and structure refinement.

Identification code	2013ncs0299 / NL2	
Empirical formula	$C_{32}H_{44}O_{12.50}PS_2$	
Formula weight	723.76	
Temperature	120(2) K	
Wavelength	0.71075 Å	
Crystal system	Triclinic	
Space group	*P*–1	
Unit cell dimensions	*a* = 12.2838(5) Å	α = 72.355(5)°
	b = 15.5187(8) Å	β = 85.430(6)°
	c = 19.4586(13) Å	γ = 84.513(6)°
Volume	3513.6(3) Å^3	
Z	4	
Density (calculated)	1.368 Mg / m^3	
Absorption coefficient	0.259 mm^{-1}	
F(000)	1532	
Crystal	Prism; Colourless	
Crystal size	0.800 × 0.200 × 0.100 mm^3	
θ range for data collection	2.988 – 27.449°	
Index ranges	$-15 \le h \le 13$, $-20 \le k \le 20$, $-25 \le l \le 25$	
Reflections collected	52696	
Independent reflections	15872 [R_{int} = 0.0682]	
Completeness to θ = 25.242°	99.3 %	
Absorption correction	Semi–empirical from equivalents	
Max. and min. transmission	1.000 and 0.730	
Refinement method	Full-matrix least-squares on F^2	
Data / restraints / parameters	15872 / 1937 / 1145	
Goodness-of-fit on F^2	1.080	
Final *R* indices [$F^2 > 2\sigma(F^2)$]	*R1* = 0.0956, *wR2* = 0.2678	
R indices (all data)	*R1* = 0.1771, *wR2* = 0.3340	
Extinction coefficient	n/a	
Largest diff. peak and hole	0.916 and –0.640 e Å^{-3}	

Diffractometer: *Rigaku AFC12* goniometer equipped with an enhanced sensitivity (HG) *Saturn724+* detector mounted at the window of an *FR-E+ SuperBright* molybdenum rotating anode generator with HF *Varimax* optics (100µm focus). **Cell determination and data collection**: *CrystalClear-SM Expert 2.0 r13* (Rigaku, 2011). **Data reduction, cell refinement and absorption correction**: *CrystalClear-SM Expert 3.1 b25* (Rigaku, 2012). **Structure solution**: SHELXS97 (G Sheldrick, G.M. (2008). Acta Cryst. A64, 112-122.) **Structure refinement**: *SHELXL-2012* (Sheldrick, G.M. (2008). Acta Cryst. A64, 112-122). **Graphics:** *ORTEP3 for Windows* (L. J. Farrugia, J. Appl. Crystallogr. 1997, 30, 565
97, 30, 565

Special details:

There is disorder in the molecules, for which various geometrical (SAME and SADI) anisotropic displacement (DELU and SIMU) restraints were used.

Table A3.2. Atomic coordinates [× 10^4], equivalent isotropic displacement parameters [Å^2 × 10^3] and site occupancy factors. U_{eq} is defined as one third of the trace of the orthogonalized U^{ij} tensor.

Atom	*x*	*y*	*z*	U_{eq}	*S.o.f.*
C1	7762(12)	4732(12)	8013(5)	55(2)	0.490(10)
C2	7420(10)	5251(9)	8471(6)	65(3)	0.490(10)
C3	7928(10)	5098(8)	9115(5)	78(3)	0.490(10)
C4	8778(10)	4426(8)	9301(5)	91(3)	0.490(10)
C5	9121(10)	3907(8)	8842(5)	80(3)	0.490(10)
C6	8612(12)	4060(10)	8198(5)	62(3)	0.490(10)
C7	6030(20)	6330(20)	8709(17)	105(8)	0.490(10)
C8	8780(20)	4764(17)	10442(11)	176(8)	0.490(10)
C9	9720(30)	2814(18)	7975(14)	94(7)	0.490(10)
C11	7265(3)	6284(3)	6703(2)	51(1)	1
C12	6448(4)	7019(3)	6598(2)	54(1)	1
C13	6684(4)	7889(3)	6229(2)	60(1)	1
C14	7729(4)	8072(3)	5969(2)	62(1)	1
C15	8579(4)	7400(3)	6066(3)	71(1)	1
C16	8331(4)	6512(3)	6437(3)	64(1)	1
C17	4552(5)	7516(4)	6769(4)	93(2)	1
C18	8963(5)	9247(4)	5503(3)	82(2)	1
C19	10269(7)	5973(9)	6492(10)	65(4)	0.47(2)
C21	5655(4)	4901(3)	7219(3)	60(1)	1
C22	5068(4)	4455(3)	7864(3)	77(1)	1
C23	3930(5)	4390(4)	7865(4)	97(2)	1
C24	3407(5)	4773(4)	7225(5)	101(2)	1
C25	3952(4)	5169(4)	6587(4)	85(2)	1
C26	5075(4)	5230(3)	6588(3)	66(1)	1
C27	5097(8)	3737(6)	9140(4)	149(4)	1
C28	1756(14)	4361(16)	8017(16)	123(7)	0.52(3)
C29	5140(6)	6141(5)	5357(4)	103(2)	1
C31	7704(6)	4410(3)	6604(3)	53(2)	0.862(4)
C32	7278(5)	3468(4)	6813(3)	64(2)	0.862(4)
C33	7824(6)	2867(4)	6370(3)	72(2)	0.862(4)
P1	7081(1)	5106(1)	7149(1)	50(1)	1
O1	6574(17)	5868(15)	8232(11)	67(3)	0.490(10)
O2	9254(11)	4279(8)	9941(5)	113(3)	0.490(10)
O3	8950(20)	3581(16)	7735(10)	71(4)	0.490(10)
O11	5425(3)	6801(2)	6884(2)	69(1)	1
O12	7873(3)	8970(2)	5627(2)	74(1)	1
O13	9099(3)	5795(2)	6579(2)	81(1)	1
O21	5663(4)	4080(3)	8456(2)	92(1)	1

O22	2281(9)	4718(19)	7309(14)	118(5)	0.52(3)
O23	5682(3)	5601(3)	5976(2)	74(1)	1
O31	9194(4)	2190(6)	5075(3)	107(2)	0.862(4)
O32	7564(5)	1514(4)	5451(3)	108(2)	0.862(4)
O33	7693(4)	2687(3)	4287(2)	84(1)	0.862(4)
S1	8026(2)	2321(1)	5004(1)	62(1)	0.862(4)
S2	7466(2)	3363(1)	5421(1)	125(1)	0.862(4)
C101	7642(12)	4857(11)	8028(4)	58(3)	0.510(10)
C102	7098(10)	5334(9)	8469(5)	65(3)	0.510(10)
C103	7355(9)	5124(7)	9187(5)	79(3)	0.510(10)
C104	8156(10)	4437(8)	9464(4)	85(3)	0.510(10)
C105	8701(9)	3960(8)	9022(5)	77(3)	0.510(10)
C106	8444(11)	4170(10)	8304(5)	59(2)	0.510(10)
C107	5609(17)	6377(19)	8629(15)	77(5)	0.510(10)
C108	7696(18)	4492(14)	10667(7)	152(8)	0.510(10)
C109	9520(20)	2849(15)	8204(12)	84(5)	0.510(10)
O101	6321(18)	5979(16)	8176(11)	74(3)	0.510(10)
O102	8365(11)	4105(7)	10164(4)	110(3)	0.510(10)
O103	8960(20)	3711(14)	7871(9)	65(3)	0.510(10)
C119	10071(11)	5881(9)	6035(10)	87(6)	0.53(2)
C128	1607(14)	4282(15)	7577(19)	112(7)	0.48(3)
O122	2341(11)	4780(20)	6999(14)	113(5)	0.48(3)
C131	7710(40)	4680(20)	6440(20)	61(4)	0.138(4)
C132	7320(30)	3754(18)	6500(20)	72(5)	0.138(4)
C133	7960(30)	3317(16)	5962(18)	87(4)	0.138(4)
O131	9040(19)	2230(30)	4940(20)	141(11)	0.138(4)
O132	7940(30)	1041(14)	5211(16)	128(8)	0.138(4)
O133	7140(30)	2540(20)	4636(12)	119(8)	0.138(4)
S101	7926(16)	1999(12)	5108(9)	101(5)	0.138(4)
S102	7389(12)	2216(8)	6076(7)	108(4)	0.138(4)
C41	7544(3)	8863(3)	2879(2)	51(1)	1
C42	8528(4)	8744(3)	3217(2)	58(1)	1
C43	8866(4)	7920(3)	3718(2)	63(1)	1
C44	8228(5)	7193(3)	3848(3)	70(1)	1
C45	7271(5)	7251(3)	3508(3)	69(1)	1
C46	6934(4)	8087(3)	3022(2)	58(1)	1
C47	10169(4)	9375(4)	3365(4)	89(2)	1
C48	8205(9)	5663(7)	4541(6)	85(3)	0.575(11)
C49	5202(5)	7576(4)	2899(4)	96(2)	1
C51	7742(4)	10850(3)	2151(2)	53(1)	1
C52	8280(4)	11398(3)	1520(2)	60(1)	1
C53	8823(4)	12130(3)	1532(3)	67(1)	1
C54	8838(4)	12338(3)	2162(3)	63(1)	1
C55	8308(4)	11848(3)	2800(3)	60(1)	1
C56	7774(4)	11109(3)	2782(2)	54(1)	1
C57	8645(6)	11741(5)	237(3)	107(2)	1

C58	10072(8)	13539(6)	1638(5)	90(3)	0.680(11)
C59	7423(5)	10575(4)	4073(2)	74(1)	1
C61	5586(3)	10192(3)	2472(2)	52(1)	1
C62	5007(4)	9812(3)	3143(2)	53(1)	1
C63	3884(4)	10054(3)	3237(3)	61(1)	1
C64	3367(4)	10690(4)	2670(3)	66(1)	1
C65	3911(4)	11112(3)	2022(3)	64(1)	1
C66	5021(4)	10847(3)	1940(2)	56(1)	1
C67	5081(5)	8909(4)	4384(3)	84(2)	1
C68	1756(5)	11663(5)	2316(4)	108(2)	1
C69	5162(6)	11662(6)	678(3)	120(3)	1
C71	7030(20)	9630(30)	1384(13)	62(3)	0.503(5)
C72	8070(17)	9062(17)	1242(9)	69(3)	0.503(5)
C73	8335(11)	9178(10)	447(8)	91(3)	0.503(5)
P41	6991(1)	9889(1)	2242(1)	52(1)	1
O41	9136(3)	9474(2)	3044(2)	67(1)	1
O42	8787(8)	6457(5)	4330(5)	76(3)	0.575(11)
O43	6018(3)	8217(2)	2651(2)	67(1)	1
O51	8253(3)	11136(2)	914(2)	80(1)	1
O52	9385(3)	13054(2)	2193(3)	90(1)	1
O53	7203(3)	10583(2)	3360(2)	59(1)	1
O61	5586(3)	9228(2)	3676(2)	61(1)	1
O62	2281(3)	10877(3)	2814(2)	87(1)	1
O63	5643(3)	11238(2)	1329(2)	72(1)	1
O71	7104(8)	7105(7)	−227(6)	101(3)	0.503(5)
O72	8907(8)	7456(8)	−183(7)	119(4)	0.503(5)
O73	7865(9)	6944(7)	908(4)	127(4)	0.503(5)
S41	7858(8)	7406(5)	154(4)	86(2)	0.503(5)
S42	7237(3)	8759(3)	37(2)	108(2)	0.503(5)
C171	7020(20)	9580(30)	1414(13)	59(3)	0.497(5)
C172	8130(18)	9102(17)	1263(10)	73(3)	0.497(5)
C173	8129(11)	8855(11)	567(9)	88(3)	0.497(5)
O171	7901(9)	7815(7)	−703(4)	118(3)	0.497(5)
O172	7229(9)	6535(8)	174(6)	124(4)	0.497(5)
O173	8966(7)	7060(7)	286(6)	104(3)	0.497(5)
S141	7893(8)	7242(5)	26(4)	75(2)	0.497(5)
S142	7072(3)	8014(3)	646(2)	105(2)	0.497(5)
O142	8257(9)	6299(7)	4305(7)	71(3)	0.425(11)
C148	9221(10)	6135(9)	4721(7)	67(4)	0.425(11)
C158	9292(16)	13415(12)	2736(8)	91(6)	0.320(11)
C301	2032(8)	9557(9)	1597(6)	179(4)	1
C302	882(6)	9795(6)	1451(4)	115(2)	1
C303	3177(9)	8425(8)	1274(6)	180(4)	1
C304	4009(11)	9066(9)	1043(8)	232(6)	1
O301	2270(7)	9021(6)	1146(5)	198(3)	1

Table A3.3. Bond lengths [Å] and angles [°].

C1–C2	1.3900	C18–H18A	0.9800
C1–C6	1.3900	C18–H18B	0.9800
C1–P1	1.844(6)	C18–H18C	0.9800
C2–O1	1.353(10)	C19–O13	1.476(9)
C2–C3	1.3900	C19–H19A	0.9800
C3–C4	1.3900	C19–H19B	0.9800
C3–H3	0.9500	C19–H19C	0.9800
C4–O2	1.366(8)	C21–C26	1.403(7)
C4–C5	1.3900	C21–C22	1.413(7)
C5–C6	1.3900	C21–P1	1.798(5)
C5–H5	0.9500	C22–O21	1.359(7)
C6–O3	1.352(10)	C22–C23	1.411(8)
C7–O1	1.425(12)	C23–C24	1.387(9)
C7–H7A	0.9800	C23–H23	0.9500
C7–H7B	0.9800	C24–C25	1.361(9)
C7–H7C	0.9800	C24–O22	1.388(11)
C8–O2	1.457(13)	C24–O122	1.410(12)
C8–H8A	0.9800	C25–C26	1.392(7)
C8–H8B	0.9800	C25–H25	0.9500
C8–H8C	0.9800	C26–O23	1.352(6)
C9–O3	1.431(12)	C27–O21	1.425(7)
C9–H9A	0.9800	C27–H27A	0.9800
C9–H9B	0.9800	C27–H27B	0.9800
C9–H9C	0.9800	C27–H27C	0.9800
C11–C16	1.405(6)	C28–O22	1.443(13)
C11–C12	1.423(6)	C28–H28A	0.9800
C11–P1	1.798(4)	C28–H28B	0.9800
C12–O11	1.365(5)	C28–H28C	0.9800
C12–C13	1.370(6)	C29–O23	1.417(6)
C13–C14	1.364(6)	C29–H29A	0.9800
C13–H13	0.9500	C29–H29B	0.9800
C14–O12	1.372(5)	C29–H29C	0.9800
C14–C15	1.386(6)	C31–C32	1.526(7)
C15–C16	1.399(6)	C31–P1	1.811(5)
C15–H15	0.9500	C31–H31A	0.9900
C16–O13	1.363(5)	C31–H31B	0.9900
C17–O11	1.447(6)	C32–C33	1.529(7)
C17–H17A	0.9800	C32–H32A	0.9900
C17–H17B	0.9800	C32–H32B	0.9900
C17–H17C	0.9800	C33–S2	1.843(6)
C18–O12	1.424(6)	C33–H33A	0.9900

C33–H33B	0.9900	C133–S102	1.851(10)
P1–C131	1.801(15)	C133–H13E	0.9900
P1–C101	1.812(6)	C133–H13F	0.9900
O13–C119	1.519(10)	O131–S101	1.434(10)
O31–S1	1.441(5)	O132–S101	1.438(10)
O32–S1	1.430(5)	O133–S101	1.414(10)
O33–S1	1.416(4)	S101–S102	2.059(9)
S1–S2	2.059(3)	C41–C42	1.392(6)
C101–C102	1.3900	C41–C46	1.423(6)
C101–C106	1.3900	C41–P41	1.807(4)
C102–O101	1.340(9)	C42–O41	1.359(5)
C102–C103	1.3900	C42–C43	1.402(6)
C103–C104	1.3900	C43–C44	1.383(7)
C103–H103	0.9500	C43–H43	0.9500
C104–O102	1.339(8)	C44–C45	1.377(7)
C104–C105	1.3900	C44–O42	1.400(8)
C105–C106	1.3900	C44–O142	1.402(10)
C105–H105	0.9500	C45–C46	1.402(6)
C106–O103	1.347(11)	C45–H45	0.9500
C107–O101	1.424(12)	C46–O43	1.350(5)
C107–H10A	0.9800	C47–O41	1.433(5)
C107–H10B	0.9800	C47–H47A	0.9800
C107–H10C	0.9800	C47–H47B	0.9800
C108–O102	1.459(12)	C47–H47C	0.9800
C108–H10D	0.9800	C48–O42	1.419(11)
C108–H10E	0.9800	C48–H48A	0.9800
C108–H10F	0.9800	C48–H48B	0.9800
C109–O103	1.432(12)	C48–H48C	0.9800
C109–H10G	0.9800	C49–O43	1.432(6)
C109–H10H	0.9800	C49–H49A	0.9800
C109–H10I	0.9800	C49–H49B	0.9800
C119–H11A	0.9800	C49–H49C	0.9800
C119–H11B	0.9800	C51–C56	1.407(6)
C119–H11C	0.9800	C51–C52	1.419(6)
C128–O122	1.457(13)	C51–P41	1.785(5)
C128–H12A	0.9800	C52–O51	1.363(6)
C128–H12B	0.9800	C52–C53	1.378(6)
C128–H12C	0.9800	C53–C54	1.361(7)
C131–C132	1.528(12)	C53–H53	0.9500
C131–H13A	0.9900	C54–O52	1.372(6)
C131–H13B	0.9900	C54–C55	1.391(6)
C132–C133	1.536(12)	C55–C56	1.385(6)
C132–H13C	0.9900	C55–H55	0.9500
C132–H13D	0.9900	C56–O53	1.360(5)

C57–O51	1.443(6)	C73–S42	1.879(10)
C57–H57A	0.9800	C73–H73A	0.9900
C57–H57B	0.9800	C73–H73B	0.9900
C57–H57C	0.9800	P41–C171	1.814(11)
C58–O52	1.388(8)	O52–C158	1.332(13)
C58–H58A	0.9800	O71–S41	1.424(9)
C58–H58B	0.9800	O72–S41	1.397(11)
C58–H58C	0.9800	O73–S41	1.425(9)
C59–O53	1.432(5)	S41–S42	2.116(6)
C59–H59A	0.9800	C171–C172	1.542(9)
C59–H59B	0.9800	C171–H17D	0.9900
C59–H59C	0.9800	C171–H17E	0.9900
C61–C66	1.389(6)	C172–C173	1.515(10)
C61–C62	1.422(6)	C172–H17F	0.9900
C61–P41	1.802(4)	C172–H17G	0.9900
C62–O61	1.352(5)	C173–S142	1.893(10)
C62–C63	1.407(6)	C173–H17H	0.9900
C63–C64	1.387(7)	C173–H17I	0.9900
C63–H63	0.9500	O171–S141	1.429(9)
C64–O62	1.363(5)	O172–S141	1.377(12)
C64–C65	1.384(7)	O173–S141	1.421(9)
C65–C66	1.397(6)	S141–S142	2.087(6)
C65–H65	0.9500	O142–C148	1.447(11)
C66–O63	1.368(5)	C148–H14A	0.9800
C67–O61	1.426(6)	C148–H14B	0.9800
C67–H67A	0.9800	C148–H14C	0.9800
C67–H67B	0.9800	C158–H15A	0.9800
C67–H67C	0.9800	C158–H15B	0.9800
C68–O62	1.441(7)	C158–H15C	0.9800
C68–H68A	0.9800	C301–O301	1.379(8)
C68–H68B	0.9800	C301–C302	1.454(8)
C68–H68C	0.9800	C301–H30A	0.9900
C69–O63	1.390(6)	C301–H30B	0.9900
C69–H69A	0.9800	C302–H30C	0.9800
C69–H69B	0.9800	C302–H30D	0.9800
C69–H69C	0.9800	C302–H30E	0.9800
C71–C72	1.539(8)	C303–O301	1.367(8)
C71–P41	1.830(10)	C303–C304	1.445(9)
C71–H71A	0.9900	C303–H30F	0.9900
C71–H71B	0.9900	C303–H30G	0.9900
C72–C73	1.514(10)	C304–H30H	0.9800
C72–H72A	0.9900	C304–H30I	0.9800
C72–H72B	0.9900	C304–H30J	0.9800

C2–C1–C6	120.0	C12–C13–H13	119.9
C2–C1–P1	113.6(6)	C13–C14–O12	115.0(4)
C6–C1–P1	126.2(6)	C13–C14–C15	122.0(4)
O1–C2–C3	126.1(9)	O12–C14–C15	123.0(5)
O1–C2–C1	113.9(9)	C14–C15–C16	117.6(4)
C3–C2–C1	120.0	C14–C15–H15	121.2
C2–C3–C4	120.0	C16–C15–H15	121.2
C2–C3–H3	120.0	O13–C16–C15	123.0(4)
C4–C3–H3	120.0	O13–C16–C11	114.2(4)
O2–C4–C3	118.9(8)	C15–C16–C11	122.7(4)
O2–C4–C5	121.1(8)	O11–C17–H17A	109.5
C3–C4–C5	120.0	O11–C17–H17B	109.5
C6–C5–C4	120.0	H17A–C17–H17B	109.5
C6–C5–H5	120.0	O11–C17–H17C	109.5
C4–C5–H5	120.0	H17A–C17–H17C	109.5
O3–C6–C5	120.9(9)	H17B–C17–H17C	109.5
O3–C6–C1	119.0(9)	O12–C18–H18A	109.5
C5–C6–C1	120.0	O12–C18–H18B	109.5
O1–C7–H7A	109.5	H18A–C18–H18B	109.5
O1–C7–H7B	109.5	O12–C18–H18C	109.5
H7A–C7–H7B	109.5	H18A–C18–H18C	109.5
O1–C7–H7C	109.5	H18B–C18–H18C	109.5
H7A–C7–H7C	109.5	O13–C19–H19A	109.5
H7B–C7–H7C	109.5	O13–C19–H19B	109.5
O2–C8–H8A	109.5	H19A–C19–H19B	109.5
O2–C8–H8B	109.5	O13–C19–H19C	109.5
H8A–C8–H8B	109.5	H19A–C19–H19C	109.5
O2–C8–H8C	109.5	H19B–C19–H19C	109.5
H8A–C8–H8C	109.5	C26–C21–C22	117.6(5)
H8B–C8–H8C	109.5	C26–C21–P1	117.3(4)
O3–C9–H9A	109.5	C22–C21–P1	125.1(4)
O3–C9–H9B	109.5	O21–C22–C23	123.4(5)
H9A–C9–H9B	109.5	O21–C22–C21	116.5(5)
O3–C9–H9C	109.5	C23–C22–C21	120.1(6)
H9A–C9–H9C	109.5	C24–C23–C22	118.7(6)
H9B–C9–H9C	109.5	C24–C23–H23	120.6
C16–C11–C12	116.0(4)	C22–C23–H23	120.6
C16–C11–P1	117.0(3)	C25–C24–C23	122.8(6)
C12–C11–P1	127.0(3)	C25–C24–O22	124.2(12)
O11–C12–C13	122.6(4)	C23–C24–O22	113.0(12)
O11–C12–C11	115.8(4)	C25–C24–O122	101.4(12)
C13–C12–C11	121.6(4)	C23–C24–O122	135.3(12)
C14–C13–C12	120.1(4)	C24–C25–C26	118.2(6)
C14–C13–H13	119.9	C24–C25–H25	120.9

C26–C25–H25	120.9	C21–P1–C31	103.7(3)
O23–C26–C25	122.0(5)	C11–P1–C101	105.8(6)
O23–C26–C21	115.6(4)	C21–P1–C101	112.0(6)
C25–C26–C21	122.4(5)	C131–P1–C101	123(2)
O21–C27–H27A	109.5	C11–P1–C1	110.1(6)
O21–C27–H27B	109.5	C21–P1–C1	114.8(6)
H27A–C27–H27B	109.5	C31–P1–C1	107.0(4)
O21–C27–H27C	109.5	C2–O1–C7	118.9(13)
H27A–C27–H27C	109.5	C4–O2–C8	118.9(12)
H27B–C27–H27C	109.5	C6–O3–C9	118.2(14)
O22–C28–H28A	109.5	C12–O11–C17	118.2(4)
O22–C28–H28B	109.5	C14–O12–C18	118.1(4)
H28A–C28–H28B	109.5	C16–O13–C19	119.0(6)
O22–C28–H28C	109.5	C16–O13–C119	115.4(6)
H28A–C28–H28C	109.5	C22–O21–C27	118.6(6)
H28B–C28–H28C	109.5	C24–O22–C28	120.6(13)
O23–C29–H29A	109.5	C26–O23–C29	118.8(5)
O23–C29–H29B	109.5	O33–S1–O32	118.3(3)
H29A–C29–H29B	109.5	O33–S1–O31	115.1(4)
O23–C29–H29C	109.5	O32–S1–O31	107.4(4)
H29A–C29–H29C	109.5	O33–S1–S2	100.5(2)
H29B–C29–H29C	109.5	O32–S1–S2	107.8(3)
C32–C31–P1	113.5(4)	O31–S1–S2	107.0(3)
C32–C31–H31A	108.9	C33–S2–S1	100.81(19)
P1–C31–H31A	108.9	C102–C101–C106	120.0
C32–C31–H31B	108.9	C102–C101–P1	114.2(6)
P1–C31–H31B	108.9	C106–C101–P1	125.2(7)
H31A–C31–H31B	107.7	O101–C102–C103	122.6(10)
C31–C32–C33	113.8(5)	O101–C102–C101	117.4(10)
C31–C32–H32A	108.8	C103–C102–C101	120.0
C33–C32–H32A	108.8	C102–C103–C104	120.0
C31–C32–H32B	108.8	C102–C103–H103	120.0
C33–C32–H32B	108.8	C104–C103–H103	120.0
H32A–C32–H32B	107.7	O102–C104–C105	114.9(7)
C32–C33–S2	109.0(4)	O102–C104–C103	124.5(7)
C32–C33–H33A	109.9	C105–C104–C103	120.0
S2–C33–H33A	109.9	C104–C105–C106	120.0
C32–C33–H33B	109.9	C104–C105–H105	120.0
S2–C33–H33B	109.9	C106–C105–H105	120.0
H33A–C33–H33B	108.3	O103–C106–C105	120.6(9)
C11–P1–C21	110.4(2)	O103–C106–C101	119.4(9)
C11–P1–C131	96.9(10)	C105–C106–C101	120.0
C21–P1–C131	107.0(16)	O101–C107–H10A	109.5
C11–P1–C31	110.6(2)	O101–C107–H10B	109.5

H10A–C107–H10B	109.5	C132–C133–S102	107.7(12)
O101–C107–H10C	109.5	C132–C133–H13E	110.2
H10A–C107–H10C	109.5	S102–C133–H13E	110.2
H10B–C107–H10C	109.5	C132–C133–H13F	110.2
O102–C108–H10D	109.5	S102–C133–H13F	110.2
O102–C108–H10E	109.5	H13E–C133–H13F	108.5
H10D–C108–H10E	109.5	O133–S101–O131	116.6(14)
O102–C108–H10F	109.5	O133–S101–O132	114.9(13)
H10D–C108–H10F	109.5	O131–S101–O132	106.5(13)
H10E–C108–H10F	109.5	O133–S101–S102	102.0(11)
O103–C109–H10G	109.5	O131–S101–S102	109.2(12)
O103–C109–H10H	109.5	O132–S101–S102	107.1(12)
H10G–C109–H10H	109.5	C133–S102–S101	100.3(8)
O103–C109–H10I	109.5	C42–C41–C46	116.8(4)
H10G–C109–H10I	109.5	C42–C41–P41	126.7(3)
H10H–C109–H10I	109.5	C46–C41–P41	116.4(3)
C102–O101–C107	119.6(14)	O41–C42–C41	116.4(4)
C104–O102–C108	117.3(9)	O41–C42–C43	121.7(4)
C106–O103–C109	118.0(13)	C41–C42–C43	121.9(4)
O13–C119–H11A	109.5	C44–C43–C42	118.7(5)
O13–C119–H11B	109.5	C44–C43–H43	120.7
H11A–C119–H11B	109.5	C42–C43–H43	120.7
O13–C119–H11C	109.5	C45–C44–C43	122.5(4)
H11A–C119–H11C	109.5	C45–C44–O42	131.0(6)
H11B–C119–H11C	109.5	C43–C44–O42	106.4(6)
O122–C128–H12A	109.5	C45–C44–O142	101.3(6)
O122–C128–H12B	109.5	C43–C44–O142	136.1(6)
H12A–C128–H12B	109.5	C44–C45–C46	117.9(5)
O122–C128–H12C	109.5	C44–C45–H45	121.0
H12A–C128–H12C	109.5	C46–C45–H45	121.0
H12B–C128–H12C	109.5	O43–C46–C45	123.0(4)
C24–O122–C128	112.7(13)	O43–C46–C41	115.0(4)
C132–C131–P1	110.8(15)	C45–C46–C41	122.0(4)
C132–C131–H13A	109.5	O41–C47–H47A	109.5
P1–C131–H13A	109.5	O41–C47–H47B	109.5
C132–C131–H13B	109.5	H47A–C47–H47B	109.5
P1–C131–H13B	109.5	O41–C47–H47C	109.5
H13A–C131–H13B	108.1	H47A–C47–H47C	109.5
C131–C132–C133	111.7(13)	H47B–C47–H47C	109.5
C131–C132–H13C	109.3	O42–C48–H48A	109.5
C133–C132–H13C	109.3	O42–C48–H48B	109.5
C131–C132–H13D	109.3	H48A–C48–H48B	109.5
C133–C132–H13D	109.3	O42–C48–H48C	109.5
H13C–C132–H13D	107.9	H48A–C48–H48C	109.5

H48B–C48–H48C	109.5	C66–C61–P41	116.6(3)
O43–C49–H49A	109.5	C62–C61–P41	125.9(3)
O43–C49–H49B	109.5	O61–C62–C63	122.5(4)
H49A–C49–H49B	109.5	O61–C62–C61	117.1(4)
O43–C49–H49C	109.5	C63–C62–C61	120.4(4)
H49A–C49–H49C	109.5	C64–C63–C62	118.6(4)
H49B–C49–H49C	109.5	C64–C63–H63	120.7
C56–C51–C52	116.3(4)	C62–C63–H63	120.7
C56–C51–P41	115.5(3)	O62–C64–C65	123.0(5)
C52–C51–P41	128.1(4)	O62–C64–C63	114.1(5)
O51–C52–C53	122.7(4)	C65–C64–C63	123.0(4)
O51–C52–C51	115.8(4)	C64–C65–C66	117.2(4)
C53–C52–C51	121.5(4)	C64–C65–H65	121.4
C54–C53–C52	119.4(4)	C66–C65–H65	121.4
C54–C53–H53	120.3	O63–C66–C61	114.8(4)
C52–C53–H53	120.3	O63–C66–C65	121.9(4)
C53–C54–O52	120.6(4)	C61–C66–C65	123.2(4)
C53–C54–C55	122.6(4)	O61–C67–H67A	109.5
O52–C54–C55	116.7(5)	O61–C67–H67B	109.5
C56–C55–C54	117.4(4)	H67A–C67–H67B	109.5
C56–C55–H55	121.3	O61–C67–H67C	109.5
C54–C55–H55	121.3	H67A–C67–H67C	109.5
O53–C56–C55	123.7(4)	H67B–C67–H67C	109.5
O53–C56–C51	113.5(4)	O62–C68–H68A	109.5
C55–C56–C51	122.7(4)	O62–C68–H68B	109.5
O51–C57–H57A	109.5	H68A–C68–H68B	109.5
O51–C57–H57B	109.5	O62–C68–H68C	109.5
H57A–C57–H57B	109.5	H68A–C68–H68C	109.5
O51–C57–H57C	109.5	H68B–C68–H68C	109.5
H57A–C57–H57C	109.5	O63–C69–H69A	109.5
H57B–C57–H57C	109.5	O63–C69–H69B	109.5
O52–C58–H58A	109.5	H69A–C69–H69B	109.5
O52–C58–H58B	109.5	O63–C69–H69C	109.5
H58A–C58–H58B	109.5	H69A–C69–H69C	109.5
O52–C58–H58C	109.5	H69B–C69–H69C	109.5
H58A–C58–H58C	109.5	C72–C71–P41	113.6(13)
H58B–C58–H58C	109.5	C72–C71–H71A	108.8
O53–C59–H59A	109.5	P41–C71–H71A	108.8
O53–C59–H59B	109.5	C72–C71–H71B	108.8
H59A–C59–H59B	109.5	P41–C71–H71B	108.8
O53–C59–H59C	109.5	H71A–C71–H71B	107.7
H59A–C59–H59C	109.5	C73–C72–C71	113.0(11)
H59B–C59–H59C	109.5	C73–C72–H72A	109.0
C66–C61–C62	117.5(4)	C71–C72–H72A	109.0

C73–C72–H72B	109.0	C173–C172–H17G	109.5
C71–C72–H72B	109.0	C171–C172–H17G	109.5
H72A–C72–H72B	107.8	H17F–C172–H17G	108.1
C72–C73–S42	111.5(8)	C172–C173–S142	110.4(9)
C72–C73–H73A	109.3	C172–C173–H17H	109.6
S42–C73–H73A	109.3	S142–C173–H17H	109.6
C72–C73–H73B	109.3	C172–C173–H17I	109.6
S42–C73–H73B	109.3	S142–C173–H17I	109.6
H73A–C73–H73B	108.0	H17H–C173–H17I	108.1
C51–P41–C61	107.0(2)	O172–S141–O173	118.5(9)
C51–P41–C41	113.5(2)	O172–S141–O171	114.6(9)
C61–P41–C41	112.7(2)	O173–S141–O171	111.2(9)
C51–P41–C171	113.0(14)	O172–S141–S142	100.7(7)
C61–P41–C171	107.7(8)	O173–S141–S142	104.0(6)
C41–P41–C171	102.9(12)	O171–S141–S142	105.9(5)
C51–P41–C71	110.6(14)	C173–S142–S141	99.5(5)
C61–P41–C71	107.8(8)	C44–O142–C148	108.1(9)
C41–P41–C71	105.1(12)	O142–C148–H14A	109.5
C42–O41–C47	118.3(4)	O142–C148–H14B	109.5
C44–O42–C48	113.0(8)	H14A–C148–H14B	109.5
C46–O43–C49	118.6(4)	O142–C148–H14C	109.5
C52–O51–C57	117.8(4)	H14A–C148–H14C	109.5
C158–O52–C54	125.3(9)	H14B–C148–H14C	109.5
C54–O52–C58	124.3(6)	O52–C158–H15A	109.5
C56–O53–C59	119.5(4)	O52–C158–H15B	109.5
C62–O61–C67	119.5(4)	H15A–C158–H15B	109.5
C64–O62–C68	116.5(5)	O52–C158–H15C	109.5
C66–O63–C69	120.9(5)	H15A–C158–H15C	109.5
O72–S41–O71	112.4(8)	H15B–C158–H15C	109.5
O72–S41–O73	112.7(8)	O301–C301–C302	98.1(7)
O71–S41–O73	114.9(9)	O301–C301–H30A	112.2
O72–S41–S42	106.2(7)	C302–C301–H30A	112.2
O71–S41–S42	102.2(5)	O301–C301–H30B	112.2
O73–S41–S42	107.3(6)	C302–C301–H30B	112.2
C73–S42–S41	101.2(5)	H30A–C301–H30B	109.8
C172–C171–P41	111.8(13)	C301–C302–H30C	109.5
C172–C171–H17D	109.3	C301–C302–H30D	109.5
P41–C171–H17D	109.3	H30C–C302–H30D	109.5
C172–C171–H17E	109.3	C301–C302–H30E	109.5
P41–C171–H17E	109.3	H30C–C302–H30E	109.5
H17D–C171–H17E	107.9	H30D–C302–H30E	109.5
C173–C172–C171	110.6(9)	O301–C303–C304	98.8(9)
C173–C172–H17F	109.5	O301–C303–H30F	112.0
C171–C172–H17F	109.5	C304–C303–H30F	112.0

O301–C303–H30G	112.0
C304–C303–H30G	112.0
H30F–C303–H30G	109.7
C303–C304–H30H	109.5
C303–C304–H30I	109.5
H30H–C304–H30I	109.5
C303–C304–H30J	109.5
H30H–C304–H30J	109.5
H30I–C304–H30J	109.5
C303–O301–C301	117.6(10)

Table A3.4. Anisotropic displacement parameters [Å^2× 10^3]. The anisotropic displacement factor exponent takes the form: $-2\pi^2[h^2a^{*2}U^{11} + \cdots + 2\,h\,k\,a^*\,b^*\,U^{12}]$.

Atom	U^{11}	U^{22}	U^{33}	U^{23}	U^{13}	U^{12}
C1	65(6)	48(5)	51(4)	−11(4)	−3(4)	−11(4)
C2	80(7)	58(5)	53(4)	−13(4)	−4(4)	3(5)
C3	92(7)	78(6)	63(5)	−19(4)	−15(5)	−1(6)
C4	101(7)	99(6)	67(5)	−12(5)	−24(5)	5(7)
C5	89(8)	72(6)	69(6)	−4(5)	−16(5)	3(6)
C6	66(6)	50(6)	62(5)	−3(4)	−7(5)	2(5)
C7	141(18)	89(10)	79(10)	−31(8)	14(14)	27(13)
C8	210(18)	208(17)	124(12)	−75(11)	−44(13)	20(15)
C9	71(10)	83(9)	116(17)	−20(10)	−11(11)	32(7)
C11	42(2)	52(2)	56(2)	−8(2)	−4(2)	−5(2)
C12	52(2)	50(2)	60(3)	−14(2)	−3(2)	−3(2)
C13	59(3)	53(2)	64(3)	−11(2)	−14(2)	−2(2)
C14	74(3)	47(2)	56(3)	0(2)	−6(2)	−7(2)
C15	54(3)	59(3)	83(3)	4(2)	9(2)	−11(2)
C16	49(3)	54(2)	75(3)	−1(2)	3(2)	−3(2)
C17	58(3)	70(4)	150(6)	−36(4)	−5(3)	14(3)
C18	85(4)	63(3)	88(4)	−3(3)	1(3)	−21(3)
C19	41(5)	87(8)	69(9)	−20(6)	−8(5)	−18(5)
C21	50(2)	51(2)	80(3)	−21(2)	9(2)	−7(2)
C22	66(3)	54(3)	106(4)	−21(3)	25(3)	−14(2)
C23	65(3)	67(3)	150(5)	−27(3)	44(3)	−21(3)
C24	45(3)	66(4)	194(6)	−46(4)	12(3)	−7(3)
C25	48(3)	65(3)	151(5)	−41(3)	−15(3)	−3(2)
C26	46(2)	54(3)	104(3)	−33(2)	−12(2)	4(2)
C27	156(8)	137(7)	110(5)	12(5)	71(5)	−23(6)
C28	56(8)	151(13)	149(14)	−23(13)	−4(8)	−18(8)
C29	102(5)	110(5)	100(4)	−35(4)	−51(4)	22(4)
C31	55(3)	49(3)	53(3)	−12(3)	−4(3)	0(3)
C32	62(3)	50(3)	80(4)	−23(3)	−7(3)	5(3)
C33	82(4)	61(3)	76(3)	−24(3)	−19(3)	13(3)
P1	43(1)	50(1)	54(1)	−9(1)	−1(1)	−7(1)
O1	82(9)	61(7)	63(6)	−26(5)	−6(5)	4(5)
O2	133(8)	134(7)	71(5)	−21(5)	−47(5)	−9(6)
O3	68(6)	63(7)	72(7)	−12(4)	−10(6)	16(5)
O11	43(2)	62(2)	100(3)	−24(2)	−1(2)	−1(2)
O12	85(3)	53(2)	74(2)	0(2)	−2(2)	−11(2)

O13	38(2)	58(2)	124(3)	8(2)	9(2)	−5(2)
O21	95(3)	76(2)	83(2)	1(2)	37(2)	−21(2)
O22	47(4)	99(7)	202(11)	−43(11)	32(5)	−18(5)
O23	64(2)	84(2)	77(2)	−27(2)	−18(2)	7(2)
O31	59(3)	158(6)	84(3)	−9(4)	−3(2)	3(3)
O32	152(5)	84(3)	93(3)	−27(3)	29(3)	−65(4)
O33	89(3)	94(3)	78(3)	−32(2)	−18(3)	−12(3)
S1	58(1)	63(1)	63(1)	−16(1)	−2(1)	−12(1)
S2	187(2)	88(1)	116(2)	−56(1)	−90(2)	64(2)
C101	62(5)	45(5)	55(4)	5(4)	−5(4)	−9(4)
C102	80(7)	56(5)	58(4)	−13(4)	−11(5)	−2(5)
C103	95(8)	73(5)	65(5)	−20(4)	−16(5)	18(6)
C104	102(7)	87(6)	60(4)	−17(4)	−22(5)	27(6)
C105	87(7)	68(5)	62(5)	−4(4)	−6(5)	13(5)
C106	61(6)	52(5)	58(4)	−9(4)	−5(4)	−4(4)
C107	82(11)	74(8)	70(8)	−23(6)	1(8)	14(8)
C108	187(17)	181(15)	65(7)	−28(9)	−5(9)	64(13)
C109	99(14)	61(7)	78(11)	−6(7)	−7(9)	12(7)
O101	85(8)	66(6)	59(5)	−9(4)	−8(5)	19(5)
O102	140(8)	117(6)	64(4)	−22(4)	−28(5)	37(6)
O103	71(6)	55(6)	67(6)	−12(4)	−20(5)	1(4)
C119	60(7)	76(7)	104(11)	−2(7)	11(7)	−2(5)
C128	49(7)	133(12)	156(17)	−39(12)	0(9)	−29(7)
O122	50(5)	97(7)	192(11)	−42(10)	20(6)	−25(5)
C131	54(9)	57(8)	65(8)	−13(8)	6(8)	9(9)
C132	71(9)	58(8)	80(9)	−12(7)	−10(9)	9(8)
C133	101(9)	68(8)	96(9)	−28(7)	−35(9)	19(8)
O131	82(12)	136(19)	150(20)	38(19)	19(13)	−6(14)
O132	160(20)	98(11)	131(18)	−42(11)	−29(17)	−8(13)
O133	91(14)	130(15)	118(11)	−22(15)	23(12)	11(14)
S101	93(9)	91(10)	126(9)	−38(8)	3(7)	−36(8)
S102	113(8)	79(6)	133(7)	−36(6)	0(6)	−5(6)
C41	46(2)	51(2)	51(2)	−7(2)	−3(2)	−3(2)
C42	54(3)	55(2)	57(3)	−8(2)	−1(2)	0(2)
C43	65(3)	63(3)	54(3)	−11(2)	−7(2)	13(2)
C44	89(4)	52(2)	57(3)	−3(2)	−2(2)	19(2)
C45	81(3)	46(2)	69(3)	−4(2)	2(2)	0(2)
C46	60(3)	50(2)	61(3)	−10(2)	−2(2)	−6(2)
C47	62(3)	93(4)	113(5)	−26(4)	−28(3)	−5(3)
C48	77(7)	59(6)	98(7)	6(5)	−7(6)	−2(5)
C49	86(4)	62(3)	137(5)	−14(3)	−12(4)	−37(3)
C51	46(2)	54(2)	55(2)	−9(2)	−3(2)	−2(2)
C52	60(3)	54(3)	61(3)	−8(2)	11(2)	−11(2)
C53	69(3)	57(3)	68(3)	−7(2)	13(2)	−17(2)

C54	53(3)	47(2)	84(3)	−11(2)	−1(2)	−8(2)
C55	49(3)	56(3)	74(3)	−20(2)	−6(2)	2(2)
C56	44(2)	52(2)	61(2)	−9(2)	−3(2)	−3(2)
C57	137(6)	120(5)	67(3)	−27(3)	34(4)	−63(5)
C58	92(7)	69(5)	101(7)	−6(4)	−3(5)	−30(5)
C59	75(4)	88(4)	57(3)	−16(3)	−14(3)	−6(3)
C61	47(2)	48(2)	57(2)	−9(2)	−5(2)	−2(2)
C62	47(2)	52(2)	57(2)	−13(2)	0(2)	−6(2)
C63	55(3)	60(3)	68(3)	−18(2)	3(2)	−12(2)
C64	43(2)	72(3)	91(3)	−35(3)	−7(2)	−1(2)
C65	61(3)	60(3)	74(3)	−20(2)	−23(2)	3(2)
C66	55(3)	53(2)	57(2)	−10(2)	−7(2)	−6(2)
C67	74(4)	94(4)	65(3)	3(3)	12(3)	−8(3)
C68	52(3)	107(5)	163(7)	−37(4)	−25(4)	11(3)
C69	124(6)	137(6)	67(4)	4(4)	−19(4)	40(5)
C71	66(7)	67(7)	51(5)	−16(5)	−3(5)	−7(6)
C72	70(6)	83(6)	65(5)	−37(5)	−12(5)	−5(5)
C73	88(7)	116(7)	77(6)	−43(6)	−2(5)	4(6)
P41	48(1)	50(1)	50(1)	−4(1)	−2(1)	−5(1)
O41	46(2)	69(2)	76(2)	−6(2)	−13(2)	−2(2)
O42	78(6)	61(4)	70(4)	5(3)	−10(5)	14(4)
O43	61(2)	56(2)	82(2)	−12(2)	−2(2)	−14(2)
O51	102(3)	75(2)	59(2)	−14(2)	21(2)	−34(2)
O52	67(2)	61(2)	140(4)	−26(2)	6(2)	−20(2)
O53	59(2)	65(2)	49(2)	−12(1)	−4(1)	−7(2)
O61	54(2)	65(2)	52(2)	1(1)	2(1)	−5(2)
O62	46(2)	99(3)	120(3)	−39(2)	−14(2)	6(2)
O63	74(2)	69(2)	57(2)	6(2)	−10(2)	1(2)
O71	66(5)	125(7)	112(7)	−33(6)	−39(5)	11(5)
O72	85(6)	124(8)	153(9)	−52(7)	43(7)	−41(6)
O73	128(8)	147(7)	84(5)	10(5)	−18(5)	−41(6)
S41	64(3)	87(3)	94(4)	−4(2)	−16(3)	−9(2)
S42	110(3)	146(3)	84(2)	−58(2)	−45(2)	31(2)
C171	62(6)	64(7)	49(5)	−12(5)	−1(5)	−9(6)
C172	68(6)	83(7)	68(6)	−25(5)	−1(5)	2(5)
C173	76(6)	115(7)	85(6)	−47(6)	6(5)	−10(5)
O171	129(8)	152(8)	54(4)	−15(4)	−5(4)	33(6)
O172	109(7)	164(8)	136(8)	−96(7)	51(7)	−76(7)
O173	63(5)	110(7)	119(7)	1(6)	−24(5)	−10(4)
S141	65(3)	97(3)	62(2)	−21(2)	6(2)	−17(2)
S142	92(3)	146(4)	90(3)	−58(3)	23(2)	−27(2)
O142	56(6)	67(5)	76(6)	3(4)	−10(5)	−7(5)
C148	66(8)	64(7)	61(7)	1(5)	−18(6)	1(6)
C158	101(14)	63(10)	108(12)	−11(8)	−48(11)	−14(9)

C301	186(8)	228(11)	134(7)	–79(7)	–38(7)	29(8)
C302	91(4)	173(7)	82(4)	–26(4)	13(4)	–61(5)
C303	181(10)	204(11)	158(8)	–55(8)	–42(8)	6(6)
C304	279(11)	172(11)	261(15)	–53(10)	–125(12)	–47(9)
O301	241(7)	170(7)	184(6)	–71(5)	12(6)	19(5)

Table A3.5. Hydrogen coordinates [× 10^4] and isotropic displacement parameters [$Å^2$ × 10^3].

Atom	*x*	*y*	*z*	U_{eq}	*S.o.f.*
H3	7695	5453	9428	94	0.490(10)
H5	9702	3448	8969	96	0.490(10)
H7A	5460	6769	8455	158	0.490(10)
H7B	6558	6641	8877	158	0.490(10)
H7C	5689	5885	9125	158	0.490(10)
H8A	9212	4593	10872	263	0.490(10)
H8B	8025	4607	10583	263	0.490(10)
H8C	8790	5419	10207	263	0.490(10)
H9A	9915	2544	7582	141	0.490(10)
H9B	9398	2365	8390	141	0.490(10)
H9C	10386	3008	8116	141	0.490(10)
H13	6120	8366	6154	72	1
H15	9305	7537	5888	86	1
H17A	3868	7265	7004	140	1
H17B	4462	7785	6250	140	1
H17C	4735	7984	6975	140	1
H18A	8946	9900	5257	124	1
H18B	9388	8918	5201	124	1
H18C	9303	9113	5967	124	1
H19A	10719	5396	6606	98	0.47(2)
H19B	10423	6313	6819	98	0.47(2)
H19C	10443	6329	5992	98	0.47(2)
H23	3530	4090	8296	116	1
H25	3576	5399	6152	102	1
H27A	5628	3486	9513	224	1
H27B	4641	3260	9123	224	1
H27C	4631	4230	9255	224	1
H28A	964	4376	7974	185	0.52(3)
H28B	1901	4732	8322	185	0.52(3)
H28C	2047	3735	8234	185	0.52(3)
H29A	5681	6358	4958	154	1
H29B	4728	6661	5466	154	1
H29C	4634	5778	5219	154	1
H31A	7564	4723	6091	63	0.862(4)
H31B	8506	4345	6651	63	0.862(4)
H32A	6479	3533	6752	77	0.862(4)
H32B	7397	3163	7330	77	0.862(4)
H33A	7569	2248	6563	87	0.862(4)
H33B	8628	2824	6402	87	0.862(4)
H103	6983	5450	9488	94	0.510(10)

H10S	9249	3490	9211	92	0.510(10)
H10A	5059	6801	8338	115	0.510(10)
H10B	6035	6704	8860	115	0.510(10)
H10C	5243	5900	9001	115	0.510(10)
H10D	7936	4202	11158	228	0.510(10)
H10E	6926	4389	10648	228	0.510(10)
H10F	7778	5145	10534	228	0.510(10)
H10G	9858	2591	7829	126	0.510(10)
H10H	8997	2439	8509	126	0.510(10)
H10I	10091	2927	8501	126	0.510(10)
H11A	10569	5332	6176	130	0.53(2)
H11B	10460	6409	6024	130	0.53(2)
H11C	9812	5958	5555	130	0.53(2)
H12A	885	4300	7390	169	0.48(3)
H12B	1538	4560	7970	169	0.48(3)
H12C	1905	3651	7759	169	0.48(3)
H13A	7536	5111	5964	73	0.138(4)
H13B	8520	4621	6469	73	0.138(4)
H13C	6527	3828	6401	86	0.138(4)
H13D	7400	3348	6995	86	0.138(4)
H13E	8743	3223	6061	105	0.138(4)
H13F	7876	3716	5461	105	0.138(4)
H43	9520	7861	3963	76	1
H45	6852	6740	3601	83	1
H47A	10516	9950	3192	134	1
H47B	10644	8901	3230	134	1
H47C	10053	9205	3891	134	1
H48A	8621	5178	4890	127	0.575(11)
H48B	8104	5472	4116	127	0.575(11)
H48C	7488	5790	4764	127	0.575(11)
H49A	4590	7757	2579	144	1
H49B	4938	7558	3391	144	1
H49C	5521	6973	2896	144	1
H53	9183	12486	1105	81	1
H55	8312	12015	3232	72	1
H57A	8570	11477	–153	160	1
H57B	9418	11831	265	160	1
H57C	8214	12326	141	160	1
H58A	10368	14017	1784	135	0.680(11)
H58B	9656	13812	1205	135	0.680(11)
H58C	10675	13129	1533	135	0.680(11)
H59A	6952	10161	4427	111	1
H59B	7274	11188	4118	111	1
H59C	8193	10372	4163	111	1
H63	3489	9789	3679	73	1
H65	3545	11563	1649	77	1

H67A	5605	8495	4705	126	1
H67B	4440	8588	4365	126	1
H67C	4852	9425	4567	126	1
H68A	981	11729	2470	162	1
H68B	1816	11590	1831	162	1
H68C	2112	12205	2308	162	1
H69A	5730	11904	304	180	1
H69B	4641	12160	732	180	1
H69C	4775	11223	538	180	1
H71A	6381	9297	1379	74	0.503(5)
H71B	6972	10206	986	74	0.503(5)
H72A	8695	9238	1448	83	0.503(5)
H72B	7976	8414	1495	83	0.503(5)
H73A	9042	8839	388	110	0.503(5)
H73B	8412	9828	190	110	0.503(5)
H17D	6430	9169	1451	71	0.497(5)
H17E	6869	10131	1006	71	0.497(5)
H17F	8720	9509	1226	88	0.497(5)
H17G	8279	8546	1668	88	0.497(5)
H17H	8863	8587	460	106	0.497(5)
H17I	7962	9409	163	106	0.497(5)
H14A	9293	5497	5012	101	0.425(11)
H14B	9151	6522	5040	101	0.425(11)
H14C	9871	6277	4394	101	0.425(11)
H15A	9752	13928	2622	136	0.320(11)
H15B	9529	12956	3178	136	0.320(11)
H15C	8527	13627	2808	136	0.320(11)
H30A	2465	10095	1456	214	1
H30B	2136	9213	2110	214	1
H30C	565	10186	1738	173	1
H30D	490	9242	1579	173	1
H30E	815	10117	936	173	1
H30F	3218	8002	979	216	1
H30G	3213	8076	1791	216	1
H30H	4735	8738	1080	347	1
H30I	3947	9466	1351	347	1
H30J	3909	9429	541	347	1

Table A3.6. Torsion angles [°].

C6–C1–C2–O1	–178.8(16)
P1–C1–C2–O1	6.6(15)
C6–C1–C2–C3	0.0
P1–C1–C2–C3	–174.6(12)
O1–C2–C3–C4	178.7(18)
C1–C2–C3–C4	0.0
C2–C3–C4–O2	–179.0(12)
C2–C3–C4–C5	0.0
O2–C4–C5–C6	179.0(12)
C3–C4–C5–C6	0.0
C4–C5–C6–O3	178.0(19)
C4–C5–C6–C1	0.0
C2–C1–C6–O3	–178.0(19)
P1–C1–C6–O3	–4.2(18)
C2–C1–C6–C5	0.0
P1–C1–C6–C5	173.8(14)
C16–C11–C12–O11	–177.3(4)
P1–C11–C12–O11	1.6(6)
C16–C11–C12–C13	3.0(7)
P1–C11–C12–C13	–178.1(3)
O11–C12–C13–C14	178.5(4)
C11–C12–C13–C14	–1.8(7)
C12–C13–C14–O12	–178.3(4)
C12–C13–C14–C15	–0.1(8)
C13–C14–C15–C16	0.7(8)
O12–C14–C15–C16	178.7(5)
C14–C15–C16–O13	–178.7(5)
C14–C15–C16–C11	0.6(8)
C12–C11–C16–O13	176.9(4)
P1–C11–C16–O13	–2.1(6)
C12–C11–C16–C15	–2.4(7)
P1–C11–C16–C15	178.6(4)
C26–C21–C22–O21	175.0(4)
P1–C21–C22–O21	–6.7(7)
C26–C21–C22–C23	–3.0(7)
P1–C21–C22–C23	175.4(4)
O21–C22–C23–C24	–177.9(5)
C21–C22–C23–C24	–0.2(8)
C22–C23–C24–C25	3.4(10)
C22–C23–C24–O22	–175.8(14)
C22–C23–C24–O122	174(2)

C23–C24–C25–C26	–3.2(9)
O22–C24–C25–C26	175.9(16)
O122–C24–C25–C26	–176.1(14)
C24–C25–C26–O23	179.0(5)
C24–C25–C26–C21	–0.3(8)
C22–C21–C26–O23	–176.1(4)
P1–C21–C26–O23	5.4(6)
C22–C21–C26–C25	3.3(7)
P1–C21–C26–C25	–175.3(4)
P1–C31–C32–C33	–178.3(4)
C31–C32–C33–S2	–65.3(6)
C16–C11–P1–C21	–163.7(4)
C12–C11–P1–C21	17.4(5)
C16–C11–P1–C131	–53(2)
C12–C11–P1–C131	128(2)
C16–C11–P1–C31	–49.5(5)
C12–C11–P1–C31	131.6(5)
C16–C11–P1–C101	75.0(6)
C12–C11–P1–C101	–104.0(6)
C16–C11–P1–C1	68.5(6)
C12–C11–P1–C1	–110.4(6)
C26–C21–P1–C11	50.4(4)
C22–C21–P1–C11	–128.0(4)
C26–C21–P1–C131	–53.9(16)
C22–C21–P1–C131	127.7(16)
C26–C21–P1–C31	–68.1(4)
C22–C21–P1–C31	113.5(4)
C26–C21–P1–C101	168.0(6)
C22–C21–P1–C101	–10.3(7)
C26–C21–P1–C1	175.5(6)
C22–C21–P1–C1	–2.8(7)
C32–C31–P1–C11	–161.1(4)
C32–C31–P1–C21	–42.8(5)
C32–C31–P1–C131	–148(8)
C32–C31–P1–C101	79.4(8)
C32–C31–P1–C1	78.9(8)
C2–C1–P1–C11	55.5(8)
C6–C1–P1–C11	–118.7(8)
C2–C1–P1–C21	–69.8(8)
C6–C1–P1–C21	116.0(8)
C2–C1–P1–C131	164.3(11)
C6–C1–P1–C131	–9.9(15)
C2–C1–P1–C31	175.7(6)
C6–C1–P1–C31	1.6(10)

C2–C1–P1–C101	–1(9)
C6–C1–P1–C101	–175(10)
C3–C2–O1–C7	–10(3)
C1–C2–O1–C7	169(2)
C3–C4–O2–C8	6.4(19)
C5–C4–O2–C8	–172.7(15)
C5–C6–O3–C9	10(3)
C1–C6–O3–C9	–172(2)
C13–C12–O11–C17	2.1(7)
C11–C12–O11–C17	–177.6(5)
C13–C14–O12–C18	164.5(5)
C15–C14–O12–C18	–13.6(7)
C15–C16–O13–C19	14.3(11)
C11–C16–O13–C19	–165.0(9)
C15–C16–O13–C119	–29.3(12)
C11–C16–O13–C119	151.4(11)
C23–C22–O21–C27	–11.0(9)
C21–C22–O21–C27	171.2(6)
C25–C24–O22–C28	–174.2(17)
C23–C24–O22–C28	5(3)
O122–C24–O22–C28	166(8)
C25–C26–O23–C29	16.0(7)
C21–C26–O23–C29	–164.6(5)
C32–C33–S2–S1	–169.3(4)
C11–P1–C101–C102	63.5(8)
C21–P1–C101–C102	–56.9(8)
C131–P1–C101–C102	173.1(11)
C31–P1–C101–C102	–174.5(5)
C1–P1–C101–C102	–171(10)
C11–P1–C101–C106	–125.2(7)
C21–P1–C101–C106	114.5(7)
C131–P1–C101–C106	–15.5(16)
C31–P1–C101–C106	–3.1(11)
C1–P1–C101–C106	1(9)
C106–C101–C102–O101	–179.0(17)
P1–C101–C102–O101	–7.1(17)
C106–C101–C102–C103	0.0
P1–C101–C102–C103	171.9(12)
O101–C102–C103–C104	178.9(18)
C101–C102–C103–C104	0.0
C102–C103–C104–O102	–171.0(13)
C102–C103–C104–C105	0.0
O102–C104–C105–C106	171.8(12)
C103–C104–C105–C106	0.0

C104–C105–C106–O103	–179.8(18)
C104–C105–C106–C101	0.0
C102–C101–C106–O103	179.8(18)
P1–C101–C106–O103	8.9(17)
C102–C101–C106–C105	0.0
P1–C101–C106–C105	–170.9(13)
C103–C102–O101–C107	–10(3)
C101–C102–O101–C107	169.0(19)
C105–C104–O102–C108	–171.0(14)
C103–C104–O102–C108	0.4(19)
C105–C106–O103–C109	19(3)
C101–C106–O103–C109	–161(2)
C25–C24–O122–C128	172.6(18)
C23–C24–O122–C128	1(3)
O22–C24–O122–C128	–24(4)
C11–P1–C131–C132	–157(3)
C21–P1–C131–C132	–44(4)
C31–P1–C131–C132	35(6)
C101–P1–C131–C132	88(4)
C1–P1–C131–C132	86(4)
P1–C131–C132–C133	–172(3)
C131–C132–C133–S102	–179(3)
C132–C133–S102–S101	160(3)
C46–C41–C42–O41	176.1(4)
P41–C41–C42–O41	–0.6(6)
C46–C41–C42–C43	–4.8(7)
P41–C41–C42–C43	178.5(4)
O41–C42–C43–C44	–177.5(4)
C41–C42–C43–C44	3.5(7)
C42–C43–C44–C45	–0.5(8)
C42–C43–C44–O42	176.5(6)
C42–C43–C44–O142	–177.6(10)
C43–C44–C45–C46	–1.0(8)
O42–C44–C45–C46	–177.1(7)
O142–C44–C45–C46	177.0(7)
C44–C45–C46–O43	179.0(5)
C44–C45–C46–C41	–0.5(7)
C42–C41–C46–O43	–176.2(4)
P41–C41–C46–O43	0.9(5)
C42–C41–C46–C45	3.3(7)
P41–C41–C46–C45	–179.6(4)
C56–C51–C52–O51	179.4(4)
P41–C51–C52–O51	–2.7(7)
C56–C51–C52–C53	1.4(7)

P41–C51–C52–C53	179.4(4)
O51–C52–C53–C54	–178.3(5)
C51–C52–C53–C54	–0.5(8)
C52–C53–C54–O52	179.0(5)
C52–C53–C54–C55	–1.1(8)
C53–C54–C55–C56	1.7(7)
O52–C54–C55–C56	–178.4(4)
C54–C55–C56–O53	–178.5(4)
C54–C55–C56–C51	–0.7(7)
C52–C51–C56–O53	177.2(4)
P41–C51–C56–O53	–1.0(5)
C52–C51–C56–C55	–0.8(7)
P41–C51–C56–C55	–179.0(4)
C66–C61–C62–O61	–174.9(4)
P41–C61–C62–O61	6.0(6)
C66–C61–C62–C63	4.2(7)
P41–C61–C62–C63	–174.9(4)
O61–C62–C63–C64	177.1(4)
C61–C62–C63–C64	–2.0(7)
C62–C63–C64–O62	179.9(4)
C62–C63–C64–C65	–1.5(7)
O62–C64–C65–C66	–179.0(4)
C63–C64–C65–C66	2.6(7)
C62–C61–C66–O63	175.0(4)
P41–C61–C66–O63	–5.8(6)
C62–C61–C66–C65	–3.1(7)
P41–C61–C66–C65	176.0(4)
C64–C65–C66–O63	–178.2(4)
C64–C65–C66–C61	–0.1(7)
P41–C71–C72–C73	–155.7(19)
C71–C72–C73–S42	–64(2)
C56–C51–P41–C61	63.2(4)
C52–C51–P41–C61	–114.8(4)
C56–C51–P41–C41	–61.8(4)
C52–C51–P41–C41	120.2(4)
C56–C51–P41–C171	–178.5(10)
C52–C51–P41–C171	3.6(10)
C56–C51–P41–C71	–179.7(9)
C52–C51–P41–C71	2.3(10)
C66–C61–P41–C51	68.2(4)
C62–C61–P41–C51	–112.7(4)
C66–C61–P41–C41	–166.3(3)
C62–C61–P41–C41	12.8(5)
C66–C61–P41–C171	–53.5(15)

C62–C61–P41–C171	125.6(15)
C66–C61–P41–C71	–50.7(15)
C62–C61–P41–C71	128.4(15)
C42–C41–P41–C51	–8.2(5)
C46–C41–P41–C51	175.1(3)
C42–C41–P41–C61	–130.0(4)
C46–C41–P41–C61	53.2(4)
C42–C41–P41–C171	114.2(12)
C46–C41–P41–C171	–62.5(12)
C42–C41–P41–C71	112.8(12)
C46–C41–P41–C71	–63.9(12)
C72–C71–P41–C51	83(3)
C72–C71–P41–C61	–160(2)
C72–C71–P41–C41	–40(3)
C72–C71–P41–C171	–71(33)
C41–C42–O41–C47	–178.4(5)
C43–C42–O41–C47	2.6(7)
C45–C44–O42–C48	–6.0(13)
C43–C44–O42–C48	177.4(8)
O142–C44–O42–C48	5.5(14)
C45–C46–O43–C49	17.9(7)
C41–C46–O43–C49	–162.5(5)
C53–C52–O51–C57	–11.0(8)
C51–C52–O51–C57	171.1(5)
C53–C54–O52–C158	167.2(11)
C55–C54–O52–C158	–12.6(12)
C53–C54–O52–C58	–8.9(9)
C55–C54–O52–C58	171.2(6)
C55–C56–O53–C59	–20.9(6)
C51–C56–O53–C59	161.1(4)
C63–C62–O61–C67	–6.3(7)
C61–C62–O61–C67	172.7(4)
C65–C64–O62–C68	–11.7(7)
C63–C64–O62–C68	167.0(5)
C61–C66–O63–C69	158.5(5)
C65–C66–O63–C69	–23.3(8)
C72–C73–S42–S41	–92.9(11)
C51–P41–C171–C172	75(3)
C61–P41–C171–C172	–167(2)
C41–P41–C171–C172	–48(3)
C71–P41–C171–C172	102(35)
P41–C171–C172–C173	–180(2)
C171–C172–C173–S142	–63(2)
C172–C173–S142–S141	–145.0(11)

C45–C44–O142–C148	–178.5(10)
C43–C44–O142–C148	–1.0(17)
O42–C44–O142–C148	10.3(12)
C304–C303–O301–C301	–71.2(13)
C302–C301–O301–C303	–160.0(9)